PALLADIUM AND GOLD CATALYSTS FOR SUSTAINABLE CHEMICAL PROCESSING

YUFEN HAO

A dissertation submitted for the degree of Doctor of Philosophy

Heriot-Watt University

School of Engineering and Physical Sciences

July 2015

Abstract

The main focus of this thesis is the investigation of sustainable routes for the production of commercially important higher and functionalised aliphatic and aromatic amines through the application of (oxide and carbon) supported palladium and gold catalysts. In the hydrogenation of butyronitrile as a model aliphatic nitrile, unsupported Pd promoted the formation of primary and secondary amines. The acid-base character of the support and available surface reactive hydrogen are critical catalyst variables. The greater acidity of Pd/C (relative to Pd/Al_2O_3) resulted in the predominant formation of the tertiary (tributyl-) amine where spillover hydrogen serves to elevate hydrogenation rate. The combination of Ba with Pd (supported bimetallic) proved effective in promoting hydrogenation activity with 100% selectivity to the secondary amine, which is attributed to a decrease in acidity and modification to Pd dispersion that enhances surface hydrogen. The feasibility of an alternative route for the synthesis of higher aliphatic secondary and tertiary amines from primary and secondary amine feedstock has been demonstrated. Control of contact time is key where the use of a multiple catalyst beds in series facilitates higher yields. This is accounted for in terms of surface reaction mechanism. This configuration was also efficient for the synthesis of benzylamine from benzonitrile.

Hydrogenation selectivity was further assessed by considering the reduction of functionalized nitroarenes (*p*-chloronitrobenzene (*p*-CNB) and *p*-nitrobenzonitrile (*p*-NBN)). It is shown that the redox nature of the support has a direct impact on the activity and selectivity response. The formation of $Pd^{\delta+}$ (on carbon) activates the nitro group with subsequent C-Cl bond scission with the formation of *p*-chloroaniline (*p*-CAN) and aniline (AN). The occurrence of $Pd^{\delta-}$ (on SiO_2 and Al_2O_3) favours interaction *via* the aromatic ring that activates both $–NO_2$ and –Cl for attack generating AN and nitrobenzene. The formation of a PdZn alloy (established by XPS analysis) in addition to Pd^0 selectively activates the $–NO_2$ group and promotes the sole formation of *p*-CAN at all levels of conversion (and close to 100%). Exclusive conversion of *p*-NBN to *p*-aminobenzonitrile was achieved over a series of oxide (CeO_2, Fe_2O_3, Fe_3O_4, TiO_2, ZrO_2 and Al_2O_3) supported (1 mol %) Au catalysts. Hydrogen uptake is structure sensitive and favoured by smaller nano-scale metal particles with a consequent increase in activity. Reaction over Au/TiO_2 delivered the highest specific hydrogenation rate, which is explained on the basis of $–NO_2$ activation at the metal-support interface that is

facilitated by $N^{\delta+}$ interaction with electron rich gold ($Au^{\delta-}$, demonstrated by XPS). This effect is shown to extend to TiO_2 supported Ag and Pd.

Supported Au is also effective in the selective hydrogenation of benzaldehye in liquid phase operation using water as a green solvent. 100% yield of the target benzyl alcohol was attained over Au/Al_2O_3 whereas Pt/Al_2O_3 generated toluene and benzene as significant (hydrogenolysis) by-products. Solvent effects were evaluated where a direct correlation between selective hydrogenation rate and dielectric constant is demonstrated and ascribed to competitive adsorption, which was more severe for less polar alcohol solvents. Solvation by polar water facilitated benzaldehyde activation. The same activity and selectivity trends were found to also apply to continuous gas phase reaction.

The results presented in this thesis demonstrate, for the first time, direct participation of the support in the catalytic hydrogenation of aliphatic nitriles over Pd-based catalysts. This can be harnessed to enhance amine production in a sustainable continuous flow gas operation process. Moreover, secondary and tertiary aliphatic amines can be selectively produced from the correspondent primary and secondary amines over Pd in continuous mode. The use of reducible supports can result in the formation of an alloy phase and surface defects with beneficial selectivity and activity effects in the production of functionalized amines. The selective catalytic action of supported Au catalysts has been established in achieving 100% yield of benzyl alcohol (from benzaldehyde) using water as a benign solvent.

Dedication

To my grandparents

Yaoer Zhang and Jiacai Hao

Acknowledgements

This thesis could not have been completed without the help and support of my supervisor, colleagues, friends and family. I would like to take this opportunity to express my utmost gratitude to them.

My greatest appreciation goes to my supervisor Professor Mark A. Keane. I thank him for the guidance, encouragement and advice that he has provided throughout my PhD studies. I do appreciate his enthusiasm for research work, rich experience in directing research projects. Thanks also goes to Dr. Fernando Cárdenas-Lizana for his patience in discussion and suggestions on the research projects and also the modification of the thesis. I would also like to thank Dr. Humphrey Yiu for his support in access to the usage of experimental equipments.

The fancial support from Scottish Overseas Research Student Awards Scheme is also acknowleged and very much appreciated for without it, I would not have been able to commence and complete this work.

I am enormously delighted to have the privilege of knowing my colleagues of past and present, namely, Noemie Perret, Xiaodong Wang, Maoshuai Li, I thank you for all the discussions/suggestions in the research projects and wonderful moments in life. I would also like to thank my friends Ivan Ku, Na Wang, Dalia Capao, Eilidh Duncan, Craig Callahan, Natalia Felenta, Gregor, Pedro, Kamil and Yi Jin for making my life easier away from PhD studies. I would personally thank my close friends Shuhua Dong, Peggy Zhu and Rajiv for their consistent support when I was through any difficult times.

My appreciation is also extended to all the technicians in Chemical engineering department for helping me with the installation/maintaining of experimental equipments. Just name a few of them, Ronnie (who has retired now); Curtis; Richard; Craig Bell etc.

Last but not least, my special gratitude goes to my parents and two younger sisters for their unconditional love and unwavering support.

Table of Contents

Lists of Tables

Lists of Figures

Lists of Schemes

Glossary

Acronyms

AAS	Atomic Absorption Spectroscopy
p-ABN	*p*-Aminobezonitrile
AN	Aniline
p-NBN	*p*-Nitrobenzonitrile
BE	Binding Energy
BBA	N-butylidene-butylamine
BEDA	But-1-eny-dibutylamine
BET	S.Brunauer, P. H. Emmett and E. Teller theory; measurement of surface area
BT	Butyronitrile
BI	Butylidenimine
p-CAN	*p*-Chloroaniline
p-CNB	*p*-Chloronitrobenzene
DBA	Di-butylamine
FID	Flame Ionisation Detector
GHSV	Gas Hourly Space Velocity
HRTEM	High Resolution Transmission Electron Microscopy
(HR)XRD	(High Resolution) X-ray Diffraction
ICP	Inductively Coupled Plasma
ICP-OES	Inductively coupled plasma-optical emission spectrometry
MBA	Mono-butylamine
NB	Nitrobenzene
PZC	Point of Zero Charge
STEM	Scanning Transmission Electron Microscopy
TBA	Tri-butylamine
TEM	Transmission Electron Microscopy
TOF	Turnover Frequency

TPD	Temperature Programmed Desorption
TPR	Temperature Programmed Reduction
XAS	X-ray Absorption Spectroscopy
XPS	X-ray Photoelectron Spectroscopy

Symbols

d_{H2}, d_{TEM}, $d_{(S)TEM}$	Mean metal diameter (using (S)TEM); (nm)
F	Inlet molar feed rate (mol h^{-1})
i.d.	Internal diameter/mm
N_i	Stoichiometric coefficient for product "*i*"
R_0	Initial rate
S	Selectivity (%)
T_{max}	Temperature maximum (K)
X	Conversion
x_i	Molar fraction of reactant/product "*i*"
λ	Wavelength in FTIR analysis (Å)
ε	Dielectric constant

List of Publications by the Candidate

[1] Y. Hao, M. Li, F. Cárdenas-Lizana, M.A. Keane, *Production of butylamine in the gas phase hydrogenation of butyronitrile over Pd/SiO_2 and Ba-Pd/SiO_2*, Catal. Struct. React. (**2015**) Accepted.

[2] Y. Hao, X. Wang, N. Perret, F. Cárdenas-Lizana, M.A. Keane, *An analysis of acid-base and metal-support effects in the gas phase hydrogenation of butyronitrile over palladium* Catal. Struct. React. 1 (**2015**) 1-8.

[3] M. Li, Y. Hao, F. Cárdenas-Lizana, M. Keane, *Selective production of furfuryl alcohol via gas phase hydrogenation of furfural over Au/Al_2O_3*, Catal. Commun. 69 (**2015**) 119-122.

[4] M. Li, Y. Hao, F. Cárdenas-Lizana, H.P. Yiu, M. Keane, *''Hydrogen-free'' hydrogenation of nitrobenzene over Cu/SiO_2 via coupling with 2-butanol dehydrogenation*, Top. Catal. (**2014**) 1-10.

[5] F. Cárdenas-Lizana, Y. Hao, M. Crespo-Quesada, I. Yuranov, X. Wang, M.A. Keane, L. Kiwi-Minsker, *Selective gas phase hydrogenation of p-chloronitrobenzene over Pd catalysts: Role of the support*, ACS Catal. 3 (**2013**) 1386-1396.

[6] Y. Hao, M. Li, F. Cárdenas-Lizana, M.A. Keane, *Selective production of benzylamine via gas phase hydrogenation of benzonitrile supported Pd catalysts*, manuscript ready for submission.

[7] Y. Hao, X. Wang, F. Cárdenas-Lizana, M.A. Keane, *Palladium promoted production of higher amines from a lower amines feedstock*, manuscript ready for submission.

[8] Y. Hao, F. Cárdenas-Lizana, M.A. Keane, *Clean production of benzyl alcohol over supported gold catlayts*, manuscript ready for submission.

[9] Y. Hao, F. Cárdenas-Lizana, M.A. Keane, *Gas phase chemoselective hydrogenation of p-nitrobenzonitrile over gold: Effect of metal particle size, support and the metal-support interface*, manuscript ready for submission

List of Presentations by the Candidate

[1] *Gas Phase Hydrogenation of p-Nitrobenzonitrile over Gold Catalysts: Effect of Particle Size and Support*, Oral presentation at the Annual Postgraduate Conference, Heriot-Watt University, June 2013.

[2] *Role of the Support in Selective Hydrogenation of p-Chloronitrobenzene over Pd Catalysts*, Oral presentation at SURCAT ECOSSE, St. Andrews University, June 2012.

[3] *Gas Phase Hydrogenation of Butyronitrile over Supported Pd Catalysts: Support Effects and Mechanistic Investigations*, Post presentation at the Poster Event, Heriot-Watt University, October 2011.

Chapter 1

Introduction and Scope of the Thesis

This Chapter provides a brief overview of the concept of sustainable chemical processes, focusing on amine production. The objectives of this PhD research are defined and the approach taken is described.

1.1 Sustainable Chemical Processing and Amine Synthesis

The apparent conflict of increasing chemical production and environmental protection has resulted in a pressing demand for the development of sustainable manufacturing processes [1]. This requires processes that operate safely and with a high degree of energy efficiency that must draw on cost-effective catalyst formulations that deliver high selectivity to the target product [2]. The concept of atom efficiency is critical in this respect, *i.e.* utilisation of all the material in the process, avoiding by-product formation, minimising waste to arrive at the optimal product yield. Amines (both aliphatic and aromatic) are widely used as intermediates in the production of agrochemicals and pharmaceuticals [3]. However, traditional synthesis routes *via* hydrogenation of nitriles or nitro-compounds typically generates low product yield and selectivity, toxic by-product formation and energy inefficiency [4]. Supported nano-scaled Pd is effective in the dissociative adsorption of H_2 [5] and has been widely adopted in catalytic hydrogenation [6,7]. Nevertheless, the application in nitrile or nitro-compound reduction is limited and existing studies have reported significant by-product formation. This is a reaction system that requires improvement to meet the requirements of sustainable chemical processing.

1.2 Scope and Organization of the Thesis

The aim of this research is to explore the catalytic selectivity in the application of Pd and Au catalysts for the synthesis of commercially valuable products. The work has covered catalyst synthesis, characterisation and process optimisation. Catalyst characterisation has involved ICP, AAS, TPR, $H_2/O_2/NH_3$ chemisorption, H_2/NH_3 TPD, (S)TEM and XPS measurements. Amines are predominantly produced *via* high pressure batch liquid phase hydrogenation of nitriles [8]. A move to continuous processes has been highlighted by the fine chemical/pharmaceutical sector as a priority to achieve higher throughput and sustainable production [9]. Palladium catalysts have been

employed in amine synthesis in **Chapter 2-6**; thesis organisation and scope are summarised in **Table 1.1**. The role of support acid-base character in affecting activity/selectivity is inconclusive from a consideration of existing literature [10-13] and is considered in **Chapter 2**. The continuous gas phase hydrogenation of butyronitrile was investigated over supported (C and Al_2O_3) Pd and the catalytic action compared with bulk (unsupported) Pd. Support acidity facilitated condensation

Table 1.1: **Scope of the studies undertaken in this thesis.**

	Reactant	Catalysts	Objective
Chapter 2	C_3H_7-C≡ N	PdO Pd/Al_2O_3 Pd/C	Role of support and spillover hydrogen
Chapter 3	C_3H_7-C≡ N	Pd/SiO_2 Ba-Pd/SiO_2	Exclusive production of primary amine
Chapter 4	C_3H_7-CH_2-NH_2 $(C_3H_7$-$CH_2)_2$-NH	Pd/Al_2O_3 Pd/C	Role of support, exclusive production of secondary and tertiary amines
Chapter 5		Pd/Al_2O_3 Pd/C	Role of support, exclusive production of primary amines
Chapter 6	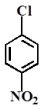	Pd/C, Pd/SiO_2, Pd/Al_2O_3 Pd/ZnO	Role of support, exclusive production of *p*-chloroaniline
Chapter 7		Supported Au *vs* Pd *vs* Ag	Role of metal particle size, support and metal-support interface
Chapter 8		Au/Al_2O_3 , Au/Fe_2O_3 Pt/Al_2O_3	Exclusive production of benzyl alcohol, solvent effect

reactions to form higher (secondary and tertiary) amines. This work is extended in **Chapter 3** by inclusion of Ba to Pd/SiO_2 to modify surface chemistry and enhance selectivity to primary amine. The controlled synthesis of higher amines is the focus of **Chapter 4**. The consequences of a switch from an aliphatic (butyronitrile) to an aromatic (benzonitrile) nitrile is developed in **Chapter 5**. Possible support effects are further examined in the hydrogenation of *p*-chloronitrobenzene (**Chapter 6**). Selectivity is further probed in reduction of nitro (-NO_2) and cyano (-C≡N) substituents on the aromatic ring (in *p*-nitrobenzonitrile), comparing the catalytic action of supported Au with Pd and Ag systems in **Chapter 7**. In order to further explore the potential of supported Au catalysts, **Chapter 8** deals with the hydrogenation of benzaldehyde in

liquid phase using water as solvent; results are compared with continuous gas phase operation. The thesis ends (**Chapter 9**) with a concluding summary and suggested future work.

1.3 References

[1] S.H. Park, C.L. Walter, *Industrial development and environmental degradation*, Edward Publ., Inc., Cheltenham, (**1998**) 14-18.

[2] D. Brennan, *Sustainable process engineering: Concepts, strategies, evaluation and implementation*, Pan Stanford Publ., Sigapore, (**2013**) 13-13.

[3] S. Gomez, J.A. Peters, T. Maschmeyer, *The reductive amination of aldehydes and ketones and the hydrogenation of nitriles: Mechanistic aspects and selectivity control*, Adv. Synth. Catal. 344 (**2002**) 1037-1057.

[4] J. Krupka, J. Pasek, *Nitrile hydrogenation on solid catalysts - new insights into the reaction mechanism*, Curr. Org. Chem. 16 (**2012**) 988-1004.

[5] A.W. Pelzer, J. Jellinek, K.A. Jackson, *H_2 reactions on palladium clusters*, J. Phys. Chem. A 117 (**2013**) 10407-10415.

[6] M. Armbrüster, M. Behrens, F. Cinquini, K. Föttinger, Y. Grin, A. Haghofer, B. Klötzer, A. Knop-Gericke, H. Lorenz, A. Ota, S. Penner, J. Prinz, C. Rameshan, Z. Révay, D. Rosenthal, N. Rupprechter, P. Sautet, R. Schlögl, L. Shao, L. Szentmiklósi, D. Teschner, D. Torres, R. Wagner, R. Widmer, G. Wowsnick, *How to control the selectivity of palladium-based catalysts in hydrogenation reactions: The role of subsurface chemistry*, ChemCatChem 4 (**2012**) 1048-1063.

[7] H.-U. Blaser, A. Indolese, A. Schnyder, H. Steiner, M. Studer, *Supported palladium catalysts for fine chemicals synthesis*, J. Mol. Catal. A: Chem. 173 (**2001**) 3-18.

[8] S. Nishimura, *Handbook of Heterogeneous Catalytic Hydrogenation for Organic Synthesis* John Wiley, New York (**2001**) 265-265.

[9] C. Jiménez-González, P. Poechlauer, Q.B. Broxterman, B.-S. Yang, D.A. Ende, J. Baird, C. Bertsch, R.E. Hannah, P. Dell'Orco, H. Noorrnan, S. Yee, R. Reintjens, A. Wells, V. Massonneau, J. Manley, *Key green engineering research areas for sustainable manufacturing: A perspective from pharmaceutical and fine chemicals manufacturers*, Org. Process Res. Dev. 15 (**2011**) 900-911.

[10] A.C. Gluhoi, P. Mărginean, U. Stănescu, *Effect of supports on the activity of nickel catalysts in acetonitrile hydrogenation*, Appl. Catal. A: Gen. 294 (**2005**) 208-214.

[11] M.J.F.M. Verhaak, A.J. Dillen, J.W. Geus, *The selective hydrogenation of acetonitrile on supported nickel catalysts*, Catal. Lett. 26 (**1994**) 37-53.

[12] P. Braos-García , P. Maireles-Torres, E. Rodríguez-Castellón , A. Jiménez-López *Gas-phase hydrogenation of acetonitrile over nickel supported on alumina- and mixed alumina/gallium oxide-pillared tin phosphate catalysts*, J. Mol. Catal. A: Chem. 168 (**2001**) 279-287.

[13] P. Braos-García, P. Maireles-Torres, E. Rodríguez-Castellón, A. Jiménez-López, *Gas-phase hydrogenation of acetonitrile on zirconium-doped mesoporous silica-supported nickel catalysts*, J. Mol. Catal. A: Chem. 193 (**2003**) 185-196.

Chapter 2

Support Effects in the Gas Phase Hydrogenation of Butyronitrile over Palladium

The effect of the support in the hydrogenation of nitriles to higher amines is inconclusive in the literature. In this Chapter the possible role of the carrier has been established by direct comparison of Pd/Al_2O_3 with Pd/C in the selective gas phase hydrogenation of butyronitrile, taking (unsupported) bulk Pd as benchmark. Catalytic performance is correlated to critical catalyst characterisation data.

2.1 Introduction

The catalytic hydrogenation of nitriles is an established route to amines, widely used as intermediates in the production of agrochemicals and pharmaceuticals [1]. This reaction is typically conducted in batch liquid phase at elevated H_2 pressure (20-45 atm [2-6]) with alkane solvents (*e.g.* hexane [5,7], heptane [3,4,6] and octane [7,8]). A move from batch to continuous processes has, however, been highlighted by the fine chemical/pharmaceutical sector as a priority to achieve higher throughput and sustainable production [9]. Nitrile hydrogenation has been conducted over supported metal (Ni [2,8,10], Co [5,8,10], Ru [3,4,6,10], Cu [4,10], Rh [3,4], Pt [3,4,10], Pd [3,4,7,10,11]) catalysts where primary amines are preferentially produced over Ru, Ni and Co, whereas Cu and Rh promote the formation of secondary amines and Pd and Pt exhibit higher selectivity to tertiary amines. It is striking that Pd, although extensively used in hydrogenation applications, has not been employed to any significant extent in nitrile reduction and the work to date has primarily considered the performance of bimetallic (Pd-Ni [3,4], Pd-Ag [4], Pd-Cu [4], Pd-Pt [12]) or (PdZn, $PdGa_5$, Pd_5Ga_2 and $Pd_{0.48}In_{0.52}$) alloy [11] catalyst formulations.

Metal oxides have been used as support in the hydrogenation of butyronitrile [3-6,10,13], benzylcyanide [3], acetonitrile [4-6,12] and lauronitrile [2]. Use of carbon as metal carrier has focused on reactions promoted by Ni [14-16] with limited work on supported Pd [13,17]. Catalytic hydrogenation has been shown to be influenced by support acid-base character [18] with conflicting results for nitrile reduction. In the hydrogenation of acetonitrile [19-22] over oxide (MgO [19,20], Al_2O_3 [19-21], Cr_2O_3

[19], SiO_2 [19,20,22], TiO_2 [19], ZrO_2 [19], ThO_2 [19], and UO_2 [19]) supported Ni, surface acidity was proposed to contribute to condensation step(s). In contrast, no apparent selectivity dependence on support acidity was observed for reaction over oxide [23] (Al_2O_3, TiO_2, SiO_2-Al_2O_3, SiO_2) and zeolite (NaY [6]) supported Ru [6], Ni [6,23], Rh [6] and Pt [6]. Given the available literature, it is difficult to establish any explicit link between catalyst performance and surface acid properties. In this report we set out to decouple the effect of metal and support in determining catalyst performance and evaluate the role of surface acidity in the gas phase continuous hydrogenation of butyronitrile, as a model aliphatic nitrile reactant, over Pd/C and Pd/Al_2O_3, taking bulk Pd as benchmark.

2.2 Experimental Method

The alumina support (Puralox, Condea Vista Co.) was used as received, butyronitrile (> 99.8%), (1 wt-%) Pd/C, (1.2 wt-%) Pd/Al_2O_3 and PdO were obtained from Sigma-Aldrich. The samples were sieved into a batch of 75 μm average diameter and activated in 60 cm^3 min^{-1} H_2 (BOC, > 99.99%) at 10 K min^{-1} to 573 K, which was maintained for 1 h. Reduction conditions to convert PdO to zero valent Pd have been established elsewhere [24]. Samples for off-line analysis were passivated in 1% v/v O_2/He at ambient temperature.

2.2.1 Catalyst Characterization

Palladium content was measured by inductively coupled plasma-optical emission spectrometry (ICP-OES, Vista-PRO, Varian Inc.) from the diluted extract in HF. Temperature programmed reduction (TPR), H_2 and NH_3 chemisorption/temperature programmed desorption (TPD) and specific surface area (SSA) measurements were conducted using the commercial CHEM-BET 3000 (Quantachrome) unit. The samples were loaded into a U-shaped Quartz cell (3.76 mm *i.d.*) and heated in 17 cm^3 min^{-1} (Brooks mass flow controlled) 5% v/v H_2/N_2 at 10 K min^{-1} to 573 ± 1 K. The effluent gas passed through a liquid nitrogen trap and changes in H_2 consumption monitored by a thermal conductivity detector (TCD) with data acquisition/manipulation using the TPR Win™ software. The reduced samples were maintained at the final temperature in H_2/N_2 until the signal returned to baseline, swept with 65 cm^3 min^{-1} N_2 for 1.5 h, cooled to ambient temperature and subjected to H_2 (or NH_3) chemisorption using a pulse (50-1000 μl) titrations. Samples were thoroughly flushed in N_2 with TPD at 10-50 K min^{-1} to 923-1173 K. The resultant profile was corrected using the TPD recorded in parallel directly following TPR to explicitly determine H_2 (or NH_3) release. SSA was

determined in a 30% v/v N_2/He flow using undiluted N_2 as internal standard. At least two cycles of N_2 adsorption-desorption were employed using the standard single point BET method. SSA and H_2/NH_3 uptake/desorption were reproducible to ±5% and the values quoted represent the mean. Supported Pd particle morphology (size and shape) was determined by transmission (TEM, JEOL JEM 2011 unit) and scanning transmission (STEM, JEOL 2200FS field emission gun-equipped unit) electron microscopy, employing Gatan DigitalMicrograph 1.82 for data acquisition/manipulation. The samples were crushed and deposited (dry) on a holey carbon/Cu grid (300 Mesh). Up to 800 individual Pd particles were counted for each catalyst to determine the surface area-weighted Pd diameter as described elsewhere [25].

2.2.2 Catalytic Procedure

Reactions were conducted (1 atm, 473 K) *in situ*, following catalyst activation, in a fixed bed vertical glass reactor (*i.d.* = 15 mm) under conditions that ensured minimal mass or heat transfer limitations. The butyronitrile reactant was delivered at a fixed calibrated flow rate *via* a glass/teflon air-tight syringe and teflon line using a microprocessor controlled infusion pump (Model 100 kd Scientific). A layer of borosilicate glass beads served as preheating zone where the reactant was vaporized and reached reaction temperature before contacting the catalyst. Isothermal conditions (±1 K) were maintained by diluting the catalyst bed with ground glass (75 μm) and the temperature was continuously monitored by a thermocouple inserted in a thermowell within the catalyst bed. A co-current flow of butryronitrile (<1% v/v) and H_2 was maintained at $GHSV = 1.0 \times 10^4$ h^{-1} with an inlet flow rate (F) of 6.9 mmol h^{-1} where H_2 was in excess (by a factor of 24) of the stoichiometric requirement for the formation of the butylidenimine intermediate. The reaction temperature (473 K) was above boiling point of butyronitrile (390-392 K) ensuring the reactant was gasified. Although the boiling point of the hydrogenation products (butylamine (350 K), dibutylamine (432.9 K) and tributylamine (487 K)) varied, the partial pressure of tributylamine calculated under the reaction temperature (175 Pa) was one magnitude lower than the saturated vapour pressure (1314 Pa) suggesting the gas phase of tributylamine (**Appendix 1**). The molar palladium (n) to F ratio spanned the range $0.3 \times 10^{-4} – 1.3 \times 10^{-3}$ h. The reactor effluent was frozen in a liquid nitrogen trap for subsequent analysis, which was made using a Perkin-Elmer Auto System XL chromatograph equipped with a flame ionisation detector, employing a DB-1 capillary column (*i.d.* = 0.33 mm, length = 30 m, film thickness = 0.20 μm). Data acquisition/manipulation was performed using the

TotalChrom Workstation Version 6.1.2 (for Windows) chromatography data system and reactant/product molar fractions (x_i) were obtained using detailed calibration plots (not shown). Fractional butyronitrile hydrogenation (X_{BT}) was obtained from

$$X_{BT} = \frac{[\mathrm{BT}]_{in} - [\mathrm{BT}]_{out}}{[\mathrm{BT}]_{in}} \quad \textbf{(2.1)}$$

where selectivity to product *i* (S_i, %) is given by

$$S_i = \frac{N_i x_i}{[\mathrm{BT}]_{in} - [\mathrm{BT}]_{out}} \times 100 \quad \textbf{(2.2)}$$

$[\mathrm{BT}]_{in}$ and $[\mathrm{BT}]_{out}$ represent inlet and outlet butyronitrile concentration, respectively, and N_i is the stoichiometric coefficient for product "*i*". Repeated reactions with different samples from the same batch of catalyst delivered raw data reproducibility better than ±6%.

2.3 Results and Discussion

2.3.1 Catalytic Procedure

The critical physico-chemical properties of the catalytic systems considered in this study are recorded in **Table 2.1**.

2.3.1.1 Pd/Al_2O_3

The TPR profile generated for Pd/Al_2O_3 is presented in **Figure 2.1(I)** where the occurrence of a negative peak (H_2 release) at 355 K can be attributed to Pd hydride decomposition [26]. The hydride is generated by H_2 absorption, which is known to proceed at H_2 partial pressures >0.02 atm [27]; a pressure of 0.05 atm during TPR was used in this work. The absence of any H_2 consumption (positive signal) prior to hydride decomposition suggests the presence of metallic Pd in advance of the temperature ramp. Palladium particle size was determined by electron microscopy and verified by H_2 chemisorption on the basis of dissociative adsorption (Pd/H stoichiometry = 1:1) [28]. Representative TEM images presented in **Figure 2.2(AI)** and **(AII)** reveal pseudo-spherical Pd particles at the nano-scale. The associated Pd size distribution histogram

Table 2. 1: Specific surface area (SSA), Pd mean particle size (from TEM/STEM (d_{TEM}) and H_2 chemisorption (d_{H_2}) measurements), H_2 uptake and release during TPD (with associated temperature of maximum release (T_{max})) and NH_3 uptake and release (with T_{max}).

Catalyst	SSA/ $m^2\ g^{-1}$	Pd size/ nm		H_2 uptake/ mmol g_{Pd}^{-1}	H_2 TPD		NH_3 uptake/ mmol g^{-1}	NH_3 TPD	
		d_{TEM}	d_{H_2}		H_2 desorbed/ mmol g_{Pd}^{-1}	T_{max}/ K		NH_3 desorbed/ mmol g^{-1}	T_{max}/ K
Pd/Al_2O_3	145	3.0	2.4	2.1	9.6	767	0.52	0.51	464
Al_2O_3	160	-	-	-	-	-	0.71	0.69	450
Pd	3		131	0.04	0.05	782			
$Pd+Al_2O_3$	133			0.04	0.09	782			
$Pd/Al_2O_3+Al_2O_3$	152			2.3	46.6	767			
Pd/C	870	2.8	2.2	2.5	79.8	785, 1173	0.94	0.92	480

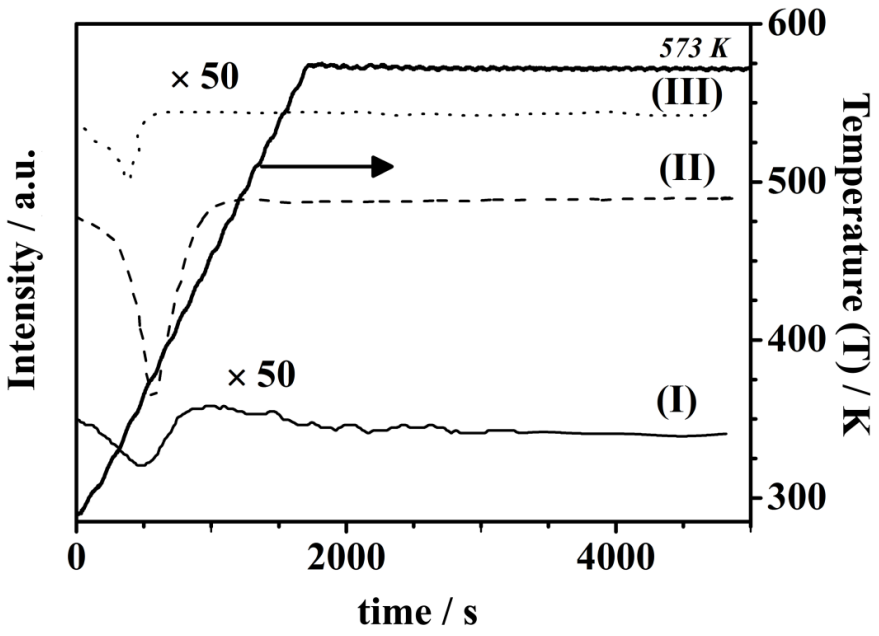

Figure 2. 1: Temperature-programmed reduction (TPR) profiles for (I) Pd/Al_2O_3 (solid line), (II) PdO (dashed line) and (III) Pd/C (dotted line).

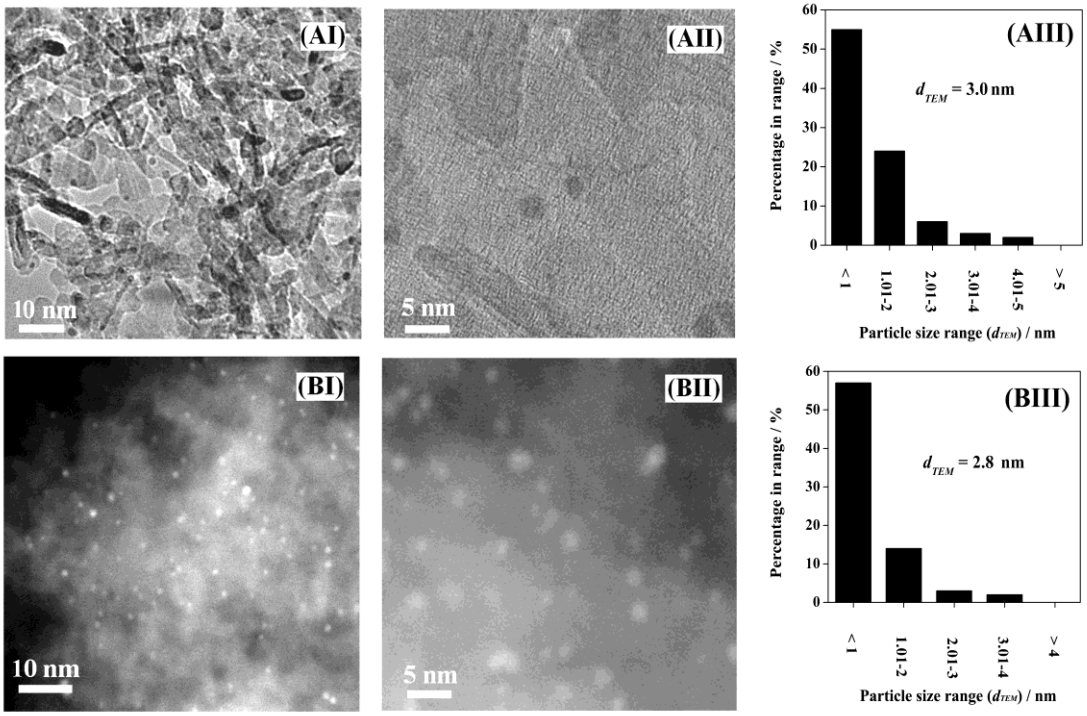

Figure 2. 2: Representative (I) medium and (II) higher magnification TEM and STEM images with associated (III) Pd particle size distributions for (A) Pd/Al_2O_3 and (B) Pd/C.

(**Figure 2.2(AIII)**) delivered a mean diameter (d_{TEM} = 3.0 nm) in good agreement with the value obtained from H_2 chemisorption (d_{H_2} = 2.4 nm). We should note that chemisorption titration measurements were conducted at H_2 partial pressure = 0.001 atm, circumventing any contribution due to hydride formation. Subsequent TPD generated the profile presented in **Figure 2.3(AI)** with H_2 release over 665-890 K. Hydrogen desorption far exceeded the amount chemisorbed (**Table 2.1**). This suggests the involvement of spillover hydrogen, *i.e*. migration of atomic hydrogen to the support following dissociation on Pd sites during TPR [29]. Alumina has been demonstrated to accommodate spillover through the action of surface hydroxyl groups [30]. The temperature related maximum H_2 release (T_{max} = 767 K) is consistent with publications demonstrating spillover desorption from alumina at $T \geq 503$ K [24,31].

There is some controversy regarding the predominant role of metal or support in nitrile hydrogenation particularly regarding condensation steps [4,21,22,32]. In order to decouple these effects, we examined bulk Pd (generated by reducing PdO) and a Pd+Al_2O_3 physical mixture, where the Pd content was equivalent to that in Pd/Al_2O_3. We should note that there was no detectable H_2 uptake or release on or from Al_2O_3, a response that is expected and in agreement with the literature [26]. The SSA recorded for Pd+Al_2O_3 (**Table 2.1**) is a composite with additive contributions from both components. TPR of PdO also generated a negative peak (**Figure 2.1(II)**) with a T_{max} (= 373 K) and associated hydride composition (H/Pd = 0.67) which differed from that measured for Pd/Al_2O_3 (T_{max} = 35 K; H/Pd = 0.05). This agrees with the reported shift in hydride decomposition to higher temperatures and increased H/Pd for larger Pd particles [26]. The appreciably lower (by a factor greater than 50) H_2 uptake on bulk Pd relative to Pd/Al_2O_3 can be related to the lower specific Pd surface area. While H_2 chemisorption was unchanged with Al_2O_3 addition, TPD from the physical mixture was measurably higher (2-fold) than that from Pd alone, suggesting the occurrence of spillover, as noted elsewhere [29]. Hydrogen spillover in catalyst+support physical combinations where the two components are well mixed [33] or present as discrete layers [34] has been demonstrated with a reported [35] spillover transport across non-contiguous surfaces. This effect was also observed for the Pd/Al_2O_3+Al_2O_3 mixture (see TPD profile in **Figure 2.3(AII)**) where H_2 released was (5 times) greater than that recorded for Pd/Al_2O_3 (**Table 2.1**).

Surface acidity was probed by NH_3 adsorption coupled with TPD; the TPD profiles for Al_2O_3 **(I)** and Pd/Al_2O_3 **(II)** are given in **Figure 2.3(B)**. The conventional

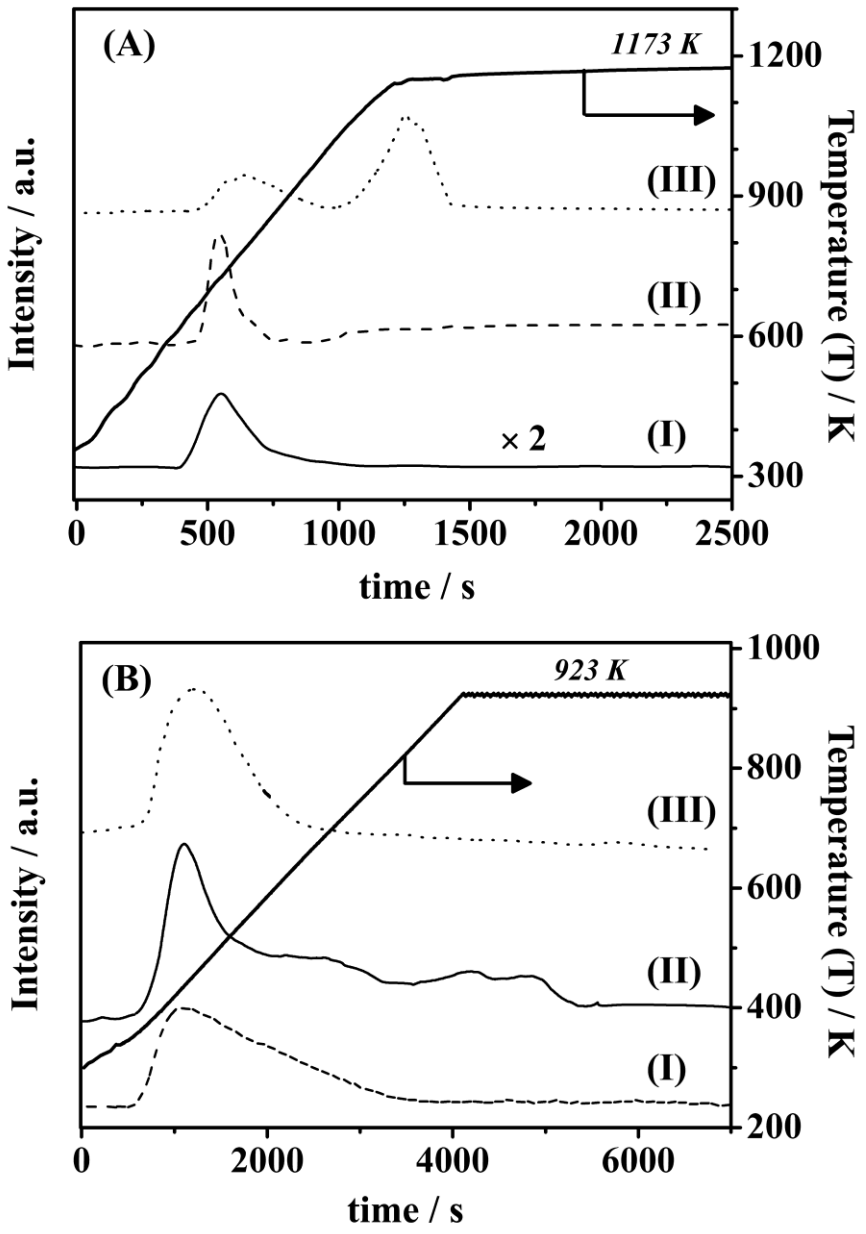

Figure 2. 3: (A) Hydrogen temperature-programmed desorption (TPD) profiles for (I) Pd/Al_2O_3 (solid line), (II) Pd/Al_2O_3+Al_2O_3 (dashed line) and (III) Pd/C (dotted line); (B) Ammonia TPD profiles for (I) Al_2O_3 (dashed line), (II) Pd/Al_2O_3 (solid line) and (III) Pd/C (dotted line).

approach (as documented in the literature) to quantifying acidity has been based solely on a measurement of NH_3 desorption [22,36,37]. This can, however, be subject to inaccuracy, notably as a result of contributions due to thermal degradation of surface functionalities, particularly dehydroxylation [38]. In this study, total acidity obtained from integration of the TPD signal matched NH_3 uptake measured in pulse chemisorption (**Table 2.1**). The reported acid site data for alumina show some disparity depending on sample pre-treatment and experimental desorption conditions, *e.g.* gas

flow and heating rates [39]. The NH_3 TPD profile for Al_2O_3 (**Figure 2.3(BI)**) is characterised by T_{max} = 450 K where the profile shape is similar to that recorded by Skotak *et al.* [40]. Surface acidity associated with Al_2O_3 is predominantly attributable to Lewis sites (Al^{3+}) [41,42] with a secondary -OH group contribution [42]. Profile generated for Pd/Al_2O_3 (**Figure 2.3(BII)**) exhibited a similar maximum (at 464 K) but the NH_3 adsorbed (and released) was measurably lower than Al_2O_3 (see **Table 2.1**). A similar effect has been reported previously [40] and explained on the basis of Pd interaction with surface acid sites, following Pd incorporation on Al_2O_3, that results in a decrease in total acidity. The NH_3 measurements recorded in this study for Pd/Al_2O_3 (0.51 ± 0.01 mmol g^{-1}, see **Table 2.1**) are very close (0.54 mmol g^{-1}) to that reported by Nam *et al.*[37].

2.3.1.2 Pd/C

In order to assess further the possible role of the metal carrier, Pd/C was examined where the SSA (870 $m^2\,g^{-1}$, **Table 2.1**) far exceeded that of Pd/Al_2O_3 and is typical of activated carbon supported metal catalysts [25]. The TPR profile of Pd/C (**Figure 2.1(III)**) exhibits a Pd hydride decomposition peak at 353 K with associated H/Pd = 0.04, close to that obtained for Pd/Al_2O_3 (H/Pd = 0.05) and suggesting an equivalent Pd size [26]. The STEM images (**Figure 2.2(BI)** and **2.2(BII)**) reveal near spherical Pd particles with a mean diameter (d_{TEM} = 2.8 nm) from the size distribution (**Figure 2.2(BIII)**) that agrees with the H_2 chemisorption (d_{H_2} = 2.2 nm, **Table 2.1**) measurement. We must stress the convergence of Pd loading (1.1 ± 0.1 wt-%), size distribution and mean (d_{TEM} = 2.9 ± 0.1 nm) for Pd/Al_2O_3 and Pd/C, which facilitates an explicit analysis of support effects. Hydrogen desorption from Pd/C was significantly greater (by a factor of over 30) than that chemisorbed (**Table 2.1**), again suggesting spillover contributions. The H_2 TPD profile for Pd/C **Figure 2.3(AIII)** shows two stages of H_2 desorption with associated T_{max} at 785 K and 1173 K and a greater total H_2 release (8-fold) relative to Pd/Al_2O_3. Differences in the amount of spillover hydrogen associated with the same metal (and size) on different carriers have been noted in the literature [43]. Spillover can be influenced by the concentration of initiating and acceptor sites and degree of contact between the participating phases [44]. We can link increased H_2 desorption from Pd/C to the greater SSA that can accommodate more spillover. Surface carboxylic and phenolic groups associated with carbonaceous materials can act as spillover acceptor sites [34]. A wide variation in acidity of carbon supported transition metal catalysts has been observed and is sensitive to carbon source and pre-treatment conditions [45,46].

The total acidity of Pd/C from NH_3 chemisorption matched the desorption measurement (0.93 ± 0.1 mmol g^{-1}) and exceeded that of Pd/Al_2O_3 (**Table 2.1**). The NH_3 TPD profile for Pd/C (**Figure 2.3(BIII)**) is characterised by a T_{max} = 480 K, equivalent to that (473-483 K) reported elsewhere for carbon supported systems [45] and ascribed to the presence of weak acid sites [47,48].

2.3.2 Gas Phase Hydrogenation of Butyronitrile

Reaction pathways in butyronitrile hydrogenation that have been reported in the literature [3,49] are presented in **Figure 2.4**. Nitrile reduction generates a reactive aldimine (butylidenimine, BI) intermediate that is hydrogenated to the primary amine (butylamine, BA, step **(I)**). Butylamine can undergo condensation with the imine in the presence of hydrogen, releasing ammonia to generate a secondary amine (dibutylamine, DBA, step **(II)**) which, in turn, can be transformed into a tertiary amine (tributylamine, TBA, step **(III)**). The reactivity of butylidenimine, in terms of hydrogenation or condensation, governs product selectivity. Fractional butyronitrile conversion (X_{BT}) over

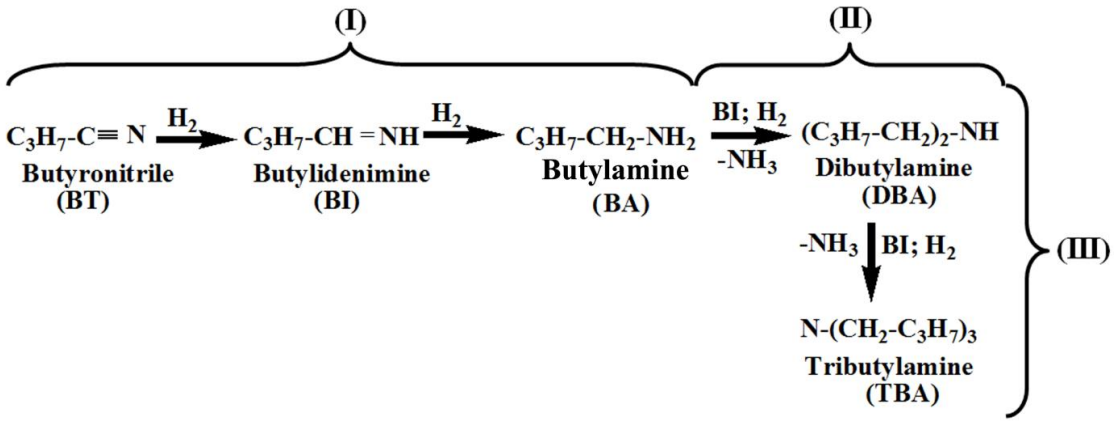

Figure 2. 4: Reaction pathways for the hydrogenation of butyronitrile (BT) to (I) primary (butylamine, BA), (II) secondary (dibutylamine, DBA) and (III) tertiary (tributylamine, TBA) amine products.

Pd/Al_2O_3 was time invariant and representative time on-stream plots are shown in **Figure 2.5(A)**. This response is significant given that (liquid and gas phase) hydrogenation of nitriles over supported Pt [6,50], Ru [6] and Ni [14,16,22] was accompanied by catalyst deactivation and a temporal decline in activity. This was attributed to: (i) agglomeration of metal particles during reaction [6,15]; (ii) occlusion of active sites by the amine product(s) [6,12,15]; (iii) catalyst coking due to the formation of dehydrogenated surface species and carbides [14,22]. These deleterious

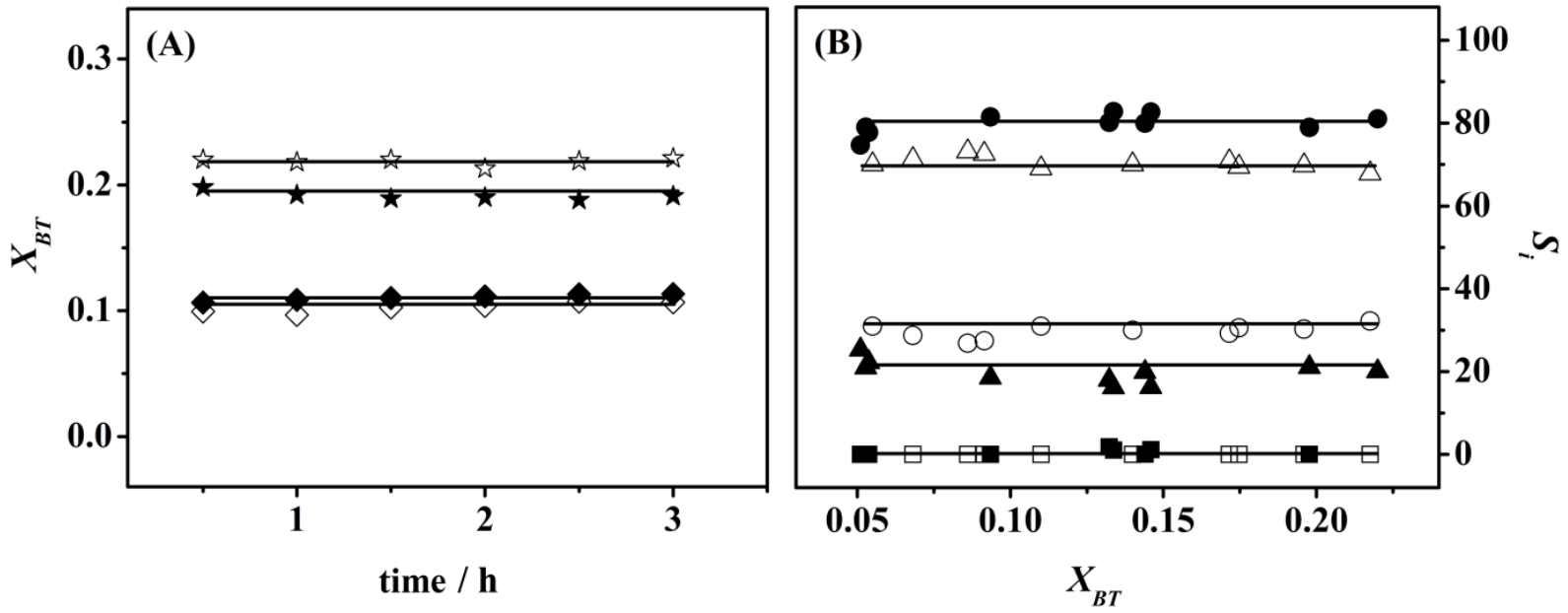

Figure 2. 5: (A) Temporal dependence of butyronitrile fractional conversion (X_{BT}) at varying n/F (0.8×10^{-3} h, ◆; 1.3×10^{-3} h,★; 0.4×10^{-3} h,◇; 0.8×10^{-3} h, ☆) and (B) Selectivity (S_i, %) to butylamine (BA, ■, □), dibutylamine (DBA, ●, ○) and tributylamine (TBA, ▲, △) as a function of X_{BT} for reaction over Pd/Al_2O_3 (solid symbols) and Pd/C (open symbols). *Reaction conditions*: T = 473 K, P = 1 atm.

effects do not appear to apply in our system. Selectivity as a function of conversion over Pd/Al_2O_3 is shown in **Figure 2.5(B)**. The secondary amine was the principal product with tributylamine as by-product and negligible butylamine formation (S_{BA} < 2%); selectivity was independent of conversion. The results suggest that once formed, butylamine participates in a condensation step with the aldimine to generate dibutylamine as the main product. The secondary amine that is produced undergoes further reaction with butylidenimine to give the tertiary amine but this step was not promoted to the same extent. Our findings are in line with the work of Huang and Sachtler [4] who reported the formation of secondary amine as the main reaction product in the conversion of butyronitrile over Pd/NaY in both liquid and gas phase operation. We should, however, note that Iwasa and co-workers [11] have reported preferential tertiary amine formation in gas phase acetonitrile hydrogenation over Pd/Al_2O_3.

An unambiguous correlation of metal and support in governing nitrile hydrogenation selectivity has yet to be established. It has been proposed that support acidity can affect product distribution [16,19,22] and Lewis and Brønsted acid sites on alumina are known to contribute to condensation reactions [19,49]. Weak adsorption of butyronitrile on Al_2O_3 with surface coordination through the nitrogen (of the -C≡N group) has been demonstrated by infrared spectroscopy [51]. Hegedűs and Máthé [52]

Table 2. 2: Butyronitrile consumption rate and product (butylamine (BA), dibutylamine (DBA) and tributylamine (TBA) selectivity (S_i) for reaction over bulk and supported Pd at an equal fractional conversion (X_{BT} = 0.15); *Reaction conditions*: T = 473 K, P = 1 atm.

Catalyst	Rate/ mol $h^{-1}mol_{Pd}^{-1}$	S_i / %		
		BA	DBA	TBA
Pd/Al_2O_3	110	0	84	16
Al_2O_3	-	-	-	-
Pd	1.7	55	45	0
$Pd+Al_2O_3$	2.5	43	52	5
$Pd/Al_2O_3+Al_2O_3$	112	0	82	18
Pd/C	183	0	30	70

proposed that the Pd phase determines selectivity while the alumina carrier only influences activity. In order to decouple these contributions, we conducted the reaction over Al_2O_3 and bulk Pd. There was no detectable conversion using the alumina support alone, which can be ascribed to the inability of Al_2O_3 to dissociate H_2 [26] and generate the reactive intermediate. The nitrile consumption rate over bulk Pd was appreciably lower (by a factor of 65) than Pd/Al_2O_3 (**Table 2.2**), which can be attributed to lower H_2 uptake/release (**Table 2.1**). Comparison of selectivity is only meaningful at a common conversion and the selectivity data presented in **Table 2.2** were obtained at X_{BT} = 0.15. Bulk Pd generated near equivalent butylamine and dibutylamine with no detectable tertiary amine formation. This suggests that the condensation reaction to generate secondary (but not tertiary) amine can proceed over Pd sites without the involvement of the support. Drawing on the pathway in **Figure 2.4**, the nitrile can be activated on bulk Pd, react with the available surface hydrogen to form imine with further hydrogenation to butylamine and condensation to dibutylamine. In contrast to Pd/Al_2O_3, the secondary amine formed on bulk Pd must desorb without further reaction. Enhanced selectivity to dibutylamine (and formation of tributylamine) exhibited by Pd/Al_2O_3 suggests a contribution due to the support and/or metal/support interface to promote condensation. Gluhoi *et al.* [19] have proposed that the metal-support interface is critical in nitrile hydrogenation. To develop this further, the reaction was conducted over a $Pd+Al_2O_3$ physical mixture, which delivered a measurably higher reaction rate than Pd alone (**Table 2.2**). The H_2 TPD results presented in **Table 2.1** establish the occurrence of spillover hydrogen on Al_2O_3 in the mixture which can account for the increased rate. Moreover, selectivity to dibutylamine was enhanced with the isolation of tributylamine in the product stream. This suggests a direct contribution of Al_2O_3 to primary (and secondary) amine condensation, where activated nitrile reacts with spillover hydrogen generated by Pd. Any contribution due to hydrogen spillover in $Pd/Al_2O_3+Al_2O_3$ was negligible and reaction rate/product distribution was essentially the same as that obtained with Pd/Al_2O_3 (**Table 2.2**). The intrinsic activity of Pd/Al_2O_3 is such that spillover due to addition of Al_2O_3 (**Table 2.1**) did not influence performance.

Pd/C delivered a significantly higher nitrile consumption rate than Pd/Al_2O_3 (**Table 2.2**), which can be linked to greater available surface reactive hydrogen (**Table 2.1**), given the equivalency of Pd particle size in both catalysts. Structure sensitivity has been proposed for gas phase nitrile hydrogenation over supported Ni [14,15] and Pt [50] with higher specific activity for larger metal particles in the 10-18 nm range. The basic character of butyronitrile (electron lone pair on nitrogen in -C≡N) must be considered in

possible nitrile interaction(s) with the support [49,51]. The greater surface acidity exhibited by Pd/C favours nitrile/amine activation and can contribute to higher reaction rate. This is consistent with the literature that has linked activity to support acidity [16,52]. Catalyst stability with time on-stream also applies to Pd/C (**Figure 2.5(A)**) where selectivity was independent of conversion (**Figure 2.5(B)**) with tributylamine as predominant product, dibutylamine as by-product and no detectable butylamine. This deviates from the selectivity response for Pd/Al_2O_3 and enhanced tertiary amine selectivity over Pd/C can be ascribed to greater surface acidity that promotes condensation [19,49]. Chen *et al.* [2] reported increased conversion of lauronitrile over more acidic catalysts (Ni/SiO_2, Ni/Al_2O_3 Ni/SiAlO) with low selectivity to the primary amine. Moreover, given the decreasing amine basicity, in the order tributylamine > dibutylamine > butylamine [53], increased surface acidity enhances amine interaction, facilitating sequential reaction (butylamine → dibutylamine → tributylamine, see **Figure 2.4**) leading to predominant tertiary amine formation.

2.4 Conclusions

This work has set out to decouple the role of metal (Pd) and support in nitrile hydrogenation. In solvent-free continuous gas phase butyronitrile hydrogenation over Pd/C and Pd/Al_2O_3 with equivalent mean Pd size (2.9 ± 0.1 nm), Pd/C exhibited appreciably higher activity that can be attributed to increased surface hydrogen (from H_2 TPD) coupled with greater surface acidity (from NH_3 chemisorption/TPD). Nitrile conversion over both catalysts was constant with time on-stream. Reaction over bulk Pd generated primary and secondary amines, indicating that condensation can proceed over Pd without support. Alumina alone was inactive but in combination with Pd (physical mixture) an increase in activity (relative to Pd) was observed and attributed to the involvement of spillover hydrogen. Addition of Al_2O_3 to bulk Pd shifted reaction to higher amines, demonstrating direct contribution of Al_2O_3 to condensation. Pd/Al_2O_3 and Pd/C generated distinct product distributions with secondary amine as principal product over Pd/Al_2O_3 and preferential tertiary amine formation over Pd/C; product selectivity was independent of conversion. The greater surface acidity of Pd/C facilitates surface interaction(s) with butylamine and dibutylamine, promoting sequential reaction with the butylidenimine intermediate, favouring tertiary amine formation.

2.5 References

[1] S. Gomez, J.A. Peters, T. Maschmeyer, *The reductive amination of aldehydes and ketones and the hydrogenation of nitriles: Mechanistic aspects and selectivity control*, Adv. Synth. Catal. 344 (**2002**) 1037.

[2] H. Chen, M. Xue, S. Hu, J. Shen, *The effect of surface acidic and basic properties on the hydrogenation of lauronitrile over the supported nickel catalysts*, Chem. Eng. J. 181–182 (**2012**) 677.

[3] Y. Huang, W.M.H. Sachtler, *On the mechanism of catalytic hydrogenation of nitriles to amines over supported metal catalysts*, Appl. Catal. A: Gen. 182 (**1999**) 365.

[4] Y. Huang, W.M.H. Sachtler, *Catalytic hydrogenation of nitriles over supported mono- and bimetallic catalysts*, J. Catal. 188 (**1999**) 215.

[5] P. Schärringer, T.E. Müller, J.A. Lercher, *Investigations into the mechanism of the liquid-phase hydrogenation of nitriles over raney-Co catalysts*, J. Catal. 253 (**2008**) 167.

[6] Y. Huang, V. Adeeva, W.M.H. Sachtler, *Stability of supported transition metal catalysts in the hydrogenation of nitriles*, Appl. Catal. A: Gen. 196 (**2000**) 73.

[7] L. Hegedűs, T. Máthé, T. Kárpáti, *Selective heterogeneous catalytic hydrogenation of nitriles to primary amines in liquid phase: Part II: Hydrogenation of benzyl cyanide over palladium*, Appl. Catal. A: Gen. 349 (**2008**) 40.

[8] A. Chojecki, M. Veprek-Heijman, T.E. Müller, P. Schärringer, S. Veprek, J.A. Lercher, *Tailoring raney-catalysts for the selective hydrogenation of butyronitrile to n-butylamine*, J. Catal. 245 (**2007**) 237.

[9] C. Jiménez-González, P. Poechlauer, Q.B. Broxterman, B.-S. Yang, D. am_Ende, J. Baird, C. Bertsch, R.E. Hannah, P. Dell'Orco, H. Noorrnan, S. Yee, R. Reintjens, A. Wells, V. Massonneau, J. Manley, *Key green engineering research areas for sustainable manufacturing: A perspective from pharmaceutical and fine chemicals manufacturers*, Org. Proc. Res. Dev. 15 (**2011**) 900.

[10] D.J. Segobia, A.F. Trasarti, C.R. Apesteguía, *Hydrogenation of nitriles to primary amines on metal-supported catalysts: Highly selective conversion of butyronitrile to n-butylamine*, Appl. Catal. A: Gen. 445-446 (**2012**) 69.

[11] N. Iwasa, M. Yoshikawa, M. Arai, *Selective hydrogenation of acetonitrile to ethylamine using palladium-based alloy catalysts*, Phys. Chem. Chem. Phys. 4 (**2002**) 5414.

[12] M.C. Carrión, B.R. Manzano, F.A. Jalón, I. Fuentes-Perujo, P. Maireles-Torres, E. Rodríguez-Castellón, A. Jiménez-López, *Gas-phase hydrogenation of acetonitrile over Pt and Pt–Pd supported on mesoporous solids: Influence of the metallic precursor*, Appl. Catal. A: Gen. 288 (**2005**) 34.

[13] J. Krupka, J. Drahonsky, A. Hlavackova, *Aminocarbene mechanism of the formation of a tertiary amine in nitrile hydrogenation on a palladium catalyst*, React. Kinet. Mech. Cat. 108 (**2013**) 91.

[14] A. Nieto-Márquez, D. Toledano, J.C. Lazo, A. Romero, J.L. Valverde, *Carbon nanospheres as novel support in the nickel catalyzed gas phase hydrogenation of butyronitrile*, Appl. Catal. A Gen. 373 (**2010**) 192.

[15] A. Nieto-Márquez, D. Toledano, P. Sánchez, A. Romero, J.L. Valverde, *Impact of nitrogen doping of carbon nanospheres on the nickel-catalyzed hydrogenation of butyronitrile*, J. Catal. 269 (**2010**) 242.

[16] A. Nieto-Márquez, V. Jiménez, A.M. Raboso, S. Gil, A. Romero, J.L. Valverde, *Influence of the chemical activation of carbon nanofibers on their use as catalyst support*, Appl. Catal. A Gen. 393 (**2011**) 78.

[17] X.-F. Guo, Y.-S. Kim, G.-J. Kim, *Hydrogenation of chiral nitrile on highly ordered mesoporous carbon-supported pd catalysts*, Catal. Today 150 (**2010**) 22.

[18] S. Santiago-Pedro, V. Tamayo-Galván, T. Viveros-García, *Effect of the acid–base properties of the support on the performance of Pt catalysts in the partial hydrogenation of citral*, Catal. Today 213 (**2013**) 101.

[19] A.C. Gluhoi, P. Mărginean, U. Stănescu, *Effect of supports on the activity of nickel catalysts in acetonitrile hydrogenation*, Appl. Catal. A: Gen. 294 (**2005**) 208.

[20] M.J.F.M. Verhaak, A.J. van_Dillen, J.W. Geus, *The selective hydrogenation of acetonitrile on supported nickel catalysts*, Catal. Lett. 26 (**1994**) 37.

[21] P. Braos-García, P. Maireles-Torres, E. Rodríguez-Castellón, A. Jiménez-López, *Gas-phase hydrogenation of acetonitrile over nickel supported on alumina- and mixed alumina/gallium oxide-pillared tin phosphate catalysts*, J. Mol. Catal. A: Chem. 168 (**2001**) 279.

[22] P. Braos-García, P. Maireles-Torres, E. Rodríguez-Castellón, A. Jiménez-López, *Gas-phase hydrogenation of acetonitrile on zirconium-doped mesoporous silica-supported nickel catalysts*, J. Mol. Catal. A: Chem. 193 (**2003**) 185.

[23] C.V. Rode, M. Arai, M. Shirai, Y. Nishiyama, *Gas-phase hydrogenation of nitriles by nickel on various supports*, Appl. Catal. A Gen. 148 (**1997**) 405.

[24] C. Amorim, X. Wang, M.A. Keane, *Application of hydrodechlorination in environmental pollution control: Comparison of the performance of supported and unsupported pd and Ni catalysts*, Chin. J. Catal. 32 (**2011**) 746.

[25] C. Amorim, M.A. Keane, *Palladium supported on structured and nonstructured carbon: A consideration of pd particle size and the nature of reactive hydrogen*, J. Colloid Interf. Sci. 322 (**2008**) 196.

[26] S. Gómez-Quero, F. Cárdenas-Lizana, M.A. Keane, *Effect of metal dispersion on the liquid phase hydrodechlorination of 2,4-dichlorophenol over Pd/Al_2O_3*, Ind. Eng. Chem. Res. 47 (**2008**) 6841.

[27] C. Shi, B.W.-L. Jang, *Nonthermal RF plasma modifications on Pd/γ-Al_2O_3 for selective hydrogenation of acetylene in the presence of ethylene*, Ind. Eng. Chem. Res. 45 (**2006**) 5879.

[28] G. Prelazzi, M. Cerboni, G. Leofanti, *Comparison of H_2 adsorption, O_2 adsorption, H_2 titration, and O_2 titration on supported palladium catalysts*, J. Catal. 181 (**1999**) 73.

[29] C. Amorim, M.A. Keane, *Catalytic hydrodechlorination of chloroaromatic gas streams promoted by Pd and Ni: The role of hydrogen spillover*, J. Hazard. Mater. 211–212 (**2012**) 208.

[30] J.T. Miller, B.L. Meyers, F.S. Modica, G.S. Lane, M. Vaarkamp, D.C. Koningsberger, *Hydrogen temperature-programmed desorption (H_2 TPD) of supported platinum catalysts*, J. Catal. 143 (**1993**) 395.

[31] B. Lin, R. Wang, X. Yu, J. Lin, F. Xie, K. Wei, *Physicochemical characterization and H_2-TPD study of alumina supported ruthenium catalysts*, Catal. Lett. 124 (**2008**) 178.

[32] A. Infantes-Molina, J. Mérida-Robles, P. Braos-García, E. Rodríguez-Castellón, E. Finocchio, G. Busca, P. Maireles-Torres, A. Jiménez-López, *Nickel supported on porous silica as catalysts for the gas-phase hydrogenation of acetonitrile*, J. Catal. 225 (**2004**) 479.

[33] A.D. Lueking, R.T. Yang, *Hydrogen spillover to enhance hydrogen storage—study of the effect of carbon physicochemical properties*, Appl. Catal. A: Gen. 265 (**2004**) 259.

[34] W.C. Conner, J.L. Falconer, *Spillover in heterogeneous catalysis*, Chem. Rev. 95 (**1995**) 759.

[35] P. Baeza, M.S. Ureta-Zañartu, N. Escalona, J. Ojeda, F.J. Gil-Llambías, B. Delmon, *Migration of surface species on supports: A proof of their role on the synergism between CoS_x or NiS_x and MoS_2 in HDS*, Appl. Catal. A: Gen. 274 (**2004**) 303.

[36] M. Turco, G. Bagnasco, C. Cammarano, P. Senese, U. Costantino, M. Sisani, *$Cu/ZnO/Al_2O_3$ catalysts for oxidative steam reforming of methanol: The role of Cu and the dispersing oxide matrix*, Appl. Catal. B: Environ. 77 (**2007**) 46.

[37] I. Nam, K.M. Cho, J.G. Seo, S. Hwang, K.-W. Jun, I.K. Song, *Production of middle distillate from synthesis gas in a dual-bed reactor through hydrocracking of wax over mesoporous Pd-Al_2O_3 composite catalyst*, Catal. Lett. 130 (**2009**) 192.

[38] L. Rodríguez-González, F. Hermes, M. Bertmer, E. Rodríguez-Castellón, A. Jiménez-López, U. Simon, *The acid properties of H-ZSM-5 as studied by NH_3-TPD and ^{27}Al-MAS-NMR spectroscopy*, Appl. Catal. A: Gen. 328 (**2007**) 174.

[39] M. Moreno-Bravo, M. Hernández-Luna, J. Alcaraz-Cienfuegos, A. Rosas-Aburto, *Fluorinated alumina for benzene propylation: Reaction scheme and heterogeneity of the acid surface*, Appl. Catal. A: Gen. 249 (**2003**) 35.

[40] M. Skotak, D. Łomot, Z. Karpiński, *Catalytic conversion of C_6-alkanes over Pd/Al_2O_3 catalysts: The effect of support acidity*, Appl. Catal. A: Gen. 229 (**2002**) 103.

[41] P.J. Chupas, C.P. Grey, *Surface modification of fluorinated aluminas: Application of solid state NMR spectroscopy to the study of acidity and surface structure*, J. Catal. 224 (**2004**) 69.

[42] C. Morterra, G. Magnacca, *A case study: Surface chemistry and surface structure of catalytic aluminas, as studied by vibrational spectroscopy of adsorbed species*, Catal. Today 27 (**1996**) 497.

[43] S.T. Srinivas, P.K. Rao, *Direct observation of hydrogen spillover on carbon-supported platinum and its influence on the hydrogenation of benzene*, J. Catal. 148 (**1994**) 470.

[44] G.L. Xu, K.Y. Shi, Y. Gao, H.Y. Xu, Y.D. Wei, *Studies of reforming natural gas with carbon dioxide to produce synthesis gas: X. The role of CeO_2 and MgO promoters*, J. Mol. Catal. A: Chem. 147 (**1999**) 47.

[45] X. Tan, W. Deng, M. Liu, Q. Zhang, Y. Wang, *Carbon nanotube-supported gold nanoparticles as efficient catalysts for selective oxidation of cellobiose into gluconic acid in aqueous medium*, Chem. Commun. (**2009,**) 7179.

[46] W. Deng, X. Tan, W. Fang, Q. Zhang, Y. Wang, *Conversion of cellulose into sorbitol over carbon nanotube-supported ruthenium catalyst*, Catal. Lett. 133 (**2009**) 167.

[47] C. Fang, D. Zhang, L. Shi, R. Gao, H. Li, L. Ye, J. Zhang, *Highly dispersed CeO_2 on carbon nanotubes for selective catalytic reduction of NO with NH_3*, Catal. Sci. Technol. 3 (**2013**) 803.

[48] D. Zhang, L. Zhang, L. Shi, C. Fang, H. Li, R. Gao, L. Huang, J. Zhang, *In situ supported MnO_x-CeO_x on carbon nanotubes for the low-temperature selective catalytic reduction of no with NH_3*, Nanoscale 5 (**2013**) 1127.

[49] I. Ortiz-Hernandez, C.T. Williams, *In situ studies of butyronitrile adsorption and hydrogenation on Pt/Al_2O_3 using attenuated total reflection infrared spectroscopy*, Langmuir 23 (**2007**) 3172.

[50] M. Arai, Y. Takada, Y. Nishiyama, *Effects of metal particle size in gas-phase hydrogenation of acetonitrile over silica-supported platinum catalysts*, J. Phys. Chem. B 102 (**1998**) 1968.

[51] M.R. Strunk, C.T. Williams, *Aliphatic nitrile adsorption on Al_2O_3 and ZrO_2 as studied by total internal reflection sum-frequency spectroscopy*, Langmuir 19 (**2003**) 9210.

[52] L. Hegedűs, T. Máthé, *Selective heterogeneous catalytic hydrogenation of nitriles to primary amines in liquid phase: Part I. Hydrogenation of benzonitrile over palladium*, Appl. Catal. A: Gen. 296 (**2005**) 209.

[53] N.L. Allinger, M.P. Cava, D.C. De Jongh, C.R. Johnson, N.A. Lebel, C.L. Stevens, *Organic chemistry*, Worth Publishers, New York, 1974.

Chapter 3

Production of Butylamine in the Gas Phase Hydrogenation of Butyronitrile over Pd/SiO_2 and $Ba\text{-}Pd/SiO_2$

In the previous Chapter, the predominant formation of tertiary (tributyl-) amine was established for reaction over Pd/C and linked to the increase surface acidity where spillover hydrogen served to elevate hydrogenation rate. In this Chapter, acidity is modified by incorporating Ba with Pd and the consequent effects in butyronitrile hydrogenation are assessed.

3.1 Introduction

Primary aliphatic amines are widely used in the textile, pharmaceutical, fine chemical and agrochemical sectors [1]. Industrial amine production is based on nitrile hydrogenation where reaction selectivity to the primary amine, circumventing secondary and even tertiary amine formation, is challenging [1,2]. Taking the hydrogenation of butyronitrile (**Figure 3.1**), partial reduction (step (I)) generates an imine (butylidenimine) as reactive intermediate that is converted (step (II)) to the target butylamine. The latter can participate in a condensation (step (III)) with the imine and reduction (step (IV)) to produce the secondary amine (dibutylamine) with NH_3 elimination. Additional condensation of dibutylamine and imine (step (V)) and subsequent hydrogenation (step (VI)) generate the tertiary amine (tributylamine) [3]. Nitrile hydrogenation has been predominantly conducted in batch liquid phase at elevated H_2 pressures (20-45 bar) [4-8]. A range of supported transition metal (Ru [5,9], Ni [4,10-12], Co [8,13], Rh [5], Cu [6], Pd [5,14] and Pt [5,14]) catalysts has been used, where Ni, Co and Ru favoured primary amine formation, Rh and Cu facilitated generation of secondary amine, Pt and Pd promoted a mixture of both amines [2]. There is evidence that catalytic activity can also be influenced by the nature of the metal where Segobia *et al*. [15], studying the liquid phase hydrogenation of butyronitrile (T = 343 K, P_{H_2} = 25 bar) over a series of SiO_2 supported metals, established the following decreasing activity sequence: Ni > Co > Pt > Ru > Cu > Pd. A move from batch to continuous processes has been highlighted by the fine chemical/pharmaceutical sector as a priority to reduce downtime and increase throughput [16]. Supported Ni catalysts have been applied in gas phase operation but low selectivity to the target primary amine

and loss of activity with time on stream are decided drawbacks [10,11,17-20]. Use of Pd/ZnO delivered high selectivity (99%) to ethylamine but low activity (conversions <6%) in acetonitrile conversion where alloy (PdZn) formation served to inhibit condensation to higher amines [21].

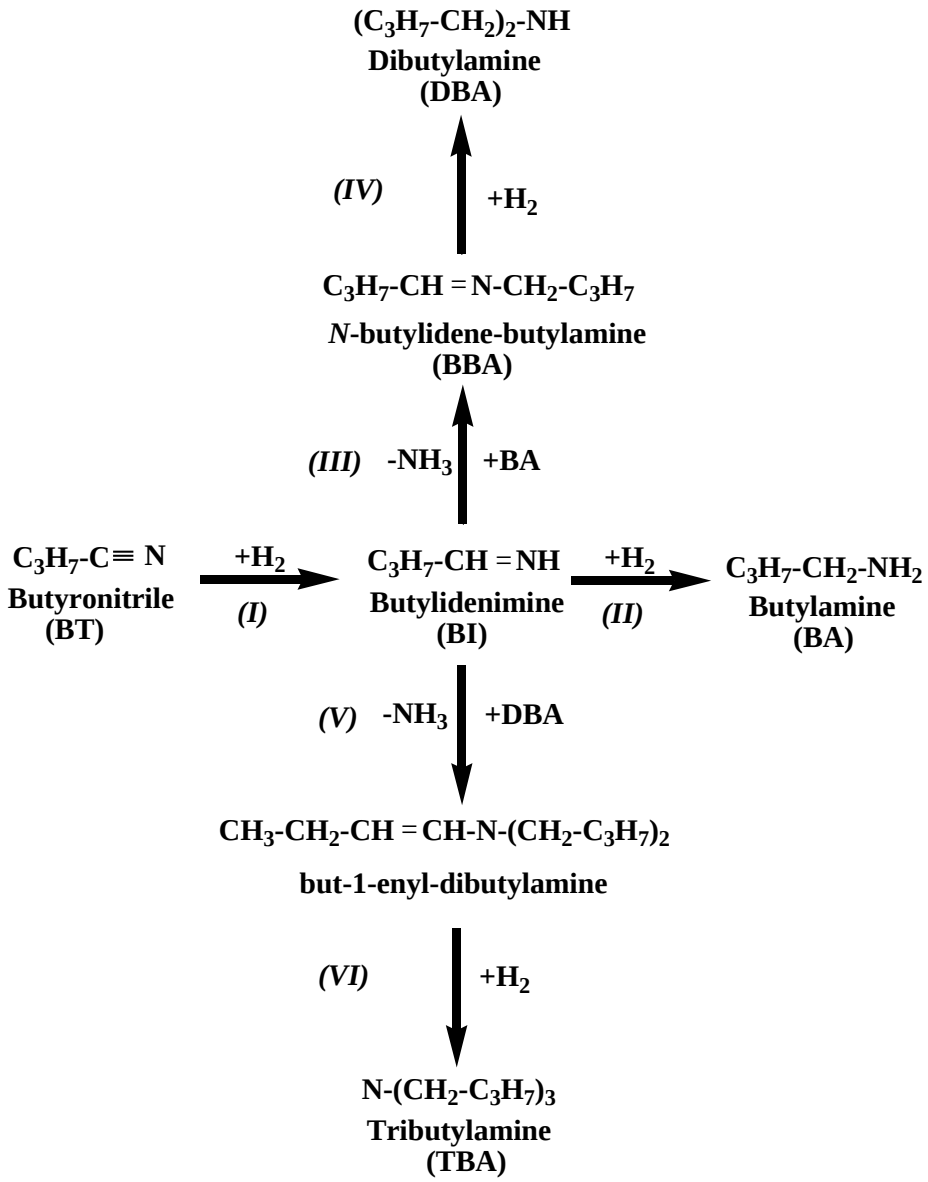

Figure 3. 1: Reaction scheme for the hydrogenation of butyronitrile.

Selectivity in nitrile reduction is affected by acid-base properties of the support and the electronic character of the metal site which, in turn, is influenced by the use of additives and/or promoters. The incorporation of ammonia provides a basic reaction medium that inhibits acid-catalysed condensation (**Figure 3.1**, steps (III) and (V)) [2]. As a corollary, support acidity is critical in terms of amine/imine surface interaction leading to higher amine production [4,19,22]. An increase in carrier basicity (by

nitrogen doping [10] and LiOH treatment [13]) has been established as a means of increasing primary amine selectivity over Ni [10] and Co [13] catalysts in the hydrogenation of butyronitrile. Modifications to the electron density of supported metal nano-particles can also influence product distribution where Branco *et al.* [23] demonstrated higher *n*-propylamine selectivity over copper-lanthanide intermetallic compounds ($LnCu_2$, Ln = La, Ce, Pr, Nd) that was ascribed to charge transfer (from the lanthanide) to Cu which inhibited condensation.

Supported nano-scale Pd is effective in dissociative adsorption of H_2 [24] and has been widely adopted in catalytic hydrogenation [25,26]. Nevertheless, application in nitrile conversion is limited due to undesired formation of secondary/tertiary amines and low activity [2,7,14,15]. In previous work, we reported a Pd-alkaline earth metal synergy that resulted in increased surface hydrogen with a consequent elevated hydrogenation rate [27]. Moreover, Ba→Pd electron donation in Pd-Ba/Al_2O_3 was demonstrated [27]. In this study, we explored the promoting effect of Ba in Pd/SiO_2 as an approach to enhanced butylamine production in gas phase butyronitrile hydrogenation.

3.2 Experimental

3.2.1 Catalyst Preparation, Activation and Characterisation

A 5% w/w Pd/SiO_2 was prepared by impregnation of fumed SiO_2 (Aldrich) with $Pd(OAc)_2$ in dimethylformamide (DMF). The DMF was removed from the impregnated sample under vacuum over 12 h at ambient temperature. The Ba-Pd complex $\{(DMF)_xBaPd(CN)_4\}_\infty$ bimetallic precursor was prepared as described elsewhere [28]. The SiO_2 support was added to a solution of the precursor in DMF to deliver a 5% w/w Pd loading (Pd/Ba = 1 mol mol^{-1}). Both samples were sieved (ATM fine test sieves) into batches of 75 μm mean particle diameter. The samples were activated by reduction in flowing (60 cm^3 min^{-1}) dry H_2 (99.99%, BOC) at 10 K min^{-1} to 573 K for 30 min, flushed in He, cooled to ambient temperature and passivated in 1% v/v O_2/He for *ex situ* analysis.

Metal loading was determined by inductively coupled plasma-optical emission spectrometry (ICP-OES, Vista-PRO, Varian Inc.) from the diluted extract of aqua regia (25% v/v HNO_3/HCl). Nitrogen adsorption/desorption, temperature programmed reduction (TPR), H_2 (and NH_3) chemisorption and temperature programmed desorption (TPD) were performed using the commercial CHEM-BET 3000 (Quantachrome) unit. The samples (0.05-0.1 g) were loaded in a U-shaped Quartz cell (3.76 mm *i. d.*),

outgassed for 30 min and the total specific surface area (SSA) recorded in a 30% v/v N_2/He flow where undiluted N_2 (99.9%) served as internal standard. At least two cycles of N_2 adsorption-desorption were employed using the standard single point BET method. TPR analysis was conducted by heating the sample in 17 cm^3 min^{-1} (Brooks mass flow controlled) 5% v/v H_2/N_2 at 10 K min^{-1} to 573 ± 1 K. The effluent gas passed through a liquid N_2 trap and changes in H_2 consumption were monitored by a thermal conductivity detector (TCD) with data acquisition/manipulation using the TPR Win™ software. The reduced sample was maintained at 573 K in H_2/N_2 until the signal returned to baseline, swept with 65 cm^3 min^{-1} N_2 for 1.5 h, cooled to ambient temperature and subjected to H_2 (or NH_3) chemisorption using a pulse (50-1000 µl) titration procedure. Any possible contribution due to Pd hydride formation can be discounted as the H_2 partial pressure (<2 Torr) in the sample cell was well below that (>11 Torr) required to generate the hydride [29]. Samples were thoroughly flushed in N_2 (65 cm^3 min^{-1}) to remove weakly bound H_2 (or NH_3) and subjected to TPD (at 10-50 K min^{-1}) to 1000-1273 K with a final isothermal hold until the signal returned to baseline. Powder X-ray diffraction (XRD) analyses were conducted on a Bruker/Siemens D500 incident X-ray diffractometer using Cu Kα radiation; samples were scanned at 0.02º $step^{-1}$ over the range $20º \leq 2\theta \leq 90º$. Diffractograms were identified using the JCPDS-ICDD Pd reference (46-1043). Palladium particle size was obtained from the Scherrer equation [30],

$$d_c = \frac{K\lambda}{\beta \cos\theta} \qquad \textbf{(3.1)}$$

Where d_c is the mean size of the ordered (crystalline) domains, K is a dimensionless shape factor (0.9), λ the X-ray wavelength (1.5056 Å), β line broadening at half the maximum intensity and θ the Bragg angle (2θ = 40.1º). Palladium particle morphology (size and shape) was determined by transmission electron microscopy analysis, conducted using a JEOL-2000 TEM/STEM microscope equipped with a UTW energy dispersive x-ray (EDX) detector (Oxford Instruments) and operated at an accelerating voltage of 200 kV. The samples were prepared by ultrasonic dispersion in 2-butanol, evaporating a drop of the resultant suspension onto a holey carbon/Cu grid (300 Mesh). Up to 800 individual particles were counted for each catalyst and the mean metal diameter (d_{TEM}) calculated from

$$d_{TEM} = \frac{\sum_i n_i d_i}{\sum_i n_i} \qquad \textbf{(3.2)}$$

where n_i is the number of particles of diameter d_i.

3.2.2 Hydrogenation of Butyronitrile

3.2.2.1 Catalytic System

The hydrogenation of butyronitrile (Sigma-Aldrich, ≥99%) was conducted *in situ*, immediately following catalyst activation at 1 atm and 473-563 K in a fixed bed vertical glass reactor (*i. d.* = 15 mm). Reactions were conducted under operating conditions that ensured negligible internal or external mass and heat transfer limitations. The nitrile reactant was delivered at a fixed calibrated flow rate (0.6 $cm^3\ h^{-1}$) *via* a glass/teflon air-tight syringe and teflon line using a microprocessor controlled infusion pump (Model 100 kd Scientific). A layer of borosilicate glass beads served as preheating zone, ensuring that the reactant was vaporised and reached reaction temperature before contacting the catalyst. Isothermal conditions (±1 K) were maintained by diluting the catalyst bed with ground glass (75 μm); the ground glass was mixed thoroughly with the catalyst before insertion in the reactor. The reaction temperature was continuously monitored using a thermocouple inserted in a thermowell within the catalyst bed. A co-current flow of butyronitrile and H_2 (<1% v/v nitrile in H_2) was maintained at *GHSV* = $1.0 \times 10^4\ h^{-1}$. The inlet nitrile flow (*F*) was constant at 6.9 mmol h^{-1} where the H_2 content was in excess (by a factor of 12 relative to the stoichiometric requirement for butylamine formation) and the gas flow rate was monitored using a Humonics (Model 520) digital flowmeter. The molar palladium (*n*) to *F* ratio spanned the range 3.4×10^{-4} – 3.4×10^{-3} h. All the reactant and proposed hydrogenation products (butylamine, dibutylamine and tributylamine) are in gas phase at this reaction condition according to the analysis in **Appendix 1**. The reactor effluent was frozen in a liquid nitrogen trap for subsequent analysis, which was made using a Perkin-Elmer Auto System XL chromatograph equipped with a programmed split/splitless injector and a flame ionisation detector, employing a DB-1 capillary column (*i. d.* = 0.33 mm, length = 50 m, film thickness = 0.20 μm). Data acquisition and manipulation were performed using the TurboChrom Workstation Version 6.1.2 (for Windows) chromatography data system and the overall reactant/product molar fractions (x_i) were obtained using detailed calibration (not shown). Fractional butyronitrile conversion (*X*) was obtained from

$$X_{BT} = \frac{[\mathrm{BT}]_{in} - [\mathrm{BT}]_{out}}{[\mathrm{BT}]_{in}} \quad \textbf{(3.3)}$$

nitrile consumption rate from

$$\text{Rate } (\mathrm{h}^{-1}) = \frac{X \times F}{n} \quad \textbf{(3.4)}$$

where selectivity to product *i* (S_i) is given by

$$S_i(\%) = \frac{N_i x_i}{\sum N_i x_i} \times 100 \quad \textbf{(3.5)}$$

$[\text{Butyronitrile}]_{in}$ and $[\text{Butyronitrile}]_{out}$ represent inlet and outlet butyronitrile concentration, respectively and N_i is the stoichiometric coefficient for product *i*. In a series of blank tests, passage of butyronitrile in a stream of H_2 through the empty reactor or over the SiO_2 support alone did not result in any detectable conversion. Repeated reactions with different samples of catalyst from the same batch delivered raw data reproducibility that was better than ±6%.

3.2.2.2 Thermodynamic Analysis

Application of thermodynamics to catalytic processes provides an important guide to the maximum conversion/selectivity possible under a given set of reaction conditions. All the reactant/product species (butyronitrile, butylamine, dibutylamine, tributylamine, H_2 and NH_3) were considered. Setting the inlet nitrile at 1 mol, product distribution at equilibrium was determined over 473-563 K at a total pressure of 1 atm, where the H_2/butyronitrile molar ratio was kept constant at 24 to mimic catalytic reaction conditions. The equilibrium calculations were made using CHEMCAD (Version 6) where the Gibbs reactor facility was applied to obtain product composition under conditions of minimised Gibbs free energy. The equation of state for fugacity employed the Soave–Redlich–Kwong approach [31]. The total Gibbs function is given by

$$G^t = \sum_{i=1}^{N} n_i \bar{G}_i = \sum_{i=1}^{N} n_i \bar{\mu}_i = \sum n_i G_i^0 + RT \sum n_i \ln \frac{\hat{f}_i}{f_i^0} \quad \textbf{(3.6)}$$

For gas phase reaction equilibrium, $\hat{f}_i = \hat{\phi}_i y_i P$, $f_i^0 = P^0$ and $\Delta G^0 = \Delta G_{f_i}^0$ and the minimum Gibbs free energy of each gaseous species and total for the system can be expressed by

$$\Delta G_{f_i}^0 + RT \ln \frac{\hat{\phi}_i y_i P}{P^0} + \sum_k \lambda_k a_{ik} = 0 \quad \textbf{(3.7)}$$

$$\sum_{i=1}^{N} n_i (\Delta G_{f_i}^0 + RT \ln \frac{\hat{\phi}_i y_i P}{P^0} + \sum_k \lambda_k a_{ik}) = 0 \quad \textbf{(3.8)}$$

according to the Lagrange undetermined multiplier method with the elemental balance constraint

$$\sum_{i=1}^{N} n_i a_{ik} = A_k \quad \textbf{(3.9)}$$

3.3 Results and Discussion

3.3.1 Catalyst Characterisation

Critical physico-chemical characteristics of Pd/SiO_2 and $Ba\text{-}Pd/SiO_2$ are given in **Table 3.1**. The total area (SSA) of Pd/SiO_2 is close to that of the SiO_2 support (200 m^2 g^{-1}). In contrast, $Ba\text{-}Pd/SiO_2$, synthesised from the bimetallic complex, exhibited a significantly lower SSA, which can be ascribed to partial pore blockage as observed for silica supported Pd/lanthanide bimetallics prepared from analogous precursors [32]. TPR generated the profiles given in **Figure 3.2** where Pd/SiO_2 **(I)** exhibited a negative peak (H_2 release) at 368 K, which can be attributed to Pd hydride decomposition [33]. The TPR profile for $Ba\text{-}Pd/SiO_2$ (**II**) is also characterised by a negative peak at 354 K, where the associated Pd hydride composition, in terms of H/Pd ratio (0.19), was markedly lower than that recorded for Pd/SiO_2 (0.34). This suggests inhibited hydride

Table 3. 1: Physico-chemical properties of SiO_2 supported Pd and Ba-Pd catalysts.

	Pd/SiO_2	$Ba\text{-}Pd/SiO_2$
SSA ($m^2\ g^{-1}$)	191	154
TPR T_{max} (K)	368[a]	354[a], 573[b]
Pd hydride (H/Pd; mol mol^{-1})	0.34	0.19
H_2 chemisorption (μmol g^{-1})	7	46
H_2 TPD (μmol g^{-1})	19	91
NH_3 chemisorption (mmol g^{-1})	0.49	0.34
NH_3 TPD (mmol g^{-1})	0.48	0.32
d_{TEM} (nm)	28	7
d_c (nm)	33	9

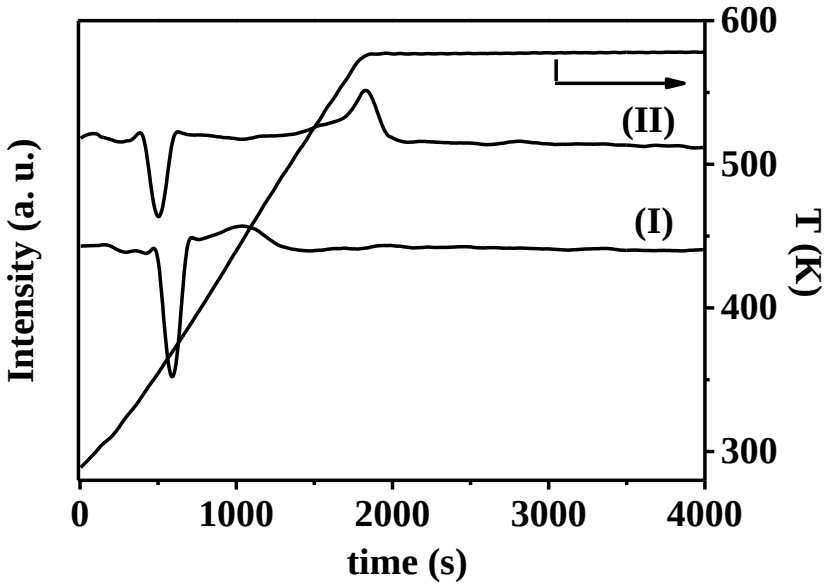

Figure 3. 2: Temperature programmed reduction (TPR) profiles for (I) Pd/SiO_2 and (II) $Ba\text{-}Pd/SiO_2$.

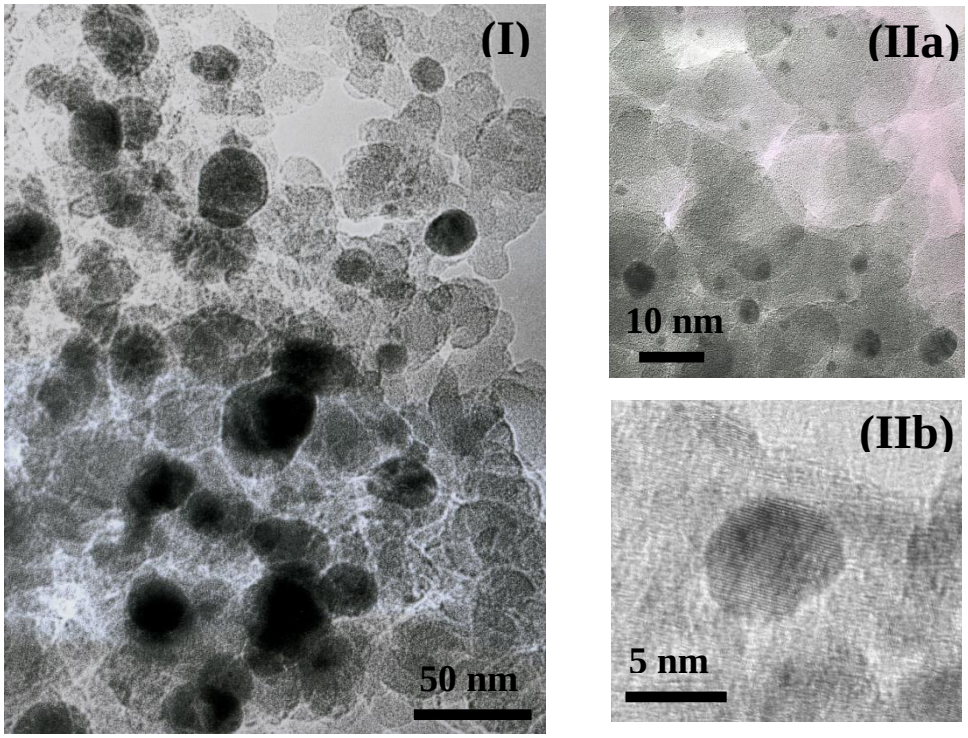

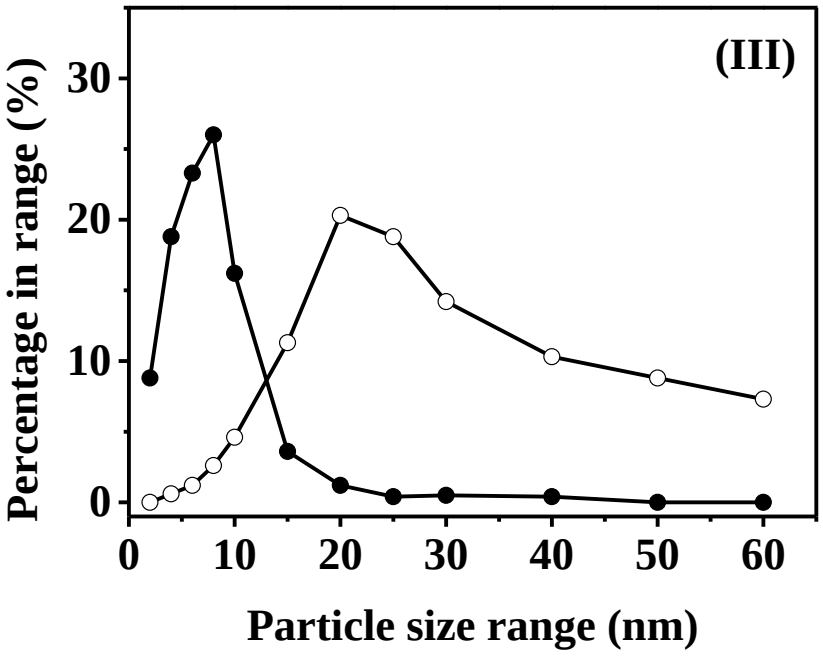

Figure 3. 3: Representative transmission electron microscopy (TEM) images of (I) Pd/SiO_2 (○) and (II) $Ba\text{-}Pd/SiO_2$ (●) with (III) associated particle size distributions.

formation due to the incorporation of Ba but can also indicate the occurrence of smaller Pd particles as size governs hydride composition with an upper H/Pd = 0.76 for bulk Pd [34]. Decomposition of supported Pd hydride has been reported to occur over the temperature range 323-373 K [34-36] where a shift to higher temperature correlates with an increase in Pd particle size [37]. A secondary H_2 consumption (positive TPRsignal) at 573 K suggests a temperature induced reduction step, which may result from stabilisation of surface Pd oxide with the addition of Ba [27]. Supported Pd size was determined by TEM analysis and representative images (with associated particle size distributions) are presented in **Figure 3.3**. Both catalysts display quasi-spherical Pd nano-particles with a narrower distribution of smaller particles on Ba-Pd/SiO_2 (mean size = 7 nm) relative to Pd/SiO_2 (mean size = 28 nm). This result is in good agreement with the mean Pd size obtained from application of the Scherrer equation to XRD line broadening (**Table 3.1,** diffractograms not shown). The incorporation of Ba can serve to minimise Pd agglomeration, leading to the formation of smaller Pd particles, as noted elsewhere [27,38]. The higher metal dispersion can account for the lower hydride decomposition temperature, associated H/Pd ratio and the greater H_2 chemisorption on

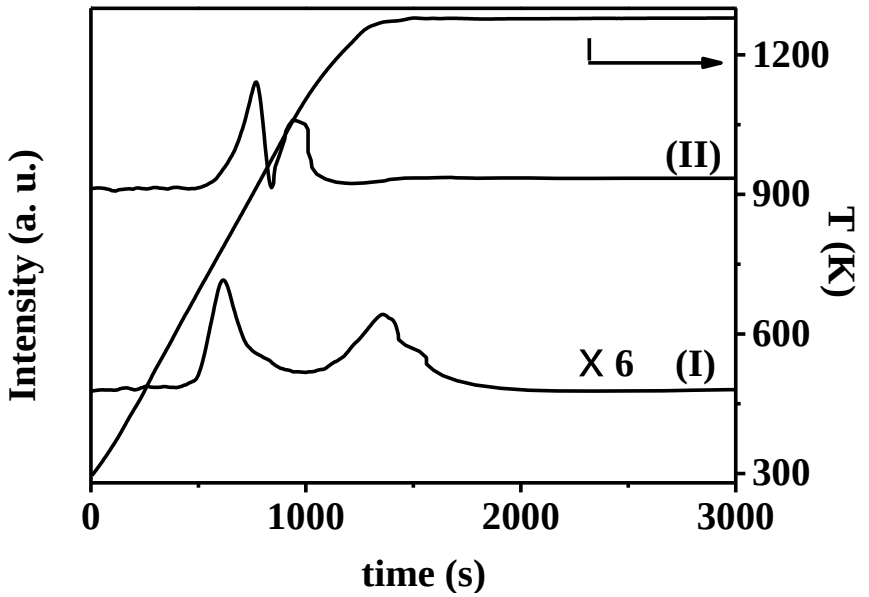

Figure 3. 4: Hydrogen temperature programmed desorption (TPD) profiles for (I) Pd/SiO_2 and (II) Ba-Pd/SiO_2.

Ba-Pd/SiO_2 relative to Pd/SiO_2 (**Table 3.1**), where smaller Pd particles facilitate dissociative H_2 adsorption [39]. Hydrogen released from both catalysts during TPD (**Table 3.1**) exceeded that adsorbed in pulse titration, diagnostic of spillover hydrogen

during TPR [40]. Hydrogen TPD from Pd/SiO_2 generated the profile given in **Figure 3.4(I)**, characterised by a two stage release with T_{max} = 775 K and 1273 K (final isothermal hold). Drawing on available literature, the lower temperature peak can be ascribed to loss of chemisorbed hydrogen from Pd [36]. This is consistent with the equivalence of H_2 desorbed over 720-980 K (6 μmol g^{-1}) with that chemisorbed (7 μmol g^{-1}, **Table 3.1**). Hydrogen release at higher (1050-1273 K) temperatures has been attributed to desorption from the support and/or metal/support interface [27,41]. The TPD profile for $Ba\text{-}Pd/SiO_2$ (**Figure 3.4(II)**) also showed two desorption peaks with a greater (by a factor of 5) amount of H_2 desorbed compared with Pd/SiO_2 (**Table 3.1**). This can be linked to the presence of smaller Pd particles that increased H_2 uptake and diffusion/spillover to the support [42]. The shift of the second H_2 desorption from $Ba\text{-}Pd/SiO_2$ to a lower temperature (relative to Pd/SiO_2) has been ascribed to Ba/surface interaction that impacts on spillover release [27].

Surface acidity was probed by NH_3 chemisorption/desorption where TPD from the silica support (**Figure 3.5(I)**) exhibited NH_3 release with T_{max} = 343 K that can be attributed to weak acid sites [43,44], Indeed, both Brønsted (hydroxyl groups acting as

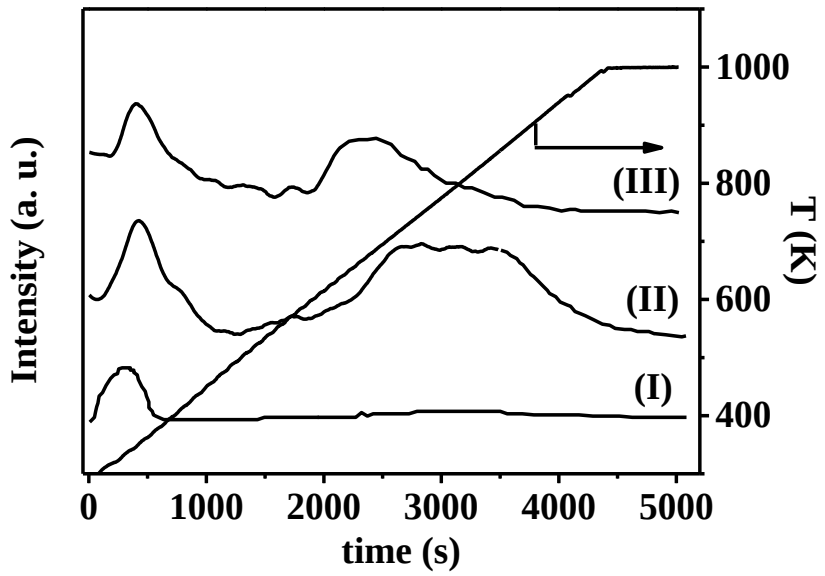

Figure 3. 5: Ammonia temperature programmed desorption (TPD) profiles for (I) SiO_2, (II) Pd/SiO_2 and (III) $Ba\text{-}Pd/SiO_2$.

proton donors) [44] and weak Lewis acid sites [43,44] have been detected on silica surfaces by FTIR spectroscopy. Integration of the NH_3 desorption signal gave a total NH_3 release that correlates well with the chemisorption measurement (0.21 ± 0.02 mmol

g^{-1}). Both Pd/SiO_2 **(II)** and $Ba\text{-}Pd/SiO_2$ **(III)** exhibited a positive peak at T_{max} = 357 K with NH_3 desorption (0.15 mmol g^{-1}) close to that observed for SiO_2 (0.19 mmol g^{-1}). A secondary higher temperature (600-1000 K) NH_3 release was also in evidence that must be linked to surface acidity generated during metal incorporation and sample treatment. Impalà *et al.* [45] reported NH_3 TPD up to 0.46 mmol g^{-1} from Pd/SiO_2, which was dependent on catalyst synthesis procedure, *i.e.* metal precursor, loading and thermal treatment. Ammonia chemisorption/desorption was lower for $Ba\text{-}Pd/SiO_2$ compared with Pd/SiO_2 (**Table 3.1**). Labalme and co-workers [46] also reported a decrease in total surface acidity as a result of Ba addition to Pt/Al_2O_3 based on NH_3 TPD, which was attributed to neutralisation of surface hydroxyl groups. We should flag prior XRD analysis of $Ba\text{-}Pd/SiO_2$ that exhibited a weak signal due to a $BaSiO_3$ phase [27], which can result in a consumption of surface acid sites. XPS analysis has shown [27] that the Pd $3d_{5/2}$ signal for $Ba\text{-}Pd/SiO_2$ appeared at a lower binding energy (by 0.5 eV) relative to Pd/SiO_2, suggesting electron donation from Ba to form an electron-rich Pd phase, which is consistent with Labalme's conclusion of electron donation from electropositive Ba to Pt on Al_2O_3 [46]. This is in line with other reports which have concluded that addition of Ba increases electron density of Pd sites [47,48]. In summary, $Ba\text{-}Pd/SiO_2$ exhibited greater dispersion of electron rich Pd with enhanced H_2 chemisorption and lower total surface acidity relative to Pd/SiO_2.

3.3.2 Butyronitrile Hydrogenation: Thermodynamic Considerations

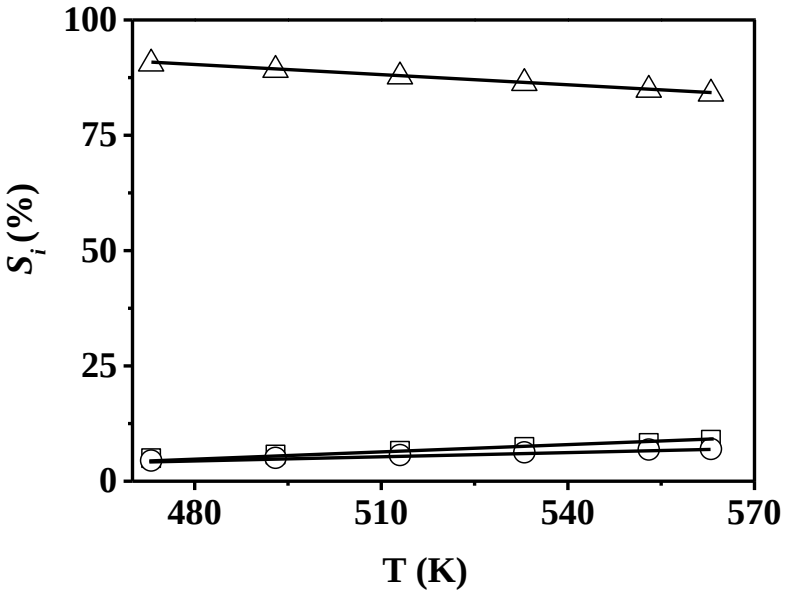

Figure 3. 6: Product selectivity (S_i) as a function of reaction temperature at thermodynamic equilibrium; butylamine (□); dibutylamine (○); tributylamine (△).

A thermodynamic analysis of butyronitrile hydrogenation was performed to determine system behavior at equilibrium. Under thermodynamic control, the nitrile reactant was fully converted under the reaction conditions employed in this study. The calculated equilibrium selectivity as a function of reaction temperature is presented in **Figure 3.6** where it can be seen that the tertiary amine is the predominant product (*S* = 83-90%). Production of equivalent amounts of butylamine and dibutylamine as by-product is favoured by increasing temperature. Preferential tertiary amine production indicates that there is no thermodynamic barrier for the coupled reduction and condensation steps shown in **Figure 3.1**.

3.3.3 Butyronitrile Hydrogenation: Catalytic Activity/Selectivity (at 473 K)

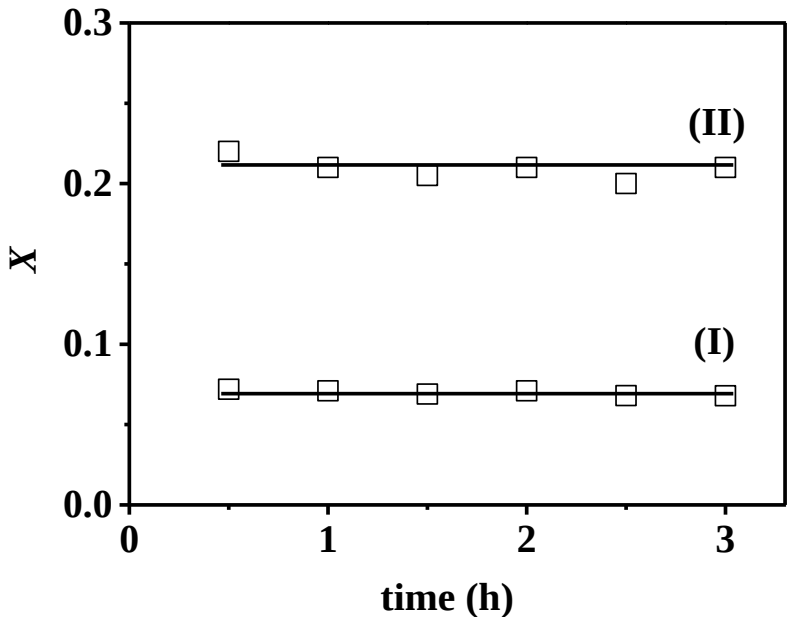

Figure 3. 7: Time on-stream butyronitrile fractional conversion (*X*) for reaction over (I) Pd/SiO_2 and (II) Ba-Pd/SiO_2; *Reaction conditions: P* = 1 atm, *T* = 473 K, *n*/*F* = 1.4 × 10^{-3} h.

Taking 473 K as a benchmark temperature, fractional butyronitrile conversion was time invariant over both Pd/SiO_2 **(I)** and Ba-Pd/SiO_2 **(II)** where the latter exhibited higher nitrile conversion (**Figure 3.7**). This is significant, given the temporal decline in activity reported in liquid [4-7,9,49] and gas phase [10,11,17,19] nitrile hydrogenation over supported Pd [5-7,9,50,51], Pt [7,52], Ru [7] and Ni [11,18,19]. Catalyst deactivation has been ascribed to metal particle agglomeration [7,10], active site occlusion by amine product(s) [7,10,14,52,53] and catalyst coking associated with the formation of dehydrogenated surface species and carbides [11,14,18,20]. The greater

levels of H_2 uptake/release exhibited by Ba-Pd/SiO_2 (**Table 3.1**) can account for the observed higher nitrile hydrogenation activity. Product distribution was invariant with

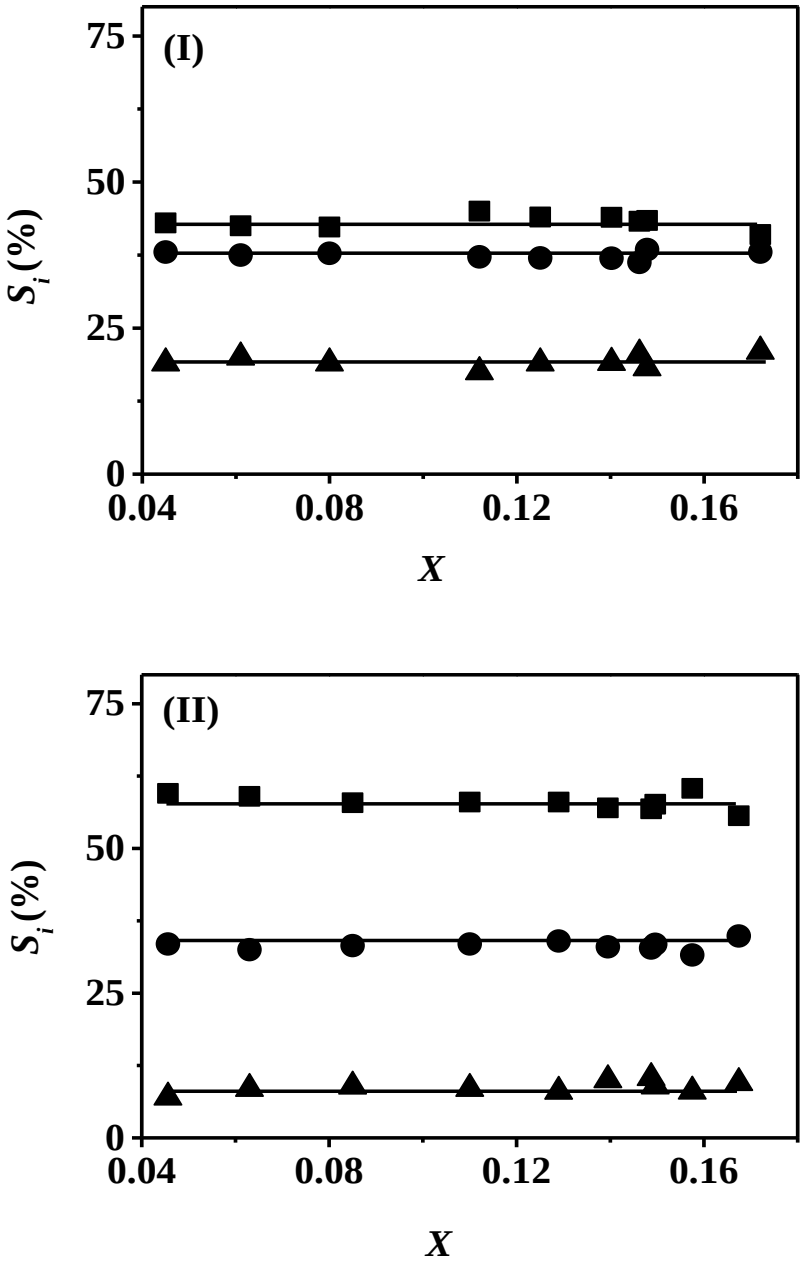

Figure 3. 8: Selectivity (S_i) to butylamine (■), dibutylamine (●) and tributylmine (▲) as a function of butyronitrile fractional conversion (X) for reaction over (I) Pd/SiO_2 and (II) Ba-Pd/SiO_2; *Reaction conditions:* P = 1 atm, T = 473 K, n/F = 3.4 × 10^{-4} – 3.4 × 10^{-3} h.

conversion (**Figure 3.8**) where butylamine was the major product, deviating from predominant tertiary amine formation under thermodynamic equilibrium (**Figure 3.6**),

demonstrating catalytic control. Nitrile transformation to amines *via* the pathway shown in **Figure 3.1** requires catalyst bifunctionality [54] where the metal phase serves to promote hydrogenation steps (steps I, II, IV and VI) and condensation of the imine intermediates with butyl- and dibutyl-amine (steps III and step V) proceeds on surface acid sites [2,4,17,18,54]. Selectivity to the target butylamine was higher over Ba-Pd/SiO_2 (**Figure 3.8(II)**) than Pd/SiO_2 (**Figure 3.8(I)**). This can be partly attributed to the lower surface acidity of the bimetallic catalyst that served to suppress condensation to secondary and/or tertiary amines. Moreover, weaker butylamine interaction with electron-rich Pd sites on Ba-Pd/SiO_2 resulting from repulsion with the $–NH_2$ function can favour desorption of the primary amine without further reaction. Branco *et al*. [23] reached a similar conclusion for the conversion of propionitrile over lanthanide-promoted Cu where the electron enriched Cu sites exhibited weaker adsorption of primary amine, limiting subsequent condensation.

3.3.4 Butyronitrile Hydrogenation: Temperature Effects

Reaction temperature is a critical variable that impacts on reactant/intermediate activation and desorption dynamics, which in turn can influence hydrogenation rate and product distribution [55]. The nitrile consumption rate delivered by Pd/SiO_2 **(I)** and Ba-Pd/SiO_2 **(II)** passed through maxima at 523 K and 493 K, respectively, as shown in **Figure 3.9**. Nieto-Márquez *et al.* [11] reported a maximum rate of butyronitrile hydrogenation over (carbon nanosphere) supported Ni catalysts at comparable temperatures that they linked to decreasing surface coverage by reactant due to thermal desorption. Reaction over Ba-Pd/SiO_2 delivered higher nitrile consumption rates with the maximum at a lower temperature (493 K). The latter can be linked to a lesser degree of butyonitrile interaction *via* the nitrogen electron lone pair at electron rich Pd sites, resulting in a more facile desorption. There is evidence in the literature [11] for a higher T_{max} in butyronitrile hydrogenation rate over smaller Ni particles with lower electron density that can be attributed to stronger C≡N adsorption and the requirement for higher desorption temperatures. In terms of product distribution, butylamine selectivity over both catalysts increased with increasing temperature to 100% at $T \geq 543$ K (**Figure 3.9**). This is quite distinct from the thermodynamic equilibrium composition (**Figure 3.6**) where tri-butylamine was the predominant product over the entire temperature range. An increase in temperature must induce desorption of the butylamine product, circumventing condensation. Cristiani and co-workers [56] have recorded an increase in

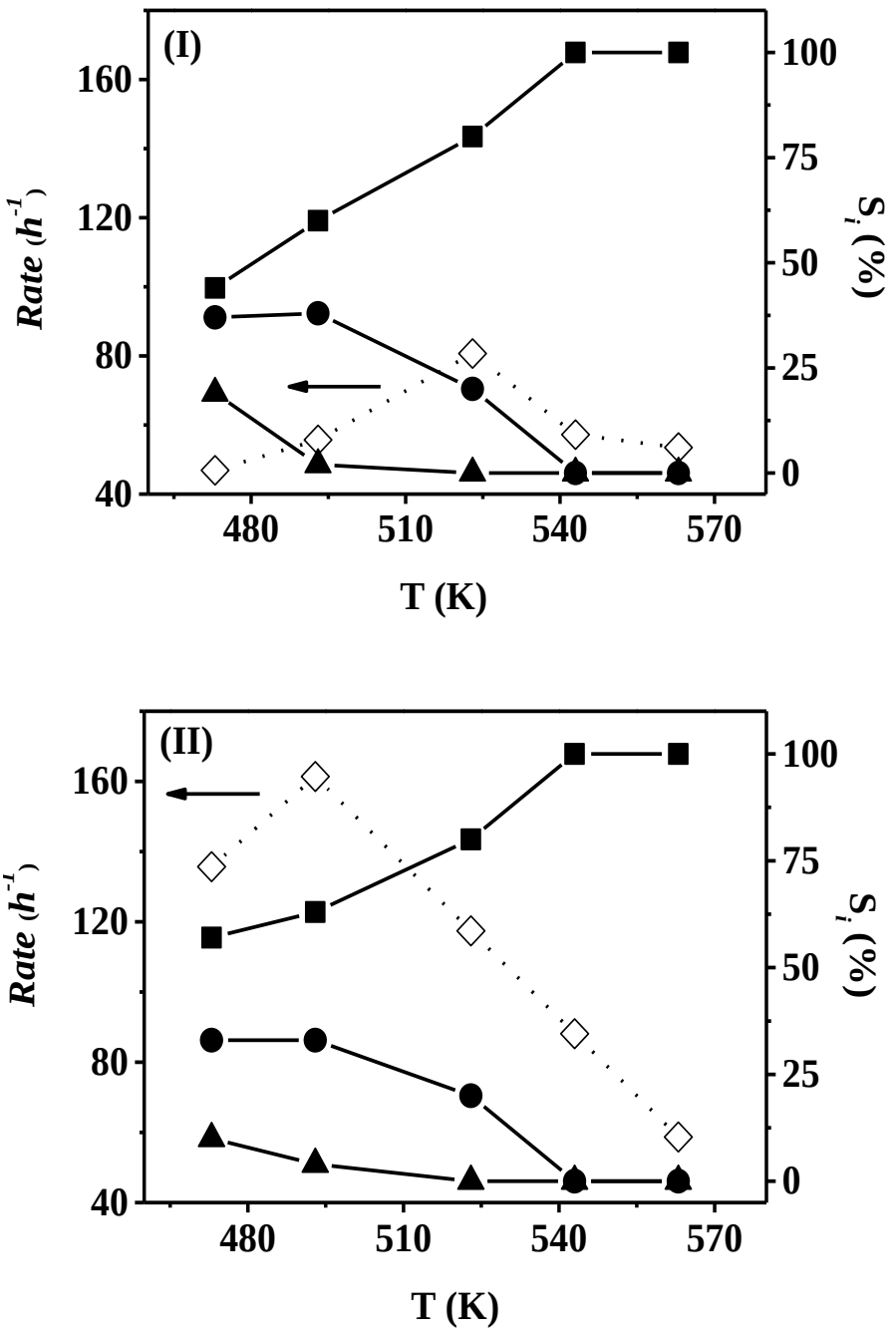

Figure 3. 9: Reaction rate (◇) and selectivity (S_i) to butylamine (■), dibutylamine (●) and tributylamine (▲) as a function of temperature for reaction over (I) Pd/SiO_2 and (II) $Ba\text{-}Pd/SiO_2$; *Reaction conditions:* P = 1 atm, $n/F = 1.4 \times 10^{-3}$ h.

primary amine formation (S = 16% - 41%) at higher temperatures (453-563 K) in stearonitrile conversion over $CuO\text{-}Cr_2O_3$. In contrast, Braos-García and co-workers [20] noted decreasing primary amine selectivity and preferential secondary amine formation with increasing temperature (378-418 K) for acetonitrile hydrogenation over mixed

alumina/gallium oxide (16% w/w Ga_2O_3) supported Ni, which they ascribed to the combined effect of amine desorption and differences in the strength of amine interaction with surface acid sites. Nieto-Márquez *et al.* [11] have proposed that the selectivity maximum is the result of contributions due to mass transfer, thermodynamic limitations and thermal poisoning. The higher butyronitrile consumption rate delivered by Ba-Pd/SiO_2 coupled with reaction exclusivity translates into higher butylamine productivity (91 mol h^{-1} mol_{Pd}^{-1}) than that achieved over Pd/SiO_2 (54 mol h^{-1} mol_{Pd}^{-1}) at 543 K. We attribute this to greater availability of surface reactive hydrogen and lower surface acidity, resulting in enhanced nitrile conversion and inhibited condensation reaction. It is important to stress that in previous reports Ni has shown higher activity and selectivity to primary amines than Pd in the liquid phase nitrile hydrogenation [6,15]. We have achieved an order of magnitude higher rate over Ba-Pd/SiO_2 with full selectivity to the target butylamine when compared with reported gas phase continuous reaction over supported Ni under similar reaction conditions (T = 493 K, 1 atm) [10]. Our results demonstrate that incorporation of an alkaline earth metal (Ba) with Pd facilitates enhanced cleaner primary amine production.

3.4 Conclusions

Ba-Pd/SiO_2 delivered a higher butyronitrile selective hydrogenation rate (91 mol h^{-1} mol_{Pd}^{-1}) to the target butylamine relative to Pd/SiO_2 (54 mol h^{-1} mol_{Pd}^{-1}). The increased rate can be attributed to greater available surface reactive hydrogen (from H_2 chemisorption coupled with TPD) on Ba-Pd/SiO_2. Lower acidity of Ba-Pd/SiO_2 (from NH_3 adsorption/TPD) served to minimise side condensation with imine and the formation of higher amines. Electron donation from electropositive Ba weakened butylamine interaction with Pd sites resulting in more facile desorption without subsequent condensation. Temperature-related activity maxima (T_{max}) are attributed to thermal desorption that limits surface coverage by reactant where T_{max} for Ba-Pd/SiO_2 (493 K) was measurably lower than Pd/SiO_2 (523 K), reflecting weaker surface interaction for the former. We have provided the first reported evidence for (i) full selectivity to primary amine in nitrile hydrogenation over supported Pd; (ii) enhanced selective hydrogenation rate (ten-fold higher compared with that supported for supported Ni) for the supported Pd-alkaline earth metal formulation.

3.5 References

[1] J. Krupka, J. Pasek, *Nitrile hydrogenation on solid catalysts - new insights into the reaction mechanism*, Curr. Org. Chem. 16 (**2012**) 988-1004.

[2] S. Gomez, J.A. Peters, T. Maschmeyer, *The reductive amination of aldehydes and ketones and the hydrogenation of nitriles: Mechanistic aspects and selectivity control*, Adv. Synth. Catal. 344 (**2002**) 1037-1057.

[3] S. Nishimura, *Handbook of Heterogeneous Catalytic Hydrogenation for Organic Synthesis* John Wiley, New York (**2001**) 265-265.

[4] H. Chen, M. Xue, S. Hu, J. Shen, *The effect of surface acidic and basic properties on the hydrogenation of lauronitrile over the supported nickel catalysts*, Chem. Eng. J. 181–182 (**2012**) 677-684.

[5] Y.Y. Huang, W.M.H. Sachtler, *On the mechanism of catalytic hydrogenation of nitriles to amines over supported metal catalysts*, Appl. Catal. A: Gen. 182 (**1999**) 365-378.

[6] Y.Y. Huang, W.M.H. Sachtler, *Catalytic hydrogenation of nitriles over supported mono- and bimetallic catalysts*, J. Catal. 188 (**1999**) 215-225.

[7] Y.Y. Huang, V. Adeeva, W.M.H. Sachtler, *Stability of supported transition metal catalysts in the hydrogenation of nitriles*, Appl. Catal. A: Gen. 196 (**2000**) 73-85.

[8] P. Schärringer, T.E. Müller, J.A. Lercher, *Investigations into the mechanism of the liquid-phase hydrogenation of nitriles over raney-Co catalysts*, J. Catal. 253 (**2008**) 167-179.

[9] Y.Y. Huang, W.M.H. Sachtler, *Concerted reaction mechanism in deuteration and H/D exchange of nitriles over transition metals*, J. Catal. 184 (**1999**) 247-261.

[10] A. Nieto-Márquez, D. Toledano, P. Sánchez, A. Romero, J. Luis Valverde, *Impact of nitrogen doping of carbon nanospheres on the nickel-catalyzed hydrogenation of butyronitrile*, J. Catal. 269 (**2010**) 242-251.

[11] A. Nieto-Márquez, D. Toledano, J. Carlos Lazo, A. Romero, J. Luis Valverde, *Carbon nanospheres as novel support in the nickel catalyzed gas phase hydrogenation of butyronitrile*, Appl. Catal. A: Gen. 373 (**2010**) 192-200.

[12] H. Chen, M.W. Xue, J.Y. Shen, *Surface properties of Ni/MgO catalysts for the hydrogenation of lauronitrile*, Catal. Lett. 135 (**2010**) 246-255.

[13] A. Chojecki, M. Veprek-Heijman, T.E. Müller, P. Schärringer, S. Veprek, J.A. Lercher, *Tailoring raney-catalysts for the selective hydrogenation of butyronitrile to n-butylamine*, J. Catal. 245 (**2007**) 237-248.

[14] M.C. Carrión, B.R. Manzano, F.A. Jalón, I. Fuentes-Perujo, P. Maireles-Torres, E. Rodríguez-Castellón, A. Jiménez-López, *Gas-phase hydrogenation of acetonitrile over Pt and Pt-Pd supported on mesoporous solids: Influence of the metallic precursor*, Appl. Catal. A: Gen. 288 (**2005**) 34-42.

[15] D.J. Segobia, A.F. Trasarti, C.R. Apesteguía, *Hydrogenation of nitriles to primary amines on metal-supported catalysts: Highly selective conversion of butyronitrile to n-butylamine*, Appl. Catal. A: Gen. 445–446 (**2012**) 69-75.

[16] C. Jiménez-González, P. Poechlauer, Q.B. Broxterman, B.-S. Yang, D.A. Ende, J. Baird, C. Bertsch, R.E. Hannah, P. Dell'Orco, H. Noorrnan, S. Yee, R. Reintjens, A. Wells, V. Massonneau, J. Manley, *Key green engineering research areas for sustainable manufacturing: A perspective from pharmaceutical and fine chemicals manufacturers*, Org. Process Res. Dev. 15 (**2011**) 900-911.

[17] A.C. Gluhoi, P. Mărginean, U. Stănescu, *Effect of supports on the activity of nickel catalysts in acetonitrile hydrogenation*, Appl. Catal. A: Gen. 294 (**2005**) 208-214.

[18] P. Braos-García, P. Maireles-Torres, E. Rodríguez-Castellón, A. Jiménez-López, *Gas-phase hydrogenation of acetonitrile on zirconium-doped mesoporous silica-supported nickel catalysts*, J. Mol. Catal. A: Chem. 193 (**2003**) 185-196.

[19] A. Nieto-Márquez, V. Jiménez, A. Manuel Raboso, S. Gil, A. Romero, J. Luis Valverde, *Influence of the chemical activation of carbon nanofibers on their use as catalyst support*, Appl. Catal. A: Gen. 393 (**2011**) 78-87.

[20] P. Braos-García , P. Maireles-Torres, E. Rodríguez-Castellón , A. Jiménez-López *Gas-phase hydrogenation of acetonitrile over nickel supported on alumina- and mixed alumina/gallium oxide-pillared tin phosphate catalysts*, J. Mol. Catal. A: Chem. 168 (**2001**) 279-287.

[21] N. Iwasa, M. Yoshikawa, M. Arai, *Selective hydrogenation of acetonitrile to ethylamine using palladium-based alloy catalysts*, Phys. Chem. Chem. Phys. 4 (**2002**) 5414-5420.

[22] S.H. Hu, M.W. Xue, H. Chen, J.Y. Shen, *The effect of surface acidic and basic properties on the hydrogenation of aromatic rings over the supported nickel catalysts*, Chem. Eng. J. 162 (**2012**) 371-379.

[23] J.B. Branco, D. Ballivet-Tkatchenko, A.P. de Matos, *Gas-phase hydrogenation of propionitrile catalyzed by $LnCu_{(2)}$ (Ln = La, Ce, Pr, Nd)*, J. Phys. Chem. C 111 (**2007**) 15084-15088.

[24] A.W. Pelzer, J. Jellinek, K.A. Jackson, *H_2 reactions on palladium clusters*, J. Phys. Chem. A 117 (**2013**) 10407-10415.

[25] M. Armbrüster, M. Behrens, F. Cinquini, K. Föttinger, Y. Grin, A. Haghofer, B. Klötzer, A. Knop-Gericke, H. Lorenz, A. Ota, S. Penner, J. Prinz, C. Rameshan, Z. Révay, D. Rosenthal, N. Rupprechter, P. Sautet, R. Schlögl, L. Shao, L. Szentmiklósi, D. Teschner, D. Torres, R. Wagner, R. Widmer, G. Wowsnick, *How to control the selectivity of palladium-based catalysts in hydrogenation reactions: The role of subsurface chemistry*, ChemCatChem 4 (**2012**) 1048-1063.

[26] H.-U. Blaser, A. Indolese, A. Schnyder, H. Steiner, M. Studer, *Supported palladium catalysts for fine chemicals synthesis*, J. Mol. Catal. A: Chem. 173 (**2001**) 3-18.

[27] E. Ding, S. Jujjuri, M. Sturgeon, S.G. Shore, M.A. Keane, *Novel one step preparation of silica supported Pd/Sr and Pd/Ba catalysts via an organometallic precursor: Application in hydrodechlorination and hydrogenation*, J. Mol. Catal. A: Chem. 294 (**2008**) 51-60.

[28] D.W. Knoeppel, J.P. Liu, E.A. Meyers, S.G. Shore, *Heterometallic one-dimensional arrays containing cyanide-bridged lanthanide(III) and transition metals*, Inorg. Chem. 37 (**1998**) 4828-4837.

[29] A.L. Bugaev, A.A. Guda, K.A. Lomachenko, V.V. Srabionyan, L.A. Bugaev, A.V. Soldatov, C. Lamberti, V.P. Dmitriev, J.A. van Bokhoven, *Temperature- and pressure-dependent hydrogen concentration in supported PdHx nanoparticles by Pd K-edge X-ray absorption spectroscopy*, J. Phys. Chem. C 118 (**2014**) 10416-10423.

[30] U. Holzwarth, N. Gibson, *The scherrer equation versus the 'debye-scherrer equation'*, Nat. Nanotechnol. 6 (**2011**) 534-534.

[31] X. Wang, S. Li, H. Wang, B. Liu, X. Ma, *Thermodynamic analysis of glycerin steam reforming*, Energy Fuel 22 (**2008**) 4285-4291.

[32] S. Jujjuri, E. Ding, S.G. Shore, M.A. Keane, *A characterization of Ln-Pd/SiO_2 (Ln=La, Ce, Sm, Eu, Gd and Yb): Correlation of surface chemistry with hydrogenolysis activity*, J. Mol. Catal. A: Chem. 272 (**2007**) 96-107.

[33] F. Menegazzo, T. Fantinel, M. Signoretto, F. Pinna, *Metal dispersion and distribution in Pd-based PTA catalysts*, Catal. Commun. 8 (**2007**) 876-879.

[34] F. Cárdenas-Lizana, Y. Hao, M. Crespo-Quesada, I. Yuranov, X. Wang, M.A. Keane, L. Kiwi-Minsker, *Selective gas phase hydrogenation of p-chloronitrobenzene over Pd catalysts: Role of the support*, ACS Catal. 3 (**2013**) 1386-1396.

[35] S. Jujjuri, M.A. Keane, *Catalytic hydrodechlorination at low hydrogen partial pressures: Activity and selectivity response*, Chem. Eng. J. 157 (**2010**) 121-130.

[36] C. Amorim, G. Yuan, P.M. Patterson, M.A. Keane, *Catalytic hydrodechlorination over Pd supported on amorphous and structured carbon*, J. Catal. 234 (**2005**) 268-281.

[37] S. Gómez-Quero, F. Cárdenas-Lizana, M.A. Keane, *Effect of metal dispersion on the liquid-phase hydrodechlorination of 2,4-dichlorophenol over Pd/Al_2O_3*, Ind. Eng. Chem. Res. 47 (**2008**) 6841-6853.

[38] F. Klingstedt, H. Karhu, A.K. Neyestanaki, L.E. Lindfors, T. Salmi, J. Väyrynen, *Barium promoted palladium catalysts for the emission control of natural gas driven vehicles and biofuel combustion systems*, J. Catal. 206 (**2002**) 248-262.

[39] A.M. Doyle, S.K. Shaikhutdinov, S.D. Jackson, H.-J. Freund, *Hydrogenation on metal surfaces: Why are nanoparticles more active than single crystals?*, Angew. Chem. Int. Ed. 42 (**2003**) 5240-5243.

[40] C. Tu, S. Cheng, *Ceria-modified palladium/activated carbon as a high-performance catalyst for crude caprolactam hydrogenation purification*, ACS Sustain. Chem. Eng. 2 (**2013**) 629-636.

[41] M. Chettibi, A.-G. Boudjahem, M. Bettahar, *Synthesis of Ni/SiO_2 nanoparticles for catalytic benzene hydrogenation*, Transition Metal Chem. 36 (**2011**) 163-169.

[42] S.D. Lin, M.A. Vannice, *Hydrogenation of aromatic hydrocarbons over supported Pt catalysts. III. Reaction models for metal surfaces and acidic sites on oxide supports*, J. Catal. 143 (**1993**) 563-572.

[43] A.V. Biradar, S.B. Umbarkar, M.K. Dongare, *Transesterification of diethyl oxalate with phenol using MoO_3/SiO_2 catalyst*, Appl. Catal. A: Gen. 285 (**2005**) 190-195.

[44] L. Óvári, F. Solymosi, *Determination of acidic centers on supported MO_2C catalysts*, J. Mol. Catal. A: Chem. 207 (**2004**) 35-40.

[45] D. Impalà, S. Franceschini, O. Piccolo, A. Vaccari, *Pd-based sol–gel catalysts for the enantioselective hydrogenation of (e)-2-methyl-2-butenoic acid*, Catal. Lett. 125 (**2008**) 243-249.

[46] V. Labalme, B. Béguin, F. Gaillard, M. Primet, *Characterisation and acid properties of some modified combustion catalysts: Pt/alumina with barium and Pt/zirconia with yttrium*, Appl. Catal. A: Gen. 192 (**2000**) 307-316.

[47] N. Mahata, K.V. Raghavan, V. Vishwanathan, M.A. Keane, *Influence of the charge transfer capacity of alkali and alkaline earth metals as promoters in*

thehydrogenation of phenol over palladium and nickel catalysts, React. Kinet. Catal. Lett. 72 (**2001**) 297-302.

[48] K. Tanikawa, C. Egawa, *Effect of barium addition on CO oxidation activity of palladium catalysts*, Appl. Catal. A: Gen. 403 (**2011**) 12-17.

[49] P. Kukula, K. Koprivova, *Structure-selectivity relationship in the chemoselective hydrogenation of unsaturated nitriles*, J. Catal. 234 (**2005**) 161-171.

[50] L. Hegedűs, T. Máthé, T. Kárpáti, *Selective heterogeneous catalytic hydrogenation of nitriles to primary amines in liquid phase part II: Hydrogenation of benzyl cyanide over palladium*, Appl. Catal. A: Gen. 349 (**2008**) 40-45.

[51] L. Hegedűs, T. Máthé, *Selective heterogeneous catalytic hydrogenation of nitriles to primary amines in liquid phase part I. Hydrogenation of benzonitrile over palladium*, Appl. Catal. A: Gen. 296 (**2005**) 209-215.

[52] M. Arai, Y. Takada, Y. Nishiyama, *Effects of metal particle size in gas-phase hydrogenation of acetonitrile over silica-supported platinum catalysts*, J. Phys. Chem. B 102 (**1998**) 1968-1973.

[53] P.F. Yang, Z.X. Jiang, P.L. Ying, C. Li, *Effect of surface composition on the catalytic performance of molybdenum phosphide catalysts in the hydrogenation of acetonitrile*, J. Catal. 253 (**2008**) 66-73.

[54] M.J.F.M. Verhaak, A.J. Dillen, J.W. Geus, *The selective hydrogenation of acetonitrile on supported nickel catalysts*, Catal. Lett. 26 (**1994**) 37-53.

[55] M.P. González-Marcos, J.I. Gutiérrez-Ortiz, C.G.-O. De Elguea, J.I. Alvarez, J.R. González-Velasco, *Control of the product distribution in the hydrogenation of vegetable oils over nickel on silica catalysts*, The Canadian Journal of Chemical Engineering 76 (**1998**) 927-935.

[56] G.G. C. Cristiani, G. Airoldi and P. Forzatti, *Catalytic hydrogenation*, studies in surface sciences and catalysis. Elsevier, Amsterdam 1986 128.

Chapter 4

Palladium Promoted Production of Higher Amines from a Lower Amine Feedstock

The results in the previous Chapters have demonstrated a distinct catalytic response in the synthesis of higher (secondary or tertiary) amines as a result of modifications in the acid-base properties of the catalyst due to variation in the nature of the support, metal dispersion and incorporation of a second metal. In this Chapter, an alternative route for the synthesis of higher aliphatic (secondary and tertiary) amines from a primary and secondary amine feedstock is demonstrated.

4.1 Introduction

Higher (secondary and tertiary) amines are commercially important in the production of a range of chemical products [1-3]. Secondary amines are key pharmacophores in biologically active compounds in the drug industry [4] while tertiary amines find widespread use as solvents in extraction processes [3]. Standard synthesis of secondary amines involves (i) *N*-alkylation of primary amines with (toxic) alkyl halides or alcohols [5,6] or (ii) reduction of imines using reducing agents (*e.g.* $NaCNBH_3$) in liquid batch mode [4]. Both approaches generate mixtures of primary, secondary and tertiary amines, as well as quaternary ammonium salts [7] where extraction of the target product necessitates multiple separation/purification steps [2,4,8]. Condensation of primary amines offers an alternative more sustainable route to secondary amines [4,9,10]. Taking mono-butylamine (MBA) as a model reactant (**Figure 4.1**), dehydrogenation generates a reactive butylidenimine (BI) intermediate, which readily reacts with MBA to form *N*-butylidene-butylamine (BBA) *via* elimination of 1 mol NH_3. BBA can be further hydrogenated to di-butylamine (DBA), which in turn leads to the formation of a tertiary amine (tri-butylamine, TBA) through the hydrogenation of but-1-eny-dibutylamine (BEDA). The limited reports on primary amine condensation have employed homogeneous Pt [4], Pd [10], Ru [11,12] and Ir [13,14] catalysts that are difficult to reuse. We should note the work of Miyazawa *et al.* [15] who proposed DBA synthesis from MBA employing physically mixed Pt/C and alumina powder under microwave irradiation but the temperature was difficult to

control, resulting in data irreproducibility. Kim *et al.* [9] studying the synthesis of secondary amine from a primary amine over Cu/Al_2O_3 reported formation of significant quantities of undesired imine by-product. Kamiguchi and co-workers [10] recorded low selectivity (<13%) to DBA in gas phase condensation over Pt/C and Pd/C with imine as the principal product where Pd/C exhibited higher reaction rate. Activated carbon [16,17] and alumina [18-22] supports bear acid sites that favour condensation reactions to generate higher amines [23,24]. Moreover the activated carbon and alumina exhibited different electron transfer between the support and the Pd metal phase that resulted in different catalytic adsorption mode of reactant which in turn impact on the catalytic performance [25], but the metal electronic effect has not been investigated in any details for the amine condensation.

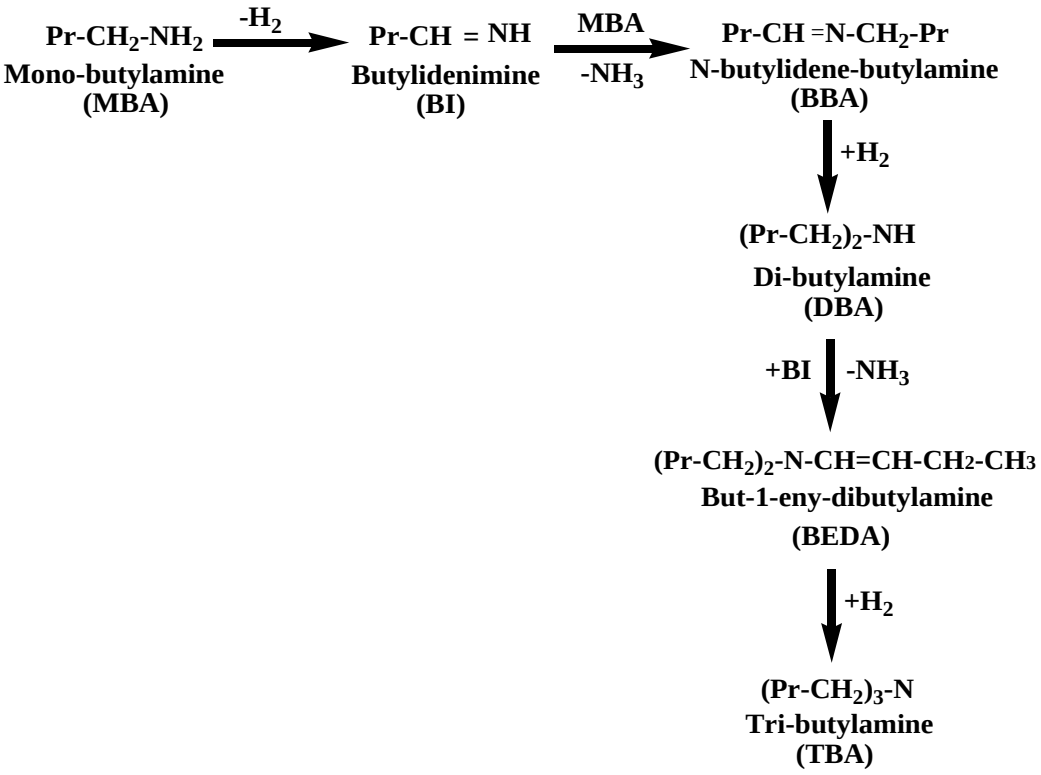

Figure 4. 1: Schematic showing the reaction pathways associated with the condensation of mono-butylamine (MBA) to higher amines (di-butylamine (DBA) and tri-butylamine (TBA)).

Tertiary amines are also predominantly produced *via* primary amine *N*-alkylation [1] and hydrogenation of nitriles over supported Pt [26,27] and Pd [28]. These approaches show the same drawbacks in terms of non-selective amine production and use of toxic agents (e.g. alkyl halides). Condensation of secondary to tertiary amines is a

possible alternative but a thorough research through the literature only revealed one patent on the preparation of tri-alkylamines from di-alkylamines using a metal chloride (e.g. ruthenium trichloride) catalyst in presence of a biphyllic ligand (as catalyst stabiliser) [29]. This homogeneous system requires downstream product/catalyst separation and there is no evidence of commercial application. Moreover, we could not find any reported reaction mechanism for di- → tri-amine transformation. An efficient amine condensation system that utilises reusable heterogeneous catalysts in continuous mode at ambient pressure represents a significant advancement in terms of green chemistry/sustainable processing. Given the higher activity recorded for Pd relative to Pt in gas phase amine condensation [10] and the established performance of Pd catalysts in dehydrogenation [30-34] and hydrogenation [35-37] (critical steps in higher amine synthesis), we have adopted supported Pd as suitable candidates for this process. In this study, Pd/C was first applied in gas phase operation to establish viability of DBA production from MBA and the catalytic response was compared with Pd/Al_2O_3. Synthesis of the tertiary amine (TBA) from DBA was also evaluated and a reaction mechanism proposed based on the catalytic results. We demonstrate that operation of catalyst beds in series serves to decrease the contact time that enhanced the further conversion of MBA and DBA which in overall facilitates full selectivity to TBA at elevated rates.

4.2 Experimental

4.2.1 Catalyst Characterisation

Commercial (1% w/w) Pd on carbon and alumina catalysts were obtained from Sigma-Aldrich. The Pd content was measured by inductively coupled plasma-optical emission spectrometry (ICP-OES, Vista-PRO, Varian Inc.) from the diluted extract in HF. Catalyst activation, H_2 chemisorption, temperature programmed desorption (TPD) and specific surface area (SSA) measurements were conducted using the CHEM-BET 3000 (Quantachrome) unit. Samples were loaded into a U-shaped Quartz cell (3.76 mm *i.d.*) and heated in 17 cm^3 min^{-1} (Brooks mass flow controlled) 5% v/v H_2/N_2 at 2 K min^{-1} to 573 ± 1 K, following the reduction procedure established previously [25]. The samples were swept with 65 cm^3 min^{-1} N_2 for 1.5 h, cooled to ambient temperature and subjected to H_2 chemisorption using a pulse (50 µl) titration procedure. The samples were thoroughly flushed in N_2 and subjected to TPD at 50 K min^{-1} (in 65 cm^3 min^{-1} N_2) to 1173 K. Hydrogen uptake and release were monitored by a thermal conductivity

detector (TCD) with data acquisition/manipulation using the TPR Win^{TM} software. SSA was recorded with a 30% v/v N_2/He flow using undiluted N_2 (99.9%) as internal standard. Three cycles of N_2 adsorption-desorption in the flow mode were employed, applying the standard single point BET method; SSA and H_2 uptake/release values were reproducible to within ±5% and the values quoted represent the mean. Palladium particle morphology (size and shape) was determined by transmission (JEOL JEM 2011 TEM unit) and scanning transmission (JEOL 2200FS field emission gun-equipped TEM unit) electron microscopy, employing Gatan DigitalMicrograph 1.82 for data acquisition/manipulation. Samples for analysis were crushed and deposited (dry) on a holey carbon/Cu grid (300 Mesh). Up to 800 individual Pd particles were counted for each catalyst and the surface area-weighted metal diameter ($d_{(S)TEM}$) calculated from

$$d_{(S)TEM} = \frac{\sum_i n_i d_i^3}{\sum_i n_i d_i^2} \qquad \textbf{(4.1)}$$

where n_i is the number of particles of diameter d_i. X-ray photoelectron spectroscopy (XPS) analyses were conducted on an Axis Ultra instrument (Kratos Analytical) under ultra-high vacuum conditions (<10^{-8} Torr) using a monochromatic Al Kα X-ray source (1486.6 eV). The source power was maintained at 150 W and the emitted photoelectrons were sampled from a 750 × 350 μm^2 area at a take-off angle = 90°. The analyser pass energy was 80 eV for survey spectra (0–1000 eV) and 40 eV for high resolution spectra (Pd 3$d_{5/2}$ and 3$d_{3/2}$). The adventitious carbon 1*s* peak was calibrated at 284.5 eV and used as an internal standard to compensate for charging effects.

4.2.2 Catalytic Procedure

The condensation (of MBA and DBA, Sigma-Aldrich, purity ≥99%) reactions were conducted *in situ*, immediately after catalyst activation, under atmospheric pressure over the temperature range 453-523 K in a fixed bed vertical glass reactor (*i.d.* = 15 mm). The reactant was delivered at a fixed calibrated flow rate to the reactor *via* a glass/teflon air-tight syringe and teflon line using a microprocessor controlled infusion pump (Model 100 kd Scientific). A layer of borosilicate glass beads served as preheating zone, ensuring the reactants were vaporised and reached reaction temperature before contacting the catalyst bed. Isothermal conditions (±1 K) were

achieved by diluting the catalyst bed with ground glass (75 μm); the ground glass was mixed thoroughly with catalyst before insertion in the reactor. Reaction temperature was continuously monitored using a thermocouple inserted in a thermowell within the catalyst bed. A co-current flow of amine and ultra pure (BOC, >99.99%) N_2 or H_2 was maintained at total $GHSV = 1 \times 10^4$ h^{-1} with an inlet amine molar flow (F) of 3.5 – 6.1 mmol h^{-1}. The boing point of reactant (mono-butylamine (350 K), di-butylamine (432.9 K) was below reaction temperature (453-523 K) ensuring the gasification. Although tributylamine showed a high boing point 487 K, the highest partial pressure (182 Pa) according to the composition of the products was still one magnitude lower than the saturated vapour pressure (1314 Pa) at 473 K suggesting the gas phase of tributylamine.

The gas (N_2 or H_2) flow rate was monitored using a Humonics (Model 520) digital flowmeter. The molar palladium (n) to F ratio spanned the range 0.3×10^{-3} – 2.5×10^{-3} h. In a series of blank tests, passage of MBA or DBA in a stream of H_2 through the empty reactor did not result in any detectable conversion. The reactor effluent was frozen in a liquid nitrogen trap for subsequent analysis by capillary GC (Perkin-Elmer Auto System XL chromatograph equipped with a programmed split/splitless injector and FID), employing a DB-1 capillary column (*i.d.* = 0.33 mm, length = 50 m, film thickness = 0.20 μm). The effluent gas from the DBA reaction was bubbled through a water trap (5 cm^3) to absrob NH_3 which is fully soluble in water at room temperature [38]. The pH is monitored (pH meter, Hanna Instruments) with time on-stream [39]. Reactant/product molar fractions (x_i) were obtained using detailed calibration (not shown). Fractional conversion (X_{reactant}), taking MBA as reactant, is given by

$$X_{MBA}\ (-) = \frac{[\text{MBA}]_{in} - [\text{MBA}]_{out}}{[\text{MBA}]_{in}} \qquad \textbf{(4.2)}$$

with product selectivity (S_i)

$$S_i\ (\%) = \frac{N_i x_i}{\sum N_i x_i} \times 100 \qquad \textbf{(4.3)}$$

where $[\text{MBA}]_{in}$ and $[\text{MBA}]_{out}$ represent the concentration of reactant entering (in) and leaving (out) the reactor and N_i is the stoichiometric coefficient for each product.

Repeated reactions with different samples from the same batch of catalyst delivered raw data reproducibility that was better than ±6%.

4.3 Results and Discussion

4.3.1 Production of DBA from MBA

The mechanism (see **Figure 4.1**) for the formation of secondary and/or tertiary amines from the corresponding mono-amine involves (i) dehydrogenation (MBA→BI), (ii) condensation with NH_3 release (BI+MBA→BBA) and (iii) hydrogenation (BBA→DBA) reactions [10]. As it is possible that the hydrogen released in dehydrogenation can participate in the subsequent reduction steps, we first assessed the requirement for H_2 in the feed by carrying out catalytic tests in N_2. Reaction over Pd/C

Table 4. 1 : Rate of di-butylamine (DBA) production (R_{DBA}) (in N_2 and H_2; P = 1 atm, T = 473 K) and physico-chemical properties of Pd/C and Pd/Al_2O_3 in terms of specific surface area (SSA), mean Pd particle size (obtained from (S)TEM ($d_{(S)TEM}$)), XPS (Pd 3$d_{5/2}$) binding energy (BE), H_2 chemisorbed and release during TPD.

Catalyst	Pd/C	Pd/Al_2O_3
R_{DBA} in N_2 ($mol_{DBA}\, h^{-1} mol_{Pd}^{-1}$)	38	17
R_{DBA} in H_2 ($mol_{DBA}\, h^{-1} mol_{Pd}^{-1}$)	104	77
SSA ($m^2\, g^{-1}$)	870	145
Pd size (nm, $d_{(S)TEM}$)	2.5	3.0
Pd 3$d_{5/2}$ BE (eV)	335.9	334.9
H_2 chemisorbed ($\times 10^{-2}$ mol mol_{Pd}^{-1})	27	22
H_2 TPD ($\times 10^{-2}$ mol mol_{Pd}^{-1})	849	102

and Pd/Al_2O_3 resulted in the sole formation of the target DBA, demonstrating effective transfer of the hydrogen generated in the dehydrogenation step for the conversion of BBA to DBA. In contrast, Kim *et al*. [9] reported that reaction in Ar over Cu/Al_2O_3 resulted only in the production of the intermediate alkylimine where a switch to H_2 was

required to further hydrogenate alkylimine to secondary amines. DBA production rate (R_{DBA}) was obtained from

$$R_{DBA}\ (\mathrm{mol_{DBA}\ h^{-1}\ mol_{Pd}^{-1}}) = \frac{X_{MBA} \times F}{2n} \qquad \textbf{(4.4)}$$

where n is molar amount of Pd catalysts. The values obtained are presented in **Table 4.1** where Pd/C shows a (two-fold) higher rate than Pd/Al_2O_3 for reaction in N_2. Activation of reactant [40,41] and/or available surface hydrogen [42] have been considered crucial in determining reaction rate in hydrogenation reactions. We have demonstrated that the support acidity favours the condensation reactions leading to the formation of higher amine in the hydrogenation of butyronitrile [42]. However, this is on the premise that nitrile has to be activated on the support [20,21] which was further reduced by the spillover hydrogen generating imine, involving in the following condensation reaction with amine to form higher amines. As we have also demonstrated that condensation reaction can take place on Pd without the involvement of any support [42]. In this study, it is feasible that amine as reactant adsorbed on Pd *via* the lone electron pair on N that acts as a Lewis base [43] which can donate electrons, through dehydrogenation to imine and then condense with amine to generate higher amines. To investigate the Pd charge

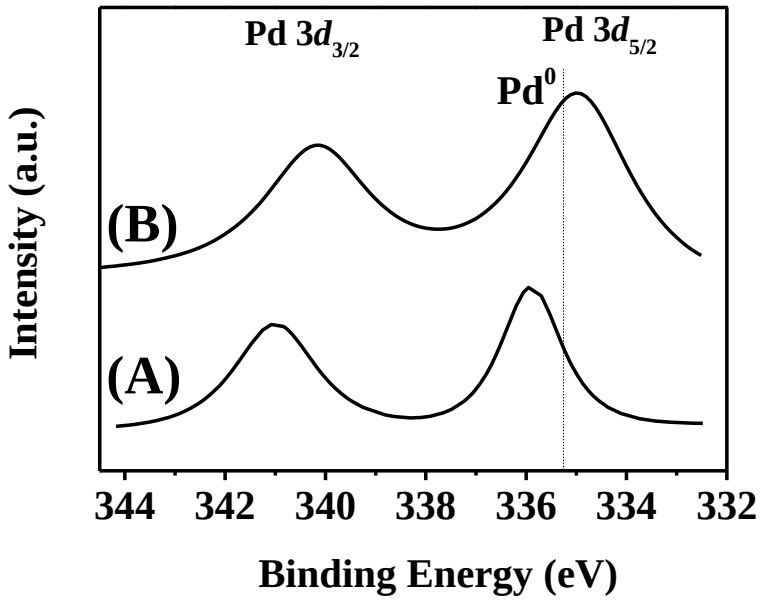

Figure 4. 2: XPS spectra over the Pd 3*d* binding energy (BE) region recorded for (A) Pd/C and (B) Pd/Al_2O_3.

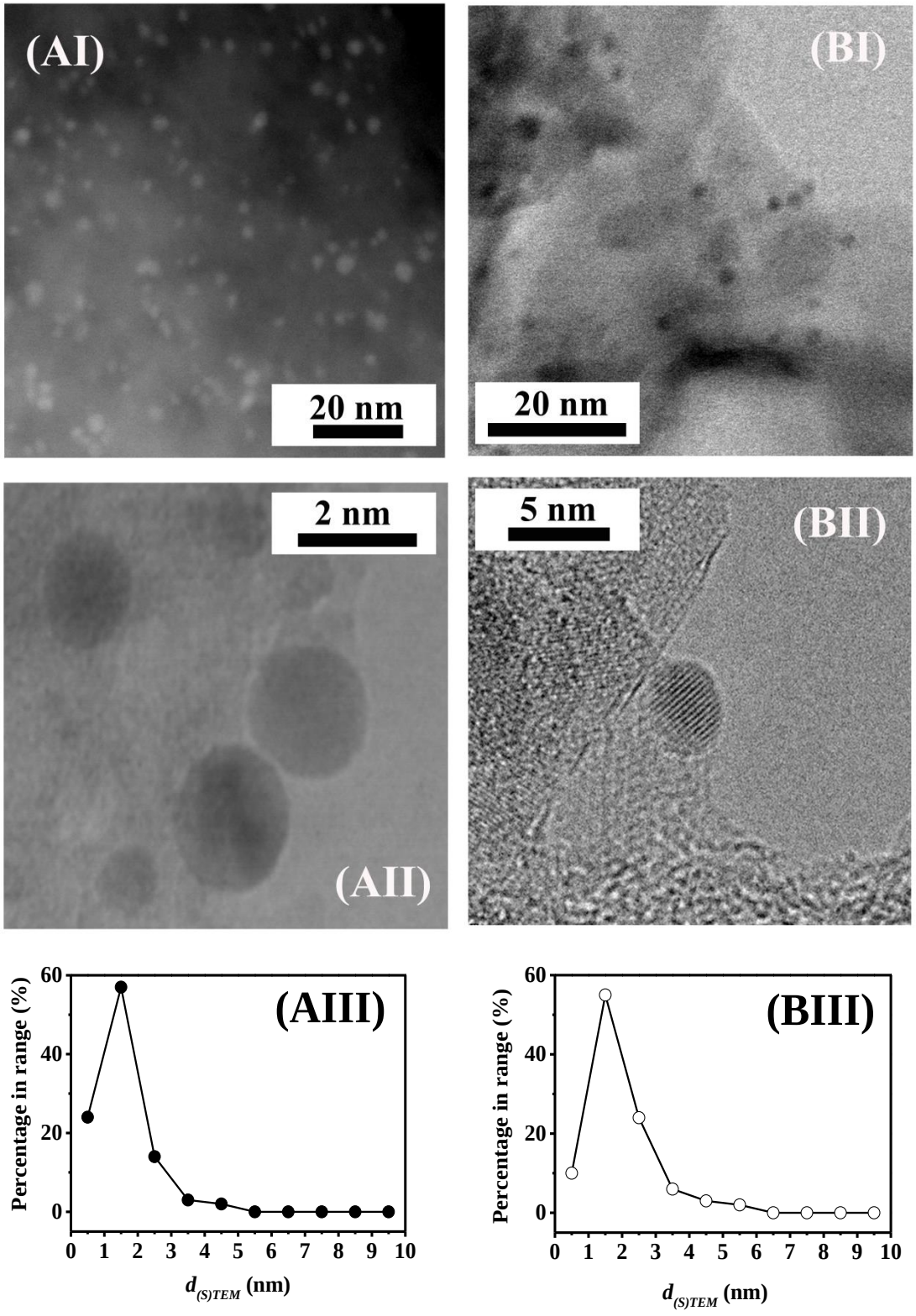

Figure 4. 3: Representative (I) medium and (II) high resolution TEM/STEM images with (III) associated Pd size distribution for (A) Pd/C and (B) Pd/Al_2O_3.

in interacting with the amine, Pd XPS analysis was conducted over the Pd 3*d* binding energy (BE) range and the resultant profiles are presented in **Figure 4.2** with BE values included in **Table 4.1**. Pd/C (**Figure 4.2(A)**) exhibited a Pd $3d_{5/2}$ signal (at 335.9 eV) that is 0.7 eV higher than metallic Pd (335.2 eV [44]), suggesting electron transfer to the carbon support with the generation of $Pd^{\delta+}$, as proposed elsewhere for nano-scale (4-12 nm) Pd on carbon [25,45]. In contrast, Pd/Al_2O_3 (**Figure 4.2(B)**) is characterised by a Pd $3d_{5/2}$ BE (334.9 eV) that is 0.3 eV lower than the metallic Pd reference, suggesting (partial) electron transfer from support to metal phase. This is in accordance with the reported occurrence of an electron-rich $Pd^{\delta-}$ (2-10 nm) phase on Al_2O_3 [25]. The STEM/TEM images provided in **Figure 4.3(I-II)** for Pd/C **(A)** and Pd/Al_2O_3 **(B)** reveal quasi-spherical particles at the nano-scale with a narrow (1-6 nm) size distribution (**Figure 4.3(III)**) and an equivalent mean (2.5-3.0 nm). The observed differences in reaction rate (**Table 4.1**) can not then be explained on the basis of Pd size. The carbon supported $Pd^{\delta+}$ facilities activation of the amine function (at the electron rich N atom) *via* electrostatic interaction, utilising the hydrogen generated in the dehydrogenation step for BBA hydrogenation. In contrast amine activation is inhibited on Pd/Al_2O_3 due to repulsion between $Pd^{\delta-}$ and $N^{\delta-}$, which can explain the lower DBA synthesis rate.

Given that DBA formation involves a hydrogenation (of BBA, **Figure 4.1**) step, the amount of surface hydrogen is an important parameter. Conversion of MBA over

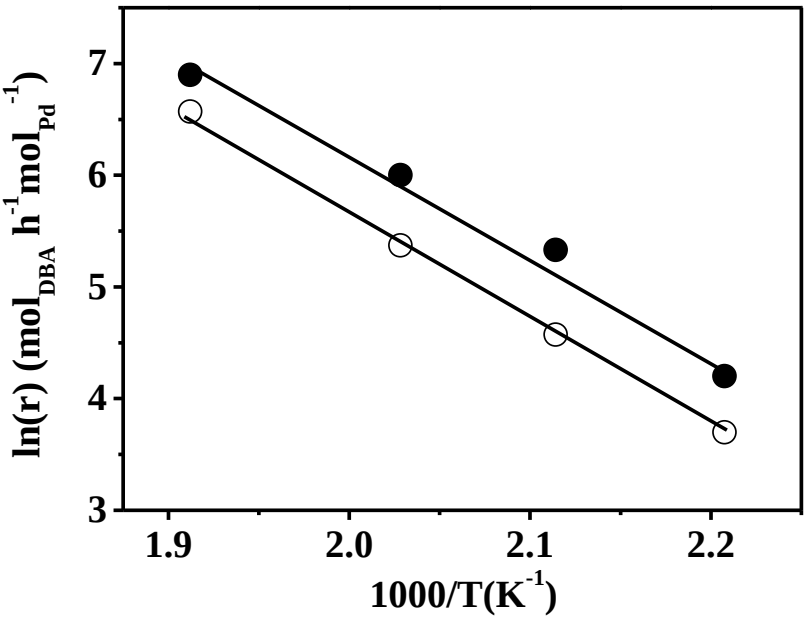

Figure 4. 4: Arrhenius plots associated with the condensation of MBA to DBA over Pd/C (●) and Pd/Al_2O_3 (○).

both catalysts in a flow of H_2 was again fully selective to DBA but at a significantly higher rate (**Table 4.1**) relative to reaction in N_2. Kamiguchi and co-workers [10], using Pd/C to promote the gas phase condensation of MBA (573-773 K), obtained BBA as the principal product and DBA as secondary product (selectivity < 13%). Exclusivity to DBA in this study was obtained at 453-523 K where higher temperatures are known to result in the desorption of amines and imines [46]. Under our reaction conditions, surface BBA hydrogenation (to DBA) proceeds without desorption. Total surface hydrogen was evaluated by H_2 TPD where, in both cases, H_2 release far exceeded that measured in the chemisorption step (**Table 4.1**). This suggests hydrogen spillover, *i.e.* H_2 dissociation on Pd sites with migration of atomic hydrogen to the support [47]. We can note studies that have established the occurrence of hydrogen spillover on activated carbon [48] and Al_2O_3 [49] supported Pd. Hydrogen desorption from Pd/C was appreciably greater than that from Pd/Al_2O_3 and can be linked to the higher SSA (**Table 4.1**) of Pd/C, which can accommodate more spillover [48]. Greater availability of surface hydrogen on Pd/C must promote the BBA→DBA step with resultant higher DBA rates (**Table 4.1**). The apparent activation energy (79 kJ mol^{-1}) from the Arrhenius plots in **Figure 4.4** converged for both catalysts and is close to that (75 ± 2 kJ mol^{-1}) reported for the formation of ethylamine over Raney nickel [50].

4.3.2 Production of TBA from DBA

Table 4. 2: Di-butylamine (DBA) consumption rate and selectivity to tri-butylamine (S_{TBA}) in single-, double- and triple- Pd/Al_2O_3 and Pd/C bed(s); *Reaction conditions*: P = 1 atm, T = 473 K, $n/F = 2.5 \times 10^{-3}$ h in H_2.

Catalyst	Pd/C		Pd/Al_2O_3	
	Rate ($mol_{DBA}\ h^{-1} mol_{Pd}^{-1}$)	S_{TBA} (%)	Rate ($mol_{DBA}\ h^{-1} mol_{Pd}^{-1}$)	S_{TBA} (%)
Single-bed	489	52	34	70
Double-bed	622	92	22	100
Triple-bed	698	100	-	-

Given the full selectivity to DBA from MBA, we explore here the feasibility of continuous TBA production from DBA as feed. The conversion of DBA over both Pd catalysts generated a mixture of MBA and TBA which is in line with a patent covering tertiary amine formation from lower amines using homogeneous catalysts ($RuCl_3 \cdot xH_2O$ and $P(C_6H_5)_3$) [29]. In terms of activity, Pd/C again delivered a significantly higher reaction rate in DBA conversion (**Table 4.2**) that can again be attributed to enhanced amine (DBA) activation on $Pd^{\delta+}$ and greater surface reactive hydrogen to promote imine (BEDA, **Figure 4.1**) hydrogenation. The selectivity response was independent of DBA conversion (**Figure 4.5**) where Pd/C generated equivalent amounts of TBA and MBA, whereas Pd/Al_2O_3 promoted preferential formation of TBA. Based on the product distributions, we propose the reaction mechanism in **Figure 4.6**. DBA adsorbs on Pd through the lone pair of electrons on N resulting in bond polarisation ($N^{\delta-}-C^{\delta+}$) with dehydrogenation to form the unsaturated imine (BBA) with polarised $N^{\delta-}=C^{\delta+}$. The

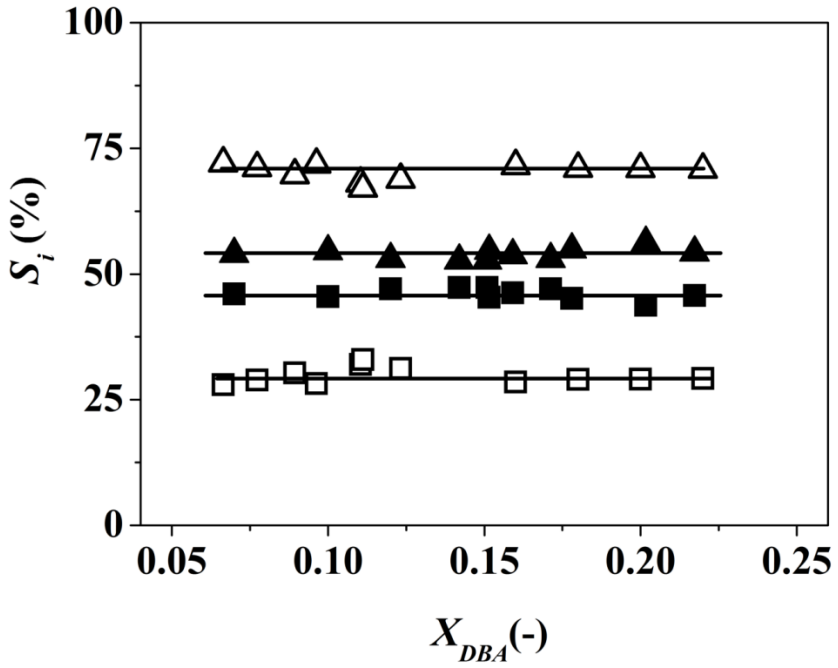

Figure 4. 5: Selectivity (S_i, %) to MBA (■, □) and TBA (▲, △) as a function of DBA fractional conversion (X_{DBA}) for reaction over Pd/C (solid symbols) and Pd/Al_2O_3 (open symbols). *Reaction conditions*: T = 4733 K, P = 1 atm; n/F = $0.3 \times 10^{-3} - 2.5 \times 10^{-3}$ h.

activated BBA can then react with adsorbed activated DBA with a surface rearrangement to generate a but-1-eny-dibutylamine (BEDA) intermediate with the release of 1 mole MBA as product. Surface hydrogenation to TBA as product then follows path (**I**) shown in **Figure 4.6**. Alternatively, the MBA formed undergoes condensation with BBA to generate TBA with loss of 1 mole NH_3 *via* path **(II)**. The

catalytic results suggest that reaction over Pd/C predominantly follows path **(I)** with rearrangement to generate a but-1-eny-dibutylamine (BEDA) intermediate with the release of 1 mole MBA as product. Surface hydrogenation to TBA as product then follows path (**I**) shown in **Figure 4.6**. Alternatively, the MBA formed undergoes condensation with BBA to generate TBA with loss of 1 mole NH_3 *via* path **(II)**. The catalytic results suggest that reaction over Pd/C predominantly follows path **(I)** with

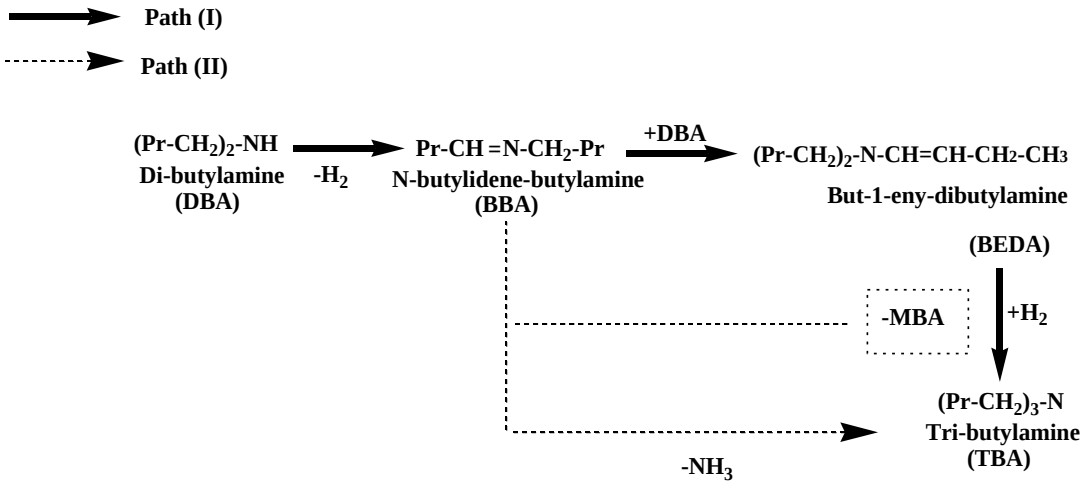

Figure 4. 6: Multiple catalyst bed reaction arrangement with associated product(s) from an inlet DBA reactant.

equi-molar production of TBA and MBA. Release of MBA from Pd/Al_2O_3 must not occur to the same extent and the reaction is directed along paths **(I)** and **(II)** with an overall greater relative enrichment of TBA in the product stream. The nitrogen in DBA bearing two electron-donating *n*-butyl chains is more electron-rich than in MBA [2] with a a consequent stronger interaction with $Pd^{\delta+}$ sites on C and competition for adsorption sites must result in a displacement of MBA from the surface by DBA reactant. On the other hand, $Pd^{\delta-}$ sites on Al_2O_3 exhibit greater repulsion with respect to DBA relative to MBA and the latter can undergo further condensation with BBA to form TBA (path **(II)**) with the release 1 mole of NH_3. This was demonstrated by pH monitoring of an aqueous trap used to collect volatiles downstream of the reactor where the far alkalinity of the exhaust stream from Pd/Al_2O_3 (pH = 9.5) relative to Pd/C (pH

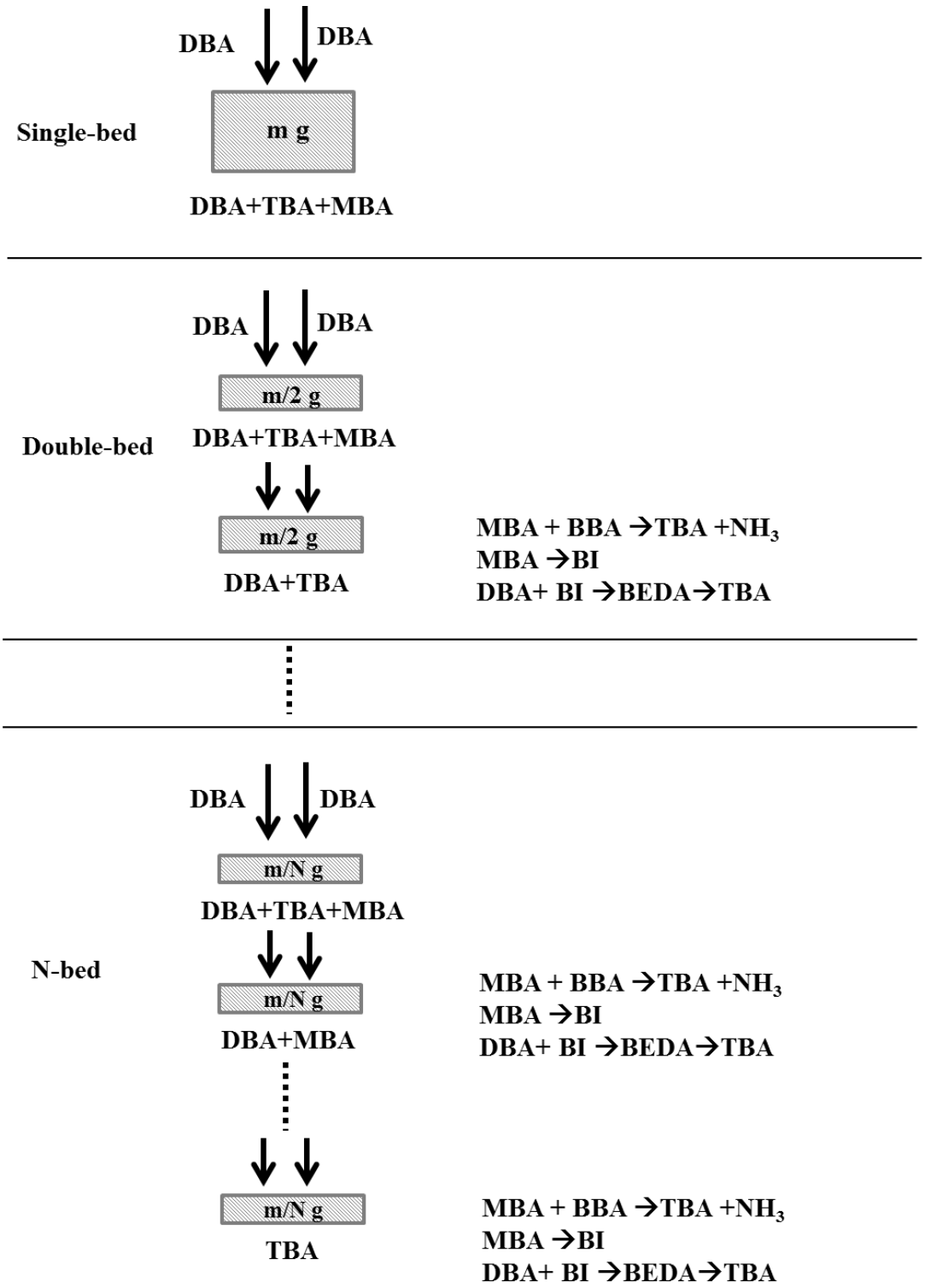

Figure 4. 7: Multiple catalyst bed reaction arrangement with associated product(s) from an inlet DBA reactant.

=7.8) establishes more NH_3 was produced from the former which corroborated the mechanism proposed for path **(II)**.

In the proposed reaction scheme, surface reaction of MBA with BBA results in higher TBA production *via* path **(II)**. Alternatively, MBA released could undergo dehydrogenation to BI which can react with DBA with further hydrogenation to TBA (**Figure 4.1**). In the single catalyst bed, a significantly component of MBA generated *via* path **(I)** enters the the product stream. Operation of a second catalyst bed in series should facilitate conversion of MBA exiting the first bed by (i) reaction with BBA generated *via* DBA dehydrogenation in the second bed (ii) dehydrogenation to BI and reaction with DBA. Both cases will lead to increased TBA yield. A simplified schematic diagram of the multiple catalyst bed arrangement and corresponding product distribution is presented in **Figure 4.7**. The experimental results obtained are provided in **Table 4.2** where the same total mass of catalyst was divided into N (= 1-3) beds with the same inlet DBA and H_2 flow rate. The contact time for each catalyst bed is decreased where MBA generated from first bed can enter the second bed for dehydrogenation generating intermediate BI reacting with DBA to form TBA until all the MBA generated were transformed to TBA with the increasing of catalyst beds. The multi-catalyst beds act as an 'recycle system' by transforming the unreacted MBA instead of releasing into the stream. An increase in overall reaction rate and TBA selectivity was observed with increasing number of beds to attain target tertiary amine exclusivity in the double-bed for Pd/Al_2O_3 and triple-bed for Pd/C. This is the first time that full selectivity to a tertiary amine from a secondary amine feedstock has been reported. The higher TBA selectivity achieved over Pd/Al_2O_3 relative to Pd/C (**Figure 4.5**) translated into a requisite lower number of catalyst beds in series to achieve full TBA selectivity.

4.4 Conclusions

We have established, for the first time, exclusive formation of higher amines (DBA and TBA) from a lower amine (MBA and DBA, respectively) feedstock over nano-scale Pd (mean size *ca*. 3 nm from TEM/STEM) supported on C and Al_2O_3 in gas phase continuous operation. Full selectivity in the conversion of MBA to DBA was attained over both catalysts with an associated apparent activation energy = 79 kJ mol^{-1}. Increased activity was recorded on switching from MBA condensation in N_2 to H_2 where Pd/C delivered a significantly higher DBA production rate. This is explained on the basis of enhanced amine activation on carbon supported $Pd^{\delta+}$ (from XPS) sites and

higher level of spillover hydrogen (from H_2 TPD). Exclusive formation of TBA (from DBA) has been achieved over both catalysts where operation of beds in series resulted in higher TBA production rates. A reaction mechanism is proposed that can account for our experimental observations. The results from this work can serve as a basis for an alternative efficient and clean continuous production of higher amines from a lower amine feedstock.

4.5 References

[1] W. He, L. Wang, C. Sun, K. Wu, S. He, J. Chen, P. Wu, Z. Yu *Pt–Sn/γ-Al_2O_3-catalyzed highly efficient direct synthesis of secondary and tertiary amines and imines*, Chem. A. Eur. J. 17 (**2011**) 13308-13317.

[2] S.A. Lawrence, *Amines: Synthesis, Properties and Applications* Cambridge University Press, Cambridge (**2004**) 73-73.

[3] X. Wang, S. Liu, T. Yu, Y. Chai, *Synthesis of tertiary aliphatic amines*, Eur. Chem. Bull. 3 (**2014**) 55-57.

[4] R.N. Salvatore, C.H. Yoon, K.W. Jung, *Synthesis of secondary amines*, Tetrahedron 57 (**2001**) 7785-7811.

[5] T.T. Dang, B. Ramalingam, S.P. Shan, A.M. Seayad, *An efficient palladium-catalyzed n-alkylation of amines using primary and secondary alcohols*, ACS Catal. 3 (**2013**) 2536-2540.

[6] L. He, Y. Qian, R.-S. Ding, Y.-M. Liu, H.-Y. He, K.-N. Fan, Y. Cao, *Highly efficient heterogeneous gold-catalyzed direct synthesis of tertiary and secondary amines from alcohols and urea*, ChemSusChem 5 (**2012**) 621-624.

[7] O. Mitsunobu, *Comprehensive organic synthesis: Heteroatom manipulation*. Vol. 6, Pergamon Press, 1993.

[8] M.S. Kwon, S. Kim, S. Park, W. Bosco, R.K. Chidrala, J. Park, *One-pot synthesis of imines and secondary amines by Pd-catalyzed coupling of benzyl alcohols and primary amines*, J. Org. Chem. 74 (**2009**) 2877-2879.

[9] I. Kim, S. Itagaki, X.J. Jin, K. Yamaguchi, N. Mizuno, *Heterogeneously catalyzed self-condensation of primary amines to secondary amines by supported copper catalysts*, Catal. Sci. Technol. 3 (**2013**) 2397-2403.

[10] S. Kamiguchi, N. Ikeda, S. Nagashima, H. Kurokawa, H. Miura, T. Chihara, *Catalytic condensation of primary amines, dehydrogenation of secondary amines,*

and dealkylation of tertiary amines over solid-state rhenium sulfide clusters with an octahedral metal framework, J. Clust. Sci. 20 (**2009**) 683-693.

[11] K. Bui-The, C. Concilio, G. Porzi, *A facile synthesis of symmetrical secondary amines from primary amines promoted by the homogeneous catalyst $RuCl_2(Ph_3P)_3$*, J. Organomet. Chem. 208 (**1981**) 249-251.

[12] S. Murahashi, N. Yoshimura, T. Tsumiyama, T. Kojima, *Catalytic alkyl group exchange reaction of primary and secondary amines*, J. Am. Chem. Soc. 105 (**1983**) 5002-5011.

[13] M. Yamashita, Y. Moroe, T. Yano, K. Nozaki, *A catalytic synthesis of dialkylamines from alkylamines using neopentyl-substituted pnp pincer–iridium complex*, Inorg. Chim. Acta 369 (**2011**) 15-18.

[14] L.L.R. Lorentz-Petersen, P. Jensen, R. Madsen, *Iridium-catalyzed condensation of primary amines to form secondary amines*, Synth.-Stuttgart (**2009**) 4110-4112.

[15] A. Miyazawa, K. Saitou, K. Tanaka, T.M. Gädda, M. Tashiro, G.K.S. Prakash, G.A. Olah, *Reaction of primary amines with Pt/C catalyst in water under microwave irradiation: A convenient synthesis of secondary amines from primary amines*, Tetrahedron Lett. 47 (**2006**) 1437-1439.

[16] C. Amorim, M.A. Keane, *Effect of surface acid groups associated with amorphous and structured carbon on the catalytic hydrodechlorination of chlorobenzenes*, J. Chem. Technol. Biothechnol. 83 (**2008**) 662-672.

[17] F. Rodríguez-Reinoso, *The role of carbon materials in heterogeneous catalysis*, Carbon 36 (**1998**) 159-175.

[18] C. Morterra, G. Magnacca, *A case study: Surface chemistry and surface structure of catalytic aluminas, as studied by vibrational spectroscopy of adsorbed species*, Catal. Today 27 (**1996**) 497-532.

[19] S. Kim, O. Byl, J.T. Yates, *Adsorption of triethylenediamine on Al_2O_3-III: Bonding to lewis acid Al^{3+} sites*, J. Phys. Chem. B 109 (**2005**) 6331-6333.

[20] I. Ortiz-Hernandez, C.T. Williams, *In situ studies of butyronitrile adsorption and hydrogenation on Pt/Al_2O_3 using attenuated total reflection infrared spectroscopy*, Langmuir 23 (**2007**) 3172-3178.

[21] M.R. Strunk, C.T. Williams, *Aliphatic nitrile adsorption on Al_2O_3 and ZrO_2 as studied by total internal reflection sum-frequency spectroscopy*, Langmuir 19 (**2003**) 9210-9215.

[22] M.C. Abello, A.P. Velasco, O.F. Gorriz, J.B. Rivarola, *Temperature-programmed desorption study of the acidic properties of γ-alumina*, Appl. Catal. A: Gen. 129 (**1995**) 93-100.

[23] P. Braos-García, P. Maireles-Torres, E. Rodríguez-Castellón, A. Jiménez-López, *Gas-phase hydrogenation of acetonitrile on zirconium-doped mesoporous silica-supported nickel catalysts*, J. Mol. Catal. A: Chem. 193 (**2003**) 185-196.

[24] M.J.F.M. Verhaak, A.J. Dillen, J.W. Geus, *The selective hydrogenation of acetonitrile on supported nickel catalysts*, Catal. Lett. 26 (**1994**) 37-53.

[25] F. Cárdenas-Lizana, Y. Hao, M. Crespo-Quesada, I. Yuranov, X. Wang, M.A. Keane, L. Kiwi-Minsker, *Selective gas phase hydrogenation of p-chloronitrobenzene over Pd catalysts: Role of the support*, ACS Catal. 3 (**2013**) 1386-1396.

[26] Y.Y. Huang, W.M.H. Sachtler, *Catalytic hydrogenation of nitriles over supported mono- and bimetallic catalysts*, J. Catal. 188 (**1999**) 215-225.

[27] M. Arai, Y. Takada, Y. Nishiyama, *Effects of metal particle size in gas-phase hydrogenation of acetonitrile over silica-supported platinum catalysts*, J. Phys. Chem. B 102 (**1998**) 1968-1973.

[28] N. Iwasa, M. Yoshikawa, M. Arai, *Selective hydrogenation of acetonitrile to ethylamine using palladium-based alloy catalysts*, Phys. Chem. Chem. Phys. 4 (**2002**) 5414-5420.

[29] Donald M. Fenton, C. Anaheim, *United states patent*, US Patent 3,726,925 (**1973**).

[30] Y. Izawa, D. Pun, S.S. Stahl, *Palladium-catalyzed aerobic dehydrogenation of substituted cyclohexanones to phenols*, Science 333 (**2011**) 209-213.

[31] R. Maatman, W. Ribbens, B. Vonk, *The role of Pd-alumina catalyst in the dehydrogenation of cyclohexane*, J. Catal. 31 (**1973**) 384-388.

[32] L. Rodríguez, D. Romero, D. Rodríguez, J. Sánchez, F. Domínguez, G. Arteaga, *Dehydrogenation of n-butane over Pd–Ga/Al_2O_3 catalysts*, Appl. Catal. A: Gen. 373 (**2010**) 66-70.

[33] M. Sobota, I. Nikiforidis, M. Amende, B.S. Zanón, T. Staudt, O. Höfert, Y. Lykhach, C. Papp, W. Hieringer, M. Laurin, D. Assenbaum, P. Wasserscheid, H.-P. Steinrück, A. Görling, J. Libuda, *Dehydrogenation of dodecahydro-n-ethylcarbazole on Pd/Al_2O_3 model catalysts*, Chem. A. Eur. J. 17 (**2011**) 11542-11552.

[34] J. Haro, R. Gómez, J.M. Ferreira, *The role of palladium in dehydrogenation of cyclohexane over Pt-Pd/Al_2O_3 bimetallic catalysts*, J. Catal. 45 (**1976**) 326-331.

[35] H.-U. Blaser, A. Indolese, A. Schnyder, H. Steiner, M. Studer, *Supported palladium catalysts for fine chemicals synthesis*, J. Mol. Catal. A: Chem. 173 (**2001**) 3-18.

[36] A.J. Yap, A.F. Masters, T. Maschmeyer, *The kinetic features of the palladium-catalyzed hydrogenolysis of nitriles and amines*, ChemCatChem 4 (**2012**) 1179-1184.

[37] M. Armbrüster, M. Behrens, F. Cinquini, K. Föttinger, Y. Grin, A. Haghofer, B. Klötzer, A. Knop-Gericke, H. Lorenz, A. Ota, S. Penner, J. Prinz, C. Rameshan, Z. Révay, D. Rosenthal, N. Rupprechter, P. Sautet, R. Schlögl, L. Shao, L. Szentmiklósi, D. Teschner, D. Torres, R. Wagner, R. Widmer, G. Wowsnick, *How to control the selectivity of palladium-based catalysts in hydrogenation reactions: The role of subsurface chemistry*, ChemCatChem 4 (**2012**) 1048-1063.

[38] G.P. Ayears, R.W. Gillett, E.R. Caeser, *Solubility of ammonia in water in the presence of atmospheric CO_2.*, Tellus 37B (**1985**) 35-40.

[39] S. Gómez-Quero, F. Cárdenas-Lizana, M.A. Keane, *Effect of metal dispersion on the liquid-phase hydrodechlorination of 2,4-dichlorophenol over Pd/Al_2O_3,* Ind. Eng. Chem. Res. 47 (**2008**) 6841-6853.

[40] M. Okamoto, T. Hirao, T. Yamaai, *Polymers as novel modifiers for supported metal catalyst in hydrogenation of benzaldehydes*, J. Catal. 276 (**2010**) 423-428.

[41] A.M.H. Rasmussen, M.N. Groves, B. Hammer, *Remote activation of chemical bonds in heterogeneous catalysis*, ACS Catal. 4 (**2014**) 1182-1188.

[42] Y. Hao, X. Wang, N. Perret, F. Cárdenas-Lizana, M.A. Keane, *An analysis of acid-base and metal-support effects in the gas phase hydrogenation of butyronitrile over palladium* Catal. Struct. React. 1 (**2015**) 1-8.

[43] J.J.W. Bakker, A.G.v.d. Neut, M.T. Kreutzer, J.A. Moulijn, F. Kapteijn, *Catalyst performance changes induced by palladium phase transformation in the hydrogenation of benzonitrile*, J. Catal. 274 (**2010**) 176-191.

[44] M. Brun, A. Berthet, J.C. Bertolini, *XPS, AES and auger parameter of Pd and PdO*, J. Electron Spectrosc. 104 (**1999**) 55-60.

[45] L. Jiang, H. Gu, X. Xu, X. Yan, *Selective hydrogenation of o-chloronitrobenzene (o-CNB) over supported pt and pd catalysts obtained by laser vaporization deposition of bulk metals*, J. Mol. Catal. A: Chem. 310 (**2009**) 144-149.

[46] P. Braos-García , P. Maireles-Torres, E. Rodríguez-Castellón , A. Jiménez-López *Gas-phase hydrogenation of acetonitrile over nickel supported on alumina- and*

mixed alumina/gallium oxide-pillared tin phosphate catalysts, J. Mol. Catal. A: Chem. 168 (**2001**) 279-287.

[47] R. Prins, *Hydrogen spillover. Facts and fiction*, Chem. Rev. 112 (**2012**) 2714-2738.

[48] C. Amorim, M.A. Keane, *Palladium supported on structured and nonstructured carbon: A consideration of Pd particle size and the nature of reactive hydrogen*, J. Colloid Interf. Sci. 322 (**2008**) 196-208.

[49] W.C. Conner, J.L. Falconer, *Spillover in heterogeneous catalysis*, Chem. Rev. 95 (**1995**) 759-788.

[50] F. Hochard, H. Jobic, J. Massardier, A.J. Renouprez, *Gas-phase hydrogenation of acetonitrile on raney-nickel catalysts - reactive hydrogen*, J. Mol. Catal. A: Chem. 95 (**1995**) 165-172.

Chapter 5

Selective Production of Benzylamine *via* Gas Phase Hydrogenation of Benzonitrile over Supported Pd Catalysts

In the previous Chapter the viability of the synthesis of higher aliphatic amines from a lower amine feed is established for the operation of multiple catalyst beds in series. That work is extended in this Chapter with a demonstration of the applicability of this methodology for the transformation of an aromatic nitrile (benzonitrile).

5.1 Introduction

Benzylamine is a versatile chemical used in the production of Vitamin H (Biotin), as an intermediate for photographic chemicals, in the manufacture of cationic paints and as an active ingredient in the synthesis of nylon fibres [1]. The hydrogenation of benzonitrile (BN), as the principal route to benzylamine (BA) [2,3], is challenging due to low selectivity as a result of undesired condensation and hydrogenolysis [4], see **Figure 5.1**. Benzylideneimine (BI) as a reactive intermediate can undergo condensation to generate dibenzylamine (DBA) with NH_3 elimination [4-6]. Toluene (TOL) can result from hydrogenolysis of the amine, diamine or even the starting nitrile [1,4]. Benzonitrile hydrogenation has been established in liquid phase under supercritical conditions at elevated H_2 pressure (6-100 bar [4,6-11]) over supported metal (Ni [6,12], Pt [10], Rh [10] and Pd [4,7-11]) catalysts. Chatterjee *et al.* [10] reported high activity and selectivity (91%) to benzylamine in supercritical CO_2 (80-100 bar) over MCM-41 supported Pd relative to Pt, Rh and Ni where the following sequence of decreasing turnover frequency (*TOF*) was established: Pd (4151 h^{-1}) > Pt (553 h^{-1}) > Rh (42 h^{-1}) > Ni (6 h^{-1}). Yoshida and co-workers [7] achieved improved benzylamine selectivity (up to 98%) over Pd/Al_2O_3 in a biphasic (CO_2 + H_2O) medium (at 70 bar), which they ascribed to benzylamine transfer into the aqueous phase that prevented undesired condensation to dibenzylamine. The energy demands associated with supercritical CO_2 lowers process efficiency. In batch liquid phase operation, Bakker *et al*. [4] reported decreasing benzylamine selectivity, in the order Pd/Al_2O_3 > Pd/C > $Pd/BaCO_3$, at a fixed benzonitrile conversion (X = 0.5) but did not provide any explanation for a possible support effect. We can also note the work of López-de Jesús *et al*. [9] where

benzylamine was generated as principal product (selectivity = 50%-72%) over Pd/Al_2O_3 with secondary formation of dibenzylamine. The nature of the solvent and use of acids have been shown to influence selectivity. Cheng *et al.* [12] observed a range of benzylamine selectivity (8%-94%) in different solvents (hexane, ethanol, H_2O, H_2O-CO_2) that was ascribed to variation in amine (and imine) solubility. Enhanced primary amine selectivity (up to 95%) over Pd/C has been achieved with the addition of sodium dihydrogen phosphate (NaH_2PO_4) [6] that reacts with the intermediate imine to inhibit secondary amine formation. However, the requirement for separation and purification unit operations to extract the target product represents a decided drawback in terms of sustainable/clean synthesis.

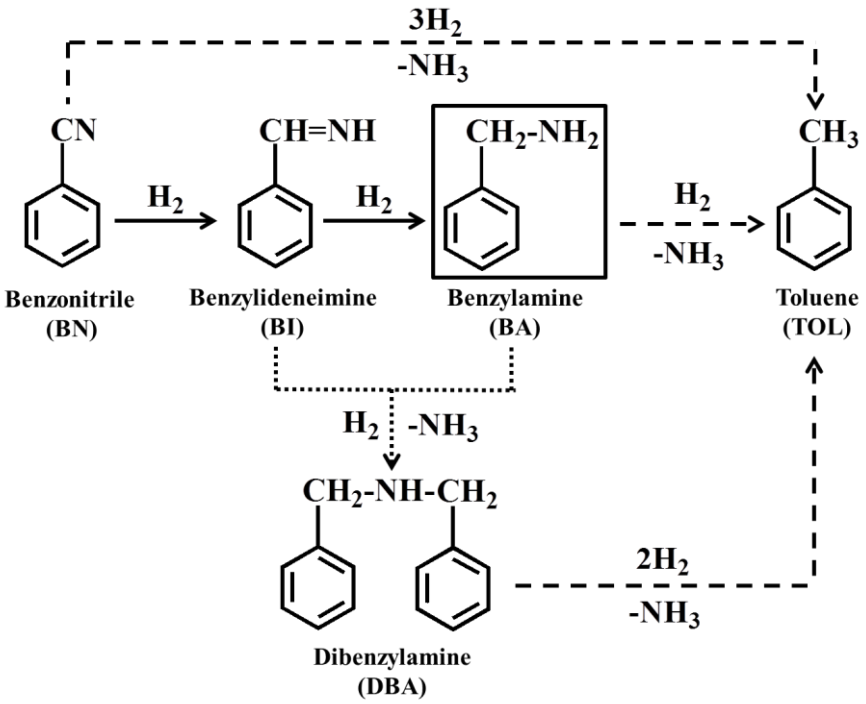

Figure 5. 1: Reaction pathways associated with the hydrogenation of benzonitrile (BN) to target (framed) benzylamine (BA, solid arrows), condensation to dibenzylamine (DBA, dotted arrows) and hydrogenolysis to toluene (TOL, dashed arrows).

A "white paper" by the American Chemical Society in conjunction with the Green Chemistry Institute and global pharmaceutical corporations ranked the move from batch to continuous processing as #1 priority to achieve sustainable chemical processes with related research given the highest strategic importance [13]. A search through literature has revealed only two studies of gas-phase continuous hydrogenation of benzonitrile [14,15]. Near exclusive (99% selectivity) benzylamine formation was

achieved over Cu-MgO (T = 513 K, WHSV= 1 h^{-1}) but with four orders of magnitude lower reaction rate (8.1×10^{-4} mol h^{-1} mol_{Cu}^{-1}) [14] relative to batch liquid phase reaction over supported Pd (4.7 mol h^{-1} mol_{Pd}^{-1}) [6]. Gas phase conversion over Ni/Al_2O_3 resulted in sole amine formation but at low conversions (<5%) [15]. We have targeted full benzylamine selectivity in the gas phase reduction of benzonitrile at high conversions, circumventing condensation and hydrogenolysis by-products. Taking the high activity exhibited by Pd in liquid phase operation [10,11], we have examined the possible role of support (carbon and alumina) on the catalytic action of Pd in gas phase reaction and consider the use of catalyst beds in series to promote amine production.

5.2 Experimental

5.2.1 Materials and Catalyst Activation

Commercial (1% wt.) Pd/C and (1.2% wt.) Pd/Al_2O_3 catalysts were obtained from Sigma-Aldrich. Prior to use, the samples were sieved to 75 μm mean diameter and activated in 60 cm^3 min^{-1} H_2 at 2 K min^{-1} to 573 K, which was maintained for 1 h to ensure the complete reduction to zero valent Pd [16]. Samples for off-line characterisation analysis were passivated in 1% v/v O_2/He at ambient temperature.

5.2.2 Catalyst Characterisation

The Pd content was measured by inductively coupled plasma-optical emission spectrometry (ICP-OES, Vista-PRO, Varian Inc.) from the diluted extract in HF. Chemisorption (H_2 and NH_3), temperature programmed desorption (TPD) and specific surface area (SSA) measurements were conducted using the commercial CHEM-BET 3000 (Quantachrome) unit. Each sample was loaded into a U-shaped Quartz cell (3.76 mm *i.d.*) and heated in 17 cm^3 min^{-1} (Brooks mass flow controlled) 5% v/v H_2/N_2 at 2 K min^{-1} to 573 ± 1 K. The reduced samples were maintained at the final temperature in a flow of H_2/N_2 until the signal returned to baseline, swept with 65 cm^3 min^{-1} N_2 for 1.5 h, cooled to ambient temperature and subjected to H_2 (or NH_3) chemisorption using a pulse (50-1000 μl) titration procedure. Samples were thoroughly flushed in N_2 and subjected to TPD (at 10-50 K min^{-1}) to 950-1200 K. The resultant profile was corrected using the TPD profile recorded in parallel directly following activation to explicitly determine H_2 (or NH_3) release. SSA was recorded with a 30% v/v N_2/He flow using undiluted N_2 (99.9%) as internal standard. Three cycles of N_2 adsorption-desorption in

the flow mode were employed to determine SSA using the standard single point BET method; SSA and H_2/NH_3 uptake/release were reproducible to within ±5% and the values quoted represent the mean. X-ray photoelectron spectroscopy (XPS) analyses were conducted on an Axis Ultra instrument (Kratos Analytical) under ultra-high vacuum conditions ($<10^{-8}$ Torr) using a monochromatic Al Kα X-ray source (1486.6 eV). The source power was maintained at 150 W and the emitted photoelectrons were sampled from a 750 × 350 μm^2 area at a take-off angle = 90°. The analyser pass energy was 80 eV for survey spectra (0–1000 eV) and 40 eV for high resolution spectra (Pd $3d_{5/2}$ and $3d_{3/2}$). The adventitious carbon 1*s* peak was calibrated at 284.5 eV and used as an internal standard to compensate for charging effects. Palladium particle morphology (shape and size) was determined by scanning transmission electron microscopy (STEM, JEOL 2200FS field emission unit), employing Gatan DigitalMicrograph 1.82 for data acquisition/manipulation. Samples for analysis were crushed and deposited (dry) on a holey carbon/Cu grid (300 Mesh). Up to 800 individual Pd particles were counted for each catalyst and the surface area-weighted mean Pd diameter (d_{STEM}) was calculated from

$$d_{STEM} = \frac{\sum_i n_i d_i^3}{\sum_i n_i d_i^2} \qquad \textbf{(5.1)}$$

where n_i is the number of particles of diameter d_i.

5.2.3 Catalytic Procedure

Reactions of benzonitrile/benzylamine (Sigma-Aldrich, purity ≥99%) were conducted *in situ*, immediately following catalyst activation, under atmospheric pressure at 353 K in a fixed bed vertical glass reactor (*i.d.* = 15 mm). The reactant was delivered as a 2-propanol (Sigma-Aldrich, purity ≥99.5%) solution at a fixed calibrated flow rate (Model 100 kd scientific microprocessor-control infusion pump) to the reactor *via* a glass/teflon *air*-tight syringe and teflon line in a co-current flow of H_2 (BOC, >99.98%, *GHSV* = 2×10^4 h^{-1}). A layer of borosilicate glass beads served as preheating zone where the organic reactant was vaporised and reached reaction temperature before contacting the catalyst. Isothermal conditions (±1 K) were maintained by diluting the catalyst bed with ground glass (75 μm); the ground glass was

mixed thoroughly with catalyst before insertion in the reactor. The reaction temperature was continuously monitored using a thermocouple inserted in a thermowell within the catalyst bed. Catalyst performance in a multiple bed arrangement was tested for Pd/Al_2O_3 where each catalyst bed was separated by glass wool (10 mm); catalyst activation followed the procedure described above. The inlet molar reactant flow rate was in the range 0.18-0.36 mmol h^{-1} where the H_2 content was up to 900 times in excess of the stoichiometric requirement for amine production. Gas flow rate was monitored using a Humonics (Model 520) digital flowmeter. The molar palladium (n) to inlet reactant ratio (n/F) spanned the range = $1.3 \times 10^{-3} – 3.6 \times 10^{-2}$ h. Although the reaction temperature (353 K) was well below the boing point of the reactant (benzonitrile) and the proposed products (benzylamine and toluene), the partial pressure for the benzonitrile was calculated according to the composition of the component and compared with the saturated vapor pressure derived from Antoine equation respectively at the reaction conditions as shown in **Appendix 2**. The inlet flow of benzonitrile showed a partial pressure of 221.9 Pa which was one magnitude lower than the saturated vapor pressure (2230 Pa) ensuring the gasification of the reactant. Benzylamine (22.5 Pa) and toluene (22.3 Pa) also exhibited a great lower partial pressure than the saturated vapor pressure of 23000 and 38636 Pa respectively, suggesting the vapor phase the products. In a series of blank tests, passage of benzonitrile or benzylamine in a stream of H_2 through the empty reactor did not result in any detectable conversion. The reactor effluent was frozen in a liquid nitrogen trap for subsequent analysis using a Perkin-Elmer Auto System XL chromatograph equipped with a programmed split/splitless injector and a flame ionization detector, employing a DB-1 capillary column (*i.d.* = 0.33 mm, length = 50 m, film thickness = 0.20 μm). Fractional benzylamine conversion (X) is given by

$$X = \frac{[Benzonitrile]_{in} - [Benzonitrile]_{out}}{[Benzonitrile]_{in}} \qquad \textbf{(5.2)}$$

with selectivity (S) to product i

$$S_i\ (\%) = \frac{[Product]_{i,\,out}}{[Benzonitrile]_{in} - [Benzonitrile]_{out}} \times 100 \qquad \textbf{(5.3)}$$

where subscripts "in" and "out" represent the reactor inlet and outlet effluent streams. Repeated reactions with different samples of catalyst delivered raw data reproducibility that was better than ±5%.

5.3 Results and Discussion

5.3.1 Pd/C: Characterisation and Catalyst Test Results

The physicochemical properties of Pd/C are summarised in **Table 5.1** where the SSA (870 m^2 g^{-1}) is close to that (875 m^2 g^{-1}) reported previously [17]. Supported Pd particle size was determined by H_2 chemisorption (assuming dissociative adsorption with H_2/Pd adsorption stoichiometry = 1/2 [18]) and validated by STEM analysis. The representative STEM image given in **Figure 5.2(I)** reveals pseudo-spherical Pd nano-particles with a narrow size distribution (<5 nm, **Figure 5.2(II)**) and mean of 2.5 nm that is in good agreement with that (2.2 nm) obtained from H_2 uptake. Hydrogen temperature programmed desorption (TPD) generated the profile presented in **Figure 5.2(III)** where a two-stage H_2 release is evident with temperature maxima (T_{max}) at 789 K and 1148 K. The lower temperature H_2 release was close to the chemisorbed component (3.1 ± 0.2 mmol g_{Pd}^{-1}). Higher temperature desorption can be attributed to spillover hydrogen generated during thermal activation [19], *i.e.* migration of atomic hydrogen to the support following dissociation at Pd sites. Desorption of spillover species has been shown to require higher temperature than release of hydrogen [20,21].

Reported surface acidities of supported metal systems has relied on NH_3 desorption measurements [19,21,22]. In this study, NH_3 chemisorption matched that released by TPD (**Table 5.1**) with an associated T_{max} = 490 K (**Figure 5.2(IV)**) that is within the range (444-573 K) reported for activated carbon supported Pd [23]. In order to gain insight into the electronic character of the Pd phase, XPS analysis over Pd 3*d* binding energy (BE) region was conducted (**Figure 5.2(V)**). The Pd $3d_{5/2}$ signal (at 335.9 eV) is 0.7 eV higher than metallic Pd (335.2 eV [24]), suggesting electron transfer to the carbon support with the generation of $Pd^{\delta+}$, as proposed elsewhere for nano-scale (4-12 nm) Pd on carbon [16,25].

Product selectivity (S_i) as a function of contact time (n/F) is presented in **Figure 5.2(VI)**. Toluene was generated as the principal product (S_i > 80%) at lower n/F (< 8 × 10^{-3} h) with secondary benzylamine formation. At extended contact time, toluene was the sole product and can be formed from direct hydrogenolysis of the nitrile reactant or

Table 5. 1: **Palladium loading, specific surface area (SSA), Pd particle size (from H_2 chemisorption and STEM analysis), H_2 and NH_3 chemisorption and release during TPD.**

Catalyst	Pd (% wt.)	SSA ($m^2\ g^{-1}$)	Pd particle size (nm)		H_2 uptake (mmol g_{Pd}^{-1})	H_2 TPD (mmol g_{Pd}^{-1})	NH_3 uptake (mmol g^{-1})	NH_3 release (mmol g^{-1})
			H_2 chemisorption	STEM				
Pd/C	1.0	870	2.2	2.5	2.5	80	0.94	0.92
Pd/Al_2O_3	1.2	145	2.4	3.0	2.1	10	0.52	0.51

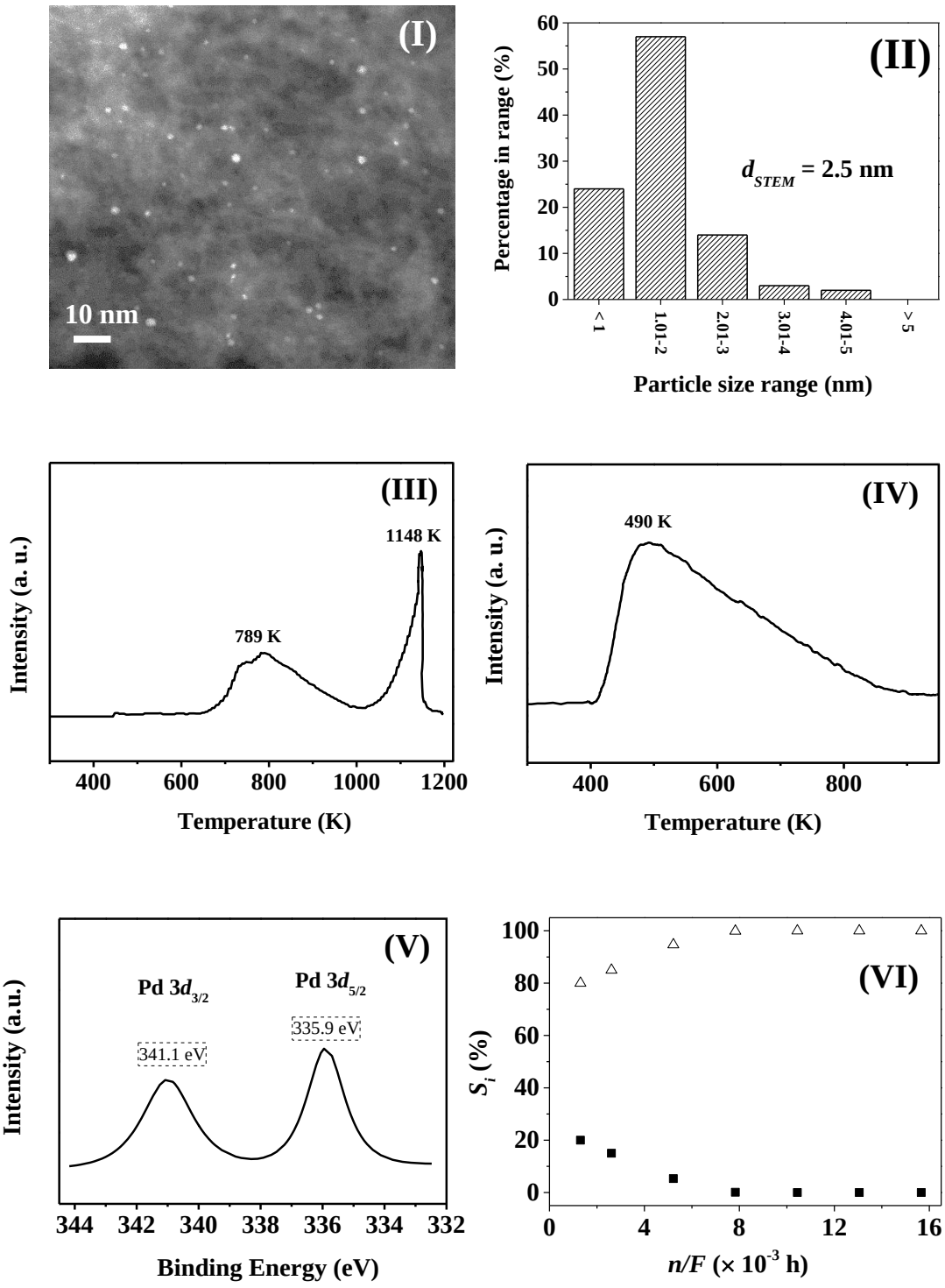

Figure 5. 2: (I) Representative STEM image with (II) associated Pd particle size distribution, (III) H_2 and (IV) NH_3 TPD profiles, (V) XPS profile and (VI) dependence of selectivity (S_i) to benzylamine (■) and toluene (△) on contact time (n/F) for Pd/C. *Reaction conditions*: T = 353 K, P_{H_2}= 1 atm.

subsequent hydrogenolysis of benzylamine and/or dibenzylamine (see dashed arrows in **Figure 5.1**). Under the same reaction conditions, use of benzylamine as feedstock generated toluene, demonstrating feasibility of this hydrogenolysis step. There was no detectable dibenzylamine, a result that deviates from liquid phase reaction systems where secondary amine formation (S < 14%) was observed over Pd/C [6,8]. This suggests that condensation of the imine intermediate with benzylamine was circumvented, possibly due to the shorter contact time in continuous gas phase continuous. Nitrile reduction to primary amine proceeds *via* a nucleophilic mechanism where hydrogen (as a weak nucleophile) attacks activated C≡N to generate the reactive imine (C=N) that undergoes further hydrogenation (to C-NH_2). A variety of nitrile adsorption modes (*i.e.* parallel, perpendicular and side-on [4]) on Pd surfaces have been proposed for nitrile hydrogenation. Nitrile interaction should be favoured *via* the lone pair electron on nitrogen with electron deficient $Pd^{\delta+}$ in a perpendicular orientation, where the adsorbed nitrile undergoes successive attack by surface dissociated hydrogen with cleavage of C-N to generate toluene. A perpendicular adsorption of the basic nitrile group on support acid sites [26-29] is also possible with hydrogenolytic bond scission by spillover hydrogen.

5.3.2 Pd/Al_2O_3: Characterisation and Catalyst Test Results

The SSA of Pd/Al_2O_3 was appreciably lower than Pd/C (**Table 5.1**) and is comparable with values (142-160 $m^2\ g^{-1}$) reported in literature [30]. The Pd phase on Al_2O_3 took the form of discrete pseudo-spherical particles (**Figure 5.3(I)**) with a similar size distribution (**Figure 5.3(II)**) and mean (3.0 nm) to Pd/C that was again in good agreement with H_2 chemisorption (**Table 5.1**). Hydrogen TPD from Pd/Al_2O_3 resulted in a broad signal (**Figure 5.3(III)**) over the 610-950 K temperature range, where the total H_2 desorbed exceeded H_2 uptake during pulse titration but was significantly lower than that measured for Pd/C (**Table 5.1**). Differences in the amount of spillover hydrogen for the same metal (and size) on different carriers have been noted in the literature [31]. Spillover can be influenced by the concentration of initiating and acceptor sites, degree of contact between participating phases and metal-support interaction(s) [32,33]. Greater H_2 desorption from Pd/C can be linked to the greater available surface area relative to Pd/Al_2O_3 that can accommodate more spillover. Ammonia desorption from Pd/Al_2O_3 (**Figure 5.3(IV)**) exhibited a lower T_{max} (470 K) relative to Pd/C, suggesting weaker interaction of NH_3 with surface acid sites. Total NH_3 release from Pd/Al_2O_3 again coincided with chemisorption and is close to that

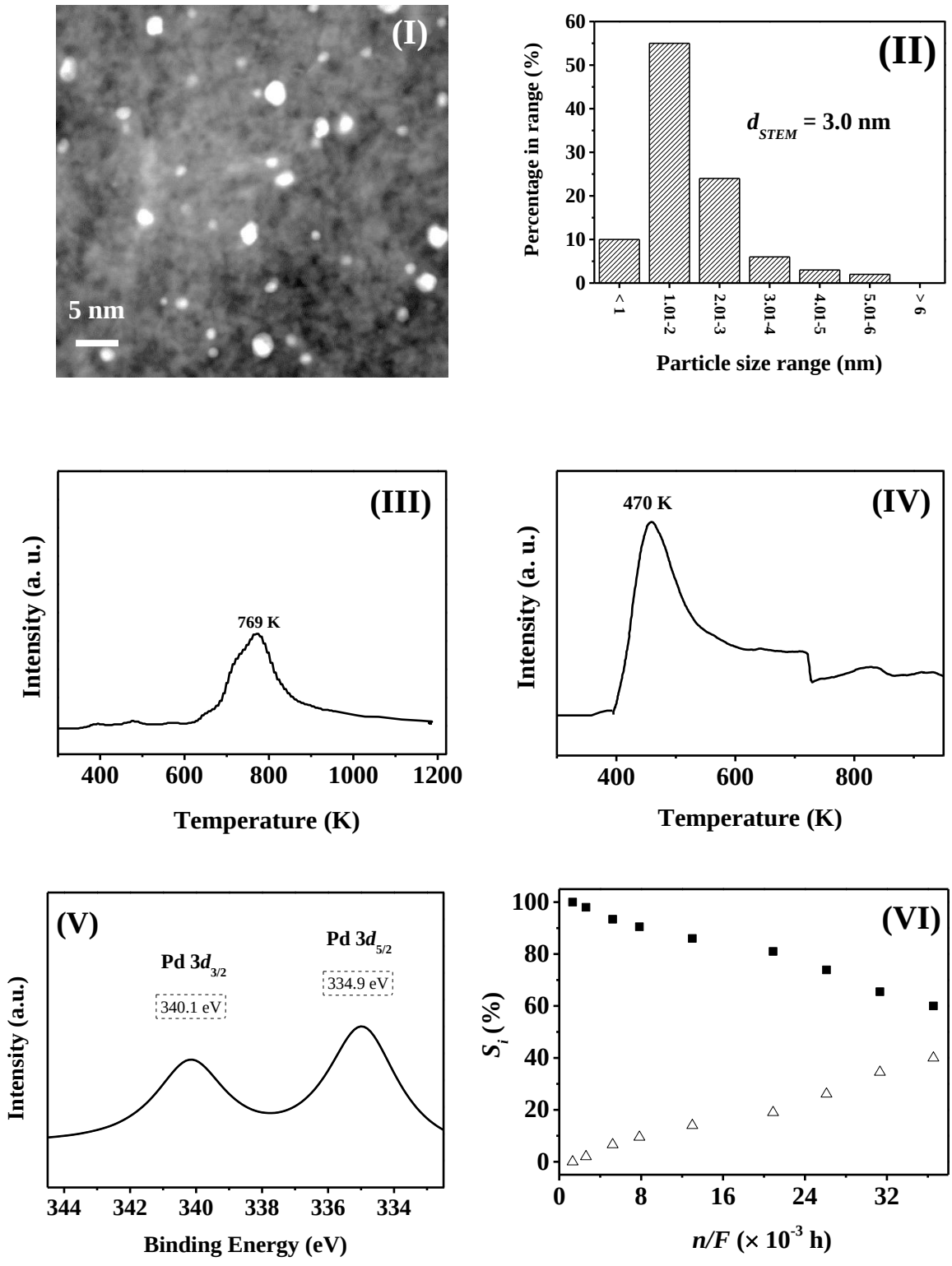

Figure 5. 3: (I) **Representative STEM image with** (II) **associated Pd particle size distribution,** (III) **H_2 and** (IV) **NH_3 TPD profiles,** (V) **XPS profile and** (VI) **dependence of selectivity (S_i) to benzylamine (■) and toluene (△) on contact time (n/F) for Pd/Al_2O_3.** ***Reaction conditions*****: T = 353 K, P_{H_2}= 1 atm.**

(0.54 $mmol_{NH_3}$ g^{-1}) reported for Pd/Al_2O_3 by Nam *et al.* [22]. Ammonia adsorption/desorption measurements confirm an appreciably greater level of surface acidity associated with Pd/C relative to Pd/Al_2O_3. The XPS profile for Pd/Al_2O_3, given in **Figure 5.3(V)**, is characterised by a Pd $3d_{5/2}$ BE that is 0.3 eV lower than the metallic Pd reference, suggesting electron transfer from support to metal phase. This is in accordance with reported electron-rich $Pd^{\delta-}$ (2-10 nm) on Al_2O_3 [16].

In contrast to Pd/C, Pd/Al_2O_3 exhibited full selectivity to the target benzylamine at low contact time ($n/F < 3 \times 10^{-3}$**)** as shown in **Figure 5.3(VI)**. This result is significant in terms of clean synthesis of benzylamine when compared with existing literature where dibenzylamine production (up to 16% selectivity) has been reported over Pd/Al_2O_3 [4,7,9]. From a consideration of Pd electronic character, a partial negative charge ($Pd^{\delta-}$) should favour interaction with a polarised carbon ($C^{\delta+}$) of the C≡N group through a side-on adsorption mode due to repulsion of $Pd^{\delta-}$ with the nitrogen lone pair. Hydrogenation of unsaturated C≡N bond to saturated amine ($C\text{-}NH_2$) reduces carbon polarity, weakening adsorption with the result that the primary amine product then can desorb without further reaction. In common with Pd/C, toluene selectivity was increased at higher n/F, indicative of a sequential pathway, *i.e.* benzonitrile → benzylamine → toluene. Reaction with benzylamine as feedstock ($n/F = 4 \times 10^{-3}$) over Pd/Al_2O_3 resulted in negligible conversion. This is in marked contrast to Pd/C which promoted hydrogenolysis of benzylamine to toluene. Taking a common fractional nitrile conversion (X = 0.2, see **Table 5.2**), Pd/Al_2O_3 delivered an appreciably higher selectivity to benzylamine (96% *vs.* 10%) but at a lower rate (by a factor of two) relative to Pd/C. This deviation in selectivity can be attributed to difference in Pd electronic

Table 5. 2: Benzonitrile hydrogenation rate (R) and selectivity (S_i, at X = 0.2) over Pd/C and Pd/Al_2O_3; *Reaction conditions*: T = 353 K; n/F = 2.6 × 10^{-3} – 3.1 × 10^{-3} h.

Catalyst	R ($mol\ h^{-1}\ mol_{Pd}^{-1}$)	$S_{i,\ X = 0.2}$ Product (%)
Pd/C	230 (527)[a]	Benzylamine (10) Toluene (90)
Pd/Al_2O_3	99 (272)[a]	Benzylamine (96) Toluene (4)

character (from XPS) that impacts on mode of adsorption of benzonitrile. As -C ≡N group could also be activated through the adsorption of nitrogen (lone pair of electron) on support acid sites [26-29], the higher nitrile consumption rate over Pd/C can be linked to greater levels of surface reactive hydrogen (H_2 TPD measurements) and the higher surface acidity.

5.3.3 Use of Catalyst Beds in Series: Enhanced Benzylamine Production over Pd/Al_2O_3

The results presented in **Figure 5.3(VI)** established full selectivity to benzylamine over Pd/Al_2O_3 at low contact time, where $X < 0.15$. This falls short in terms of the productivity required for practical applications where reaction exclusivity must be targeted at high conversion. An increase in n/F served to increase conversion (**Figure 5.3(VI)**) but this was accompanied by undesired toluene formation. Given that hydrogenolysis to toluene was suppressed over Pd/Al_2O_3 at low contact time when using either nitrile or amine as feedstock, a configuration based on several discrete catalyst beds in series, each operated at low n/F, should serve to increase overall nitrile conversion while retaining hydrogenation selectivity. The multiple catalysts beds served as a 'recycle system' by controling of contact time facilitates selective transformation of benzonitrile to benzylamine where any unreacted feedstock is converted to the target product in the subsequent catalyst beds and the amine is

Table 5. 3 : Selectivity (at X = 0.45 and 0.6) and benzonitrile hydrogenation rate (R) using multiple Pd/Al_2O_3 catalyst beds in series; *Reaction conditions*: T = 353 K; $n/F = 1.2 \times 10^{-2}$ h.

Catalyst Beds	$S_{i,\ X=0.45}$ (%)		$S_{i,\ X=0.6}$ (%)		R
	Benzylamine	Toluene	Benzylamine	Toluene	(h^{-1})
Single-bed	78	22	62	38	48
Double-bed	93	7	90	10	75
Triple-bed	97	3	96	4	84
Quadruple-bed	100	0	100	0	99

carried through without further reaction. The application of catalyst beds in series is atypical in hydrogenation processes. Dual-bed catalyst systems have been used for NO_x

and NO_2 treatment in lean burn natural gas [34,35] where increased activity and selectivity (to N_2 and O_2) were obtained with different catalyst bed composition operating at different temperatures. Use of a dual catalyst bed in simultaneous oxidation of CH_4 to C_2H_4 and syngas also involved different catalysts and temperatures [36]. The multi-bed catalyst arrangement and the associated reaction rates and product selectivity are given in **Table 5.3**. The same total mass of catalyst was divided equally into N (= 1-4) beds with the same inlet benzonitrile and H_2 flow rate. Selectivity is assessed at two representative nitrile conversions (X= 0.45 and 0.60). An increase in overall reaction rate and benzylamine selectivity (to 100%) was observed with increasing bed number

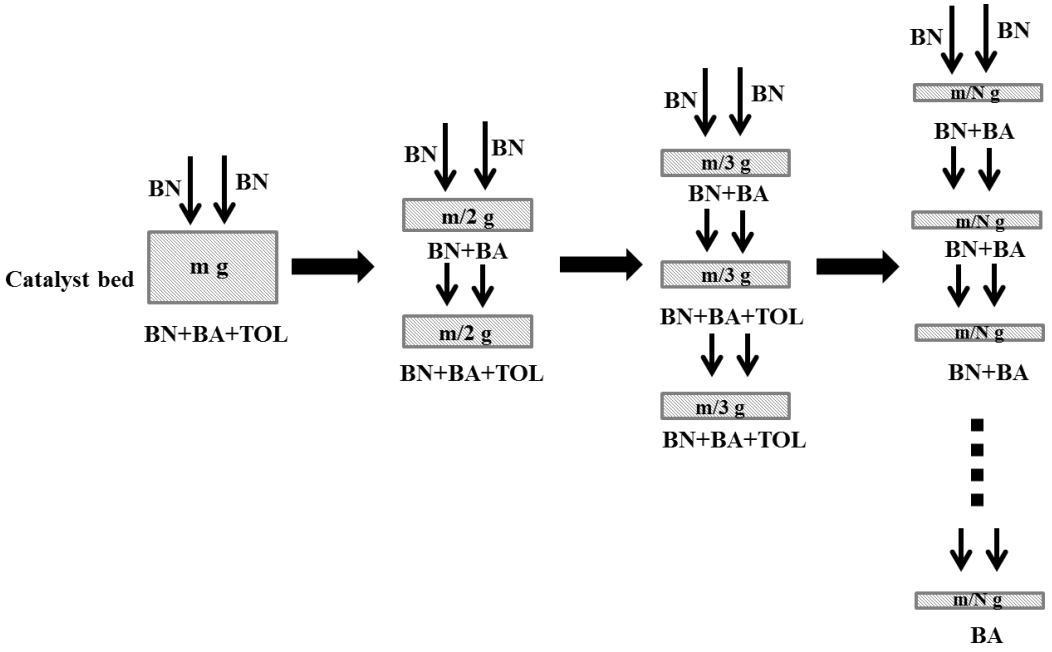

Figure 5. 4: Schematic diagram for multiple Pd/Al_2O_3 catalyst beds in series with reactant and product distribution (N is the total number of beds).

up to the quadruple bed arrangement. In principle this system should achieve 100% amine selectivity and complete benzonitrile consumption with increasing number of catalsyt beds, as shown in **Figure 5.4**. Our results demonstrate for the first time the beneficial effect of multi-beds of the same catalyst in series to enhance selective amine formation. We have achieved a rate (99 mol h^{-1} mol_{Pd}^{-1}) with full selectivity to benzylamine that is higher by a factor of 10^5 than that (8.1×10^{-4} mol h^{-1} mol_{Cu}^{-1}) reported for over Cu-MgO (at 513 K) [14] which showed the highest selectivity to benzylamine (99%) in gas phase continuous reaction in the existing literature. We have

established that the use of catalyst beds in series under isothermal conditions is an effective means of delivering high and exclusive benzylamine throughput.

5.4 Conclusions

Gas phase continuous hydrogenation of benzonitrile over Pd/C (mean Pd size = 2.5 nm) generated toluene as principal product with higher nitrile consumption rates than Pd/Al_2O_3 (mean Pd size = 3.0 nm), ascribed to greater surface acidity and levels of reactive (spillover) hydrogen. Electron transfer to the activated carbon support with the formation of $Pd^{\delta+}$ (from XPS analysis) favours a perpendicular adsorption of benzonitrile through the nitrogen lone pair with hydrogen attack to generate consecutively, imine, amine and toluene. The occurrence of $Pd^{\delta-}$ on Al_2O_3 results in a side-on activation of benzonitrile and desorption of benzylamine as exclusive product at $n/F < 3 \times 10^{-3}$; hydrogenolysis to toluene was observed at higher n/F. Utilisation of multiple Pd/Al_2O_3 beds in series serves to control contact time while retaining full selectivity to benzylamine with a rate of selective hydrogenation far greater than that reported previously.

5.5 References

[1] J. Krupka, J. Pasek, *Nitrile hydrogenation on solid catalysts - new insights into the reaction mechanism*, Curr. Org. Chem. 16 (**2012**) 988-1004.

[2] S. Nishimura, *Handbook of heterogeneous catalytic hydrogenation for organic synthesis* John Wiley, New York (**2001**) 265-265.

[3] S.A. Lawrence, *Amines: synthesis, properties and applications* Cambridge University Press, Cambridge (**2004**) 73-73.

[4] J.J.W. Bakker, A.G.v.d. Neut, M.T. Kreutzer, J.A. Moulijn, F. Kapteijn, *Catalyst performance changes induced by palladium phase transformation in the hydrogenation of benzonitrile*, J. Catal. 274 (**2010**) 176-191.

[5] S.P. Bawane, S.B. Sawant, *Reaction kinetics of the liquid-phase hydrogenation of benzonitrile to benzylamine using raney nickel catalyst*, Chem. Eng. J. 103 (**2004**) 13-19.

[6] L. Hegedűs, T. Máthé, *Selective heterogeneous catalytic hydrogenation of nitriles to primary amines in liquid phase part I. Hydrogenation of benzonitrile over palladium*, Appl. Catal. A: Gen. 296 (**2005**) 209-215.

[7] H. Yoshida, Y. Wang, S. Narisawa, S. Fujita, R. Liu, M. Arai, *A multiphase reaction medium including pressurized carbon dioxide and water for selective hydrogenation of benzonitrile with a Pd/Al_2O_3 catalyst*, Appl. Catal. A: Gen. 456 (**2013**) 215-222.

[8] A.J. Yap, A.F. Masters, T. Maschmeyer, *The kinetic features of the palladium-catalyzed hydrogenolysis of nitriles and amines*, ChemCatChem 4 (**2012**) 1179-1184.

[9] Y. López-de Jesús, C. Johnson, J. Monnier, C. Williams, *Selective hydrogenation of benzonitrile by alumina-supported Ir–Pd catalysts*, Top. Catal. 53 (**2010**) 1132-1137.

[10] M. Chatterjee, H. Kawanami, M. Sato, T. Ishizaka, T. Yokoyama, T. Suzuki, *Hydrogenation of nitrile in supercritical carbon dioxide: A tunable approach to amine selectivity*, Green Chem. 12 (**2010**) 87-93.

[11] O. Domínguez-Quintero, S. Martínez, Y. Henríquez, L. D'Ornelas, H. Krentzien, J. Osuna, *Silica-supported palladium nanoparticles show remarkable hydrogenation catalytic activity*, J. Mol. Catal. A: Chem. 197 (**2003**) 185-191.

[12] H. Cheng, X. Meng, C. Wu, X. Shan, Y. Yu, F. Zhao, *Selective hydrogenation of benzonitrile in multiphase reaction systems including compressed carbon dioxide over Ni/Al_2O_3 catalyst*, J. Mol. Catal. A: Chem. 379 (**2013**) 72-79.

[13] C. Jiménez-González, P. Poechlauer, Q.B. Broxterman, B.-S. Yang, D.A. Ende, J. Baird, C. Bertsch, R.E. Hannah, P. Dell'Orco, H. Noorrnan, S. Yee, R. Reintjens, A. Wells, V. Massonneau, J. Manley, *Key green engineering research areas for sustainable manufacturing: A perspective from pharmaceutical and fine chemicals manufacturers*, Org. Process Res. Dev. 15 (**2011**) 900-911.

[14] R.K. Marella, K.S. Koppadi, Y. Jyothi, K.S. Rama Rao, D.R. Burri, *Selective gas-phase hydrogenation of benzonitrile into benzylamine over Cu-MgO catalysts without using any additives*, New J. Chem. 37 (**2013**) 3229-3235.

[15] C.V. Rode, M. Arai, M. Shirai, Y. Nishiyama, *Gas-phase hydrogenation of nitriles by nickel on various supports*, Appl. Catal. A: Gen. 148 (**1997**) 405-413.

[16] F. Cárdenas-Lizana, Y. Hao, M. Crespo-Quesada, I. Yuranov, X. Wang, M.A. Keane, L. Kiwi-Minsker, *Selective gas phase hydrogenation of p-chloronitrobenzene over Pd catalysts: Role of the support*, ACS Catal. 3 (**2013**) 1386-1396.

[17] C. Amorim, X. Wang, M.A. Keane, *Application of hydrodechlorination in environmental pollution control: Comparison of the performance of supported and unsupported pd and Ni catalysts*, Chin. J. Catal. 32 (**2011**) 746-755.

[18] G. Prelazzi, M. Cerboni, G. Leofanti, *Comparison of H_2 adsorption, O_2 adsorption, H_2 titration, and O_2 titration on supported palladium catalysts*, J. Catal. 181 (**1999**) 73-79.

[19] P. Braos-García, P. Maireles-Torres, E. Rodríguez-Castellón, A. Jiménez-López, *Gas-phase hydrogenation of acetonitrile on zirconium-doped mesoporous silica-supported nickel catalysts*, J. Mol. Catal. A: Chem. 193 (**2003**) 185-196.

[20] B. Lin, R. Wang, X. Yu, J. Lin, F. Xie, K. Wei, *Physicochemical characterization and H_2 TPD study of alumina supported ruthenium catalysts*, Catal. Lett. 124 (**2008**) 178-184.

[21] M. Turco, G. Bagnasco, C. Cammarano, P. Senese, U. Costantino, M. Sisani, *Cu/ZnO/Al_2O_3 catalysts for oxidative steam reforming of methanol: The role of Cu and the dispersing oxide matrix*, Appl. Catal. B: Environ. 77 (**2007**) 46-57.

[22] I. Nam, K. Cho, J. Seo, S. Hwang, K.-W. Jun, I. Song, *Production of middle distillate from synthesis gas in a dual-bed reactor through hydrocracking of wax over mesoporous Pd-Al_2O_3 composite catalyst*, Catal. Lett. 130 (**2009**) 192-197.

[23] R. Puskás, A. Sápi, A. Kukovecz, Z. Kónya, *Comparison of nanoscaled palladium catalysts supported on various carbon allotropes*, Top. Catal. 55 (**2012**) 865-872.

[24] M. Brun, A. Berthet, J.C. Bertolini, *XPS, AES and auger parameter of Pd and PdO*, J. Electron Spectrosc. 104 (**1999**) 55-60.

[25] L. Jiang, H. Gu, X. Xu, X. Yan, *Selective hydrogenation of o-chloronitrobenzene (o-CNB) over supported Pt and Pd catalysts obtained by laser vaporization deposition of bulk metals*, J. Mol. Catal. A: Chem. 310 (**2009**) 144-149.

[26] M.R. Strunk, C.T. Williams, *Aliphatic nitrile adsorption on Al_2O_3 and ZrO_2 as studied by total internal reflection sum-frequency spectroscopy*, Langmuir 19 (**2003**) 9210-9215.

[27] I. Ortiz-Hernandez, C.T. Williams, *In situ studies of butyronitrile adsorption and hydrogenation on Pt/Al_2O_3 using attenuated total reflection infrared spectroscopy*, Langmuir 23 (**2007**) 3172-3178.

[28] J. Rasko, J. Kiss, *Adsorption and surface reactions of acetonitrile on Al_2O_3-supported noble metal catalysts*, Appl. Catal. A: Gen. 298 (**2006**) 115-126.

[29] S. Kim, O. Byl, J.T. Yates, *Adsorption of triethylenediamine on Al_2O_3-III: Bonding to lewis acid Al^{3+} sites*, J. Phys. Chem. B 109 (**2005**) 6331-6333.

[30] S. Gómez-Quero, F. Cárdenas-Lizana, M.A. Keane, *Effect of metal dispersion on the liquid-phase hydrodechlorination of 2,4-dichlorophenol over Pd/Al_2O_3*, Ind. Eng. Chem. Res. 47 (**2008**) 6841-6853.

[31] S.T. Srinivas, P.K. Rao, *Direct observation of hydrogen spillover on carbon-supported platinum and its influence on the hydrogenation of benzene*, J. Catal. 148 (**1994**) 470-477.

[32] P.A. Sermon, G.C. Bond, *Studies of hydrogen spillover. Part 4.-factors affecting hydrogen spillover and its reversal*, J. Chem. Soc.-Faraday Trans. 76 (**1980**) 889-900.

[33] G. Xu, K. Shi, Y. Gao, H. Xu, Y. Wei, *Studies of reforming natural gas with carbon dioxide to produce synthesis gas: X. The role of CeO_2 and MgO promoters*, J. Mol. Catal. A: Chem. 147 (**1999**) 47-54.

[34] P. Gawade, A.-M.C. Alexander, R. Clark, U.S. Ozkan, *The role of oxidation catalyst in dual-catalyst bed for after-treatment of lean burn natural gas exhaust*, Catal. Today 197 (**2012**) 127-136.

[35] J. Pérez-Ramírez, J.M. García-Cortés, F. Kapteijn, M.J. Illán-Gómez, A. Ribera, C. Salinas-Martínez de Lecea, J.A. Moulijn, *Dual-bed catalytic system for NO_x–N_2O removal: A practical application for lean-burn deNOx HC-SCR*, Appl. Catal. B: Environ. 25 (**2000**) 191-203.

[36] C. Hu, J. Wu, H. Zhang, S. Qin, *Dual catalyst bed for the oxidation of CH_4 simultaneously to C_2H_4 and syngas*, AIChE J. 53 (**2007**) 2925-2931.

Chapter 6

Selective Gas Phase Hydrogenation of *p*-Chloronitrobenzene over Pd Catalysts: Role of the Support

It has been established in Chapter 5 the interaction between support (C and Al_2O_3) and Pd affected the electronic status of Pd that resulted in different adsorption mode of reactant. The support effect was further studied in the gas phase hydrogenation of *p*-chloronitrobenzene over supported (C, Al_2O_3 SiO_2 and ZnO) Pd catalysts.

6.1 Introduction

Functionalised anilines are key intermediates in the synthesis of fine chemicals, herbicides, pesticides, dyes and pigments [1]. Amine production *via* nitroarene hydrogenation has been promoted using a range of (carbon [2-5], Al_2O_3 [6-10], SiO_2 [11-13], TiO_2 [14-17], CeO_2 [18], Fe_2O_3 [18-20], Fe_3O_4 [19], SnO_2 [21], CeO_2 [18,22] and polymer [23]) supported metal (Pd [2-7,16,24], Pt [11,20,23,25,26], Ru [21,26-28], Rh [29], Ni [8,10,14,30], Cu [31], Ag [13,32] and Au [33,34]) catalysts. Taking the hydrogenation of *p*-chloronitrobenzene (*p*-CNB), undesired C-Cl scission (**Scheme 6.1**) is difficult to circumvent, particularly at high conversions [33,35]. To date, *p*-CNB hydrogenation has focused on liquid phase batch reactions at high H_2 pressure (up to 60 atm) [30]. A move from batch to continuous operation has been identified [36] as a priority for sustainable production in the pharmaceutical and fine chemical sectors. We have demonstrated [34] exclusive $–NO_2$ reduction (but at low reaction rate) in the continuous gas phase hydrogenation of substituted nitroarenes over supported Au. In examining the role of Pd as promoter to increase activity, selective *p*-chloroaniline (*p*-CAN) production was achieved for Au/Pd $\geq$ 20 [9]. Increasing the Pd content delivered higher rates but with the formation of nitrobenzene (NB). This is consistent with the literature on gas [16] and liquid [7,35] phase operation that has demonstrated non-selective CNB hydrogenation over supported Pd, generating aniline (AN) [7,16,35], NB [7,16,35] and azo-compounds [16] as by-products.

Catalytic activity/selectivity in nitro-group reduction can be governed by the electronic [18,22] and crystallographic [15] character of the metal phase that is, in turn, influenced by interactions with the carrier [12,37]. Support acid-base properties can impact on metal dispersion with electron transfer resulting in the formation of partially

charged *nano*-scale particles [38,39]. Sangeetha *et al.* [40] observed higher activity in the hydrogenation of NB over Pd/hydrotalcite relative to Pd/MgO and Pd/γ-Al_2O_3, which they linked to enhanced Pd dispersion due to support basicity. Higher *p*-CAN selectivity (from CNB) has also been achieved with the incorporation of metal cations (Cr^{3+}/Cr^{2+} [41] and Sn^{4+} [7]) on supported Pd and associated with enhanced polarization of the N=O bond [7]. When reducible oxides are used as carriers, partial reduction of the support can lead to alloy formation [42]. Recent work has demonstrated selective hydrogenation of functionalized alkynes over PdZn alloy [43,44]. The formation of a PdZn phase, established by high-resolution X-ray diffraction/absorption spectroscopy, has been shown to enhance selectivity in the hydrogenation of 1-pentyne to pentenes (relative to Pd/SiO_2) [45] and acetonitrile to ethylamine (compared with Pd black) [46]. Use of supported Pd catalysts to achieve high selectivity in the conversion of *p*-CNB to *p*-CAN represents a challenge. We have set out to identify the critical variable(s) that control $–NO_2$ group reduction selectivity by examining a range of (commercial and laboratory synthesised) catalysts with varying Pd content, support and method of preparation. We compare the catalytic action of bulk (unsupported) Pd with that of Pd supported on three distinct carriers; (i) activated carbon; (ii) *non*-reducible oxides (SiO_2 and Al_2O_3); (iii) ZnO.

6.2 Experimental

6.2.1 Catalyst Preparation and Activation

The activated carbon support (AC, 905 m^2 g^{-1}) was obtained from NORIT (UK) and subjected to a demineralization treatment (1 M HNO_3 under continuous stirring at 500 rpm for 7 days) to remove any residual metal that could contribute to the hydrogenation process. The AC support was thoroughly washed with deionized water (until pH of the wash water approached 7) and oven-dried at 383 K for 12 h. The oxide supports, SiO_2 (Cab-O-Sil M-5, Cabot), Al_2O_3 (Puralox, Condea Vista Co.) and ZnO (Aldrich) were used as received. A series of (AC, SiO_2 and Al_2O_3) supported Pd catalyst precursors were prepared by standard impregnation (with $Pd(NO_3)_2$ at 363 K) and denoted as Pd/AC-I, Pd/SiO_2 and Pd/Al_2O_3-III. The impregnated samples were oven dried at 393 K for 12 h. In addition, Pd/Al_2O_3-I, Pd/ZnO and Pd/ZnO-PVP were prepared by deposition of *ex-situ* synthesized monodispersed Pd^0 nanoparticles. In the case of Pd/Al_2O_3-I and Pd/ZnO, an aqueous solution of $PdCl_2$ (Fluka, >99 %) and $Na_2MoO_4 \cdot H_2O$ (Fluka, >99 %) (Pd/Mo mol ratio = 1) was heated at 368 K (under

continuous stirring, 500 rpm) until complete evaporation. The solid residue was dissolved in water and contacted (at ambient temperature) with a continuous flow of H_2 (100 cm^3 min^{-1}) for 30 min. This procedure has been demonstrated [47] to result in the formation of uniform Pd^0 nanoparticles stabilised by molybdate anions. The *ex-situ* synthesis of monodispersed PVP (poly N-vinyl-2-pyrrolidone, Aldrich) stabilised Pd nanoparticles followed the method described by Lim *et al.* [48]. A known mass (0.277 g) of PVP and ascorbic acid (0.156 g, 99%, Aldrich), which acts as reducing agent, were dissolved in 15 cm^3 water at 368-371 K. An aqueous solution of $PdCl_2$ (0.088 g, 60% Pd, Aldrich) and NaCl (0.058 g, 99.5%, Fluka) was added under constant agitation (*ca.* 500 rpm) with an instantaneous change in color (from brown to black), indicative of Pd reduction and colloid formation [48]. The colloidal solution was kept under agitation at 368-371 K for 3 h, cooled and diluted with 75 cm^3 acetone and left for 12 h. The colorless liquid was decanted and the black viscous residue dissolved to give an homogeneous and stable Pd(PVP) colloidal solution. Palladium deposition (on ZnO) was achieved *via* adsorption where the support (*ca.* 2 g) was immersed and stirred in the Pd colloidal solution for *ca.* 2 h, the slurry filtered and dried in air at ambient temperature. Two commercial supported catalysts (Pd/AC-II and Pd/Al_2O_3-II, Aldrich) and bulk PdO (Aldrich) were also examined. Prior to use, the catalysts were sieved into a batch of 75 μm average diameter and reduced in 60 cm^3 min^{-1} H_2 at 10 K min^{-1} to 573 K, which was maintained for 1 h. Samples for off-line analysis were passivated in 1% v/v O_2/He at ambient temperature.

6.2.2 Catalyst Characterisation

The Pd content was measured by inductively coupled plasma-optical emission spectrometry (ICP-OES, Vista-PRO, Varian Inc.) from the diluted extract in HF. Temperature programmed reduction (TPR), H_2 and CO chemisorption and BET surface area were determined using the commercial CHEM-BET 3000 (Quantachrome) unit. The samples were loaded into a U-shaped Quartz cell (3.76 mm i.d.) and heated in 17 cm^3 min^{-1} (Brooks mass flow controlled) 5% v/v H_2/N_2 at 10 K min^{-1} to 573±1 K. The effluent gas passed through a liquid N_2 trap and H_2 consumption monitored by a thermal conductivity detector (TCD) with data acquisition/manipulation using the TPR Win™ software. The reduced samples were maintained at 573 K until the signal returned to baseline, swept with 65 cm^3 min^{-1} N_2 for 1.5 h, cooled to ambient temperature and subjected to H_2 (or CO) chemisorption using a pulse (10 μl) titration procedure. In a

series of blank tests, chemisorption measurements on each support (AC, Al_2O_3, SiO_2 and ZnO) did not result in any detectable uptake. BET areas were recorded with a 30% v/v N_2/He flow using pure N_2 (99.9%) as internal standard. At least two cycles of N_2 adsorption-desorption in the flow mode were employed to determine total surface area using the standard single point method. BET surface area, H_2 and CO uptake were reproducible to within ±5 %; the values quoted represent the mean.

X-ray photoelectron spectroscopy (XPS) analyses were conducted on an Axis Ultra instrument (Kratos Analytical) under ultra-high vacuum conditions ($<10^{-8}$ Torr) using a monochromatic Al Kα X-ray source (1486.6 eV). The source power was maintained at 150 W and the emitted photoelectrons were sampled from a 750×350 μm^2 area at a take-off angle = 90°. The analyser pass energy was 80 eV for survey spectra (0–1000 eV) and 40 eV for high resolution spectra (Pd $3d_{5/2}$ and Pd $3d_{3/2}$). The adventitious carbon 1*s* peak was calibrated at 284.5 eV and used as an internal standard to compensate for any charging effects. Spectra curve fitting and quantification were performed with the Casa XPS software, using relative sensitivity factors provided by Kratos. Palladium particle morphology and size were determined by transmission electron microscopy analysis; JEOL JEM 2011 HRTEM unit with a UTW energy dispersive X-ray detector (Oxford Instruments) operated at an accelerating voltage of 200 kV using Gatan Digital Micrograph 3.4 for data acquisition/manipulation. The samples for analysis were crushed and deposited (dry) on a holey carbon/Cu grid (300 Mesh). Mean Pd size was based on a count of up to 800 individual Pd particles.

6.2.3 Hydrogenation of p-Chloronitrobenzene (p-CNB)

6.2.3.1 Catalytic System

The hydrogenation of *p*-CNB (Sigma-Aldrich, purity ≥99 %) as a solution in ethanol (Sigma-Aldrich, ≥99 %) was carried out *in situ*, immediately after catalyst activation, under atmospheric pressure at 453 K in a fixed bed vertical glass reactor (*i.d.* = 15 mm). The operating conditions ensured negligible heat/mass transport constraints. A layer of borosilicate glass beads served as preheating zone where the *p*-CNB reactant was vaporized and reached reaction temperature before contacting the catalyst. Isothermal conditions (±1 K) were ensured by diluting the catalyst bed with ground glass (75 μm). The reaction temperature was continuously monitored using a thermocouple inserted in a thermowell within the catalyst bed. *p*-CNB was delivered at a fixed calibrated flow rate to the reactor *via* a glass/teflon air-tight syringe and teflon

line using a microprocessor controlled infusion pump (Model 100 kd Scientific). A *co*-current flow of *p*-CNB and ultra pure (BOC, >99.99 %) H_2 (<1 % v/v *p*-CNB in H_2) was maintained at $GHSV = 2\times10^4$ h^{-1} with an inlet flow (F) over the range 2.4×10^{-4} – 7×10^{-4} mol h^{-1}. The H_2 content was up to 110 times in excess of the stoichiometric requirement for hydrogenation to *p*-CAN and the flow rate was monitored using a Humonics (Model 520) digital flowmeter. The molar Pd (n) to F ratio spanned the range 1×10^{-3} – 9×10^{-3} h. Although the reaction temperate (453 K) are below the boiling point of the reactant and the proposed products, the partial pressure for each component ($P_{p\text{-}CNB}$ = 140.2 Pa; $P_{p\text{-CAN}}$ = 27.9 Pa; P_{NB} = 27.9 Pa; P_{AN} = 27.9 Pa) is far lower than the saturated vapour pressure ($P^*_{p\text{-}CNB}$ =1188 Pa; $P^*_{p\text{-CAN}}$ = 70997.6 Pa; P^*_{NB} = 46130.4 Pa; P^*_{AN} = 91200.3 Pa) at the reaction conditions (**Appendix 3**) suggesting all the components are in gas phase. In a series of blank tests, passage of *p*-CNB in a stream of H_2 through the empty reactor or over the support alone did not result in any detectable conversion.

6.2.3.2 Analytical Method and Activity/Selectivity Measurements

The composition of the reactant/product(s) mixtures was determined using a Perkin-Elmer Auto System XL chromatograph equipped with a programmed split/splitless injector and a flame ionization detector, employing a DB-1 capillary column (*i.d.* = 0.33 mm, length = 30 m, film thickness = 0.20 μm). Data acquisition and manipulation were performed using the TotalChrom Workstation Version 6.1.2 (for Windows) chromatography data system and the overall reactant/product molar fractions (x_i) were determined from detailed calibration plots (not shown). Fractional hydrogenation ($X_{p\text{-}CNB}$) was obtained from

$$X_{p-CNB} = \frac{[p-CNB]_{in} - [p-CNB]_{out}}{[p-CNB]_{in}} \qquad \textbf{(6.1)}$$

where selectivity with respect to *p*-CAN is given by

$$S_{p-CAN}(\%) = \frac{[p-CAN]_{out}}{[p-CNB]_{in} - [p-CNB]_{out}} \times 100 \qquad \textbf{(6.2)}$$

Repeated reactions with different samples from the same batch of catalyst delivered conversion/selectivity values that were reproducible to within ± 7 %.

6.3 Results and Discussion

6.3.1 Catalyst Characterisation

Characterisation measurements for the series of Pd catalysts studied are presented in **Tables 6.1** and **6.2**. Commercial and laboratory synthesized samples exhibiting a range of Pd loading (0.9-10.2 % w/w) and BET area (2-875 m^2 g^{-1}) have been used in this work to promote *p*-CNB hydrogenation. We must stress that a very broad set of Pd catalysts were chosen in order to establish critical characteristics that determine activity and selectivity.

Table 6. 1: Catalyst source or preparation method (for laboratory synthesised samples), Pd loading, BET surface area and hydrogenation performance in terms of product selectivities at a common fractional *p*-CNB conversion ($X_{p\text{-}CNB}$ = 0.2).

Catalyst	Catalyst Source/ Peparation	Pd loading (% w/w)	BET area (m^2 g^{-1})	$S_{X_{p\text{-}CNB}=0.2}$ (%)		
				p-CAN	AN	NB
Pd[a]	Commercial	-	2	29	55	16
Pd/AC-I[b]	Prepared by impregnation	5.5	875	74	0	26
Pd/AC-II	Commercial	10.2	826	38	52	10
Pd/SiO_2[b]	Prepared by impregnation	7.7	178	0	90	10
Pd/Al_2O_3-I[b]	Prepared by deposition	0.9	157	0	78	22
Pd/Al_2O_3-II	Commercial	1.2	160	0	38	62
Pd/Al_2O_3-III[b]	Prepared by impregnation	6.9	173	0	68	32
Pd/ZnO[b]	Prepared by deposition	4.7	8	100	0	0

[a]generated by reduction of PdO; [b]laboratory synthesised

Table 6. 2: Temperature and H/Pd ratio associated with Pd hydride decomposition and Pd nanoparticle size obtained from TEM (d_{TEM}), CO (d_{CO}) and H_2 (d_{H_2}) chemisorption.

Catalyst	Pd hydride		Pd nanoparticle size		
	T (K)	H/Pd (mol mol^{-1})	d_{TEM} (nm)	d_{CO} (nm)	d_{H_2} (nm)
Pd	377	0.67	-	-	-
Pd/AC-I	365	0.29	11.7	8.2	129.0
Pd/AC-II	373	0.16	4.4	19.9	4.7
Pd/SiO_2	362	0.36	12.6	36.7	9.4
Pd/Al_2O_3-I	343	0.25	6.4	28.8	4.1
Pd/Al_2O_3-II	355	0.05	2.4	2.3	2.0
Pd/Al_2O_3-III	377	0.33	9.6	49.0	25.0
Pd/ZnO	356	0.22	6.5	14.6	4.0

6.3.1.1 Palladium Particle Size

Representative temperature programmed reduction (TPR) profiles (for PdO, Pd/AC-II, Pd/Al_2O_3-II and Pd/ZnO) are presented in **Figure 6.1**. Each profile is characterised by the appearance of a negative peak at 343-377 K (**Table 6.2**) that can be attributed to Pd hydride decomposition. Ambient temperature H_2 absorption is known to generate β-phase Pd hydride when the H_2 partial pressure exceeds 0.02 atm [49,50]; P_{H2} during TPR in this work = 0.05 atm. The hydride is thermally unstable and decomposes during thermal treatment to release H_2 over the temperature range 342-386 K [51-53]. Hydride composition, presented in **Table 6.2** as H/Pd ratio, is known to depend on Pd particle size [10,54] where H/Pd decreases with decreasing size (increasing metal dispersion) [51] to approach zero for Pd size <2.5 nm [51,55]. Bulk Pd, as our

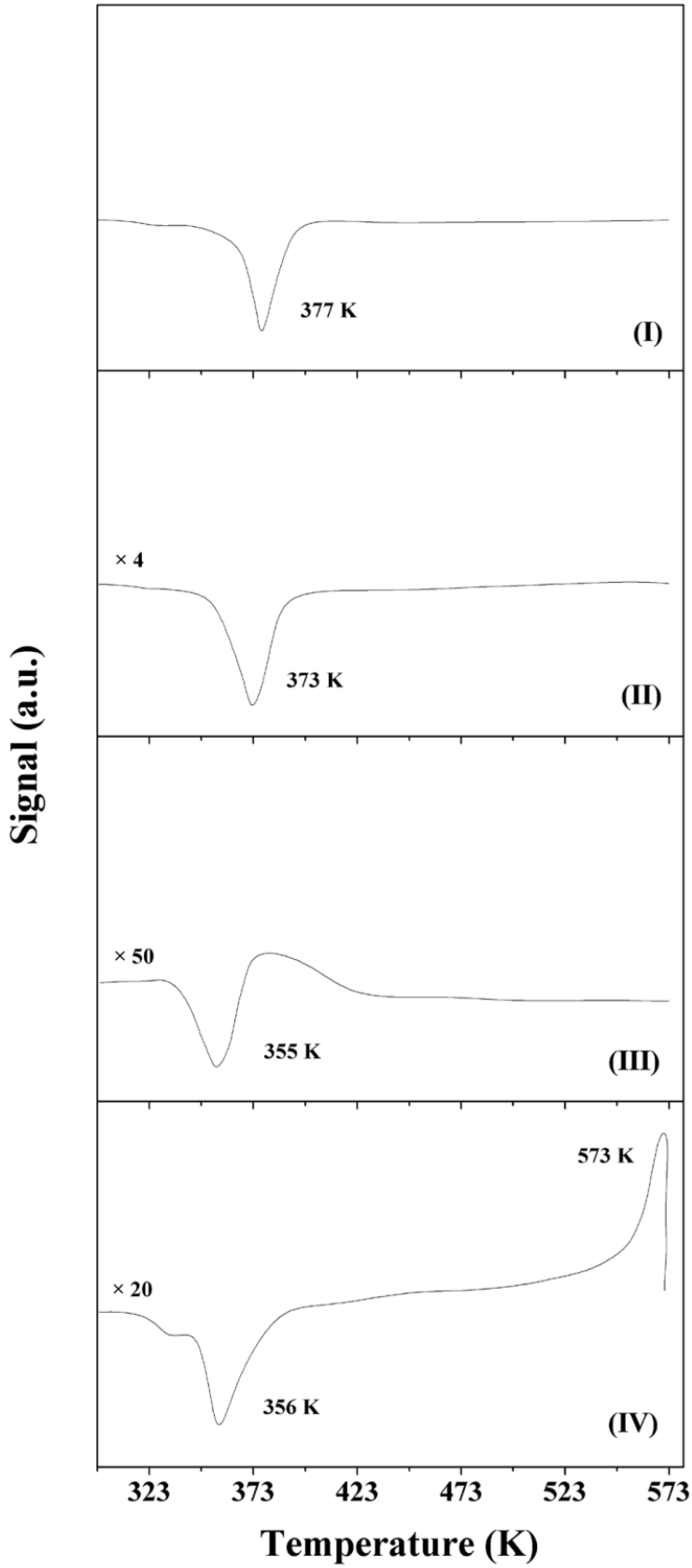

Figure 6. 1: Temperature-programmed reduction (TPR) profiles for (I) bulk PdO, (II) Pd/AC-II (III) Pd/Al_2O_3-II and (IV) Pd/ZnO.

benchmark, is characterized by the highest H/Pd (0.67), a result in good agreement with values (0.66-0.73) reported in the literature [54,56]. Considering the supported catalysts, the commercial Pd/Al_2O_3-II exhibited the lowest H/Pd (0.05) while the remaining systems generated ratios in the range 0.16-0.36, characteristic of Pd particles of 3-24 nm [56,57]. The positive signal at higher temperature (T_{max} = 573 K) for Pd/ZnO (**Figure 6.1 (IV)**) has been observed previously and linked to: (i) secondary reduction of an oxidised Pd component or reduction of ZnO (or $ZnCl_2$) at the metal/support interface [58]; (ii) simultaneous reduction of Pd^{2+} and Zn^{2+} resulting in the formation of PdZn particles [59].

The (mean) Pd particle sizes determined from TEM and (CO and H_2) chemisorption are given in **Table 2**. Consistent values for all three measurements were obtained in the case of Pd/Al_2O_3-II (2.2±0.2 nm), which agree with the low associated H/Pd from TPR analysis. However, there are inconsistencies in the results generated with each technique for the other supported Pd samples. We should note that there is a dearth of published studies recording Pd particle sizes using more than one analytical methodology. Taking an overview of the published work on supported metals in general, both agreement [4,51,60-62] and disagreement [52,62-64] have resulted from the estimation of metal particle size using gas chemisorption and TEM analysis. The discrepancy can be linked to limitations associated with these techniques. In the case of chemisorption, a source of error can result from a partial (or total) active phase occlusion by residual precursor species *post*-activation that serve to suppress uptake, leading to an *over*-estimation of metal particle size [63,64]. CO chemisorption delivered a range of Pd sizes that do not correlate directly with Pd hydride composition and deviate significantly from values obtained from H_2 uptake and TEM. This may be the result of applying a fixed Pd/CO adsorption stoichiometry [52,65] (surface metal atoms/CO molecules chemisorbed = 2), as has been the standard approach for carbon and oxide supported Pd systems [66,67]. However, CO can adsorb on Pd in both linear (Pd:CO = 1:1) [68] and bridged (Pd:CO = 2:1) [68,69] forms and this appears to depend on the nature of the support [70] and Pd size [71]. Hydrogen chemisorption is commonly employed to estimate Pd dispersion [63,72] where a dissociative adsorption (Pd:H stoichiometry = 1:1) is applied. Prelazzi *et al.* [73], in reviewing the available literature, have identified instances of good agreement between H_2 uptake (taking Pd:H = 1:1) and TEM data. In this study, Pd sizes obtained from H_2 chemisorption differ from the TEM derived values but both methods delivered an equivalent trend in terms of increasing (or decreasing) size across the group of catalysts. Particle size measurements

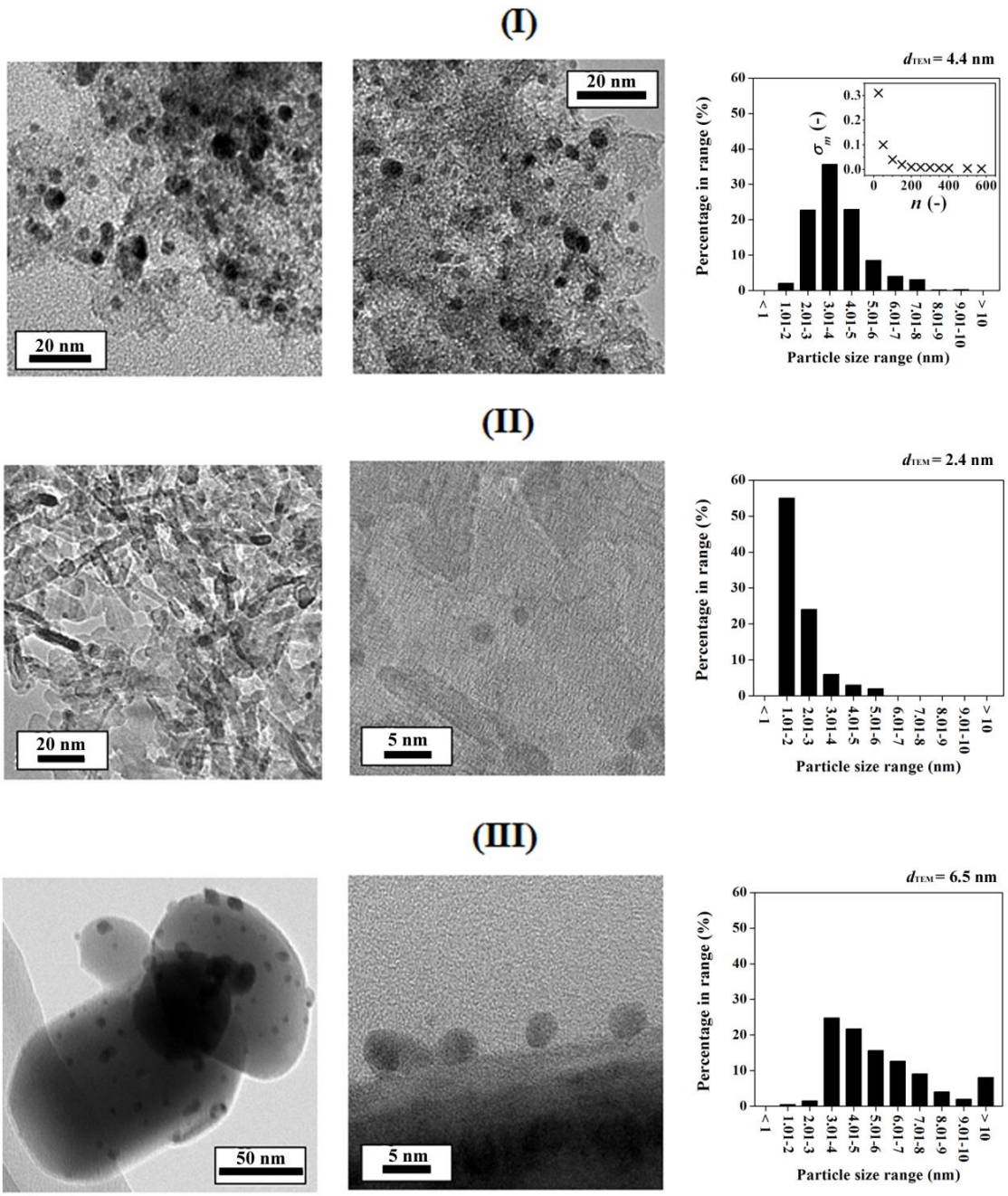

Figure 6. 2: Representative TEM images and Pd nanoparticle size distributions for (I) Pd/AC-II (with standard deviation of the mean (σ_m) as a function of the number of Pd particles counted (n)), (II) Pd/Al_2O_3-II and (III) Pd/ZnO.

from H_2 chemisorption can be compromised due to hydrogen spillover, *i.e.* dissociative chemisorption on metal sites with transport to the support surface [74], which results in an apparent higher Pd dispersion (*under*-estimation of metal size) due to additional H_2 consumption. Indeed, there is evidence in the literature for hydrogen spillover under ambient conditions for carbon [75] and oxide [76] supported Pd. We should flag

Pd/AC-I that exhibits an unfeasibly large Pd size (129.0 nm) based on H_2 chemisorption. This can result from occlusion of Pd surface sites by amorphous carbon associated with the support, as noted elsewhere [64], leading to inhibited H_2 uptake.

Electron microscopy as an imaging technique provides a particle size distribution from which the mean can be determined. There are certain limitations in the application of this method, as highlighted in the review of Matyi *et al.* [65] and recently published analysis by Liu [77]. This approach provides a two dimensional imaging of three dimensional nanoparticulate structures where the occurrence of irregular morphologies, as a result of metal-support interactions, presents problems in terms of consistent diameter measurement. Accurate diameter estimation can also be compromised by poor contrast between the support and metal(s) phases while apparatus detection limit (sizes below 1-2 nm [78]) can also lead to inaccurate sizes. Representative TEM micrographs and associated Pd particle size distributions on carbonaceous, reducible and *non*-reducible oxide carriers are presented in **Figure 6.2**. The supported metal phase exhibits a *pseudo*-spherical morphology with particles predominantly <10 nm. It is critical in TEM analysis that the particle population used for size estimation is representative of the entire ensemble of crystallites. Taking Pd/C-II as an example, the standard deviation of the mean (σ_m) is presented as a function of Pd particle count (inset to **Figure 6.2 (I)**), following the approach reported previously [78]. It can be seen that σ_m is sensitive to the total number of Pd particles counted and σ_m invariance (at counts >200) ensures that the size distribution is truly representative. Invariance of the mean applies to all the d_{TEM} values recorded in **Table 6.2**. While the combination of techniques used in this study should be complementary, our results suggest that the chemisorption measurements (particularly CO) do not give a reliable measure of Pd size. TEM analysis delivers the more valid Pd size information where particle counting is conducted with statistical rigour. Hydrogen uptake capacity is, nonetheless, an important consideration in H_2 mediated catalysis. The correlation between H_2 uptake (at ambient temperature) and mean Pd size (from TEM) is presented in **Figure 6.3 (I)**, where there is a clear increase in H_2 chemisorption capacity with decreasing Pd NP size (12.6→2.4 nm). This tendency is in agreement with published literature [51,57] showing enhanced H_2 chemisorption for smaller Pd particles.

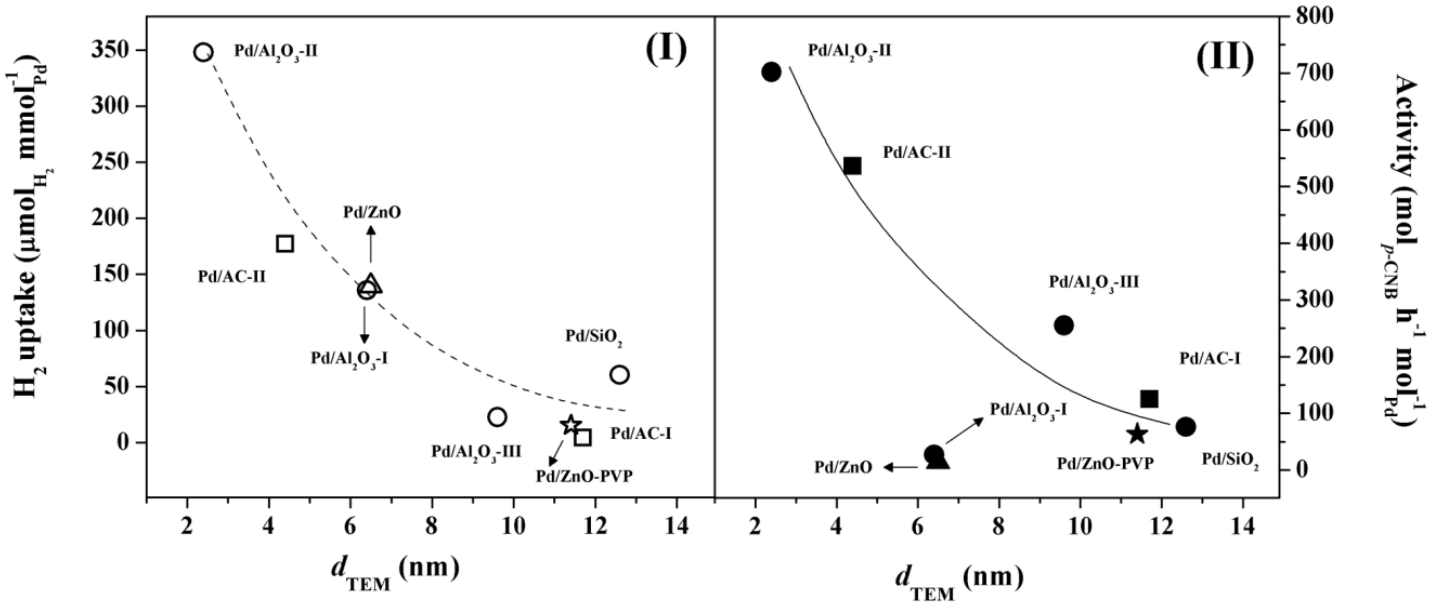

Figure 6. 3: Relationship between Pd nanoparticle size (d_{TEM}) and (I) H_2 chemisorption (open symbols; dashed line) and (II) *p*-CNB transformation rate (solid symbols; solid line); Pd supported on AC (□, ■), *non*-reducible oxides (○,●) and ZnO (Pd/ZnO: △,▲; Pd/ZnO-PVP; ★,☆)

6.3.1.2 Palladium Electronic Characteristics

In order to gain insight into the electronic character of the Pd phase, XPS analysis over the Pd 3*d* binding energy (BE) region was conducted with peak deconvolution, as shown in **Figure 6.4** for Pd/ZnO. It is known that the support can impact on the electronic properties of the metallic phase *via* metal-support interactions [79], which are more pronounced for Pd particles at the nano-scale. Taking bulk Pd as benchmark, the

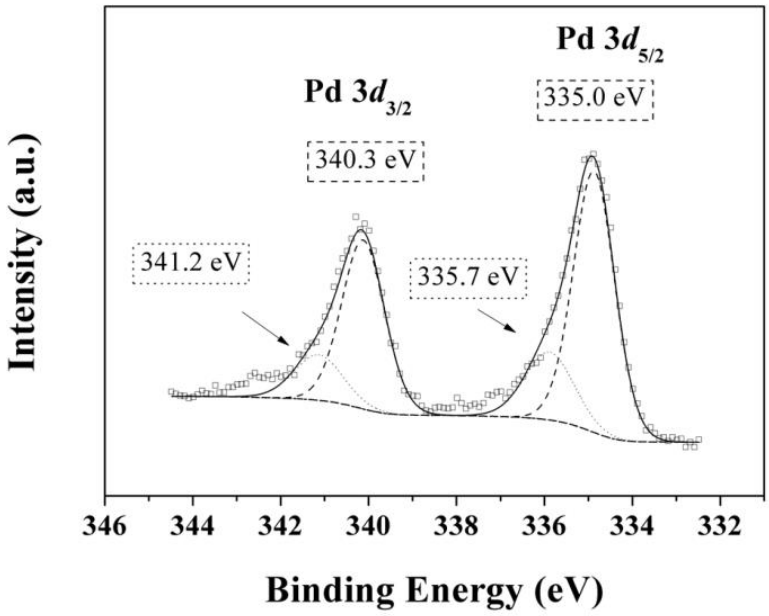

Figure 6. 4: XPS spectrum over the Pd 3*d* region for Pd/ZnO: XPS experimental data are represented by symbols (□) while the lines are the result of spectra curve fitting with independent contributions due to Pd^0 (dashed line) and PdZn alloy (dotted line) from peak deconvolution.

core level Pd $3d_{5/2}$ BE (= 335.3 eV) is in good agreement with the value (335.2 ± 0.2 eV) reported by Briggs and Seah [80] for Pd^0. In order to explicitly probe modification(s) to Pd electron density due to particle size, we present the relationship between d_{TEM} and Pd $3d_{5/2}$ BE in **Figure 6. 5**. The BE values exhibited a measurable increase (334.7→334.9 eV) with decreasing mean Pd size (6.4→2.4 nm) for the Al_2O_3 system, as has been noted elsewhere [81]. Moreover, the BE showed a marked dependence on the support. Palladium on AC exhibits a Pd $3d_{5/2}$ BE that is *ca.* 0.6 eV higher than bulk Pd, suggesting electron transfer from Pd to the carbon support resulting in a partial positively charged metal phase ($Pd^{\delta+}$). Jiang and co-workers [82] observed a positive displacement (*ca.* 1.1 eV) for carbon supported Pd (3-12 nm) when compared with bulk Pd that they ascribed to metal-support interactions. Ramos *et al.* [83] reported

a shift to higher BE for Pd/C that was attributed to electronic transfer associated with residual surface Cl. Gómez-Sainero *et al.* [84] have also demonstrated the occurrence of electron-deficient Pd (3.8-10.5 nm) on a carbon carrier. They linked this to the presence

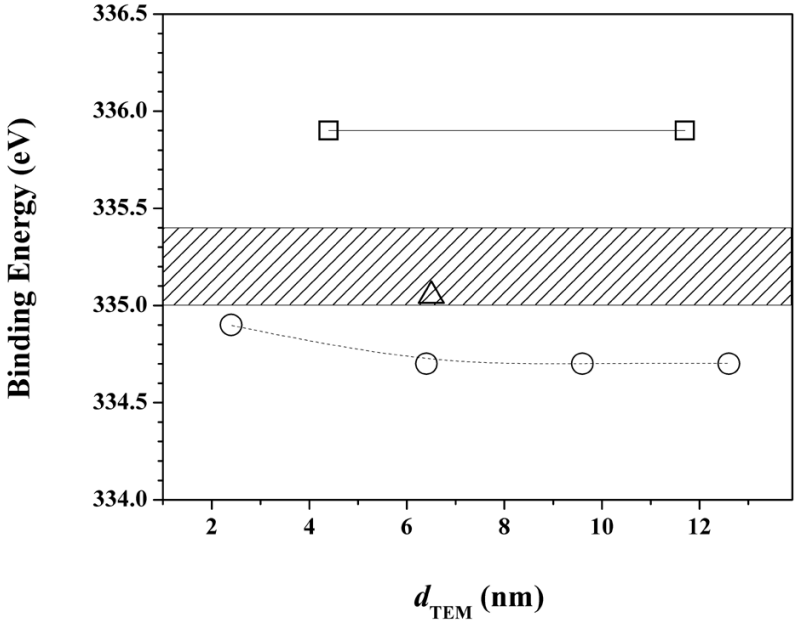

Figure 6. 5: Relationship between binding energy (BE) of the Pd $3d_{5/2}$ signal and Pd nanoparticle size (d_{TEM}) for Pd supported on activated carbon (□), *non*-reducible oxides SiO_2 and Al_2O_3 (○) and ZnO (△). *Note*: shaded area illustrates the BE region that is characteristic of Pd^0 [80].

of surface species (*e.g.* HCl and NO_x) generated during catalyst preparation/activation that serve to modify the electron density of the Pd sites with the formation of supported Pd^{n+}. The presence of $Pd^{\delta-}$ on Al_2O_3 and SiO_2 follows from the observed lower (by 0.4-0.6 eV) BE (relative to bulk Pd), as shown in **Figure 6.5**. Oxidic supports have been found to influence the electronic properties of supported transition metals where a change in the electron density of Ru (2-10 nm) on MgO, Al_2O_3 and SiO_2 has been attributed to interaction with surface OH groups [85]. The Pd $3d_{5/2}$ spectrum for Pd/ZnO (**Figure 6.4**) suggests the presence of two distinct surface Pd species. The main component shows a BE (335.0 eV) close to the reference for zero valent Pd [80] while a secondary component exhibits a signal shifted to higher BE (by 0.7 eV) and can be attributed to the occurrence of PdZn [58]. The formation of an intermetallic PdZn alloy phase after H_2 treatment at $T \geq 373$ K has been demonstrated by HRXRD and XAS [45] but the mechanism is still a matter of some debate. Hong *et al.* [76] have proposed the growth of a thin PdZn alloy phase at the metal-support interface resulting in a strong anchoring of the metal that serves to inhibit sintering. Alternatively, reversible

migration and transformation of ZnO (to Zn) on Pd can result in the partial/total coverage of Pd clusters and the ultimate formation of a PdZn outerlayer [58].

6.3.2 Correlation of Catalyst Characteristics with Catalytic Performance

6.3.2.1 Activity

The catalytic response of supported metal nanoparticles in hydrogenation reactions can be governed by electronic [86] and/or geometric [87,88] considerations. A series of experiments were conducted to investigate the effect of particle size on catalyst performance where an increase in activity with decreasing Pd size (12.6→2.4 nm) is apparent from the entries in **Figure 6.3 (II)**. The results suggest that the nature of the carrier (carbon *vs.* oxide) or catalyst source (laboratory synthesized or commercial) does not impact significantly on rate, which is determined by Pd size. Indeed, similar activity was obtained for catalysts with an equivalent mean Pd size on different supports (Pd/AC-I (11.7 nm) and Pd/SiO_2 (12.6 nm)) while, taking a common support (Pd/AC-I (11.7 nm) and Pd/AC-II (4.4 nm)), a four-fold higher activity was recorded for the catalyst bearing smaller Pd particles. This response has also been observed for gas phase *p*-CNB hydrogenation over supported Au [22] but we provide here the first report of Pd size effects in this reaction. We should note that the opposite trend has been reported for batch liquid phase *p*-CNB hydrogenation where higher activities were recorded for Pt/Al_2O_3 with lower metal dispersion and ascribed to stabilization of the negatively charged reaction transition state on larger Pt particles [89]. A salient feature of the data generated in this study is the match of activity dependence on Pd size with that of H_2 chemisorption (**Figure 6.3 (I)**). Increased rate can be attributed to greater surface hydrogen, which is a feature of greater Pd dispersion. We should flag Pd/Al_2O_3-I and Pd/ZnO, synthesized by deposition of ($Na_2MoO_4 \cdot H_2O$) stabilized monodispersed Pd nanoparticles prepared *ex situ*, that deviate from the general trend in delivering lower activities. This can result from residual surface stabilizer *post*-activation that occludes active sites and inhibits rate, as has been reported for the hydrogenation of acetylene [90]. Indeed, XPS analysis has established the presence of surface Mo species (≤1% w/w) in activated Pd/Al_2O_3-I and Pd/ZnO that is consistent with an earlier report of a Pd nanoparticulate catalyst prepared using $Na_2MoO_4 \cdot H_2O$ as stabilizer [43]. Zina and Ghorbel [91] have demonstrated that inclusion of Mo in zeolite supported Pd suppressed 1,3-butadiene hydrogenation activity, which was linked to the formation of Pd_nMo_m clusters. It should, however, be noted that H_2 chemisorption on Pd/Al_2O_3-I and

Pd/ZnO was consistent with the general trend line shown in **Figure 6.3 (I)**. This suggests that any Mo remaining from the stabilizer does not impact on H_2 uptake but must influence *p*-CNB adsorption/activation.

6.3.2.2 Selectivity

The main reaction pathways in the hydrogenation of *p*-CNB are identified in **Scheme 6.1** where nitro group reduction (step I) generates the target amine (*p*-CAN). Dechlorination of *p*-CNB (step II) results in the formation of nitrobenzene (NB), which

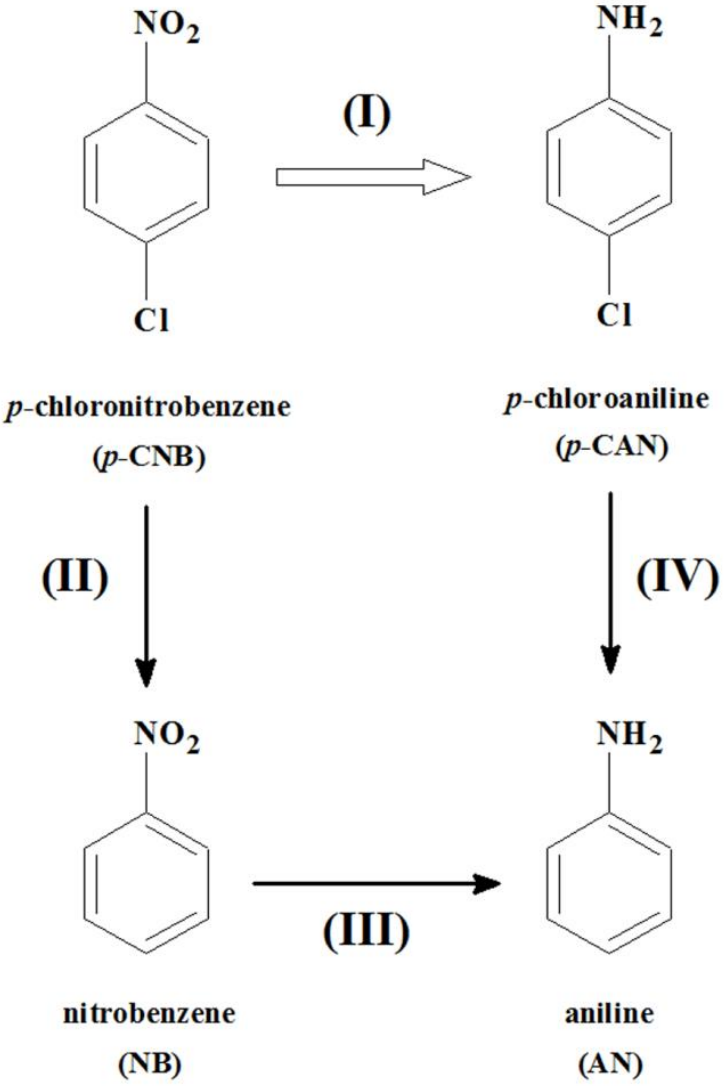

Scheme 6. 1: Reaction scheme for the hydrogenation of *p*-chloronitrobenzene (*p*-CNB). The targeted route (I) to *p*-chloroaniline (*p*-CAN) is given by the open arrow.

can undergo further hydrogenation (step III) or dechlorination of *p*-CAN (step IV) to give, in both cases, aniline (AN). Reaction over the Pd catalysts in this study generated *p*-CAN, NB and/or AN in varying proportions. In such a parallel/sequential reaction mechanism, selectivity is only meaningful at an equivalent level of conversion ($X_{p\text{-}CNB}$), which we set at 0.2 in **Table 6.1**. Bulk Pd was employed as benchmark, serving as an index against which Pd particle size and Pd-support effects can be evaluated. Reaction over unsupported Pd generated all three products with the principal formation of AN (composite hydrodechlorination and hydrogenation). Taking an overview of the catalytic response exhibited by the supported catalysts, three groups emerge, *i.e.* Pd on carbon, *non*-reducible oxides and ZnO, which are separated by the dashed lines in **Tables 6.1 and 6.2**. Carbon supported Pd (Pd/AC) promoted hydrogenation and hydrodechlorination steps with *p*-CAN selectivity that deviated from that observed for bulk Pd. Palladium on *non*-reducible Al_2O_3 and SiO_2 did not generate any detectable *p*-CAN but exhibited hydrodechlorination character (to produce NB and AN). In marked contrast, Pd/ZnO was 100% selective to *p*-CAN. The latter is a very significant finding as, to the best of our knowledge, there have been no reports demonstrating reaction exclusivity to *p*-CAN in the gas phase hydrogenation of *p*-CNB over supported Pd.

Given the distinct selectivity response for the three groupings, one catalyst (commercial Pd/AC-II and Pd/Al_2O_3-II and laboratory synthesised Pd/ZnO) was chosen from each group for further comprehensive catalyst testing; the relationships between conversion ($X_{p\text{-}CNB}$) and selectivity (S_i) are shown in **Figure 6.6** and the activation mode of *p*-chloronitrobenzene over Pd catalysts are shown in **Figure 6.7**. At low $X_{p\text{-}CNB}$ (<0.05), *p*-CAN was the principal product over bulk Pd (**Figure 6.6 (I)**) with the preferential formation of AN at higher conversions and NB as a secondary product. This suggests Pd activation of both $-NO_2$ and $-Cl$ functionalities and is in agreement with published literature showing that dechlorination [92] and nitro-group reduction [41] are promoted over unsupported Pd. The switch in selectivity to C–Cl bond scission and AN formation can be linked to the electron-donating character of the $-NH_2$ function (relative to electron-withdrawing $-Cl$ and $-NO_2$), which can induce electron transfer *via* the benzene ring, increasing C−Cl polarity [93,94] and facilitating hydrogenolytic attack by dissociated H (**Figure 6.7 (I)**). In the case of Pd/AC-II (**Figure 6.6 (II)**), *p*-CAN and AN were the principal products with trace formation of NB. XPS measurements are consistent with the formation of $Pd^{\delta+}$ in Pd/AC. The activation mode of *p*-CNB over Pd/AC was shown in **Figure 6.7 (II)**, the nitro group exhibits a higher relative electronegativity than the *para*-substitued Cl where the ring inductive and

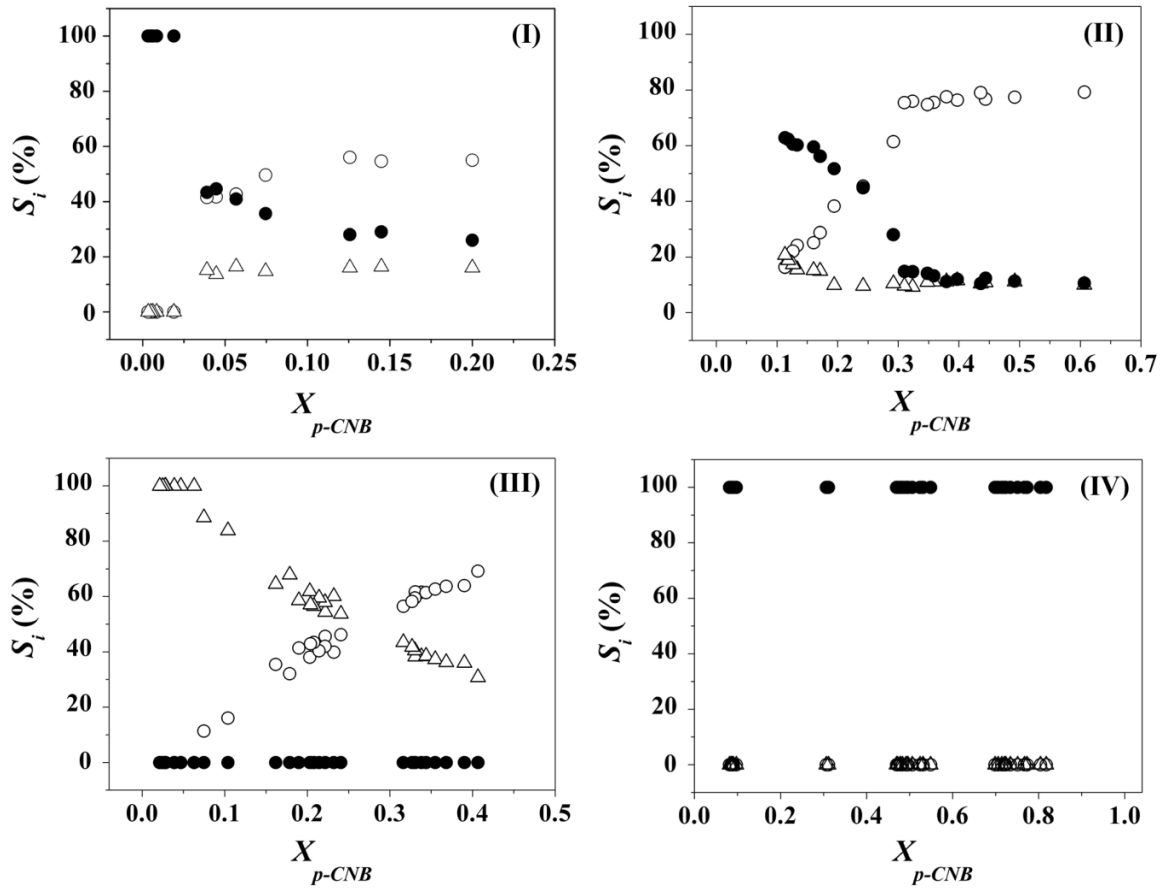

Figure 6. 6: Selectivity (S_i) to *p*-CAN (●), AN (○) and NB (△) as a function of *p*-CNB fractional conversion ($X_{p\text{-}CNB}$) for reaction over (I) bulk Pd (II) Pd/AC-II (III) Pd/Al_2O_3-II and (IV) Pd/ZnO.

conjugative effects serve to increase the electron density of $–NO_2$ [93] with activation at electron-deficient Pd to generate *p*-CAN formation, as reported elsewhere [95,96]. In common with bulk Pd, a decrease in selectivity to *p*-CAN with increased AN is in evidence at higher $X_{p\text{-}CNB}$ (>0.3), indicating a sequential mechanism *via* steps (I) and (IV) (**Scheme 6.1**). Functionalised chlorobenzenes can interact with $Pd^{\delta+}$ through the Cl substituent with a weakening of the C-Cl [97], facilitating hydrogenolysis to AN. In contrast, NB and AN were the only products generated over Pd/Al_2O_3-II (**Figure 6.6 (III)**), where an increase in conversion (>0.3) was accompanied by higher AN selectivity, suggesting that dechlorination preceded NB hydrogenation, *i.e.* reaction *via* steps (II) and (III) in Scheme 1. Both $−NO_2$ and –Cl functions can reduce the electron density of the benzene ring, favouring interaction with $Pd^{\delta-}$ in Pd/Al_2O_3-II, where both substituents are activated (**Figure 6.7 (III)**). The ring carbon bonded to Cl is more susceptible to hydrogenolytic attack as it bears the lowest electron density of all the carbons in the ring [93], leading to NB formation with further hydrogenation to AN.

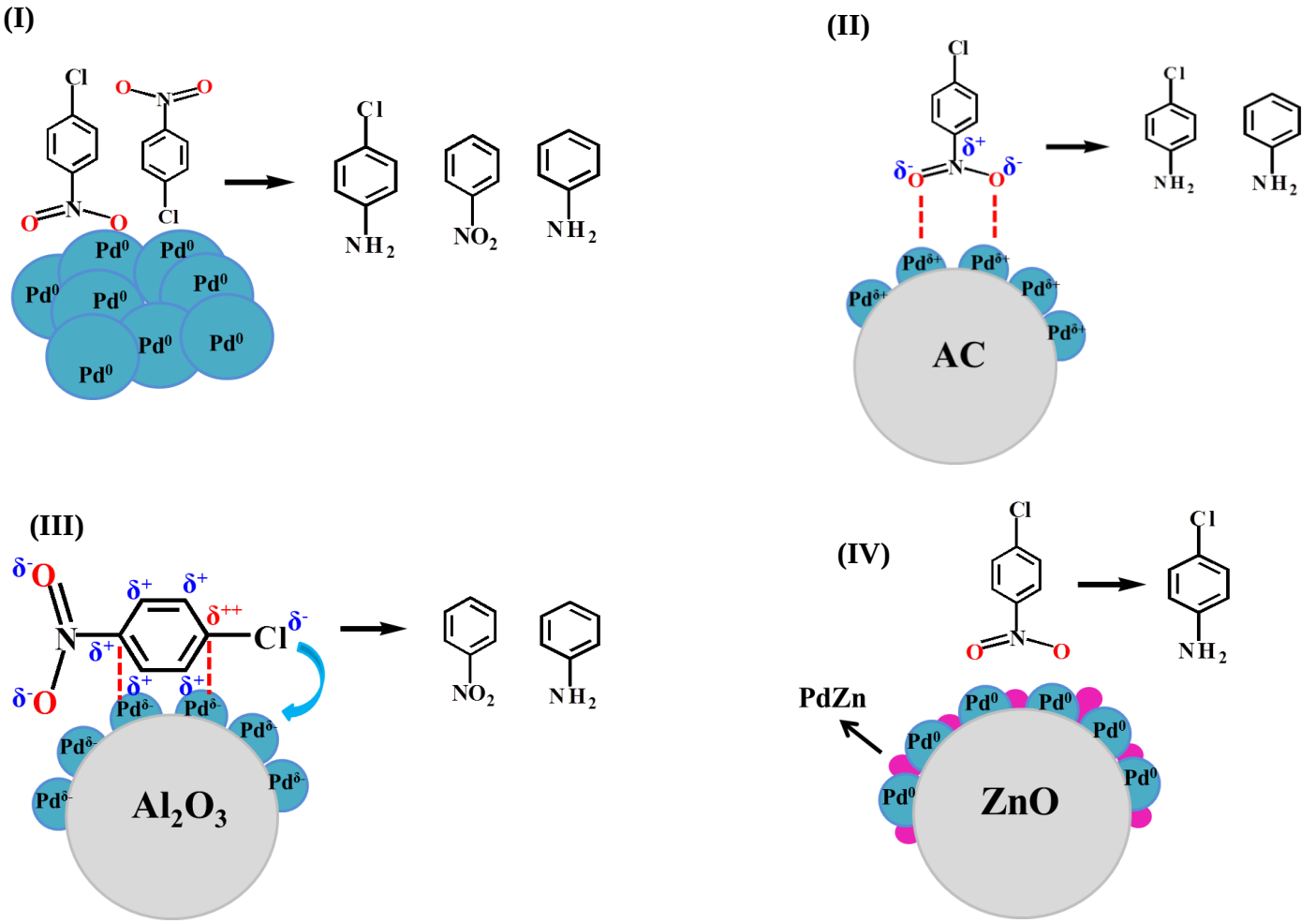

Figure 6.7 : The activation mode of *p*-chloronitrobenzene over Pd catalysts: (I) bulk Pd; (II) Pd/AC; (IV) Pd/Al_2O_3 and (IV) Pd/ZnO.

Reaction over Pd/ZnO (**Figure 6.6 (IV)**) generated *p*-CAN as the sole product, regardless of conversion, *i.e.* exclusive reaction *via* path (I) in **Scheme 6.1**. The Pd/ZnO catalyst is characterized by a Pd $3d_{5/2}$ core level BE close to that of the reference Pd (**Figure 6.5**). As both hydrodechlorination and hydrogenation were promoted over bulk Pd, a similar product distribution should be expected for Pd/ZnO. However, the formation of PdZn alloy, demonstrated by XPS (**Figure 6.4**), must influence *p*-CNB adsorption and surface reaction (**Figure 6.7 (IV)**). Sárkány *et al.* [58] reported the complete suppression of butane formation in the hydrogenation of 1,3-butadiene due to the formation of a PdZn intermetallic phase and attributed this to weaker diene/surface interaction. Iwasa *et al.* [46] recorded enhanced selectivity to primary amine in acetonitrile hydrogenation over Pd/ZnO, ascribing this to differences in substrate and/or intermediate adsorption strength relative to other supported Pd catalysts. XPS analysis has established the formation of zero valent Pd with a lesser (34 % w/w) PdZn component. We envisage H_2 dissociation on Pd^0 to generate surface reactive hydrogen where *p*-CNB interaction with the PdZn phase selectively activates the $–NO_2$ function. Indeed, reaction of *p*-CAN over Pd/ZnO delivered AN as the sole product where the rate (1.6 $mol_{p\text{-CAN}}\ h^{-1}\ mol_{Pd}^{-1}$) was appreciable lower than that (13.5 $mol_{p\text{-CAN}}\ h^{-1}\ mol_{Pd}^{-1}$) recorded for *p*-CNB as reactant. This is consistent with exclusivity to *p*-CAN where path (IV) (in Scheme 1) does not contribute to the overall process for Pd/ZnO.

6.3.2.3 Role of the Stabilizer in Determining Pd/ZnO Performance

In order to establish the possible effect of the stabilizer on the catalytic response exhibited by the catalysts synthesised using the colloid route with $Na_2MoO_4{\cdot}H_2O$, an additional ZnO supported Pd was prepared, employing PVP as stabilizer (see Experimental section), which we label Pd/ZnO-PVP. The as-prepared sample was calcined at 873 K as there is evidence in the literature for the removal of capping polymers at $T \geq 550$ K [98]. There was no detectable (on the basis of XPS analysis, not shown) surface nitrogen associated with the calcined sample, indicating effective PVP removal. Subsequent TPR activation, following the same procedure applied to Pd/ZnO (see Experimental section), generated an equivalent XPS response (profile not shown) with a principal Pd^0 (BE = 335.0 eV) and secondary PdZn (31% w/w, BE = 335.7 eV) component. Palladium particle size distribution from TEM analysis delivered a larger mean Pd size (11.4 nm) for Pd/ZnO-PVP relative to Pd/ZnO (6.5 nm) that can be attributed to sintering during the calcination step. Reaction of *p*-CNB over Pd/ZnO-PVP resulted in the sole formation of the target *p*-CAN. Reaction exclusivity in nitro-group

reduction for both ZnO supported Pd catalysts can be explicitly attributed to the supported PdZn phase. Pd/ZnO-PVP delivered a greater hydrogenation rate than Pd/ZnO (**Figure 6.3 (II)**) although the former exhibited larger Pd particle size. This confirms rate inhibition by residual Mo in the case of Pd/ZnO. The correlation of H_2 chemisorption (**Figure 6.3 (I)**) and activity (**Figure 6.3 (II)**) with Pd size for Pd/ZnO-PVP coincides with the general trend. Our results demonstrate enhanced hydrogenation activity for smaller nano-scale Pd particles irrespective of support, rate suppression due to the presence of residual (Mo-containing) stabilizer and PdZn promotion of full selectivity to *p*-CAN.

6.4 Conclusions

We have established that the support (activated carbon (AC), *non*-reducible (SiO_2, Al_2O_3) and reducible (ZnO) oxides) can influence catalytic performance in Pd promoted gas phase hydrogenation of *p*-CNB. Characterisation of Pd particle size by TEM, H_2 and CO chemisorption has been assessed where the former is shown to give the most reliable results when particle counting is statistically robust. Chemisorption leads to erroneous values arising from (i) the application of an exclusive adsorption stoichiometry factor, (ii) possible Pd site occlusion and/or (iii) contribution due to spillover. Reaction rate and surface hydrogen both increase with decreasing mean Pd size (from 12.6 to 2.4 nm). A lower rate was recorded for particles prepared by a colloidal deposition technique, which is due to site blocking by residual Mo from the stabilizer ($Na_2MoO_4 \cdot H_2O$). Use of PVP as stabilizer (Pd/ZnO-PVP) circumvents Pd poisoning but the calcination step required to remove the polymer induces Pd agglomeration, which impacts on H_2 uptake and hydrogenation rate. Bulk Pd, used as a benchmark, promoted composite hydrodechlorination/hydrogenation to generate *p*-CAN, AN and NB. XPS analysis has demonstrated electron transfer from Pd to AC with the generation of $Pd^{\delta+}$ that activates both –Cl and $–NO_2$ functions with preferential *p*-CAN formation at low *p*-CNB conversion and increased selectivity to AN in subsequent dechlorination at higher conversions. Palladium supported on Al_2O_3 and SiO_2 was *non*-selective to *p*-CAN, exhibiting hydrodechlorination character with preferential NB formation at lower conversion and AN as major product at higher conversion. This can be accounted for in terms of repulsion between $–NO_2$ and –Cl and surface $Pd^{\delta-}$ leading to adsorption *via* the benzene ring, which facilitates hydrogen attack of both substituents. In complete contrast, Pd/ZnO (and Pd/ZnO-PVP) delivered *p*-CAN as the

sole product, which is linked to the formation of a PdZn alloy that serves to activate the nitro function without further dechlorination.

6.5 Reference

[1] P.F. Vogt, J.J. Gerulis, *Ullmann's encyclopedia of industrial chemistry. "Aromatic amines"*, Wiley-VCH, Weinheim, 2005.

[2] N. Bouchenafa-Saïb, P. Grange, P. Verhasselt, F. Addoun, V. Dubois, *Effect of oxidant treatment of date pit active carbons used as Pd supports in catalytic hydrogenation of nitrobenzene*, Appl. Catal. A: Gen. 286 (**2005**) 167.

[3] V. Kratky, M. Kralik, M. Mecarova, M. Stolcova, L. Zalibera, M. Hronec, *Effect of catalyst and substituents on the hydrogenation of chloronitrobenzenes*, Appl. Catal. A: Gen. 235 (**2002**) 225.

[4] G. Neri, M.G. Musolino, C. Milone, D. Pietropaolo, S. Galvagno, *Particle size effect in the catalytic hydrogenation of 2,4-dinitrotoluene over Pd/C catalysts*, Appl. Catal. A: Gen. 208 (**2001**) 307.

[5] D.J. Suh, T.-J. Park, S.-K. Ihm, *Characteristics of carbon-supported palladium catalysts for liquid-phase hydrogenation of nitroaromatics*, Ind. Eng. Chem. Res. 31 (**1992**) 1849.

[6] V. Vishwanathan, V. Jayasri, P.M. Basha, *Vapor phase hydrogenation of o-chloronitrobenzene (o-CNB) over alumina supported palladium catalyst – a kinetic study*, React. Kinet. Catal. Lett. 91 (**2007**) 291.

[7] Q. Xu, X.-M. Liu, J.-R. Chen, R.-X. Li, X.-J. Li, *Modification mechanism of Sn^{4+} for hydrogenation of p-chloronitrobenzene over PVP-Pd/γ-Al_2O_3*, J. Mol. Catal. A: Chem. 260 (**2006**) 299.

[8] X. Meng, H. Cheng, Y. Akiyama, Y. Hao, W. Qiao, Y. Yu, F. Zhao, S.-I. Fujita, M. Arai, *Selective hydrogenation of nitrobenzene to aniline in dense phase carbon dioxide over Ni/γ-Al_2O_3: Significance of molecular interactions*, J. Catal. 264 (**2009**) 1.

[9] F. Cárdenas-Lizana, S. Gómez-Quero, A. Hugon, L. Delannoy, C. Louis, M.A. Keane, *Pd-promoted selective gas phase hydrogenation of p-chloronitrobenzene over alumina supported au*, J. Catal. 262 (**2009**) 235.

[10] F. Cárdenas-Lizana, S. Gómez-Quero, M.A. Keane, *Clean production of chloroanilines by selective gas phase hydrogenation over supported Ni catalysts*, Appl. Catal. A: Gen. 334 (**2008**) 199.

[11] Y. Takenaka, T. Kiyosu, J.-C. Choi, T. Sakakura, H. Yasuda, *Selective synthesis of n-aryl hydroxylamines by the hydrogenation of nitroaromatics using supported platinum catalysts*, Green Chem. 11 (**2009**) 1385.

[12] X.D. Wang, M.H. Liang, J.L. Zhang, Y. Wang, *Selective hydrogenation of aromatic chloronitro compounds*, Curr. Org. Chem. 11 (**2007**) 299.

[13] Y. Chen, C. Wang, H. Liu, J. Qiu, X. Bao, *Ag/SiO_2: A novel catalyst with high activity and selectivity for hydrogenation of chloronitrobenzenes*, Chem. Commun. 42 (**2005**) 5298.

[14] X.-C. Meng, H.-Y. Cheng, S.-I. Fujita, Y.-F. Hao, Y.-J. Shang, Y.-C. Yu, S.-X. Cai, F.-Y. Zhao, M. Arai, *Selective hydrogenation of chloronitrobenzene to chloroaniline in supercritical carbon dioxide over Ni/TiO_2: Significance of molecular interactions*, J. Catal. 269 (**2010**) 131.

[15] F. Cárdenas-Lizana, S. Gómez-Quero, H. Idriss, M.A. Keane, *Gold particle size effects in the gas-phase hydrogenation of m-dinitrobenzene over Au/TiO_2*, J. Catal. 268 (**2009**) 223.

[16] L.M. Sikhwivhilu, N.J. Coville, B.M. Pulimaddi, J. Venkatreddy, V. Vishwanathan, *Selective hydrogenation of o-chloronitrobenzene over palladium supported nanotubular titanium dioxide derived catalysts*, Catal. Commun. 8 (**2007**) 1999.

[17] D.P. He, X.D. Jiao, P. Jiang, J. Wang, B.Q. Xu, *An exceptionally active and selective $Pt-Au/TiO_2$ catalyst for hydrogenation of the nitro group in chloronitrobenzene*, Green Chem. 14 (**2012**) 111.

[18] F. Cárdenas-Lizana, S. Gómez-Quero, N. Perret, M.A. Keane, *Gold catalysis at the gas-solid interface: Role of the support in determining activity and selectivity in the hydrogenation of m-dinitrobenzene*, Catal. Sci. Technol. 1 (**2011**) 652.

[19] F. Cárdenas-Lizana, S. Gómez-Quero, L. Kiwi-Minsker, M.A. Keane, *Gold nano-particles supported on hematite and magnetite as highly selective catalysts for the hydrogenation of nitro-aromatics*, Int. J. Nanotech. 9 (**2012**) 92.

[20] J. Zhang, Y. Wang, H. Ji, Y. Wei, N. Wu, B. Zuo, Q. Wang, *Magnetic nancomposite catalysts with high activity and selectivity for selective hydrogenation of ortho-chloronitrobenzene*, J. Catal. 229 (**2005**) 114.

[21] B. Zuo, Y. Wang, Q. Wang, J. Zhang, N. Wu, L. Peng, L. Gui, X. Wang, R. Wang, D. Yu, *An efficient ruthenium catalyst for selective hydrogenation of ortho-chloronitrobenzene prepared via assembling ruthenium and tin oxide nanoparticles*, J. Catal. 222 (**2004**) 493.

[22] F. Cárdenas-Lizana, S. Gómez-Quero, N. Perret, M.A. Keane, *Support effects in the selective gas phase hydrogenation of p-chloronitrobenzene over gold*, Gold Bull. 42 (**2009**) 124.

[23] K. Xu, Y. Zhang, X. Chen, L. Huang, R. Zhang, J. Huang, *Convenient and selective hydrogenation of nitro aromatics with a platinum nanocatalyst under ambient pressure*, Adv. Synth. Catal. 353 (**2011**) 1260.

[24] F. Figueras, B. Coq, *Hydrogenation and hydrogenolysis of nitro-, nitroso-, azo-, azoxy- and other nitrogen-containing compounds on palladium*, J. Mol. Catal. A: Chem. 173 (**2001**) 223.

[25] F. Zhao, Y. Ikushima, M. Arai, *Hydrogenation of nitrobenzene with supported platinum catalysts in supercritical carbon dioxide: Effects of pressure, solvent, and metal particle size*, J. Catal. 224 (**2004**) 479.

[26] M. Liu, J. Zhang, J. Liu, W.W. Yu, *Synthesis of PVP-stabilized Pt/Ru colloidal nanoparticles by ethanol reduction and their catalytic properties for selective hydrogenation of ortho-chloronitrobenzene*, J. Catal. 278 (**2011**) 1.

[27] M. Liu, W. Yu, H. Liu, *Selective hydrogenation of o-chloronitrobenzene over polymer-stabilized ruthenium colloidal catalysts*, J. Mol. Catal. A: Chem. 138 (**1999**) 295.

[28] A. Tijani, B. Coq, F. Figuéras, *Hydrogenation of para-chloronitrobenzene over supported ruthenium-based catalysts*, Appl. Catal. 76 (**1991**) 255.

[29] Y. Jang, S. Kim, S.W. Jun, B.H. Kim, S. Hwang, I.K. Song, B.M. Kim, T. Hyeon, *Simple one-pot synthesis of Rh-Fe_3O_4 heterodimer nanocrystals and their applications to a magnetically recyclable catalyst for efficient and selective reduction of nitroarenes and alkenes*, Chem. Commun. 47 (**2011**) 3601.

[30] X. Meng, H. Cheng, S.-I. Fujita, Y. Yu, F. Zhao, M. Arai, *An effective medium of H_2O and low-pressure CO_2 for the selective hydrogenation of aromatic nitro compounds to anilines*, Green Chem. 13 (**2011**) 570.

[31] K.N. Rao, B.M. Reddy, S.-E. Park, *Superior copper promoted bimetallic catalysts for chemoselective hydrogenation of ortho-chloro-nitrobenzene*, Catal. Commun. 11 (**2009**) 142.

[32] F. Cárdenas-Lizana, Z.M.d. Pedro, S. Gómez-Quero, M.A. Keane, *Gas phase hydrogenation of nitroarenes: A comparison of the catalytic action of titania supported gold and silver*, J. Mol. Catal. 326 (**2010**) 48.

[33] H.U. Blaser, H. Steiner, M. Studer, *Selective catalytic hydrogenation of functionalized nitroarenes: An update*, ChemCatChem 1 (**2009**) 210.

[34] F. Cárdenas-Lizana, S. Gómez-Quero, M.A. Keane, *Ultra-selective gas phase catalytic hydrogenation of aromatic nitro compounds over Au/Al_2O_3*, Catal. Commun. 9 (**2008**) 475.

[35] J.-J. Zou, Z. Xiong, L. Wang, X. Zhang, Z. Mi, *Preparation of $Pd\text{-}B/\gamma\text{-}Al_2O_3$ amorphous catalyst for the hydrogenation of tricyclopentadiene*, J. Mol. Catal. A: Chem. 271 (**2007**) 209.

[36] C. Jiménez-González, P. Poechlauer, Q.B. Broxterman, B.-S. Yang, D.A. Ende, J. Baird, C. Bertsch, R.E. Hannah, P. Dell'Orco, H. Noorrnan, S. Yee, R. Reintjens, A. Wells, V. Massonneau, J. Manley, *Key green engineering research areas for sustainable manufacturing: A perspective from pharmaceutical and fine chemicals manufacturers*, Org. Proc. Res. Dev. 15 (**2011**) 900.

[37] B. Coq, F. Figuéras, *Structure-activity relationships in catalysis by metals: Some aspecs of particle size, bimetallic and supports effects*, Coord. Chem. Rev. 178-180 (**1998**) 1753.

[38] A.Y. Stakheev, I.S. Mashkovskii, G.N. Baeva, N.S. Telegina, *Specific features of the catalytic behavior of supported palladium nanoparticles in heterogeneous catalytic reactions*, Russ. J. Gen. Chem. 80 (**2010**) 618.

[39] A.Y. Stakheev, W.M.H. Sachtler, *Determination by X-ray photoelectron-spectroscopy of the eelectronic sstate of pd clusters in Y-zeolite*, J. Chem. Soc. Faraday Trans. 87 (**1991**) 3703.

[40] P. Sangeetha, K. Shanthi, K.S.R. Rao, B. Viswanathan, P. Selvam, *Hydrogenation of nitrobenzene over palladium-supported catalysts—effect of support*, Appl. Catal. A: Gen. 353 (**2009**) 160.

[41] X. Yang, H. Liu, H. Zhong, *Hydrogenation of o-chloronitrobenzene over polymer-stabilized palladium-platinum bimetallic colloidal clusters*, J. Mol. Catal. A: Chem. 147 (**1999**) 55.

[42] F. Cárdenas-Lizana, S. Gómez-Quero, M.A. Keane, *Gas phase hydrogenation of m-dinitrobenzene over alumina supported Au and Au-Ni alloy* Catal. Lett. 127 (**2009**) 25.

[43] N. Semagina, M. Grasemann, N. Xanthopoulos, A. Renken, L. Kiwi-Minsker, *Structured catalyst of Pd/ZnO on sintered metal fibers for 2-methyl-3-butyn-2-ol selective hydrogenation*, J. Catal. 251 (**2007**) 213.

[44] M. Crespo-Quesada, M. Grasemann, N. Semagina, A. Renken, L. Kiwi-Minsker, *Kinetics of the solvent-free hydrogenation of 2-methyl-3-butyn-2-ol over a structured Pd-based catalyst*, Catal. Today 147 (**2009**) 247.

[45] M.W. Tew, H. Emerich, J.A.v. Bokhoven, *Formation and characterization of PdZn alloy: A very selective catalyst for alkyne semihydrogenation*, J. Phys. Chem. C 115 (**2011**) 8457.

[46] N. Iwasa, M. Yoshikawa, M. Arai, *Selective hydrogenation of acetonitrile to ethylamine using palladium-based alloy catalysts*, Phys. Chem. Chem. Phys. 4 (**2002**) 5414.

[47] G.M. Maksimova, A.L. Chuvilin, E.A. Moroz, V.A. Likholobov, K.I. Matveev, *Preparation of colloidal solutions of noble metals stabilized by polyoxometalates and supported catalysts based on these solutions*, Kinet. Catal. 45 (**2004**) 870.

[48] B. Lim, M.J. Jiang, J. Tao, P.H.C. Camargo, Y. Zhu, Y. Xia, *Shape-controlled synthesis of Pd nanocrystals in aqueous solutions*, Adv. Funct. Mater. 19 (**2009**) 189.

[49] W.J. Shen, M. Okumura, Y. Matsumura, M. Haruta, *The influence of the support on the activity and selectivity of Pd in CO hydrogenation*, Appl. Catal. A: Gen. 213 (**2001**) 225.

[50] C. Shi, B.W.-L. Jang, *Nonthermal RF plasma modifications on Pd/γ-Al_2O_3 for selective hydrogenation of acetylene in the presence of ethylene*, Ind. Eng. Chem. Res. 45 (**2006**) 5879.

[51] S. Gómez-Quero, F. Cárdenas-Lizana, M.A. Keane, *Effect of metal dispersion on the liquid phase hydrodechlorination of 2,4-dichlorophenol over Pd/Al_2O_3*, Ind. Eng. Chem. Res. 47 (**2008**) 6841.

[52] C. Amorim, M.A. Keane, *Effect of surface acid groups associated with amorphous and structured carbon on the catalytic hydrodechlorination of chlorobenzenes*, J. Chem. Technol. Biotechnol. 83 (**2008**) 662.

[53] C.M. Mendez, H. Olivero, D.E. Damiani, M.A. Volpe, *On the role of Pd β-hydride in the reduction of nitrate over Pd based catalyst*, Appl. Catal. B: Environ. 84 (**2008**) 156.

[54] M. Boudart, H.S. Hwang, *Solubility of hydrogen in small particles of palladium*, J. Catal. 39 (**1975**) 44.

[55] S.B. Ziemecki, J.B. Michel, G.A. Jones, *Hydride formation as a measure of alloying in bimetallic systems containing palladium*, React. Sol. 2 (**1986**) 187.

[56] C. Amorim, M.A. Keane, *Palladium supported on structured and nonstructured carbon: A consideration of pd particle size and the nature of reactive hydrogen*, J. Colloid Interface Sci. 322 (**2008**) 196.

[57] S. Jujjuri, M.A. Keane, *Catalytic hydrodechlorination at low hydrogen partial pressures: Activity and selectivity response*, Chem. Eng. J. 157 (**2010**) 121.

[58] A. Sárkány, Z. Zsoldos, B. Furlong, J.W. Hightower, L. Guczi, *Hydrogenation of 1-butene and 1,3-butadiene mixtures over Pd/ZnO catalysts*, J. Catal. 141 (**1993**) 566.

[59] M.G. Musolino, C. Busacca, F. Mauriello, R. Pietropaolo, *Aliphatic carbonyl reduction promoted by palladium catalysts under mild conditions*, Appl. Catal. A: Gen. 379 (**2010**) 77.

[60] M. Bonarowska, B. Burda, W. Juszczyk, J. Pielaszek, Z. Kowalczyk, Z. Karpiński, *Hydrodechlorination of CCl_2F_2 (CFC-12) over Pd-Au/C catalysts*, Appl. Catal. B: Environ. 35 (**2001**) 13.

[61] A.L. Bonivardi, M.A. Baltanas, *Preparation of Pd/SiO_2 catalysts for methanol synthesis. 3. Exposed metal fraction and hydrogen solubility*, J. Catal. 138 (**1992**) 500.

[62] J.L. Benitez, G.D. Angel, *Effect of chlorine released during hydrodechlorination of chlorobenzene over Pd, Pt and Rh supported catalysts*, React. Kinet. Catal. Lett. 70 (**2000**) 67.

[63] T. Janiak, J. Okal, *Effectiveness and stability of commercial Pd/C catalysts in the hydrodechlorination of meta-substituted chlorobenzenes*, Appl. Catal. B: Environ. 92 (**2009**) 384.

[64] N. Krishnankutty, M.A. Vannice, *The effect of pretreatment on Pd/C catalysts. 1. Adsorption and absorption properties*, J. Catal. 155 (**1995**) 312.

[65] R.J. Matyi, L.H. Schwartz, J.B. Butt, *Particle-size, particle-size distribution, and related measurements of supported metal-catalyts*, Catal. Rev.-Sci. Eng. 29 (**1987**) 41.

[66] P. Canton, G. Fagherazzi, M. Battagliarin, F. Menegazzo, F. Pinna, N. Pernicone, *Pd/CO average chemisorption stoichiometry in highly dispersed supported Pd/γ-Al_2O_3 catalysts*, Langmuir 18 (**2002**) 6530.

[67] F. Pinna, F. Menegazzo, M. Signoretto, P. Canton, G. Fagherazzi, N. Pernicone, *Consecutive hydrogenation on benzaldehyde over Pd catalysts - influence of supports and sulfphur poisoning*, Appl. Catal. A: Gen. 219 (**2001**) 195.

[68] K.I. Hadjiivanov, G.N. Vayssilov, *Characterization of oxide surfaces and zeolites by carbon monoxide as an IR probe molecule* Adv. Catal. 47 (**2002**) 307.

[69] E.A. Sales, J. Jove, M.d.J. Mendes, F. Bozon-Verduraz, *Palladium, palladium–tin, and palladium–silver catalysts in the selective hydrogenation of hexadienes: TPR, mössbauer, and infrared studies of adsorbed CO*, J. Catal. 195 (**2000**) 88.

[70] A. Guerrero-Ruiz, S. Yang, Q. Xin, A. Maroto-Valiente, M. Benito-Gonzalez, I. Rodriguez-Ramos, *Comparative study by infrared spectroscopy and microcalorimetry of the CO adsorption over supported palladium catalysts*, Langmuir 16 (**2000**) 8100.

[71] L.-L. Sheu, Z. Karpinksi, W.M.H. Sachtler, *Effects of palladium particle-size and palladium silicie formation on fourier-transform infrared-spectra of CO adsorbed on Pd/SiO_2 catalysts*, J. Phys. Chem. 93 (**1989**) 4890.

[72] S. Jujjuri, E. Ding, S.G. Shore, M.A. Keane, *A characterization of Ln-Pd/SiO_2 (Ln=La, Ce, Sm, Eu, Gd and Yb): Correlation of surface chemistry with hydrogenolysis activity*, J. Mol. Catal. A: Chem. 272 (**2007**) 96.

[73] G. Prelazzi, M. Cerboni, G. Leofanti, *Comparison of H_2 adsorption, O_2 adsorption, H_2 titration, and O_2 titration on supported palladium catalysts*, J. Catal. 181 (**1999**) 73.

[74] W.C. Conner, J.L. Falconer, *Spillover in heterogeneous catalysis*, Chem. Rev. 95 (**1995**) 759.

[75] B.D. Adams, C.K. Ostrom, S. Chen, A. Chen, *High-performance Pd-based hydrogen spillover catalysts for hydrogen storage*, J. Phys. Chem. C 114 (**2010**) 19875.

[76] C.-T. Hong, C.-T. Yeh, F.-H. Yu, *Effect of reduction and oxidation treatments on Pd/ZnO catalysts*, Appl. Catal. 48 (**1989**) 385.

[77] J. Liu, *Advanced electron microscopy of metal-support interactions in supported metal catalysts*, ChemCatChem 3 (**2011**) 934.

[78] J.R. Anderson, K.C. Pratt, *Introduction to characterization and testing of catalysts*, Academic Press, Sidney, 1985.

[79] D.R. Baer, D.J. Gaspar, P. Nachimuthu, S.D. Techane, D.G. Castner, *Application of surface chemical analysis tools for characterization of nanoparticles*, Anal. Bioanal. Chem. 396 (**2010**) 983.

[80] D. Briggs, M.P. Seah, *Practical surface analysis by auger and x-ray photo-electron spectroscopy*, first ed., Wiley, Chichester, 1983.

[81] S. Hub, L. Hilaire, R. Touroude, *Hydrogenation of but-1-yne and but-1-ene on palladium catalysts. Particle size effect*, Appl. Catal. 36 (**1988**) 307.

[82] L. Jiang, H. Gu, X. Xu, X. Yan, *Selective hydrogenation of o-chloronitrobenzene (o-CNB) over supported Pt and Pd catalysts obtained by laser vaporization deposition of bulk metals*, J. Mol. Catal. A: Chem. 310 (**2009**) 144.

[83] A.L.D. Ramos, P.D.S. Alves, D.A.G. Aranda, M. Schmal, *Characterization of carbon supported palladium catalysts: Inference of electronic and particle size effects using reaction probes*, Appl. Catal. A: Gen. 277 (**2004**) 71.

[84] L.M. Gómez-Sainero, X.L. Seoane, J.L.G. Fierro, A. Arcoya, *Liquid-phase hydrodechlorination of CCl_4 to $CHCl_3$ on Pd/carbon catalysts: Nature and role of Pd active species*, J. Catal. 209 (**2002**) 279.

[85] Y.V. Larichev, B.L. Moroz, V.I. Bukhtiyarov, *Electronic state of ruthenium deposited onto oxide supports: An XPS study taking into account the final state effects*, Appl. Surf. Sci. 258 (**2011**) 1541.

[86] P. Tribolet, L. Kiwi-Minsker, *Palladium on carbon nanofibers grown on metallic filters as novel structured catalyst*, Catal. Today 105 (**2005**) 337.

[87] N. Semagina, A. Renken, L. Kiwi-Minsker, *Palladium nanoparticle size effect in 1-hexyne selective hydrogenation*, J. Phys. Chem. C 111 (**2007**) 13933.

[88] M. Crespo-Quesada, A. Yarulin, M.S. Jin, Y.N. Xia, L. Kiwi-Minsker, *Structure sensitivity of alkynol hydrogenation on shape- and size-controlled palladium nanocrystals: Which sites are most active and selective?*, J. Am. Chem. Soc. 133 (**2011**) 12787.

[89] B. Coq, A. Tijani, F. Figuéras, *Particle size effect on the kinetics of p-chloronitrobenzene hydrogenation over platinum/alumina catalysts.*, J. Mol. Catal. 68 (**1991**) 331.

[90] M. Crespo-Quesada, J.M. Andanson, A. Yarulin, B. Lim, Y.N. Xia, L. Kiwi-Minsker, *UV-ozone cleaning of supported poly(vinylpyrrolidone)-stabilized palladium nanocubes: Effect of stabilizer removal on morphology and catalytic behavior*, Langmuir 27 (**2011**) 7909.

[91] M.S. Zina, A. Ghorbel, in: E.v. Steen, M. Claeys, L.H. Callanan (Eds.), *Recents advances in the science and technology of zeolites and related materials*, Elsevier Science Ltd., Cape Town, 2004, pp. 2364-2370.

[92] C. Amorim, X. Wang, M.A. Keane, *Application of hydrodechlorination in environmental pollution control: Comparison of the performance of supported and unsupported pd and Ni catalysts*, Chin. J. Catal. 32 (**2011**) 746.

[93] B. Zhao, Y.W. Chen, *Hydrogenation of p-chloronitrobenzene on Mo, La, Fe, and W-modified NiCoB nanoalloy catalysts*, J. Non-Cryst. Solids 356 (**2010**) 839.

[94] H. Li, Q. Zhao, H. Li, *Selective hydrogenation of p-chloronitrobenzene over Ni–P–B amorphous catalyst and synergistic promoting effects of B and P*, J. Mol. Catal. A: Chem. 285 (**2008**) 29.

[95] W. Tu, S. Cao, L. Yang, W. Wang, *Modification effects of magnetic supports and bimetallic structures on palladium nanocluster catalysts*, Chem. Eng. J. 143 (**2008**) 244.

[96] H. Liu, M. Liang, C. Xiao, N. Zheng, X. Feng, Y. Liu, J. Xie, Y. Wang, *An excellent Pd-based nanocomposite catalyst for the selective hydrogenation of para-chloronitrobenzene*, J. Mol. Catal. A: Chem. 308 (**2009**) 79.

[97] T. Yoneda, T. Takido, K. Konuma, *Hydrodechlorination reactivity of para-substituted chlorobenzenes over platinum/carbon catalyst*, J. Mol. Catal. A: Chem. 265 (**2007**) 80.

[98] I. Lee, R. Morales, M.A. Albiter, F. Zaera, *Synthesis of heterogeneous catalysts with well shaped platinum particles to control reaction selectivity*, Proc. Natl. Acad. Sci. U. S. A. 105 (**2008**) 15241.

Chapter 7

Gas Phase Chemoselective Hydrogenation of *p*-Nitrobenzonitrile over Gold: Effect of Metal Particle Size, Support and the Metal-Support Interface

In the preceding Chapter, support redox character was established as a critical catalyst feature that determined performance in the hydrogenation of *p*-chloronitrobenzene. That work is extended in this Chapter with a demonstration of generic support effects for the hydrogenation of *p*-nitrobenzonitrile over supported (CeO_2, Fe_2O_3, Fe_3O_4, TiO_2, ZrO_2 and Al_2O_3) Au, Ag and Pd catalysts.

7.1 Introduction

Catalytic hydrogenation by gold is attracting growing research interest as a result of the high chemoselectivity achieved in the reduction of unsaturated functionalities, *i.e.* C≡C [1], C=C [2], C=O [3] and -NO_2 [4], in the presence of other reactive groups. The enhanced selectivity exhibited by Au nanoparticles has been attributed to geometric and electronic properties, which are influenced by interactions with the support [5,6]. Reducible oxide carriers bear a higher number of nucleation sites that facilitate the formation of smaller Au particles (< 9 nm) [7,8]. Hydrogenation rate has shown a dependence on Au size over the 2-9 nm range, notably in -NO_2 [8-10] and -C=O [11] reduction. This has been ascribed to enhanced H_2 dissociation on smaller Au particles [10,12] which is the rate limiting step [13]. Lower rates have also observed for Au particles ≤3 nm and linked to a loss of metallic character [14,15] that inhibits H_2 dissociation. On the other hand, there are studies [11,16] that claim Au particles smaller than 3 nm provide the predominant contribution to hydrogenation activity. Claus and co-workers [17,18] have proposed an Au size effect in C=O adsorption/activation where the occurrence of multiple twinned particles resulted in a lower turnover frequency (TOF) in acrolein hydrogenation. Gold particle shape at the nanoscale determines the principal exposed crystal plane and this can impact on the catalytic response as demonstrated in the hydrogenation of acrolein over Au/TiO_2 and Au/ZrO_2 [15,17,19]. The electronic character of the Au site is an additional consideration that can influence the mode of reactant adsorption [20,21] though the possible catalytic effect is not well

understood with conflicting reports in the literature. In the selective reduction of C=O (relative to C=C), Liu *et al*. [22] and Milone *et al.* [21] reported that $Au^{\delta-}$ (generated as a result of electron transfer from TiO_2, FeO(OH), α-Fe_2O_3 and γ-Fe_2O_3 supports) served to enhance C=O hydrogenation. Lenz and co-workers [23] attributed selectivity to Au morphology, discounting any catalytic effect due to support redox properties or Au charge. In addition to the possible role of the carrier to influence catalytic performance by modifying geometric and/or electronic properties of Au nanoparticles, there is also the possibility of a direct contribution *via* reactant activation at surface coordinatively unsaturated sites [24]. The possibility of reactant (notably -NO_2) activation at the support and/or metal-support interface has been overlooked. Haruta and Daté [25] have suggested that reaction at the interface can dictate rates over Au/TiO_2. Xiong and co-workers [26] attributed the high activity and selectivity in –NO_2 reduction over Ni/TiO_2 to a strong polarisation of the N=O bond at support oxygen vacancies (TiO_x).

Given the high selectivity exhibited by supported nano-scale Au in the production of functionalized amines [27], we have investigated the role of the carrier in determining the catalytic response in the gas phase hydrogenation of *p*-nitrobenzonitrile (*p*-NBN) to *p*-aminobenzonitrile (*p*-ABN). The amine product is used in the synthesis of a diversity of agrochemicals, pharmaceuticals, dyestuffs, urethanes and fine chemicals [28]. We have examined a series of oxide carriers (Al_2O_3, ZrO_2, TiO_2, CeO_2, Fe_2O_3 and Fe_3O_4) with varying redox properties that can impact on (i) Au particle size and electronic properties and (ii) -NO_2 activation for reaction. We further probe support effects by examining selected supported Ag and Pd systems that are active and selective in –NO_2 reduction [4].

7.2 Experimental

7.2.1 Materials and Chemicals

The oxide supports (Al_2O_3, CeO_2, TiO_2), precursors for the synthesis of ZrO_2, Fe_2O_3 and Fe_3O_4 ($ZrOCl_2{\cdot}8H_2O$ and $Fe(NO_3)_3{\cdot}9H_2O$ (> 99%)), Au, Ag and Pd precursors ($HAuCl_4$ (99.999%), $AgNO_3$ (99.99%) and $Pd(NO_3)_2$ (99.99%)) were obtained from Sigma-Aldrich. All the gases (O_2, H_2, N_2 and He) used were of high purity (99.9%, BOC gases). The *p*-nitrobenzonitrile (*p*-NBN reactant (Aldrich (≥98%)), solvent (1-butanol, Riedel-de Haen (≥ 99.5%)) and urea (Riedel-de Häen (≥ 99%)) were used as received.

7.2.2 Catalyst Preparation

The zirconia support precursor was prepared by precipitation with dropwise addition of $ZrOCl_2 \cdot 8H_2O$ (0.1 M, 800 cm^3) to aqueous NH_3 (2.5 M, 120 cm^3) under vigorous stirring (300 rpm) until pH = 9.3 with the formation of $Zr(OH)_4$ according to [29, 30]:

$$ZrOCl_2 \cdot 8H_2O + NH_3 \cdot H_2O \rightarrow Zr(OH)_4 + NH_3 + 2HCl + 6H_2 \quad \textbf{(7.1)}$$

Temporal pH changes were measured with a crystal-body electrode coupled to a data logging and collection system (Pico Technology), calibrated with standard buffer solutions (pH = 7 and 10). The resultant hydrogel was washed thoroughly with deionised water until Cl-free ($AgNO_3$ test), dried at 373 K for 24 h and calcined (1 K min^{-1}) in flowing air (60 cm^3 min^{-1}) at 673 K for 5 h [31].

$$Zr(OH)_4 \rightarrow ZrO_2 + 2H_2O \quad \textbf{(7.2)}$$

Iron oxide (Fe_2O_3) was prepared by precipitation in basic media [10]

$$2[Fe(NO_3)_3 \cdot 9H_2O] + 3Na_2CO_3 \rightarrow 2Fe(OH)_3 + 6NaNO_3 + 3CO_2 + 15H_2O \quad \textbf{(7.3)}$$

where 100 cm^3 aqueous Na_2CO_3 (1 M) was heated to 358 K under constant agitation (300 rpm) with dropwise addition of $Fe(NO_3)_3 \cdot 9H_2O$ (300 cm^3, 1 M). Basic conditions (pH > 7.3) were maintained during precipitation by adding Na_2CO_3 (five additions of 10 g). The solid hydroxide was subsequently aged for 2 h to increase specific surface area (SSA) [32], washed with warm distilled water until the wash water exhibited neutral pH and dried for 3 days at 353 K (2 K min^{-1}) in pure He (60 cm^3 min^{-1}) to produce hematite

$$2Fe(OH)_3 \rightarrow Fe_2O_3 + 3H_2O \quad \textbf{(7.4)}$$

A series of 1 mol % supported metal (Au, Ag and Pd) catalysts were prepared by deposition-precipitation using urea as basification agent. An aqueous mixture of urea (*ca.* 10-fold urea excess) and 400 cm^3 (5×10^{-4} M) metal precursor ($HAuCl_4$, $AgNO_3$ and $Pd(NO_3)_2$) was added with the support. The suspension was stirred and heated to 353 K (at 2 K min^{-1}) and the pH progressively increased (from pH = 3 ~ 4) to reach *ca.* 8 after 3 h as a result of the thermally induced urea decomposition.

$$NH_2\text{-}CO\text{-}NH_2 + 3H_2O \xrightarrow{T=353K} 2NH_4^+ + 2OH^- + CO_2 \quad \textbf{(7.5)}$$

The solid obtained was separated by centrifugation, washed with deionised water (with centrifugation between each washing) and dried in He (45 cm^3 min^{-1}) at 373 K (at 2 K min^{-1}) for 5 h. Au/Fe_3O_4 was obtained from the reduction of Au/Fe_2O_3 as discussed in detail elsewhere [33]. All the samples were sieved to 75 μm average particle diameter (ATM fine test sieves). Prior to use, the catalyst precursors were activated in 60 cm^3 min^{-1} H_2 at 2 K min^{-1} to 423-573 K, which was maintained for 1 h. Prior temperature programmed reduction (TPR) analysis has established full reduction of the supported metal precursor under these conditions [10,34,35].

7.2.3 Catalyst Characterisation

The metal content was measured by absorption atomic spectroscopy using a Shimadzu AA-6650 spectrometer with an air-acetylene flame from the diluted extract in aqua regia (25% v/v HNO_3/HCl). Hydrogen (and O_2) chemisorption and SSA were measured using the commercial CHEM-BET 3000 (Quantachrome) unit. Samples were loaded into a U-shaped quartz cell (3.76 mm *i. d.*) and heated in 17 cm^3 min^{-1} (Brooks mass flow controlled) 5% v/v H_2/N_2 at 2 K min^{-1} to 423-573 K. The samples were swept with 65 cm^3 min^{-1} N_2 for 1.5 h, cooled to reaction temperature (423 K) and subjected to H_2 (or O_2) chemisorption using a pulse (10 μl) titration procedure. Pulse introduction was repeated until the signal area was constant, indicating surface saturation. SSA values were recorded with a 30% (v/v) N_2/He flow; pure N_2 (99.9%) served as the internal standard. At least two cycles of N_2 adsorption–desorption in the flow mode were used to determine SSA using the standard single point BET method. SSA and H_2/O_2 uptake values were reproducible to ±5% and the values quoted are the mean. The degree of support reduction (in the case of supported Au catalysts) was determined from O_2 uptake where it has been demonstrated previously that there is a negligible contribution from Au to total O_2 adsorbed [36]. X-ray photoelectron spectroscopy (XPS) analyses were conducted on an Axis Ultra instrument (Kratos Analytical) under ultra-high vacuum conditions (<10^{-8} Torr) using a monochromatic Al Kα X-ray source (1486.6 eV). The source power was maintained at 150 W and the emitted photoelectrons were sampled from a 750 × 350 μm^2 area at a take-off angle = 90°. The adventitious carbon 1*s* peak was calibrated at 284.5 eV and used as an internal standard to compensate for charging effects. Metal particle morphology (size and shape) was

determined by (scanning) transmission electron microscopy; JEOL JEM 2011 HRTEM unit with a UTW energy dispersive X-ray detector (Oxford Instruments) operated at an accelerating voltage of 200 kV using Gatan Digital Micrograph 3.4 for data acquisition/manipulation. Samples were crushed and deposited (dry) on a holey carbon/Cu grid (300 Mesh). Up to 800 individual metal particles were counted for each catalyst and the surface area weighted mean metal diameter (*d*) calculated from

$$d = \frac{\sum_i n_i d_i^3}{\sum_i n_i d_i^2} \qquad \textbf{(7.6)}$$

where n_i is the number of particles of diameter d_i.

7.2.4 Catalytic Procedure

Reactions were carried out *in situ*, immediately after activation (as above), in a continuous flow fixed bed vertical glass reactor (*i. d.* = 15 mm) at 423 K and 1 atm where operating conditions ensured negligible heat/mass transport limitations. A layer of borosilicate glass beads served as a preheating zone, ensuring that the *p*-NBN reactant was vaporised and reached reaction temperature before contacting the catalyst. Isothermal conditions (±1 K) were maintained by diluting the catalyst bed with ground glass (75 μm); the ground glass was mixed thoroughly with catalyst before insertion into the reactor. Reaction temperature was continuously monitored by a thermocouple inserted in a thermowell within the catalyst bed. A butanolic solution of *p*-NBN was delivered *via* a glass/teflon air-tight syringe using a microprocessor controlled infusion pump (Model 100 kd Scientific) at a fixed calibrated flow rate. A co-current flow of *p*-NBN and H_2 was maintained at $GHSV = 2 \times 10^4$ h^{-1} with an inlet *p*-NBN flow (*F*) in the range $4.0 \times 10^{-5} – 7.2 \times 10^{-5}$ mol h^{-1}; the molar metal (*n*) to *F* ratio spanned the range $1.6 \times 10^{-3} – 6.8 \times 10^{-3}$ h. The calculated partial pressure of *p*-NBN (157.4 Pa) was one magnitude lower than the saturated vapour pressure (6672 Pa) at this reaction conditions ensuring the gasification of the components. The reactor effluent was frozen in a liquid nitrogen trap for subsequent analysis, which was made using a Perkin-Elmer Auto System XL gas chromatograph equipped with a programmed split/splitless injector and a flame ionisation detector, employing a DB-1 50 m × 0.20 mm *i.d.*, 0.33 μm film thickness capillary column (J&W Scientific). Data acquisition and manipulation were performed using the TotalChrom Workstation Version 6.1.2 (for Windows) chromatography data

system and reactant/product molar fractions (x_i) were obtained using detailed calibration plots (not shown). Fractional conversion ($X_{p\text{-}NBN}$) was obtained from

$$X_{p\text{-}NBN}\,(\text{-}) = \frac{[p\text{-NBN}]_{in} - [p\text{-NBN}]_{out}}{[p\text{-NBN}]_{in}} \qquad \textbf{(7.7)}$$

-where selectivity with respect to p-aminobenzonitrile (*p*-ABN) was calculated as

$$S_{p\text{-}ABN}\,(\%) = \frac{[p\text{-ABN}]_{out}}{[p\text{-NBN}]_{in} - [p\text{-NBN}]_{out}} \times 100 \qquad \textbf{(7.8)}$$

$[p\text{-NBN}]_{in}$ and $[p\text{-NBN}]_{out}$ represent *p*-NBN concentrations in the inlet and outlet streams, respectively. In a series of blank tests, passage of *p*-NBN in a stream of H_2 through the empty reactor or over each oxide support alone did not result in any detectable conversion. Repeated reactions with different samples from the same batch of catalyst delivered raw data that were reproducible to within ±7%.

7.3 Results and Discussion

Each oxide supported (Au, Ag and Pd) catalyst was prepared by deposition-precipitation to deliver an equivalent metal loading (1 mol %). The test reactant (*p*-NBN) bears two reducible substituents (-C≡N and $-NO_2$) on the aromatic ring. All the catalysts in this study promoted exclusive production of *p*-ABN in the gas phase hydrogenation of *p*-NBN. This differs from non-selective reaction reported for Raney Ni [37] where both unsaturated groups (-C≡N and $-NO_2$) were reduced.

7.3.1 Effect of Au Particle Size

The oxide supported Au catalysts exhibited a mean diameter in the range 3-8 nm. Taking Au/Al_2O_3 (**A**) and Au/TiO_2 (**B**) as representatives, electron microscopy images **(I)** and associated Au size distributions **(II)** are presented in **Figure 7.1**. Both catalysts exhibit quasi-spherical Au particles at the nano-scale, which was a feature of all the samples given in **Table 7.1**. There is no obvious correlation between (surface area weighted) mean Au size and SSA although Fe_3O_4 with the lowest area (11 $m^2\,g^{-1}$) bore the largest Au nanoparticles (mean= 7.6 nm). Carrier surface area alone does not govern Au dispersion and the surface properties (*e.g.* acid-base, redox) of the support must be taken into consideration. In the synthesis of supported metals by deposition-

precipitation, the point of zero charge (PZC) of the support is a critical variable that determines the solution pH requirements to ensure precursor-support interaction. When

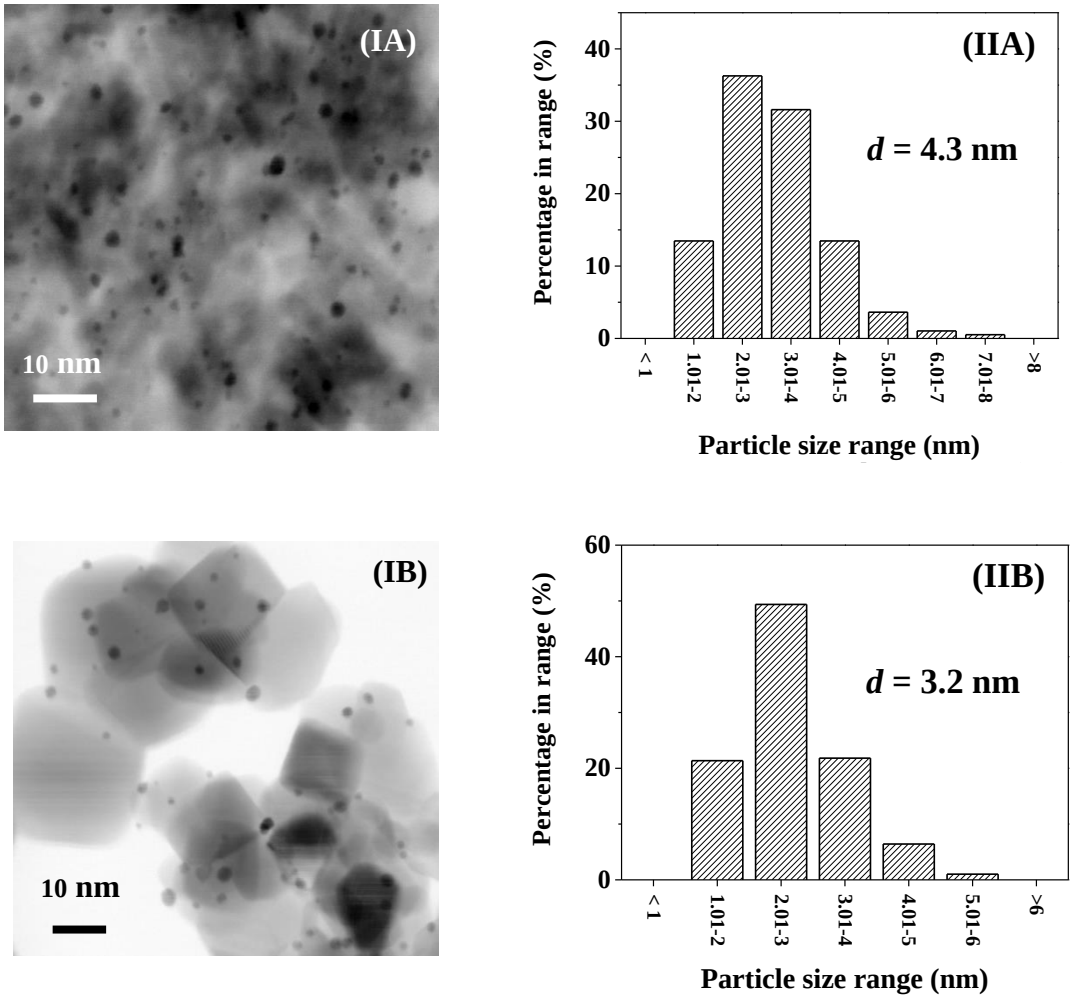

Figure 7. 1: (I) Representative electron microscopy images with (II) associated Au size distribution for (A) Au/Al_2O_3 and (B) Au/TiO_2.

the solution pH < PZC, the support surface bears a positive charge, favouring the interaction with anions species ($[Au(OH)_xCl_{4-x}]^-$) in solution and a pH in excess of PZC leads to a surface affinity for cationic species. It has been established [38] that in aqueous solution $AuCl_4^-$ undergoes sequential substitution of Cl^- with OH^- at pH = 4, 4.6, 6.5, and 9 at which point $Au(OH)_4^-$ is the predominant species. Solution pH during synthesis (≤ 8) facilitated deposition of the anionic precursor on the supports (PZC = 6.0-8.1, **Table 7.1**). It has been reported elsewhere [39] that a partial reduction of the oxide support results in metal-support interactions that impact on Au particle size where smaller nanoparticles are formed on reducible supports with a greater number of

nucleation sites [7,8,14]. Support reducibility was probed by O_2 uptake measurements post-TPR where the results (in Table 1) are in good agreement with support redox potential (E_0) [40,41]. Those supports (CeO_2 and Fe_2O_3) that exhibited the greater degree of reduction also generated the smallest Au particle sizes (**Table 7.1**).

Table 7. 1: Mean Au particle size (*d*, from TEM/STEM), specific surface area (SSA), pH point of zero charge (PZC), redox potential (E_0) and oxygen uptake.

Catalyst	*d* (nm)	SSA ($m^2\ g^{-1}$)	PZC	E_0 (V)	O_2 Uptake ($mmol\ mol_{support}^{-1}$)
Au/CeO_2	2.9	59	6.0	1.61	23
Au/Fe_2O_3	3.0	38	8.1	0.75	27
Au/Fe_3O_4	7.6	11	6.8	0.085	14
Au/TiO_2	3.2	52	6.0	-0.56	0.4
Au/ZrO_2	7.0	94	7.4	-1.55	0.3
Au/Al_2O_3	4.3	158	7.0	-1.66	0.1

Hydrogen dissociation on Au is the key controlling step in catalytic hydrogenation [42] and is dependent on metal site coordination number [43] and temperature [10]. Hydrogen chemisorption was measured at reaction temperature (423 K) and is presented as a function of mean Au particle size in **Figure 7.2(A)**. An increase in uptake with decreasing Au size is evident over the 4-8 nm range. This is consistent with previous work [31] where smaller particles bearing a higher fraction of low coordinated Au sites have been shown to enhance H_2 dissociation [44]. Uptake on catalysts (Au/CeO_2, Au/Fe_2O_3 and Au/TiO_2) with a mean Au size of *ca.* 3 nm was suppressed, which can be attributed to the loss of metallic character at the 1-3 nm size scale with a switch from conductor to semiconductor that limits H_2 dissociation [45-47]. The lower uptake on Au/TiO_2 (experimental point (6)) relative to Au/Al_2O_3 (experimental point (3)) can be linked to the greater proportion of Au particles <3 nm in the former, as established from the size histograms in **Figure 7.1(II)**). The turnover frequencies (TOF, rate per active site) presented in **Figure 7.2(B)** was obtained from Au dispersion (surface $atom_{Au}$ total $atom_{Au}^{-1}$) determined by electron microscopy [48]. The dependence of TOF with mean

Au size coincided with that observed for H_2 uptake, suggesting a direct correlation of hydrogenation rate with H_2 dissociation capacity. The latter is sensitive to Au size

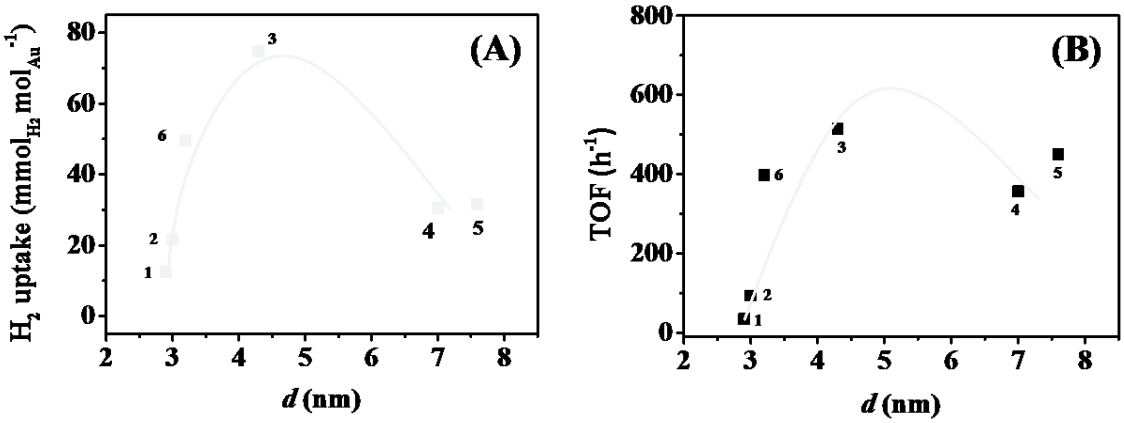

Figure 7. 2: Variation of (A) H_2 chemisorption and (B) *p*-NBN turnover frequency (TOF) with Au particle size (*d*) for (1) Au/CeO_2, (2) Au/Fe_2O_3, (3) Au/Al_2O_3, (4) Au/ZrO_2, (5) Au/Fe_3O_4 and (6) Au/TiO_2.

which is influenced by the nature of the support, notably in terms of reducibility. However, the carrier can also contribute to activity *via p*-NBN activation on the support or at the support-metal interface.

7.3.1 Support Effects

Analysis of possible contributions due to the support must consider activity normalised with respect to H_2 uptake capacity. The specific rate (*r*, per mol H_2) is presented as a function of support E_0 in **Figure 7.3**. A decrease in *r* with increasing E_0 suggests greater intrinsic $–NO_2$ reduction efficiency over less reducible oxide supports. Similar specific rates were attained over catalysts with comparable redox potential but different Au sizes, as illustrated by points **3** (Au/Al_2O_3, E_0 = -1.66 eV, *d* = 4.3 nm) and **4** (Au/ZrO_2, E_0 = -1.55 eV, *d* = 7.0 nm). Taking a similar Au particle size (7.3 ± 0.3 nm, see points **4** and **5** in **Figure 7.3**), the catalyst with the lower support redox potential (Au/ZrO_2, E_0 = -1.55 eV) delivered a specific rate that was a factor of two higher than that obtained over the catalyst with higher E_0 (Au/Fe_3O_4, E_0 = 0.085 eV). This is the first attempt to correlate hydrogenation activity of supported Au with support redox properties. It is known that the oxide support can contribute to reactant activation through surface co-ordinatively unsaturated sites, *i.e.* oxygen vacancies, formed during catalyst activation/TPR [49] at temperatures over the 400-1273 K range [50,51]. Baker *et al*. [52] employing density functional calculations proposed the activation of C=O *via*

the oxygen vacancies on TiO_2. We envision in this work that the $–NO_2$ group is adsorbed *via* surface oxygen vacancies on the support, resulting in strong interactions which serve to stabilise the nitro group and lower catalytic activity.

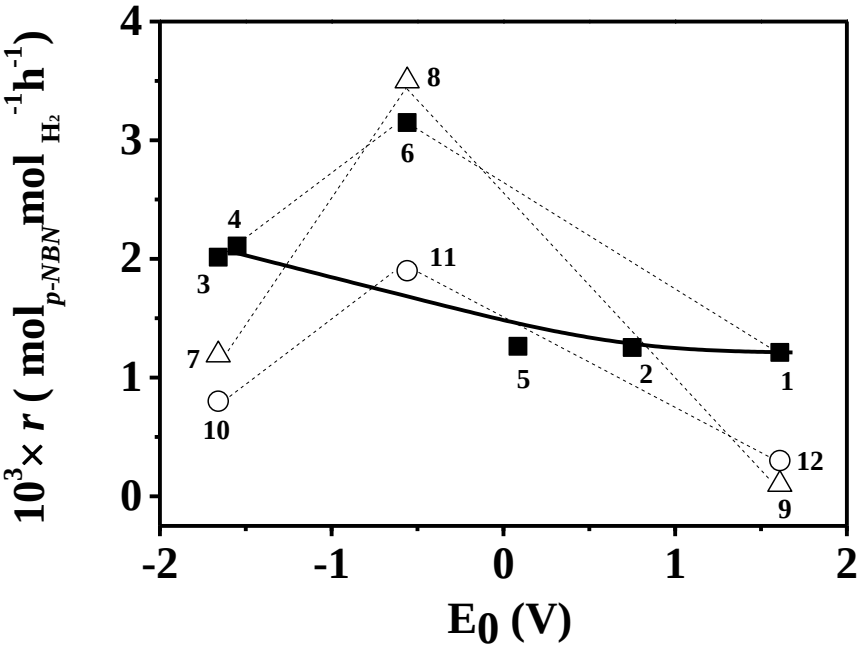

Figure 7. 3: Variation of specific (per mol of H_2) rate (r) with support redox potential (E_0) for reaction over supported Au (■), Ag (△) and Pd (○): ((1) Au/CeO_2; (2) Au/Fe_2O_3; (3) Au/Al_2O_3; (4) Au/ZrO_2; (5) Au/Fe_3O_4; (6) Au/TiO_2; (7) Ag/Al_2O_3; (8) Ag/TiO_2; (9) Ag/CeO_2; (10) Pd/Al_2O_3; (11) Pd/TiO_2; (12) Pd/CeO_2. (Note: rate over Pd was obtained at $x_{p\text{-NBN}}$ = 0.1 using 10% v/v H_2 in He as carrier gas)

It can be seen that Au/TiO_2, characterised by relatively low E_0 and limited oxygen vacancies (from O_2 uptake measurements in **Table 7.1**), deviated significantly from the general trend to deliver a clear maximum in specific hydrogenation rate (**Figure 7.3**). A comprehensive search through literature has revealed that in oxidation reactions the Au-support interface either constitutes the catalytically active site or plays an essential role in governing catalyst performance [53,54]. A possible contribution due to the interface in hydrogenation applications has yet to be definitively established. Given that H_2 activation on Au is an activated process any modification to the electronic properties of the Au site at the boundary with the support can affect the hydrogenation response. This is supported by the work of Corma *et al.* [27,55] who explained (based on DFT calculations) high selectivity in $–NO_2$ reduction in liquid phase hydrogenation over Au/TiO_2 to weak adsorption of the nitrocompound on Au atoms at the nano-particle

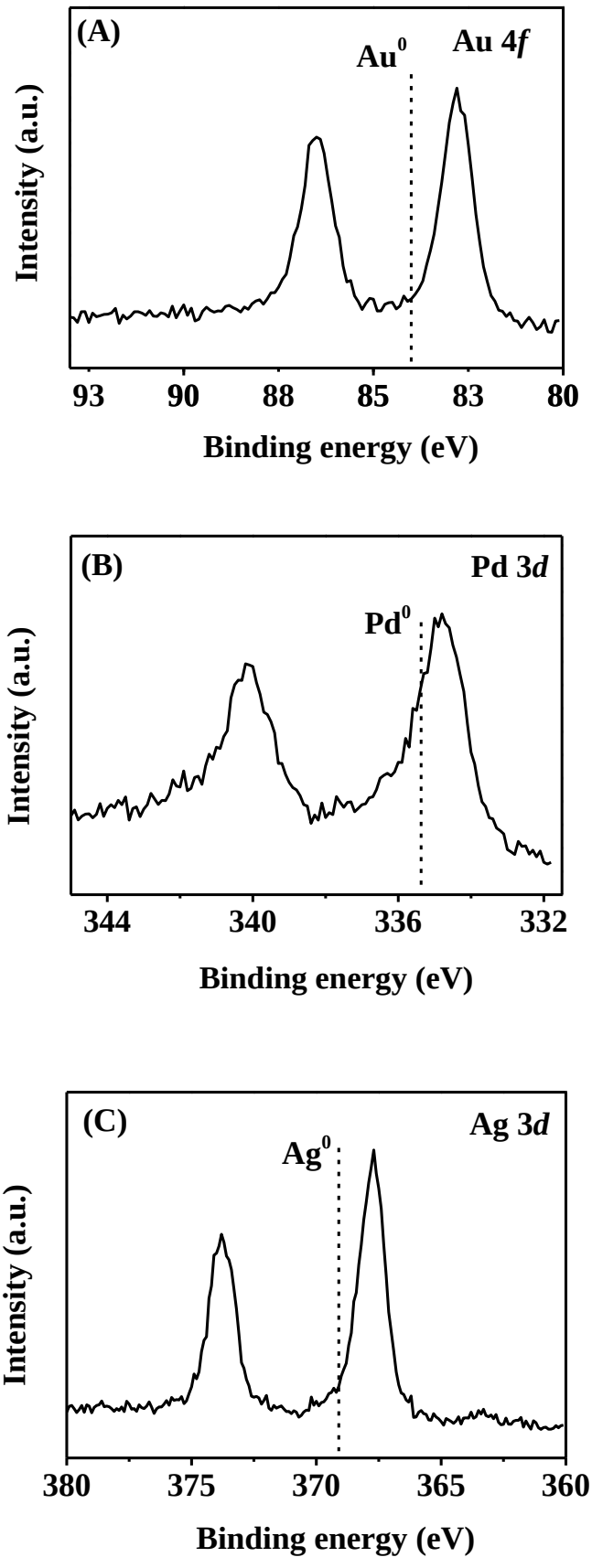

Figure 7. 4: XPS spectra over the Au 4*f*, Pd 3*d* and Ag 3*d* regions for (A) Au/TiO_2, (B) Pd/TiO_2 and (C) Ag/TiO_2.

edge. Hugon *et al*. [56] claimed that the support (TiO_2, Al_2O_3, ZrO_2 and CeO_2) did not influence Au activity in the hydrogenation of 1,3-butadiene. On the other hand, there is a number of studies that have showed superior activity and selectivity for Au/TiO_2 relative to other oxide supported Au catalysts (Au/Al_2O_3, Au/Fe_2O_3 and Au/ZrO_2) but a coherent explanation of this effect was not provided [57,58]. We employed XPS to characterise Au electronic structure and the Au 4*f* profile for Au/TiO_2 is shown in **Figure 7.4(A)**. The recorded Au $4f_{7/2}$ binding energy (BE) of 82.8 eV was significantly lower than that for reference metallic Au (84.0 eV [59]), suggesting electron transferral from TiO_2 to generate $Au^{\delta-}$. This is in accordance with the work of Schimpt *et al.* [60] who reported a down shift of 0.9 eV in BE for nano-sized (5 nm) Au on TiO_2 compared with bulk gold. It is known that support redox character can influence the electron properties of the supported Au phase [5]. The $4f_{7/2}$ BE for Au on oxide supports exhibiting E_0 extremes (CeO_2 (E_0 = 1.61V) and Al_2O_3 (E_0 = -1.66V)) can be compared in **Table 7.2**. In both cases, the measured BE was similar and lower than metallic Au but the shift was not as great as that recorded for Au/TiO_2. This suggests greater

Table 7. 2: XPS Au $4f_{7/2}$, Pd $3d_{5/2}$ and Ag $3d_{5/2}$ binding energies (BE) for Al_2O_3, TiO_2 and CeO_2 supported catalysts.

Metal	Binding energy (eV)		
	Al_2O_3	TiO_2	CeO_2
Au $4f_{7/2}$	83.3	82.8	83.4
Pd $3d_{5/2}$	334.9	334.7	335.3
Ag $3d_{5/2}$	367.7	367.5	368.4

electron-enrichment of Au on TiO_2 due to a lower interfacial energy [61] with a more facile charge transfer from TiO_2. The nitro group can be activated at the Au-TiO_2 interface with polarized $N^{\delta+}$ interacting with $Au^{\delta-}$ *via* electrostatic effects while $O^{\delta-}$ is adsorbed on the support. The cooperative effect of TiO_2 (with lower E_0/reducibility) and an electron-enriched Au must enhance -NO_2 group activation. Somorjai and co-workers [62,63] reached a similar conclusion for the catalytic action of oxide (TiO_x, ZrO_x, TaO_x, FeO_x, etc) supported Rh in the hydrogenation of acetone and CO with carbonyl activation at the metal site through the carbon where the oxygen interacts with a Lewis acid site on the support.

7.3.2 Catalytic Response over TiO_2 Supported Ag and Pd

Metal-support interactions have been suggested for a range of TiO_2 supported group VIII metals [64]. The superior activity and selectivity achieved over TiO_2 supported Pt [65-71], Ni [26,72], Pd [73] and Rh [74] in the hydrogenation of –C=O [66-68], -NO_2 [26,69,71,72], CO_2 [65,74] and CO [73] have been ascribed to: (i)

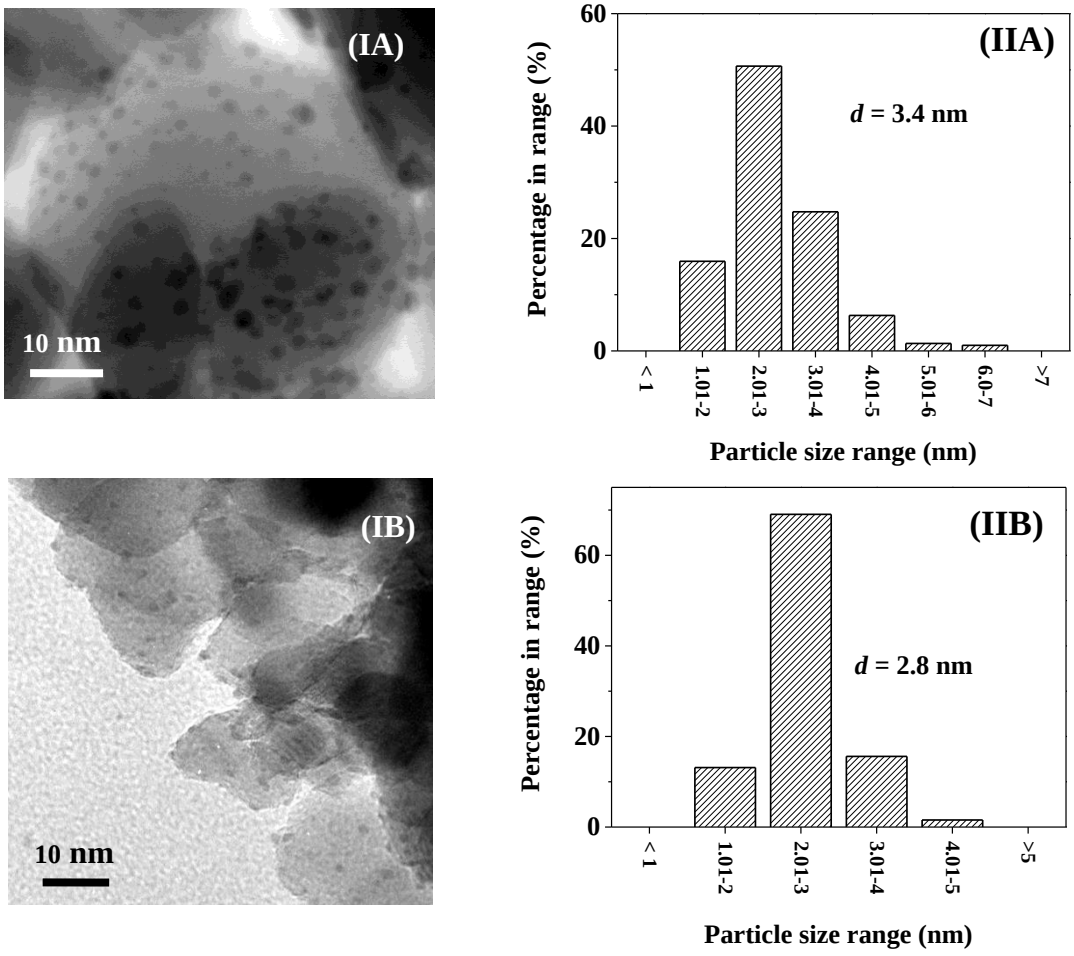

Figure 7. 5: (I) Representative electron microscopy images with (II) associated metal particle size distribution for TiO_2 supported (A) Pd and (B) Ag.

superficial support reduction leading to the formation of TiO_x that facilitates H_2 dissociation; (ii) TiO_x decoration of the metal surface resulting in enhanced reactant activation; (iii) metal-TiO_2 interaction that modifies the electronic character of the active site. To evaluate if the support effect observed for Au/TiO_2 extended to other metals we examined *p*-NBN hydrogenation TiO_2 supported Ag and Pd, comparing the catalytic response with that recorded for Al_2O_3 and CeO_2 supported systems. Mean Ag and Pd particle size on TiO_2 was similar (2.8-3.4 nm) with comparable size distribution

of peudo-spherical particles (**Figure 7.5**). XPS analysis has revealed a downward shift of 0.7 eV in Pd $3d_{5/2}$ BE for Pd/TiO_2 (**Figure 7.4(B)**) relative to metallic Pd (335.4 eV[75]), suggesting electron donation from the support to generate $Pd^{\delta-}$. The Pd $3d_{5/2}$ BE for Pd/Al_2O_3 and Pd/CeO_2 are higher than Pd/TiO_2 with the value measured for Pd/CeO_2 close to the metallic reference (**Table 7.2**). A similar trend applies to the supported Ag samples where the Ag $3d_{5/2}$ BE (**Figure 7.4(C)**) for Ag/TiO_2 was lower than metallic Ag (368.1 eV [76]) with a greater downward shift than Ag/Al_2O_3 and Ag/CeO_2 (**Table 7.2**). The XPS results indicate formation of an electron rich nano-scale Pd and Ag phase on TiO_2. The cooperative or tandem metal and support effect in terms of nitro-group activation at the metal-support interface observed for Au-TiO_2 should also apply. This is borne out in **Figure 7.3** where the specific hydrogenation rate over Ag and Pd pass through a maximum for Ag/TiO_2 and Ag/TiO_2. The maxima for Ag/TiO_2 and Au/TiO_2 coincide where the lower value for Pd/TiO_2 with an appreciably higher H_2 dissociation capacity [77] must reflect less efficient use of H_2 in *p*-NBN hydrogenation.

7.4 Conclusion

A series of 1 mol % oxide (CeO_2, Fe_2O_3, Fe_3O_4, TiO_2, ZrO_2 and Al_2O_3) supported Au catalysts were prepared by deposition-precipitation to generate nano-scale Au particles with (surface area weighted) mean diameters in the 3-8 nm range. All the catalysts were tested in the gas phase hydrogenation of *p*-NBN with full selectivity to *p*-ABN. A decrease in Au size (from 4 to 8 nm) was accompanied by an increase in H_2 chemisorption under reaction conditions. Lower uptake on Au particles $\leq$ 3 nm was recorded and attributed to a loss of metallic character and inhibited H_2 dissociation at this length scale. The dependence of *p*-NBN *TOF* on Au size coincided with that for H_2 uptake. Specific rate normalised with respect to H_2 uptake showed a dependence on support reducibility where interaction with surface oxygen vacancies served to stabilise the nitro-group and inhibit activity. Gold on TiO_2 deviated from the trend with respect to redox potential, showing a maximum in specific rate that can be ascribed to $-NO_2$ activation at the metal-support interface *via* electrostic interaction of polarized $N^{\delta+}$ with electron rich Au ($Au^{\delta-}$) and $O^{\delta-}$ adsorbed on the support. This rate maximum extends to Ag and Pd on TiO_2.

7.5 References

[1] T. Mitsudome, K. Kaneda, *Gold nanoparticle catalysts for selective hydrogenations*, Green Chem. 15 (**2013**) 2636-2654.

[2] L. McEwan, M. Julius, S. Roberts, J.Q. Fletcher, *A review of the use of gold catalysts in selective hydrogenation reactions* Gold Bull. 43 (**2010**) 298-306.

[3] M. Li, X. Wang, N. Perret, M.A. Keane, *Enhanced production of benzyl alcohol in the gas phase continuous hydrogenation of benzaldehyde over* Au/Al_2O_3, Catal. Commun. 46 (**2014**) 187-191.

[4] F. Cárdenas-Lizana, M.A. Keane, *The development of gold catalysts for use in hydrogenation reactions*, J. Mater. Sci. 48 (**2013**) 543-564.

[5] A. Corma, H. Garcia, *Supported gold nanoparticles as catalysts for organic reactions*, Chem. Soc. Rev. 37 (**2008**) 2096-2126.

[6] A. Wolf, F. Schüth, *A systematic study of the synthesis conditions for the preparation of highly active gold catalysts*, Appl. Catal. A: Gen. 226 (**2002**) 1-13.

[7] B.K. Min, W.T. Wallace, D.W. Goodman, *Support effects on the nucleation, growth, and morphology of gold nano-clusters*, Surf. Sci. 600 (**2006**) L7-L11.

[8] F. Cárdenas-Lizana, S. Gómez-Quero, N. Perret, M.A. Keane, *Support effects in the selective gas phase hydrogenation of p-chloronitrobenzene over gold*, Gold Bull. 42 (**2009**) 124-132.

[9] H.-U. Blaser, H. Steiner, M. Studer, *Selective catalytic hydrogenation of functionalized nitroarenes: An update*, ChemCatChem 1 (**2009**) 210-221.

[10] F. Cárdenas-Lizana, S. Gómez-Quero, N. Perret, M.A. Keane, *Gold catalysis at the gas-solid interface: Role of the support in determining activity and selectivity in the hydrogenation of m-dinitrobenzene*, Catal. Sci. Technol. 1 (**2011**) 652-661.

[11] E. Bus, R. Prins, J.A. van Bokhoven, *Origin of the cluster-size effect in the hydrogenation of cinnamaldehyde over supported Au catalysts*, Catal. Commun. 8 (**2007**) 1397-1402.

[12] F. Cárdenas-Lizana, S. Gómez-Quero, H. Idriss, M.A. Keane, *Gold particle size effects in the gas-phase hydrogenation of m-dinitrobenzene over* Au/TiO_2, J. Catal. 268 (**2009**) 223-234.

[13] P. Serna, P. Concepción, A. Corma, *Design of highly active and chemoselective bimetallic gold–platinum hydrogenation catalysts through kinetic and isotopic studies*, J. Catal. 265 (**2009**) 19-25.

[14] F. Cárdenas-Lizana, S. Gómez-Quero, M.A. Keane, *Exclusive production of chloroaniline from chloronitrobenzene over Au/TiO_2 and Au/Al_2O_3*, ChemSusChem 1 (**2008**) 215-221.

[15] P. Claus, A. Brückner, C. Mohr, H. Hofmeister, *Supported gold nanoparticles from quantum dot to mesoscopic size scale: Effect of electronic and structural properties on catalytic hydrogenation of conjugated functional groups*, J. Am. Chem. Soc. 122 (**2000**) 11430-11439.

[16] R. Zanella, C. Louis, S. Giorgio, R. Touroude, *Crotonaldehyde hydrogenation by gold supported on TiO_2: Structure sensitivity and mechanism*, J. Catal. 223 (**2004**) 328-339.

[17] C. Mohr, H. Hofmeister, P. Claus, *The influence of real structure of gold catalysts in the partial hydrogenation of acrolein*, J. Catal. 213 (**2003**) 86-94.

[18] P. Claus, H. Hofmeister, C. Mohr, *Identification of active sites and influence of real structure of gold catalysts in the selective hydrogenation of acrolein to allyl alcohol*, Gold Bull. 37 (**2004**) 181-186.

[19] C. Mohr, H. Hofmeister, J. Radnik, P. Claus, *Identification of active sites in gold-catalyzed hydrogenation of acrolein*, J. Am. Chem. Soc. 125 (**2003**) 1905-1911.

[20] Y. Liu, Y. Luo, Z. Wei, *Selectivity of gold catalysts for selective hydrogenation of cinnamaldehyde*, Asian J. Chem. 25 (**2013**) 8617-8620.

[21] C. Milone, R. Ingoglia, A. Pistone, G. Neri, F. Frusteri, S. Galvagno, *Selective hydrogenation of α,β-unsaturated ketones to α,β-unsaturated alcohols on gold-supported catalysts*, J. Catal. 222 (**2004**) 348-356.

[22] Y.X. Liu, Y.M. Luo, Z.J. Wei, *Selectivity of gold catalysts for selective hydrogenation of cinnamaldehyde*, Asian. J. Chem. 25 (**2013**) 8617-8620.

[23] J. Lenz, B.C. Campo, M. Alvarez, M.A. Volpe, *Liquid phase hydrogenation of α,β-unsaturated aldehydes over gold supported on iron oxides*, J. Catal. 267 (**2009**) 50-56.

[24] A. Saadi, Z. Rassoul, M.M. Bettahar, *Gas phase hydrogenation of benzaldehyde over supported copper catalysts*, J. Mol. Catal. A: Chem. 164 (**2000**) 205-216.

[25] M. Haruta, M. Daté, *Advances in the catalysis of au nanoparticles*, Appl. Catal. A: Gen. 222 (**2001**) 427-437.

[26] J. Xiong, J. Chen, J. Zhang, *Liquid-phase hydrogenation of o-chloronitrobenzene over supported nickel catalysts*, Catal. Commun. 8 (**2007**) 345-350.

[27] A. Corma, P. Serna, *Chemoselective hydrogenation of nitro compounds with supported gold catalysts*, Science 313 (**2006**) 332-334.

[28] S. Nishimura, *Handbook of Heterogeneous Catalytic Hydrogenation for Organic Synthesis* John Wiley, New York (**2001**) 265-265.

[29] R. Rana, S. Pratihar, S. Bhattacharyya, *Effect of powder treatment on the crystallization behaviour and phase evolution of Al_2O_3–high ZrO_2 nanocomposites*, J. Mater. Sci. 41 (**2006**) 7025-7032.

[30] M. Taguchi, S. Takami, T. Adschiri, T. Nakane, K. Sato, T. Naka, *Simple and rapid synthesis of ZrO_2 nanoparticles from $Zr(OET)_4$ and $Zr(OH)_4$ using a hydrothermal method*, CrystEngComm 14 (**2012**) 2117-2123.

[31] N. Perret, X.D. Wang, T. Onfroy, C. Calers, M.A. Keane, *Selectivity in the gas-phase hydrogenation of 4-nitrobenzaldehyde over supported au catalysts*, J. Catal. 309 (**2014**) 333-342.

[32] D. Andreeva, V. Idakiev, T. Tabakova, A. Andreev, R. Giovanoli, *Low-temperature water-gas shift reaction on Au/α-Fe_2O_3 catalyst*, Appl. Catal. A: Gen. 134 (**1996**) 275-283.

[33] S. Gómez-Quero, F. Cárdenas-Lizana, M.A. Keane, *Unique selectivity in the hydrodechlorination of 2,4-dichlorophenol over hematite-supported Au*, J. Catal. 303 (**2013**) 41-49.

[34] F. Cárdenas-Lizana, Z.M. de Pedro, S. Gómez-Quero, M.A. Keane, *Gas phase hydrogenation of nitroarenes: A comparison of the catalytic action of titania supported gold and silver*, J. Mol. Catal. A: Chem. 326 (**2010**) 48-54.

[35] C. Amorim, X. Wang, M.A. Keane, *Application of hydrodechlorination in environmental pollution control: Comparison of the performance of supported and unsupported pd and Ni catalysts*, Chin. J. Catal. 32 (**2011**) 746-755.

[36] G. Bond, C. Louis, D.T. Thompson, *Catalysis by Gold in Catalytic Science Series*, G. J. Hutchings (Ed.) Imperial College Press, London, (**2006**).

[37] K. Koprivova, L. Cerveny, *Hydrogenation of nitrobenzonitriles using raney nickel catalyst*, Res. Chem. Intermediat. 34 (**2008**) 93-101.

[38] F. Moreau, G.C. Bond, *Preparation and reactivation of Au/TiO_2 catalysts*, Catal. Today 122 (**2007**) 260-265.

[39] J. Radnik, C. Mohr, P. Claus, *On the origin of binding energy shifts of core levels of supported gold nanoparticles and dependence of pretreatment and material synthesis*, Phys. Chem. Chem. Phys. 5 (**2003**) 172-177.

[40] S. Salasc, V. Perrichon, M. Primet, M. Chevrier, N. Mouaddib-Moral, *Oxygen titration of spill-over hydrogen in ceria and ceria–alumina supported platinum–*

rhodium catalysts: Application to the determination of the ceria surface in contact with metal, J. Catal. 189 (**2000**) 401-409.

[41] S. Salasc, V. Perrichon, M. Primet, N. Mouaddib-Moral, *Titration by oxygen of the spill-over hydrogen adsorbed on ceria–zirconia supported palladium–rhodium catalysts*, J. Catal. 206 (**2002**) 82-90.

[42] M. Pan, A.J. Brush, Z.D. Pozun, H.C. Ham, W.-Y. Yu, G. Henkelman, G.S. Hwang, C.B. Mullins, *Model studies of heterogeneous catalytic hydrogenation reactions with gold*, Chem. Soc. Rev. 42 (**2013**) 5002-5013.

[43] J.A. van Bokhoven, J.T. Miller, *D electron density and reactivity of the d band as a function of particle size in supported gold catalysts*, J. Phys. Chem. C 111 (**2007**) 9245-9249.

[44] C. Kartusch, J. van Bokhoven, *Hydrogenation over gold catalysts: The interaction of gold with hydrogen*, Gold Bull. 42 (**2009**) 343-348.

[45] L. Stievano, S. Santucci, L. Lozzi, S. Calogero, F.E. Wagner, *197 Au mössbauer study of gold particles obtained by evaporation of metallic gold on mylar*, J. Non-cryst. Solids 232–234 (**1998**) 644-649.

[46] Q. Guo, K. Luo, K.A. Davis, D.W. Goodman, *Initial growth of au on oxides*, Surf. Interface Anal. 32 (**2001**) 161-165.

[47] H.G. Boyen, T. Herzog, G. Kästle, F. Weigl, P. Ziemann, J. Spatz, M. Möller, R. Wahrenberg, M. Garnier, P. Oelhafen, *X-ray photoelectron spectroscopy study on gold nanoparticles supported on diamond*, Phys. Rev. B 65 (**2002**) 075412.

[48] J.J.F. Scholten, A.P. Pijpers, A.M.L. Hustings, *Surface characterization of supported and nonsupported hydrogenation catalysts*, Catal. Rev. 27 (**1985**) 151-206.

[49] N. Perret, X. Wang, J.J. Delgado, G. Blanco, X. Chen, C.M. Olmos, S. Bernal, M.A. Keane, *Selective hydrogenation of benzoic acid over au supported on CeO_2 and $Ce_{0.62}Zr_{0.38}O_2$: Formation of benzyl alcohol*, J. Catal. 317 (**2014**) 114-125.

[50] J. Strunk, W.C. Vining, A.T. Bell, *A study of oxygen vacancy formation and annihilation in submonolayer coverages of TiO_2 dispersed on MCM-48*, J. Phys. Chem. C 114 (**2010**) 16937-16945.

[51] J. Paier, C. Penschke, J. Sauer, *Oxygen defects and surface chemistry of ceria: Quantum chemical studies compared to experiment*, Chem. Rev. 113 (**2013**) 3949-3985.

[52] L.R. Baker, G. Kennedy, M. van Spronsen, A. Hervier, X. Cai, S. Chen, L.-W. Wang, G.A. Somorjai, *Furfuraldehyde hydrogenation on titanium oxide-supported*

platinum nanoparticles studied by sum frequency generation vibrational spectroscopy: Acid–base catalysis explains the molecular origin of strong metal–support interactions, J. Am. Chem. Soc. 134 (**2012**) 14208-14216.

[53] Y.Y. Wu, N.A. Mashayekhi, H.H. Kung, *Au-metal oxide support interface as catalytic active sites*, Catal. Sci. Technol. 3 (**2013**) 2881-2891.

[54] M. Kotobuki, R. Leppelt, D.A. Hansgen, D. Widmann, R.J. Behm, *Reactive oxygen on a Au/TiO_2 supported catalyst*, J. Catal. 264 (**2009**) 67-76.

[55] M. Boronat, P. Concepcion, A. Corma, S. Gonzalez, F. Illas, P. Serna, *A molecular mechanism for the chemoselective hydrogenation of substituted nitroaromatics with nanoparticles of gold on TiO_2 catalysts: A cooperative effect between gold and the support*, J. Am. Chem. Soc. 129 (**2007**) 16230-16237.

[56] A. Hugon, L. Delannoy, C. Louis, *Supported gold catalysts for selective hydrogenation of 1,3-butadiene in the presence of an excess of alkenes*, Gold Bull. 41 (**2008**) 127-138.

[57] M. Okumura, T. Akita, M. Haruta, *Hydrogenation of 1,3-butadiene and of crotonaldehyde over highly dispersed au catalysts*, Catal. Today 74 (**2002**) 265-269.

[58] H. Sakurai, A. Ueda, T. Kobayashi, M. Haruta, *Low-temperature water-gas shift reaction over gold deposited on TiO_2*, Chem. Commun. (**1997**) 271-272.

[59] M. Baron, O. Bondarchuk, D. Stacchiola, S. Shaikhutdinov, H.J. Freund, *Interaction of gold with cerium oxide supports: CeO_2(111) thin films vs CeO_x nanoparticles*, J. Phys. Chem. C 113 (**2009**) 6042-6049.

[60] S. Schimpf, M. Lucas, C. Mohr, U. Rodemerck, A. Brückner, J. Radnik, H. Hofmeister, P. Claus, *Supported gold nanoparticles: In-depth catalyst characterization and application in hydrogenation and oxidation reactions*, Catal. Today 72 (**2002**) 63-78.

[61] F. Cosandey, *Epitaxy, interfacial energy and atomic structure of Au/TiO_2 interfaces*, Philos. Mag. 93 (**2013**) 1197-1218.

[62] A.B. Boffa, C. Lin, A.T. Bell, G.A. Somorjai, *Lewis acidity as an explanation for oxide promotion of metals: Implications of its importance and limits for catalytic reactions*, Catal. Lett. 27 (**1994**) 243-249.

[63] K.J. Williams, A.B. Boffa, M. Salmeron, A.T. Bell, G.A. Somorjai, *The effects of titania overlayers on C_2H_4/CO/H_2 reactions over a Rh foil*, Catal. Lett. 11 (**1991**) 77-88.

[64] S.J. Tauster, *Strong metal-support interactions*, Accounts Chem. Res. 20 (**1987**) 389-394.

[65] S.S. Kim, H.H. Lee, S.C. Hong, *A study on the effect of support's reducibility on the reverse water-gas shift reaction over pt catalysts*, Appl. Catal. A: Gen. 423 (**2012**) 100-107.

[66] M. Englisch, A. Jentys, J.A. Lercher, *Structure sensitivity of the hydrogenation of crotonaldehyde over Pt/SiO_2 and Pt/TiO_2*, J. Catal. 166 (**1997**) 25-35.

[67] M.A. Vannice, D. Poondi, *The effect of metal-support interactions on the hydrogenation of benzaldehyde and benzyl alcohol*, J. Catal. 169 (**1997**) 166-175.

[68] M.A. Vannice, *The influence of msi (metal-support interactions) on activity and selectivity in the hydrogenation of aldehydes and ketones*, Top. Catal. 4 (**1997**) 241-248.

[69] H. Rojas, G. Borda, P. Reyes, M. Brijaldo, J. Valencia, *Liquid-phase hydrogenation of m-dinitrobenzene over platinum catalysts*, J. Chil. Chem. Soc. 56 (**2011**) 793-798.

[70] G. Kennedy, L.R. Baker, G.A. Somorjai, *Selective amplification of C=O bond hydrogenation on Pt/TiO_2: Catalytic reaction and sum- frequency generation vibrational spectroscopy studies of crotonaldehyde hydrogenation*, Angew. Chem. Int. Edit. 53 (**2014**) 3405-3408.

[71] X. Han, R. Zhou, G. Lai, X. Zheng, *Influence of support and transition metal (Cr, Mn, Fe, Co, Ni and Cu) on the hydrogenation of p-chloronitrobenzene over supported platinum catalysts*, Catal. Today 93–95 (**2004**) 433-437.

[72] J. Chen, N. Yao, R. Wang, J. Zhang, *Hydrogenation of chloronitrobenzene to chloroaniline over Ni/TiO_2 catalysts prepared by sol-gel method*, Chem. Eng. J. 148 (**2009**) 164-172.

[73] W.J. Shen, M. Okumura, Y. Matsumura, M. Haruta, *The influence of the support on the activity and selectivity of pd in co hydrogenation*, Appl. Catal. A: Gen. 213 (**2001**) 225-232.

[74] T. Szailer, E. Novak, A. Oszko, A. Erdohelyi, *Effect of H_2S on the hydrogenation of carbon dioxide over supported Rh catalysts*, Top. Catal. 46 (**2007**) 79-86.

[75] M. Brun, A. Berthet, J.C. Bertolini, *XPS, AES and auger parameter of Pd and PdO*, J. Electron Spectrosc. 104 (**1999**) 55-60.

[76] P. Prieto, V. Nistor, K. Nouneh, M. Oyama, M. Abd-Lefdil, R. Díaz, *XPS study of silver, nickel and bimetallic silver-nickel nanoparticles prepared by seed-mediated growth*, Appl. Surf. Sci. 258 (**2012**) 8807-8813.

[77] X. Wang, N. Perret, M.A. Keane, *The role of hydrogen partial pressure in the gas phase hydrogenation of p-chloronitrobenzene over alumina supported au and pd: A consideration of reaction thermodynamics and kinetics*, Chem. Eng. J. 210 (**2012**) 103-113.

Chapter 8

Clean Production of Benzyl Alcohol over Supported Catalysts

Exclusive -NO_2 group reduction over Au has been established in previous Chapters. With a view to demonstrate the applicability of gold for sustainable chemical production, the selective hydrogenation of benzaldehye (to benzyl alcohol) has been examined in both (batch) liquid and (continous) gas phase operation using water as a green solvent; solvent effects in the catalytic response have been evaluated.

8.1 Introduction

The production of benzyl alcohol by the selective reduction of benzaldehyde is an important commercial process due to the multiple industrial applications of the alcohol

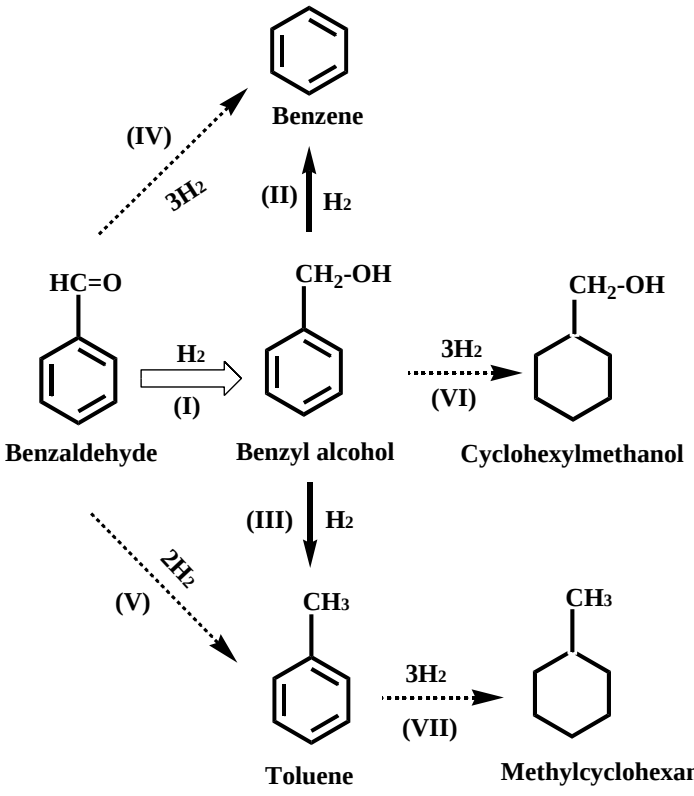

Scheme 8. 1: Reaction pathway associated with benzaldehyde hydrogenation; pathway to the target alcohol (open arrow), by-products detected in this work (solid arrows) and reported in the literature [1] (dashed arrows).

as solvent for ink, paints and lacquers [2]. Oxide supported Ru [3], Pd [4,5], Ni [6,7] Cu

[8] and Pt [9,10] catalysts have been employed in both liquid and gas phase operation. The target of 100% benzyl alcohol yield remains a challenge where undesired hydrogenolysis (to toluene and/or benzene, **Scheme 8. 1**, paths II-V) is difficult to circumvent and reported yields are in the 39-75% range [3-7,9,10]. To date, liquid phase operation using Pt-based catalysts have provided the best results. Li and co-workers [11-13] have achieved 98-99% yield over supported Pt in biphasic (water+benzaldehyde) media at high H_2 pressure (40 bar) [11-13]. They ascribed this result to (i) product transfer to the aqueous phase that avoids readsorption and further reaction, (ii) hydrophobicity of the catalyst surface that favours desorption of benzyl alcohol and (iii) the formation of electron deficient ($Pt^{\delta+}$) nanoparticles that facilitates activation of the C=O function. The energy demands due to the high working pressure and the multi-stepped (template synthesis [14,15], etching [16], washing of the surfactant [17] and deposition of a modifier [14]) catalyst preparation are decided drawbacks for industrial implementation. The role of the metal site electronic character is inconclusive as higher alcohol yield has also been ascribed to electron rich $Pd^{\delta-}$ [18], favouring alcohol desorption.

It has been demonstrated that supported Au [19,20] exhibits enhanced selectivity in the reduction of polyfunctional reactants relative to group VIII metals, notably in the batch liquid phase conversion of aldehydes (crotonaldehyde [21], citral [22] and acrolein [23]). The oxidation state of catalytically active gold is still a matter of debate where zero valent [24], anionic [25] and cationic [26] Au species have been proposed as the active site for hydrogenation. In hydrogenation applications, Au/Al_2O_3 and Au/Fe_2O_3 are among the most widely studied catalysts where at a similar Au size (2-5 nm), electron transfer from Al_2O_3 generates $Au^{\delta-}$ [27-29] while the greater electronegativity of Fe_2O_3 [30] results in electron transfer to the support [31]. Milone *et al.* [32] have proposed that the electronic character of nano-scale Au particles can influence activation of the C=O group with enhanced selectivity for carbonyl group (relative to C=C) reduction over $Au^{\delta-}$ in the conversion of *α,β*-unsaturated ketones to α,β-unsaturated alcohols. The role of Au site electronic character in aldehyde activation and the resultant hydrogenation rate has not been conclusively established.

Catalytic hydrogenation in the liquid phase can be influenced by the solvent [33]. Differences in catalytic activity have been linked to solvent polarity parameters, notably dipolar moment (μ), dielectric constant (ε) [34-36], capacity for hydrogen-bonding (α) [36,37] and H_2 solubility [34]. Aramendía [38] *et al.* and Bertero [35] and co-workers found that acetophone hydrogenation rate decreased with increasing ε of C_1-C_3 alcohols,

which they ascribed to solvation effects that impact on reactant adsorption. In contrast, Wan *et al.* [36] observed an increased 2-butanone hydrogenation rate with increasing ε due to hydrogen bonding that lowered the activation energy barrier. Enhanced hydrodehalogenation activity in polar solvents was explained on the basis of stabilisation of the arenium intermediate [33]. Drelinkiewicza [34] *et al.* concluded that acetophenone hydrogenation was more influenced by the solvent polarity than H_2 solubility. Ethanol [5,12] and alkanes (n-octane [4] and dodecane [18]) have been used as solvents in the liquid phase hydrogenation of benzaldehyde. Water as an innocuous and green reaction medium has not been considered to any great extent. It is, nonetheless, worth flagging the work of Wang and co-workers [39] which demonstrated higher activity in the chemoselective hydrogenation of α,β-unsaturated carbonyl compounds in water relative to organic solvents (ethanol, isopropanol, dioxane and cyclohexane) over Au/CeO_2 although the authors did not offer an explanation for this effect. We provide here the first reported application of Au/Al_2O_3 in the hydrogenation of benzaldehyde in aqueous solution. We have employed a commercial Pt/Al_2O_3 as benchmark catalyst and examined the role of solvent (*n*-pentanol, *n*-butanol, ethanol, H_2O and ethanol + H_2O mixtures) and possible Au site electronic effects (with testing of Au/Fe_2O_3).

8.2 Experimental

8.2.1 Materials

Reagents ($Fe(NO_3)_3.9H_2O$, Na_2CO_3, $HAuCl_4$ (99.999%), Sigma-Aldrich and urea (, ≥99%), Riedel-de Häen) were used as received. The Pt/Al_2O_3 catalyst (0.7% w/w) was obtained from Aldrich and Al_2O_3 from Puralox, Condea Vista. Co.. All the gases used (H_2, N_2, O_2, He) were of high purity (99.9%, BOC gases). The reactants (benzaldehyde, *p*-cyanobenzaldehyde and *p*-tolualdehyde, Aldrich, ≥98%), solvents (ethanol, *n*-butanol, *n*-pentanol, Aldrich, ≥99.5%) and urea (Riedel-de Häen, ≥99%) were used without further purification.

8.2.2 Catalyst Preparation and Activation

The Fe_2O_3 support was prepared as described elsewhere [40]. An aqueous solution (100 cm^3) of Na_2CO_3 (1 M) was placed into a three-necked round-bottom flask and heated (2 K min^{-1}) in a water bath to 363 K under constant agitation (300 rpm) using a vertically mounted glass impeller. An aqueous solution of $Fe(NO_3)_3 \cdot 9H_2O$ (300 cm^3, 1

M) was then added dropwise (300 cm^3 h^{-1}) *via* a glass/Teflon air-tight syringe and Teflon line by means of a microprocessor-controlled infusion pump (100 kd Scientific). Basic conditions (pH > 7.3) were maintained during precipitation with the addition of Na_2CO_3. The solid hydroxide was subsequently aged for 2 h to enhance surface area [41], washed with distilled water until the wash water showed pH ~7 and dried by heating in a flow of He (60 cm^3 min^{-1}) at 2 K min^{-1} to 353 K, which was maintained for 3 days. Gold (1% w/w) on Al_2O_3 and Fe_2O_3 were prepared by deposition-precipitation using urea as basification agent. An aqueous mixture of urea (*ca.* 10-fold urea excess) and $HAuCl_4$ in water (100 cm^3, 25×10^{-3} g cm^{-3}, pH= 2) was added to the support (*ca.* 10 g). The suspension was stirred and heated to 353 K (at 2 K min^{-1}) and the pH progressively increased to reach *ca.* 7 after 3 h as a result of the thermally induced urea decomposition.

$$NH_2\text{-}CO\text{-}NH_2 + 3H_2O \xrightarrow{T=353K} 2NH_4^+ + 2OH^- + CO_2 \qquad \textbf{(8.1)}$$

The solid obtained was separated by centrifugation, washed with deionised water (with centrifugation between each washing) and dried in He (45 cm^3 min^{-1}) at 2 K min^{-1} to 373 K, which was maintained for 5 h. All the samples were sieved to 75 μm average particle diameter (ATM fine test sieves). Prior to use in catalysis, the samples were activated in 60 cm^3 min^{-1} H_2 at 2 K min^{-1} to a final activation temperature (423 K (Au/Fe_2O_3 [40]), 523 K (Au/Al_2O_3 [42]) and 773 K (Pt/Al_2O_3) [43]) that ensured full reduction of the supported metal precursor. Post activation, the samples were cooled to 298 K and passivated in 1% v/v O_2/He for off-line analysis.

8.2.3 Catalyst Characterisation

The metal (Au and Pt) content was measured by inductively coupled plasma-optical emission spectrometry (ICP-OES, Vista-PRO, Varian Inc.) from the diluted extract in HF. Catalyst activation and chemisorption (353 K) measurements were conducted using the commercial CHEM-BET 3000 (Quantachrome) unit. The sample was loaded into a U-shaped quartz cell (3.76 mm *i. d.*), heated in 17 cm^3 min^{-1} (Brooks mass flow controlled), 5% v/v H_2/N_2 at 2 K min^{-1} to the 423-773 K and kept at the final isothermal hold until a return to the baseline. The samples were swept with 65 cm^3 min^{-1} N_2 for 1.5 h, cooled to 353 K and subjected to H_2 chemisorption using a pulse (10-50 μl) titration procedure. Hydrogen pulse introduction was repeated until the signal area was constant,

indicating surface saturation. Metal particle morphology (size and shape) was determined by scanning transmission (JEOL 2200FS field emission gun-equipped TEM unit) electron microscopy, employing Gatan DigitalMicrograph 1.82 for data acquisition/manipulation. Samples were dispersed in acetone and deposited on a holey carbon/Cu grid (300 Mesh). Up to 1000 individual particles were counted for each catalyst and the surface area mean metal (Au, Pt) diameter (d_{STEM}) was calculated from

$$d_{STEM} = \frac{\sum_i n_i d_i}{\sum_i n_i} \qquad \textbf{(8.2)}$$

where n_i is the number of particles of diameter d_i. XPS spectra were collected on a SPECS (Phoibos MCD 150) X-ray photoelectron spectrometer, using an Al Kα ($h\nu$ = 1486.6 eV) X-ray source. Binding energies were calibrated with respect to the C-C/C-H component of the C 1*s* peak (binding energy = 284.7 eV); spectra processing employed the Casa XPS software package [44].

8.2.4 Catalytic System

The liquid phase hydrogenation of benzaldehyde (T = 353 K; P = 9.0 bar) was carried out in a commercial batch stirred stainless steel reactor (100 cm^3 autoclave, Parr reactor) equipped with a H_2 supply system (GCE-Druva). The temperature was maintained at 353 ± 1 K by a process controller (Scientific & Medicine Products Ltd). At the beginning of each run, the benzaldehyde (or *p*-cyanobenzaldehyde or *p*-tolualdehyde) solution (40 cm^3, 0.05 M) and catalyst were charged and flushed three times with H_2. The system was then heated to the reaction temperature, pressurised, and the stirring engaged (time t = 0 for reaction) at 300-1100 rpm. In a series of blank tests, no measurable conversion was detected for reactions conducted in the absence of catalyst. The initial molar reactant to metal ratio spanned the range 2×10^3 - 11.0×10^3. A liquid sampling system *via* syringe with in-line filters allowed a controlled withdrawal of aliquots ($\leq$1.0 cm^3) from the reactor. The concentration of the organic species in the bulk liquid phase was determined from the total mass balance in the reaction mixture. The fractional conversion of benzaldehyde ($X_{Benzaldehyde}$) is defined as

$$X_{Benzaldehyde}(-) = \frac{[Benzaldehyde]_0 - [Benzaldehyde]}{[Benzaldehyde]_0} \qquad \textbf{(8.3)}$$

where subindex '0' refers to initial concentration. Initial benzaldehyde consumption rate (R_0) was determined from a linear regression of the temporal benzaldehyde concentration profiles at $X_{Benzaldehyde}$ < 0.25 [45]. Selectivity to benzyl alcohol ($S_{Benzylalcohol}$) is given by

$$S_{Benzylalcohol} = \frac{[Benzylalcohol]}{[Benzylalcohol]_0 - [Benzylalcohol]} \times 100 \qquad \textbf{(8.4)}$$

The gas phase hydrogenation of benzaldehyde (T = 413 K; P = 1 bar) was carried out in a fixed bed vertical glass tubular reactor (15 mm *i.d.)* under negligible internal or external mass and heat transfer limitations as described elsewhere [46]. Benzaldehyde (0.05 M aqueous solution) was delivered at a fixed calibrated flow rate to the reactor *via* a glass/teflon air-tight syringe and teflon line using a microprocessor controlled infusion pump (Model 100 kd Scientific). A co-current flow of benzaldehyde and H_2 was maintained at a GHSV=2×10^4 h^{-1} with an inlet reactant molar flow (F) = 6.0×10^{-5} mol h^{-1}. The molar metal to inlet molar organic feed rate (n/F) ratio spanned the range 3×10^{-3}– 42×10^{-3} h. The partial pressure of benzaldehyde (27.5 Pa) and the only product benzyl alcohol (2.7 Pa) were calculated which were at least 3 magnitude lower than the saturated partial pressure ($P^*_{benzaldehyde}$ =34266.8 Pa, $P^*_{benzyl\ alcohol}$ = 12614.7 Pa) at this reaction conditions (**Appendix 4**) ensuring the gasification of all the components. Passage of reactant in a stream of H_2 through the empty reactor did not result in any detectable conversion. The fractional conversion of benzaldehyde ($X_{Benzaldehyde}$) is defined as

$$X_{Benzaldehyde}(-) = \frac{[Benzaldehyde]_{in} - [Benzaldehyde]_{out}}{[Benzaldehyde]_{in}} \qquad \textbf{(8.5)}$$

where 'in' and 'out' refer to the inlet and outlet streams. Selectivity to benzyl alcohol ($S_{Benzylalcohol}$) is given by

$$S_{Benzylalcohol} = \frac{[Benzylalcohol]_{out}}{[Benzaldehyde]_{in} - [Benzaldehyde]_{out}} \times 100 \qquad \textbf{(8.6)}$$

The composition of reaction/product mixtures was analysed by gas chromatography

using a Perkin-Elmer AutoSystem XL chromatograph equipped with a programmed split/splitless injector and a flame ionisation detector, employing a DB-1 capillary column (*i.d.* = 0.33 mm, length = 50 m, film thickness = 0.20 μm). Data acquisition and manipulation were performed using the TotalChrom Workstation (Version 6.3.2 for Windows) chromatography data system. Repeated reaction runs with the same batch of catalyst delivered conversion/selectivity values that were reproducible to within ±5%.

8.3 Results and Discussion

8.3.1 Catalyst Characterisation

The metal loading, particle size (from STEM analysis), H_2 chemisorption and XPS binding energy (BE) over the Au $4f_{7/2}$ region are given in **Table 8.1**. Both supported Au catalysts (Au/Al_2O_3 and Au/Fe_2O_3) exhibit similar metal content and mean Au diameter with a common narrow size distribution 1-8 nm (**Figure 8.1**). This equivalence facilitates a direct comparison of the catalytic response. Hydrogen uptake on supported Au is sensitive to Au size where dissociative adsorption is favoured on smaller particles [47], which contributes to enhanced hydrogenation rate [47]. However,

Table 8. 1: Metal content, mean metal particle size (d_{STEM}), H_2 chemisorption (T = 353 K), XPS binding energies (BE) over Au $4f_{7/2}$ region and reaction rates in the liquid phase hydrogenation of benzaldehyde (T = 353 K, P = 9 bar).

	Au/Al_2O_3	Au/Fe_2O_3	Pt/Al_2O_3
Metal content w/w (%)	1.1	1.0	0.7
d_{STEM} (nm)	3.6	2.2	1.7
H_2 uptake (μmol g^{-1})	2.8	0.9	22.7
BE $4f_{7/2}$ (eV)	83.4	84.2	-
[a]R_0 (h^{-1})	78	73	446
[b]R_0 (h^{-1})	23	14	58

[a]initial rate obtained for reaction in water

[b]initial rate obtained for reaction in ethanol

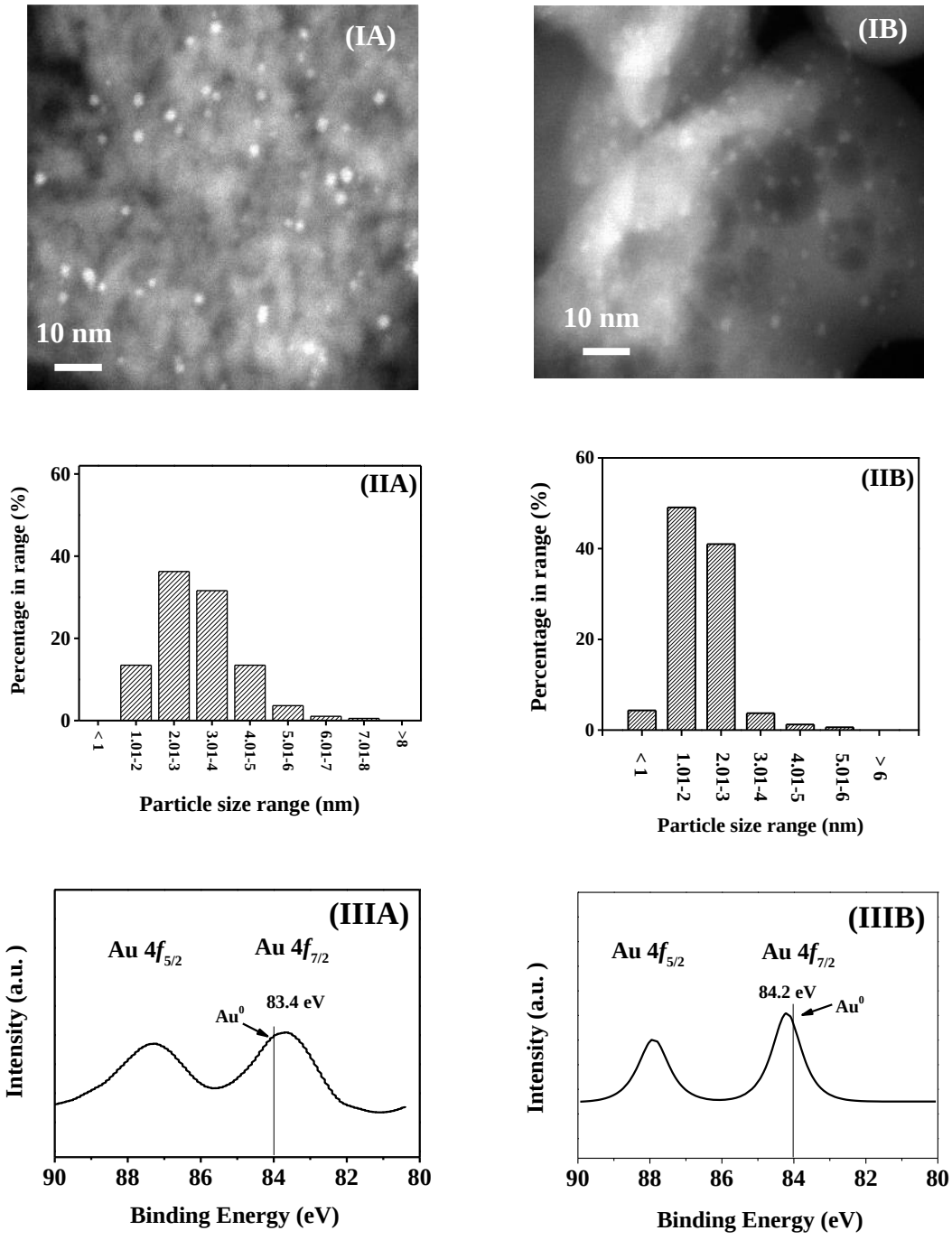

Figure 8. 1: (I) Representative STEM images with (II) associated particle size distribution and (III) XPS spectra over the Au 4*f* binding energy region for (A) Au/Al_2O_3 and (B) Au/Fe_2O_3.

there is evidence that Au particles in the 1-3 nm range exhibit a switch from conductor

to semiconductor that limits H_2 dissociation [48-50]. The lower H_2 uptake on Au/Fe_2O_3 relative to Au/Al_2O_3 (**Table 8.1**) can be linked to the greater proportion of Au particles < 3 nm in the former (**Figure 8.1(II)**). The XPS profile for Au/Al_2O_3 (**Figure 8.1(III)**) is characterised by a Au $4f_{7/2}$ binding energy (BE) = 83.4 eV that is lower than that reported for metallic gold (84.0 eV [51]), suggesting support→metal electron transfer resulting in the formation of $Au^{\delta-}$ and which is consistent with the literature [27-29]. In contrast, Au/Fe_2O_3 shows a Au $4f_{7/2}$ BE = 84.2 eV close to the metallic reference and agrees with the data (84.3 ± 0.1 eV) reported by Capos *et al.* [31]. Alumina supported Pt (0.7% w/w) used as a benchmark shows pseudo-spherical Pt nanoparticles (**Figure 8.2(I)**) with sizes in the range 1-7 nm (**Figure 8.2(II)**) and a mean = 1.7 nm. Hydrogen chemisorption on Pt/Al_2O_3 (**Table 8.1**) was an order of magnitude greater than that obtained for the Au catalysts and can be attributed to the greater capacity of Pt to dissociate H_2 [52,53].

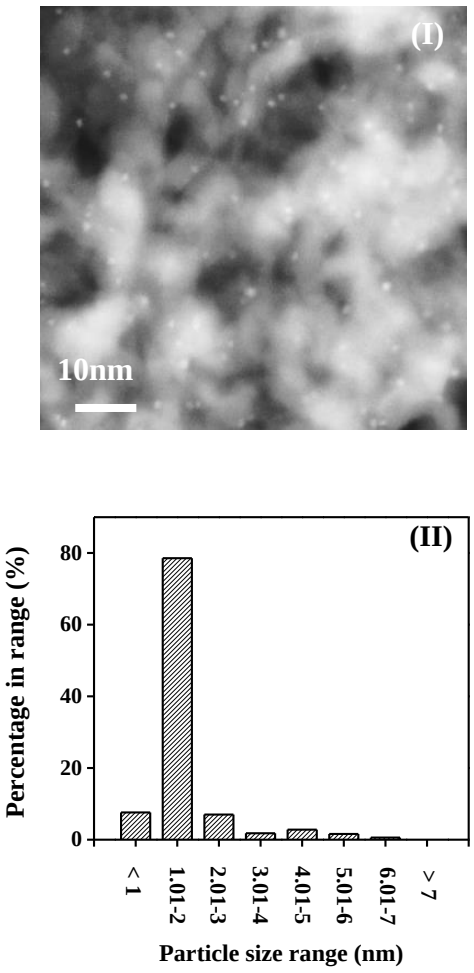

Figure 8. 2: (I) Representative STEM image with (II) associated particle size distribution for Pt/Al_2O_3.

8.3.2 Liquid Phase Hydrogenation of Benzaldehyde

8.3.2.1 Reaction under Kinetic Control

Benzaldehyde hydrogenation rate was determined from the linear variation of concentration with time, as shown in **Figure 8.3(I)**. In order to minimise diffusion and mass transfer limitations and ensure the reaction is operated under kinetic control, we have examined the effect of variations in agitation speed and catalyst mass on reaction rate as two well-established diagnostic methodologies to assess external and internal mass transfer constrains [54-56]. An increase in stirring speed from 300 to 700 rpm was accompanied by a proportional increase in rate, which remained constant at higher stirring speeds (**Figure 8.3(IA)**). This is indicative of minimal gas-liquid/liquid-solid mass transfer contributions to hydrogenation rate [57,58]. Based on these results, the stirring speed was set at 900 rpm for subsequent tests. Rate was invariant over the range of catalyst masses presented in (**Figure 8.3(IB)**), confirming chemical control where external or internal transport constrains do not contribute to the catalytic response [57].

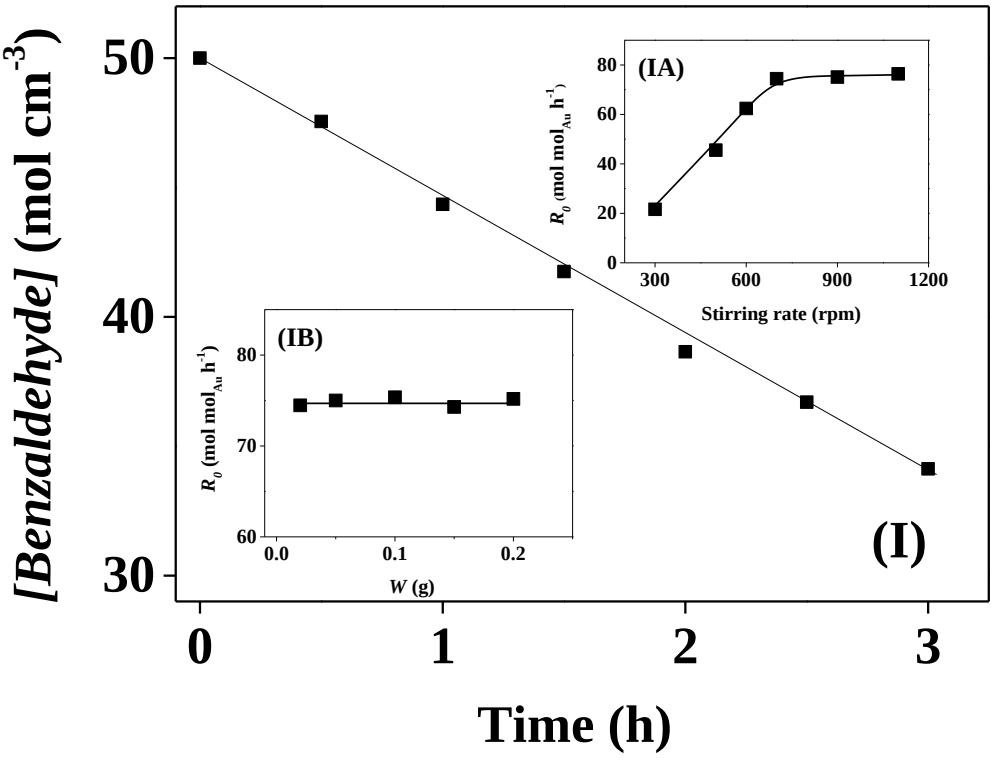

Figure 8. 3: (I) Variation of benzaldehyde concentration (*[Benzaldehyde]*) with time; dependence of initial benzaldehyde consumption rate (R_0) in water with (IA) stirring speed and (IB) mass of catalyst for reaction over Au/Al_2O_3. *Reaction conditions*: T = 353 K, P = 9 bar.

8.3.2.2 Catalytic Performance: Supported Au vs. Pt.

The temporal hydrogenation of benzaldehyde over Au/Fe_2O_3, Au/Al_2O_3 and Pt/Al_2O_3 can be compared in **Figure 8.4.** Both Au catalysts exhibited full selectivity to the target alcohol at all levels of benzaldehyde conversions (**Figure 8.4(I)**) to deliver 100% benzyl alcohol yield. Reaction selectivity is challenging in benzaldehyde hydrogenation with possible by-products shown in **Scheme 8.1**. Step I represents the target reduction of carbonyl group where subsequent hydrogenolysis results in the formation of benzene (step II) and toluene (step III) [59,60]. Benzene and toluene can also be formed directly from benzaldehyde (step IV and V) [59]. Further hydrogenation of benzyl alcohol to cyclohexylmethanol (step VI) has been reported for Ru/C [61] with toluene reduction to methylclohexane (step VII) over Ni/Al_2O_3 [7]. The reaction was prolonged for a further 15 h after complete benzaldehyde conversion (**Figure 8.4(II)**) where the benzyl alcohol product did not undergo further reaction. Benzyl alcohol production rate over Au/Al_2O_3 was equivalent or slightly higher than Au/Fe_2O_3 which may be related to the higher H_2 uptake (**Table 8.1**) but there is no compelling evidence for any effect due to Au site electron density. The reaction rate recorded for Pt/Al_2O_3 was significantly higher (**Table 8.1**), which can be attributed to the greater H_2 chemisorption capacity. A deviation in selectivity is apparent where Pt/Al_2O_3 promoted hydrogenolysis to toluene and benzene with a lower yield (95%) to benzyl alcohol at full benzaldehyde conversion. Moreover, at extended reaction times, benzene and toluene production was increased with decreasing selectivity to benzyl alcohol (87%), suggesting a sequential hydrogenation and hydrogenolysis (steps II and III) over Pd/Al_2O_3. It has been proposed [8] that benzaldyde hydrogenation over Cu/Al_2O_3 proceeds by a nucleophilic attack where the carbonyl function is activated *via* interaction with Lewis acid sites on Al_2O_3. Reactive hydrogen (as nucleophile) can be supplied by H_2 dissociation on the supported Au phase. In the hydrogenation of substituted benzaldehydes bearing -C≡N and -C=O in the *para* position, Au/Al_2O_3 exhibited full selectivity in generating the corresponding alcohol with decreasing activity in the order: *p*-cyanobenzaldehyde (89 h^{-1}) > benzaldehyde (26 h^{-1}) > *p*-tolualdehyde (13 h^{-1}). The electron withdrawing -C≡N group acts to lower the electron density of the -C=O function (*p*-cyanobenzaldehyde), facilitating nucleophilic attack whereas $–CH_3$ as an electron donating group (in *p*-tolualdehyde) renders -C=O more electron-rich, inhibited activation.

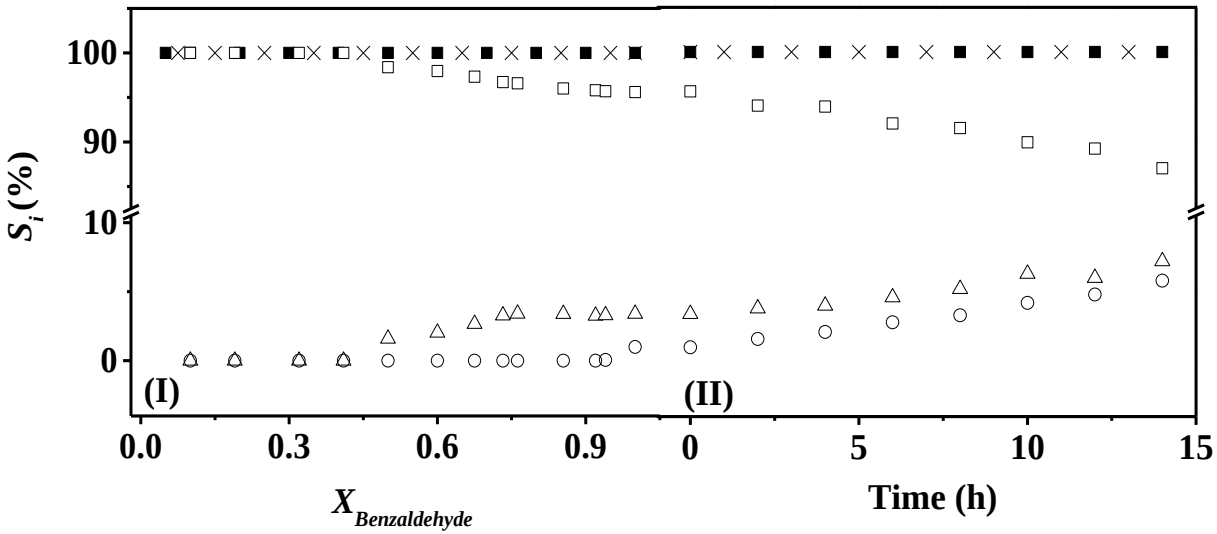

Figure 8. 4: Selectivity (S_i) as a function of (I) benzaldehyde fractional conversion ($X_{Benzaldehyde}$) and (II) time after 100% conversion of benzaldehyde (in water) had been reached over Au/Al_2O_3 (solid symbols), Pt/Al_2O_3 (open symbols) and Au/Fe_2O_3 (crosses); benzyl alcohol (■, □, ×), benzene (△) and toluene (○). *Reaction conditions*: T = 353 K, P = 9 bar.

8.3.2.3 Solvent Effects

The solvent in batch liquid phase catalytic operation serves to dissolve the reactant and/or products but can also interact with the catalyst surface and influence performance [57], benzaldehyde hydrogenation rate was consistently lower in ethanol relative to water (**Table 8.1**). Solvents effects in the catalytic hydrogenation of unsaturated aldehyde/ketones have been reported and associated with variations in H_2 solubility [34], polarity [34-36] and solvent-catalyst surface interactions [57]. The increased rate in aqueous media can not be due to H_2 solubility [33] considerations as under reaction conditions (T = 353 K, P = 9.0 bar) solubility is higher in ethanol (3.7 μmol cm^{-3}) than water (0.8 μmol cm^{-3}). The dependence of benzaldehyde hydrogenation rate (over Au/Al_2O_3) on solvent dielectric constant (ε) is presented in **Figure 8.5**; ε for water+ethanol mixtures was calculated according to the method outlined elsewhere [33]. It can be seen that rate increased with increasing ε with the highest value obtained in pure water. This response can reflect competitive adsorption between solvent and

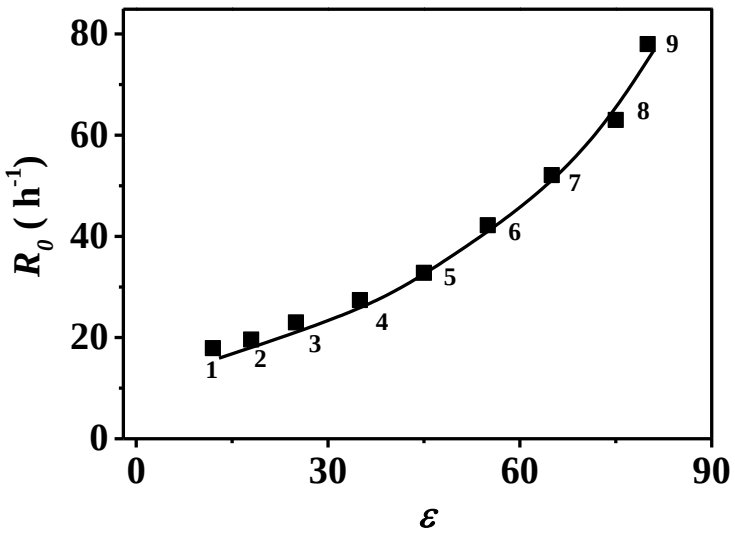

Figure 8. 5: Variation in initial rate (R_0) as a function of solvent dielectric constant (ε) for reaction in (1) pentanol; (2) butanol; (3) ethanol; ethanol:H_2O = (4) 5:1; (5) 3:1; (6) 1:1; (7) 0.6:1; (8) 0.8:1; (9) H_2O for the hydrogenation of benzaldehyde over Au/Al_2O_3. *Reaction conditions*: T = 353 K, P = 9 bar.

reactant on the catalyst or interaction of solvent with the reactant. The dielectric constant provides a measure of solvent capacity to interact with electron deficient or charged surface sites and is related to polarity [62]. Both H_2O [63] and alcohol [64] can adsorption on the Lewis acid sites (Al^{3+}) of Al_2O_3 through the oxygen of the hydroxyl

group. The greater electron density of the hydroxyl oxygen in alcohols results in stronger interaction that increases with increasing chain length of the alcohol. Competition of solvent and aldehyde for adsorption sites [8] will impact on hydrogenation rate where increased surface affinity for the solvent inhibits benzaldehyde activation, resulting in lower reaction rate. The rate decrease is inversely proportional to the polarity of the solvent (pentanol < butanol < ethanol < H_2O). The solvent can also influence reactant activation as a result of hydrogen bonding between protic solvents and the -C=O function [36,37]. Akpa *et al.* [65] employed DFT calculations to investigate 2-butanone hydrogenation in water over Ru/SiO_2 and concluded that the stronger interaction between water and 2-butanone (by hydrogen bonding) dramatically lowers the activation energy barrier and should enhance reaction rate. Catalyst (Ru/C) testing has shown higher 2-butanone hydrogenation rate in solvents with higher ε [36]. In contrast, Bertero *et al.* [35] and Aramendía *et al.* [38] reported a decrease in acetophenone hydrogenation rate with increasing ε due to solvation that inhibited the adsorption step. It should, however, be noted that these reactions were not under chemical control and mass transport rate can contribute to the overall measured activity.

8.3.3 Gas Phase Hydrogenation of Benzaldehyde

We extended our analysis to consider if the catalytic response of the three catalysts with respect to the rate and selectivity observed in batch liquid phase extended to continuous gas phase operation. The results are summarised in **Figure 8.6**. As in the liquid phase (**Figure 8.6(A)**), Au/Al_2O_3 delivered a measurably higher reaction rate than Au/Fe_2O_3 in gas phase mode that was again appreciably lower than Pt/Al_2O_3 (**Figure 8.6(B)**). Reaction exclusivity to benzyl alcohol in the liquid phase also applied to gas phase reaction where Pt/Al_2O_3 again promoted hydrogenolysis to generate toluene and benzene as significant by-products. The critical catalytic trends apply to both modes of operation and are insensitive to reaction phase, differences in contact/residence time, H_2 pressure and reaction temperature.

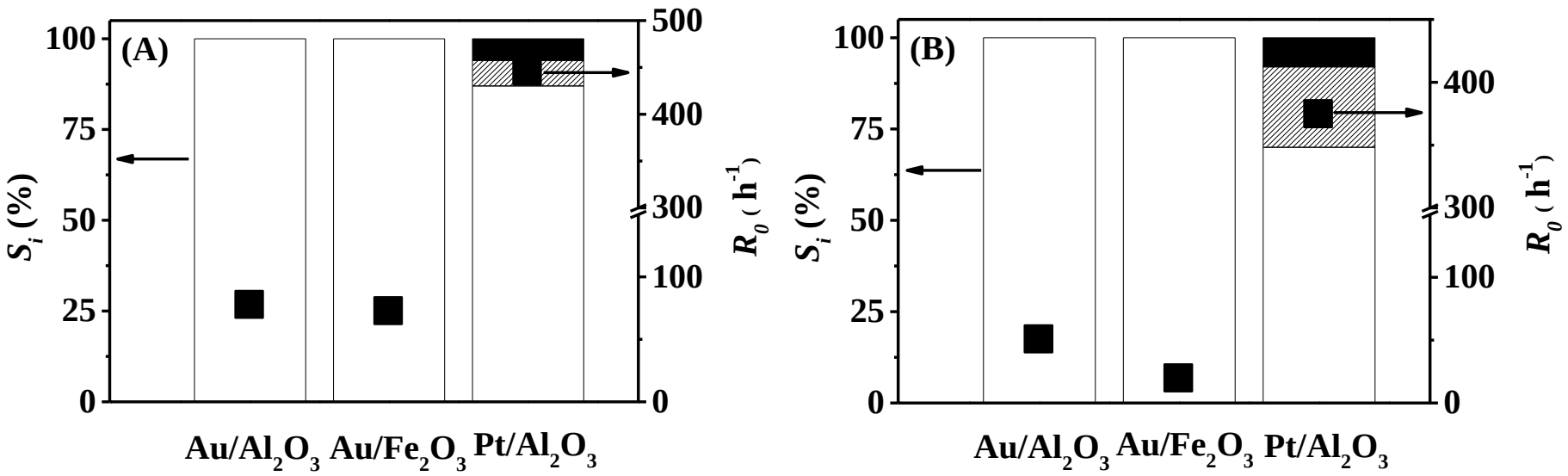

Figure 8. 6: Initial rate (R_0) (■) and selectivity (S_i) to benzyl alcohol (open bars), benzene (hatched bars) and toluene (solid bar) over Au/Al_2O_3, Pt/Al_2O_3 and Au/Fe_2O_3 in (A) liquid (T = 353 K, P = 9 bar) and (B) gas phase (T = 413 K, P = 1 bar) hydrogenation of benzaldehyde using water as solvent.

8.4 Conclusions

The liquid phase (T = 353 K, P_{H2} = 9.0 bar) hydrogenation of benzaldehyde over (1% w/w) Au/Al_2O_3 and Au/Fe_2O_3 bearing nanoscale Au particles (mean size = 2.2-3.6 nm) was fully selective with 100% yield of the target benzyl alcohol. XPS analysis suggests differences in the electronic character of the Au sites on both supports but this had no apparent significant effect on hydrogenation rate or selectivity. Reaction over (0.7% w/w) Pt/Al_2O_3 (mean Pt size = 1.7 nm) generated the alcohol with toluene and benzene as significant (hydrogenolysis) by-products. The appreciably higher reaction rate recorded for Pt/Al_2O_3 can be attributed to greater H_2 chemisorption capacity. The reaction proceeded *via* a nucleophilic mechanism where the presence of an electron-withdrawing ring substituent (-C≡N) in the *para*- position had an activating effect that served to increase reaction rate while an electron-donating substituent (-C=O) lowered rate. A correlation has been established between solvent dielectric constant (ε) and hydrogenation rate over Au/Al_2O_3. This is accounted for in terms of (i) competition for active sites that is more pronounced for alcohol with lower ε and (ii) reactant solvation facilitated by hydrogen bonding with solvents with higher ε that generated higher rates. Exclusivity to benzyl alcohol over supported Au in batch liquid phase extends to continuous operation in the gas phase, opening a number of potential opportunities for cleaner aromatic alcohol production.

8.5 References

[1] N. Perret, F. Cardenas-Lizana, M.A. Keane, *Selective hydrogenation of benzaldehyde to benzyl alcohol over Au/Al_2O_3*, Catal. Commun. 16 (**2011**) 159-164.

[2] J. Scognamiglio, L. Jones, D. Vitale, C.S. Letizia, A.M. Api, *Fragrance material review on benzyl alcohol*, Food Chem. Toxicol. 50, Supplement 2 (**2012**) S140-S160.

[3] L. Song, K. Li, X. Li, P. Wu, *One-pot synthesis of highly ordered Ru-containing mesoporous polymers/silica for benzaldehyde hydrogenation*, React. Kinetic. Mech. Cat. 104 (**2011**) 99-109.

[4] F. Pinna, F. Menegazzo, M. Signoretto, P. Canton, G. Fagherazzi, N. Pernicone, *Consecutive hydrogenation of benzaldehyde over Pd catalysts: Influence of supports and sulfur poisoning*, Appl. Catal. A: Gen. 219 (**2001**) 195-200.

[5] D. Divakar, D. Manikandan, G. Kalidoss, T. Sivakumar, *Hydrogenation of benzaldehyde over palladium intercalated bentonite catalysts: Kinetic studies*, Catal. Lett. 125 (**2008**) 277-282.

[6] S. Liu, X. Fan, X. Yan, X. Du, L. Chen, *Catalytic reduction of benzaldehyde to toluene over Ni/γ-Al_2O_3 in the presence of aniline and H_2*, Appl. Catal. A: Gen. 400 (**2011**) 99-103.

[7] A. Saadi, R. Merabti, Z. Rassoul, M.M. Bettahar, *Benzaldehyde hydrogenation over supported nickel catalysts*, J. Mol. Catal. A: Chem. 253 (**2006**) 79-85.

[8] A. Saadi, Z. Rassoul, M.M. Bettahar, *Gas phase hydrogenation of benzaldehyde over supported copper catalysts*, J. Mol. Catal. A: Chem. 164 (**2000**) 205-216.

[9] M. Arai, A. Obata, Y. Nishiyama, *The influence of reduction methods and conditions on the activity of alumina-supported platinum catalysts for the liquid phase hydrogenation of benzaldehyde in ethanol*, J. Catal. 166 (**1997**) 115-117.

[10] M. Han, H. Zhang, Y. Du, P. Yang, Z. Deng, *Catalytic hydrogenation of benzaldehydes over platinum nanoparticles immobilized on magnesium aluminate spinel under mild conditions*, React. Kinetic. Mech. Cat. 102 (**2011**) 393-404.

[11] X. Li, W. Zheng, H. Pan, Y. Yu, L. Chen, P. Wu, *Pt nanoparticles supported on highly dispersed TiO_2 coated on SBA-15 as an efficient and recyclable catalyst for liquid-phase hydrogenation*, J. Catal. 300 (**2013**) 9-19.

[12] Y. Ding, X. Li, B. Li, H. Wang, P. Wu, *Pt nanoparticles entrapped in ordered mesoporous carbons for liquid-phase hydrogenation of unsaturated compounds*, Catal. Commun. 28 (**2012**) 147-151.

[13] X. Li, Y. Shen, L. Song, H. Wang, H. Wu, Y. Liu, P. Wu, *Efficient hydrogenation of benzaldehydes over mesopolymer-entrapped pt nanoparticles in water*, Chem. Asian J. 4 (**2009**) 699-706.

[14] J. Yang, J. Zhang, L. Zhu, S. Chen, Y. Zhang, Y. Tang, Y. Zhu, Y. Li, *Synthesis of nano titania particles embedded in mesoporous SBA-15: Characterization and photocatalytic activity*, J. Hazard. Mater. 137 (**2006**) 952-958.

[15] F. Zhang, Y. Meng, D. Gu, Y. Yan, C. Yu, B. Tu, D. Zhao, *A facile aqueous route to synthesize highly ordered mesoporous polymers and carbon frameworks with Ia3d bicontinuous cubic structure*, J. Am. Chem. Soc. 127 (**2005**) 13508-13509.

[16] D. Zhao, J. Feng, Q. Huo, N. Melosh, G.H. Fredrickson, B.F. Chmelka, G.D. Stucky, *Triblock copolymer syntheses of mesoporous silica with periodic 50 to 300 angstrom pores*, Science 279 (**1998**) 548-552.

[17] B. Li, X. Li, Y. Ding, P. Wu, *Ordered mesoporous carbons with Ia3d symmetry supported Pt catalyst for efficient asymmetric hydrogenation*, Catal. Lett. 142 (**2012**) 1033-1039.

[18] M. Okamoto, T. Hirao, T. Yamaai, *Polymers as novel modifiers for supported metal catalyst in hydrogenation of benzaldehydes*, J. Catal. 276 (**2010**) 423-428.

[19] T. Mitsudome, K. Kaneda, *Gold nanoparticle catalysts for selective hydrogenations*, Green Chem. 15 (**2013**) 2636-2654.

[20] F. Cárdenas-Lizana, M.A. Keane, *The development of gold catalysts for use in hydrogenation reactions*, J. Mater. Sci. 48 (**2013**) 543-564.

[21] J. Lenz, B.C. Campo, M. Alvarez, M.A. Volpe, *Liquid phase hydrogenation of α,β-unsaturated aldehydes over gold supported on iron oxides*, J. Catal. 267 (**2009**) 50-56.

[22] C. Milone, M.L. Tropeano, G. Gulino, G. Neri, R. Ingoglia, S. Galvagno, *Selective liquid phase hydrogenation of citral on Au/Fe_2O_3 catalysts*, Chem. Commun. (**2002**) 868-869.

[23] P. Claus, H. Hofmeister, C. Mohr, *Identification of active sites and influence of real structure of gold catalysts in the selective hydrogenation of acrolein to allyl alcohol*, Gold Bull. 37 (**2004**) 181-186.

[24] R. Liu, Y. Yu, K. Yoshida, G. Li, H. Jiang, M. Zhang, F. Zhao, S.-i. Fujita, M. Arai, *Physically and chemically mixed TiO_2-supported pd and au catalysts: Unexpected synergistic effects on selective hydrogenation of citral in supercritical CO_2*, J. Catal. 269 (**2010**) 191-200.

[25] P. Claus, A. Brückner, C. Mohr, H. Hofmeister, *Supported gold nanoparticles from quantum dot to mesoscopic size scale: Effect of electronic and structural properties on catalytic hydrogenation of conjugated functional groups*, J. Am. Chem. Soc. 122 (**2000**) 11430-11439.

[26] X. Zhang, H. Shi, B.-Q. Xu, *Comparative study of Au/ZrO_2 catalysts in CO oxidation and 1,3-butadiene hydrogenation*, Catal. Today 122 (**2007**) 330-337.

[27] N. Perret, X.D. Wang, T. Onfroy, C. Calers, M.A. Keane, *Selectivity in the gas-phase hydrogenation of 4-nitrobenzaldehyde over supported au catalysts*, J. Catal. 309 (**2014**) 333-342.

[28] S. Arrii, F. Morfin, A.J. Renouprez, J.L. Rousset, *Oxidation of CO on gold supported catalysts prepared by laser vaporization: Direct evidence of support contribution*, J. Am. Chem. Soc. 126 (**2004**) 1199-1205.

[29] G.M. Veith, A.R. Lupini, S.J. Pennycook, G.W. Ownby, N.J. Dudney, *Nanoparticles of gold on γ-Al_2O_3 produced by dc magnetron sputtering*, J. Catal. 231 (**2005**) 151-158.

[30] J. Portier, P. Poizot, G. Campet, M.A. Subramanian, J.M. Tarascon, *Acid–base behavior of oxides and their electronic structure*, Solid State Sci. 5 (**2003**) 695-699.

[31] C.H. Campos, M. Jofré, C.C. Torres, B. Pawelec, J.L.G. Fierro, P. Reyes, *Chemoselective hydrogenation of o-, p- and m-chloronitrobenzene at ambient temperature on Au/Fe_2O_3 catalysts*, Appl. Catal. A: Gen. 482 (**2014**) 127-136.

[32] C. Milone, R. Ingoglia, A. Pistone, G. Neri, F. Frusteri, S. Galvagno, *Selective hydrogenation of α,β-unsaturated ketones to α,β-unsaturated alcohols on gold-supported catalysts*, J. Catal. 222 (**2004**) 348-356.

[33] S. Gómez-Quero, F. Cárdenas-Lizana, M.A. Keane, *Solvent effects in the hydrodechlorination of 2,4-dichlorophenol over Pd/Al_2O_3*, AIChE J. 56 (**2010**) 756-767.

[34] A. Drelinkiewicza, A. Waksmundzka, W. Makowski, J.W. Sobczak, A. Król, A. Zieba, *Acetophenone hydrogenation on polymer–palladium catalysts. The effect of polymer matrix*, Catal. Lett. 94 (**2004**) 143-156.

[35] N.M. Bertero, A.F. Trasarti, C.R. Apesteguía, A.J. Marchi, *Solvent effect in the liquid-phase hydrogenation of acetophenone over Ni/SiO_2: A comprehensive study of the phenomenon*, Appl. Catal. A: Gen. 394 (**2011**) 228-238.

[36] H. Wan, A. Vitter, R.V. Chaudhari, B. Subramaniam, *Kinetic investigations of unusual solvent effects during Ru/C catalyzed hydrogenation of model oxygenates*, J. Catal. 309 (**2014**) 174-184.

[37] B. Ren, M. Zhao, L. Dong, G. Li, *Catalytic hydrogenation of 2,4-dinitroethylbenzene to 2,4-diaminoethylbenzene over Ni/HY catalysts: The solvent effect*, Catal. Commun. 50 (**2014**) 92-96.

[38] M.A. Aramendía, V. Borau, J.F. Gómez, A. Herrera, C. Jiménez, J.M. Marinas, *Reduction of acetophenones over Pd/$AlPO_4$ catalysts. Linear free energy relationship (LFER)*, J. Catal. 140 (**1993**) 335-343.

[39] M.-M. Wang, L. He, Y.-M. Liu, Y. Cao, H.-Y. He, K.-N. Fan, *Gold supported on mesostructured ceria as an efficient catalyst for the chemoselective hydrogenation of carbonyl compounds in neat water*, Green Chem. 13 (**2011**) 602-607.

[40] F. Cárdenas-Lizana, S. Gómez-Quero, N. Perret, M.A. Keane, *Gold catalysis at the gas-solid interface: Role of the support in determining activity and selectivity in the hydrogenation of m-dinitrobenzene*, Catal. Sci. Technol. 1 (**2011**) 652-661.

[41] D. Andreeva, V. Idakiev, T. Tabakova, A. Andreev, R. Giovanoli, *Low-temperature water-gas shift reaction on Au/α-Fe_2O_3 catalyst*, Appl. Catal. A: Gen. 134 (**1996**) 275-283.

[42] F. Cárdenas-Lizana, Z.M. de Pedro, S. Gómez-Quero, M.A. Keane, *Gas phase hydrogenation of nitroarenes: A comparison of the catalytic action of titania supported gold and silver*, J. Mol. Catal. A: Chem. 326 (**2010**) 48-54.

[43] S.S. Kim, H.H. Lee, S.C. Hong, *A study on the effect of support's reducibility on the reverse water-gas shift reaction over pt catalysts*, Appl. Catal. A: Gen. 423–424 (**2012**) 100-107.

[44] F. Cardenas-Lizana, S. Gomez-Quero, G. Jacobs, Y. Ji, B.H. Davis, L. Kiwi-Minsker, M.A. Keane, *Alumina supported Au-Ni: Surface synergism in the gas phase hydrogenation of nitro-compounds*, J. Phys. Chem. C 116 (**2012**) 11166-11180.

[45] S. Gómez-Quero, F. Cárdenas-Lizana, M.A. Keane, *Effect of metal dispersion on the liquid-phase hydrodechlorination of 2,4-dichlorophenol over Pd/Al_2O_3*, Ind. Eng. Chem. Res. 47 (**2008**) 6841-6853.

[46] M. Li, X. Wang, N. Perret, M.A. Keane, *Enhanced production of benzyl alcohol in the gas phase continuous hydrogenation of benzaldehyde over Au/Al_2O_3*, Catal. Commun. 46 (**2014**) 187-191.

[47] L. McEwan, M. Julius, S. Roberts, J.Q. Fletcher, *A review of the use of gold catalysts in selective hydrogenation reactions* Gold Bull. 43 (**2010**) 298-306.

[48] L. Stievano, S. Santucci, L. Lozzi, S. Calogero, F.E. Wagner, *197 Au mössbauer study of gold particles obtained by evaporation of metallic gold on mylar*, J. Non-cryst. Solids 232–234 (**1998**) 644-649.

[49] Q. Guo, K. Luo, K.A. Davis, D.W. Goodman, *Initial growth of Au on oxides*, Surf. Interface Anal. 32 (**2001**) 161-165.

[50] H.G. Boyen, T. Herzog, G. Kästle, F. Weigl, P. Ziemann, J. Spatz, M. Möller, R. Wahrenberg, M. Garnier, P. Oelhafen, *X-ray photoelectron spectroscopy study on gold nanoparticles supported on diamond*, Phys. Rev. B 65 (**2002**) 075412.

[51] M.P. Seah, I.S. Gilmore, G. Beamson, *XPS: Binding energy calibration of electron spectrometers 5—re-evaluation of the reference energies*, Surf. Interface Anal. 26 (**1998**) 642-649.

[52] B. Hammer, J.K. Nørskov, *Why gold is the noblest of all the metals*, Nature 376 (**1995**) 238-240.

[53] E. Bus, J.T. Miller, J.A. van Bokhoven, *Hydrogen chemisorption on Al_2O_3-supported gold catalysts*, J. Phys. Chem. B 109 (**2005**) 14581-14587.

[54] C. Wan, Y. An, G. Xu, W. Kong, *Study of catalytic hydrogenation of n-ethylcarbazole over ruthenium catalyst*, Int. J. Hydrogen Energy 37 (**2012**) 13092-13096.

[55] J. Wood, L. Bodenes, J. Bennett, K. Deplanche, L.E. Macaskie, *Hydrogenation of 2-butyne-1,4-diol using novel bio-palladium catalysts*, Ind. Eng. Chem. Res. 49 (**2010**) 980-988.

[56] P.A. Rautanen, J.R. Aittamaa, A.O.I. Krause, *Solvent effect in liquid-phase hydrogenation of toluene*, Ind. Eng. Chem. Res. 39 (**2000**) 4032-4039.

[57] U.K. Singh, M.A. Vannice, *Kinetics of liquid-phase hydrogenation reactions over supported metal catalysts — a review*, Appl. Catal. A: Gen. 213 (**2001**) 1-24.

[58] S.P. Bawane, S.B. Sawant, *Reaction kinetics of the liquid-phase hydrogenation of benzonitrile to benzylamine using raney nickel catalyst*, Chem. Eng. J. 103 (**2004**) 13-19.

[59] D. Haffad, U. Kameswari, M.M. Bettahar, A. Chambellan, J.C. Lavalley, *Reduction of benzaldehyde on metal oxides*, J. Catal. 172 (**1997**) 85-92.

[60] M.A. Vannice, D. Poondi, *The effect of metal-support interactions on the hydrogenation of benzaldehyde and benzyl alcohol*, J. Catal. 169 (**1997**) 166-175.

[61] P. Kluson, L. Cerveny, *Hydrogenation of substituted aromatic compounds over a ruthenium catalyst*, J. Mol. Catal. A: Chem. 108 (**1996**) 107-112.

[62] C. Reichardt, *Solvents and solvent effect in organic chemistry* John Wiley, New York (**2004**) 289-289.

[63] K.C. Hass, W.F. Schneider, A. Curioni, W. Andreoni, *The chemistry of water on alumina surfaces: Reaction dynamics from first principles*, Science 282 (**1998**) 265-268.

[64] S. Cai, K. Sohlberg, *Adsorption of alcohols on γ-alumina (1 1 0 c)*, J. Mol. Catal. A: Chem. 193 (**2003**) 157-164.

[65] B.S. Akpa, C. D'Agostino, L.F. Gladden, K. Hindle, H. Manyar, J. McGregor, R. Li, M. Neurock, N. Sinha, E.H. Stitt, D. Weber, J.A. Zeitler, D.W. Rooney, *Solvent effects in the hydrogenation of 2-butanone*, J. Catal. 289 (**2012**) 30-41.

Chapter 9

Summary and Future Work

9.1 General Conclusions

The main objective of this thesis is to investigate alternative cleaner routes for the sustainable production of aliphatic and aromatic amines with multiple industrial applications. This work has focused on the use of (oxide and carbon) supported Pd and Au catalysts with detailed characterisation to allow correlation of structure with performance. Reaction mechanism underpinning each process has also been considered. Supported Pd promotes the continuous hydrogenation of aliphatic amines with time on-stream stability but delivers a mixture of higher amines. The work has tackled selectivity issues, taking a series of approaches directed at maximising exclusive formation of a target secondary or tertiary amines by modifying the catalyst formulation. The acid-base character of the support plays a critical role where acidic carriers with high specific surface area (*e.g.* Pd on C) promote condensation leading to the preferential formation of tertiary amines. The work has demonstrated a major contribution due to spillover hydrogen to elevate overall hydrogenation rate. The incorporation of a second metal (Ba) has been shown to be an effective means of controlling catalytic performance through a modification of the surface chemistry that influences reactant (nitrile) activation and reaction. Production of higher (secondary and tertiary) from a mono- and di- amine feed has been established where metal site electronic character is critical. Contact time is a crucial process variable where the use of multiple catalyst beds in series facilitates enhanced product output. This applies to the production of both aliphatic and aromatic amines from a nitrile feedstock. The effect of the support has been demonstrated in the hydrogenation of functionalized nitrocompounds. Exclusive nitro-group reduction has been established in the presence of other reducible (nitrile and chloride) functionalities. The redox character of the support is key where the exclusive nitro-group reduction is promoted using ZnO (linked to PdZn alloy formation) and the presence of oxygen vacancies (in TiO_2) enhance significantly hydrogenation rate. With the overarching theme of process selectivity and sustainability, the work was extended to consider the catalytic action of supported Au in hydrogenation applications. Preliminary data have established full selectivity in benzaldehyde hydrogenation to deliver 100% yield of the target alcohol in water as

solvent. This represents a significant improvement over conventional supported Pt application and is a system that warrants further research.

9.2 Future Directions

9.1.1 Selective Hydrogenation of Substituted Aliphatic and Aromatic Nitriles

The work presented in **Chapters 2** and **4** have established fine-tuned selectivity control in the synthesis of secondary and tertiary aliphatic amines. An extension of the work to more complex functionalized aliphatic nitriles is necessary to fully exploit these findings. Such is the case for example the selective hydrogenation of 1,6-hexanedinitrile to 6-aminohexanenitrile, a key intermediate in the production of nylon-6 [1]. The highest reported selectivity (87%) has been attained in batch liquid phase operation over (pyrophoric unstable) Raney Ni-P [3]. Exclusive target amine production is challenging due to condensation and cyclisation reactions [2]. Drawing on the database and approaches taken in this thesis, improvements over current state of the art are anticipated. Of particular relevance in this respect is the work presented in **Chapter 3** where the changes in surface chemistry resulting from the incorporation of Ba with Pd can address existing shortfalls in the reported literature. Given the reported preferential formation of primary amines over Ni [3], this metal warrants consideration applying the methods described in this thesis. Use of a basic support (*e.g*. MgO [4]) can serve to minimise condensation reactions and enhance selectivity to 6-aminohexanenitrile.

9.1.2 Liquid Phase Hydrogenation of Aromatic Nitrocompounds in Aqueous Solution over Au/TO_2 and Au/Al_2O_3

As established in **Chapter 8**, water as solvent promotes the selective hydrogenation of benzaldehyde to benzyl alcohol over Au/Al_2O_3. This reaction system requires further exploration. It is proposed to extend the work with an examination of solvent effects in the hydrogenation of aromatic nitrocompounds, (e.g. *p*-chloronitrobenzene). This would establish whether the competitive adsorption and solvation effects are generic or particular to the system studied in this thesis. Support (TiO_2) effects in terms of–NO_2 group activation are noted in **Chapter 7** and there is evidence in the literature of contributions due to the acid-base properties of Al_2O_3 [5]. The liquid phase hydrogenation of aromatic nitrocompounds in a range of solvents over Au/TiO_2 and Au/Al_2O_3 requires further work.

9.1.3 Selective Hydrogenation of Levulinic acid to γ-valerolactone Using Au Catalysts

Sustainability is the driver for the work conducted in this thesis. Currently, feedstock and the energy source for chemical processing are derived from fossil fuels (coal, petroleum oil and natural gas). However fossil reserves are finite and their consumption is accompanied by emission of greenhouse gas which causes the global warming. One response is to draw on renewable resources. Use of catalysts to convert biomass and biomass derivatives has been the subject of intensive research over the last decade [6,7]. Levulinic acid is recognised as a biomass derived platform chemical [8]. Selective reduction yields γ-valerolactone, used as petrol and diesel additive [9]. Drawing on the selective catalytic action of Au catalysts in C=O reduction to –C-OH (**Chapter 8**) a programme of study is proposed to examine the role of support in the hydrogenation of levulinic acid over Au.

9.2 Reference

[1] S. Nishimura, *Handbook of Heterogeneous Catalytic Hydrogenation for Organic Synthesis* John Wiley, New York (**2001**) 265-265.

[2] M. Serra, P. Salagre, Y. Cesteros, F. Medina, J.E. Sueiras, *Evolution of several ni and Ni-MgO catalysts during the hydrogenation reaction of adiponitrile*, Appl. Catal. A: Gen. 272 (**2004**) 353-362.

[3] J. Krupka, J. Pasek, *Nitrile hydrogenation on solid catalysts - new insights into the reaction mechanism*, Curr. Org. Chem. 16 (**2012**) 988-1004.

[4] H. Chen, M. Xue, S. Hu, J. Shen, *The effect of surface acidic and basic properties on the hydrogenation of lauronitrile over the supported nickel catalysts*, Chem. Eng. J. 181–182 (**2012**) 677-684.

[5] K.-i. Shimizu, Y. Miyamoto, T. Kawasaki, T. Tanji, Y. Tai, A. Satsuma, *Chemoselective hydrogenation of nitroaromatics by supported gold catalysts: Mechanistic reasons of size- and support-dependent activity and selectivity*, J. Phys. Chem. C 113 (**2009**) 17803-17810.

[6] M. Besson, P. Gallezot, C. Pinel, *Conversion of biomass into chemicals over metal catalysts*, Chem. Rev. 114 (**2013**) 1827-1870.

[7] P. Gallezot, *Conversion of biomass to selected chemical products*, Chem. Soc. Rev. 41 (**2012**) 1538-1558.

[8] S. Derle, P. Parikh, *Hydrogenation of levulinic acid and γ-valerolactone: Steps towards biofuels*, Biomass Conversion and Biorefinery 4 (**2014**) 293-299.

[9] P.P. Upare, J.-M. Lee, D.W. Hwang, S.B. Halligudi, Y.K. Hwang, J.-S. Chang, *Selective hydrogenation of levulinic acid to γ-valerolactone over carbon-supported noble metal catalysts*, J. Ind. Eng. Chem. 17 (**2011**) 287-292.

Appendix 1

Hydrogenation of butyronitrile (BT) at T = 473 K, P = 1 atm,

$$6\ BT + H_2 \rightarrow MBA + DBA + TBA + 3NH_3$$

To calculate the molar fraction of each component at X_{BT} = 25%,

$F_{BT} = 6.9 \times 10^{-3} \times 25\% = 1.75 \times 10^{-3}$ mol·h^{-1}

$F_{BA} = F_{DBA} = F_{TBA} = 1/6\ F_{BT} = 1/6 \times 1.75 \times 10^{-3} = 0.2875 \times 10^{-3}$ mol·h^{-1}

$$F_{H_2} = \frac{\frac{60 \times 0.001}{22.4}}{\frac{1}{60}} = 160 \times 10^{-3}\ \text{mol·h}^{-1}$$

Molar fraction of tributylamine (TBA),

$$x_{TBA} = \frac{0.2875}{6.9 \times (1 - 25\%) + 0.2875 + 0.2875 + 0.2875 + 160} = 1.7 \times 10^{-3}$$

$P_{TBA} = P_{Total} \times x_{TBA} = 101325 \times 1.7 \times 10^{-3} = 175$ Pa

To calculate the saturated vapour pressure (P_{TBA}*) of tributylamine at T = 473 K,

$$T_B = 364.7\ \text{K},\ P_B = 0.01\ \text{Bar}$$

T_B, temperature of boiling point;

P_B, vapour pressure at boiling point temperature

$$\frac{P_B}{T_B} = \frac{P_{TBA}^*}{473}$$

$$\frac{0.01}{364.7} = \frac{P^*}{473}$$

$$P_{TBA}^* = 0.01297\ \text{Bar} = 0.01297 \times 101325 \times 0.98692 = 1314.1\ \text{Pa}$$

$$P_{TBA} << P_{TBA}^*$$

Tributylamine produced was in the vapour phase.

Appendix 2

Hydrogenation of benzonitrile (BN) at T = 353 K, P = 1 atm,

$$2BN + 3H_2 \rightarrow BA + TOL + NH_3$$

$$C_{BN} = 0.3 \text{ mol·L}^{-1}$$

$$C_{2\text{-propanol}} = 12.67 \text{ mol·L}^{-1}$$

(1) To calculate the molar fraction of each component in the inlet flow,

$$F_{BN} = 0.3 \times 1.2 \times 10^{-3} = 0.36 \times 10^{-3} \text{ mol·h}^{-1}$$

$$F_{2\text{-propanol}} = 12.67 \times 1.2 \times 10^{-3} = 3.8 \times 10^{-3} \text{ mol·h}^{-1}$$

$$F_{H_2} = \frac{\frac{60 \times 0.001}{22.4}}{\frac{1}{60}} = 160 \times 10^{-3} \text{ mol·h}^{-1}$$

$$x_{BN} = \frac{0.36}{0.36 + 3.8 + 160} = 2.19 \times 10^{-3}$$

$$x_{2\text{-propanol}} = \frac{3.8}{0.36 + 3.8 + 160} = 23.1 \times 10^{-3}$$

$$x_{H_2} = \frac{160}{0.36 + 3.8 + 160} = 0.975$$

$$P_{BN} = P_{Total} \times x_{BN} = 101325 \times 2.19 \times 10^{-3} = 221.9 \text{ Pa}$$

To calculate the saturated vapour pressure of benzonitrile (P_{BN}*) at T = 353 K, according to Antoine equation,

$$\log P_{BN}^* = A - \frac{B}{T + C}$$

P_{BN}* = Saturated vapour pressure (bar)

T = Temperature (K)

The coefficient A, B and C for benzonitrile in the temperature range 301.4 - 463.8 K are,

A = 4.85401; B = 2110.572; C = -28.331

$$\log P_{BN}^* = 4.8540 - \frac{2110.572}{353 - 28.331} = -1.646$$

P_{BN}* = 0.02256 Bar = 0.02256 × 101325 × 0.98692 = 2230 Pa

$P_{BN} << P_{BN}$*

Benzonitrile was in the gas phase at this reaction conditions.

(2) To calculate the molar fraction of each component at the X_{BN} = 10%, with benzylamine as product,

$$BN + 2H_2 \rightarrow BA$$

F_{BN} = 0.3 × 1.2 × 10^{-3} × (1-10%) = 0.324 × 10^{-3} mol·h^{-1}

F_{BA} = 0.36 × 10^{-3} × 10% = 0.036 × 10^{-3} mol·h^{-1}

$F_{2\text{-}propanol}$ = 12.67 × 1.2 × 10^{-3} = 3.8 × 10^{-3} mol·h^{-1}

F_{H_2} = 160 × 10^{-3} mol·h^{-1}

Molar fraction of each component in the flow,

$$x_{BN} = \frac{0.324}{0.324+0.036+3.8+160} = 2.08 \times 10^{-3}$$

$$x_{BA} = \frac{0.036}{0.324+0.036+3.8+160} = 2.22 \times 10^{-4}$$

$P_{BN} = P_{Total} \times x_{BN}$ = 101325 × 2.08 × 10^{-3} = 210.8 Pa

$P_{BA} = P_{Total} \times x_{BA}$ = 101325 × 2.22 × 10^{-4} = 22.5 Pa

To calculate the saturated vapour pressure of benzylamine (P_{BA}*) at T = 353 K, according to Antoine equation,

$$logP_{BA}^* = A - \frac{B}{T+C}$$

P_{BA}* = Saturated vapour pressure (bar)

T = Temperature (K)

The coefficient A, B and C for benzylamine (BA) are, A = 4.8271; B = 2003.528; C = -41.973

$$logP_{BA}^* = 4.8271 - \frac{2003.528}{353-41.973} = -1.615$$

$$P_{BA}^* = 0.02256 \text{ Bar} = 0.024266 \times 101325 \times 0.98692 = 23000 \text{ Pa}$$

$$P_{BN} << P_{BN}^*$$

$$P_{BA} << P_{BA}^*$$

Benzonitrile and benzylamine were in the gas phase at this reaction conditions.

(3) To calculate the molar fraction of each component at the X_{BN} = 20%, with the production of benzylamine and toluene,

$$2BN + 3H_2 \rightarrow BA + TOL + NH_3$$

Likewise, to calculate the composition,

$F_{BN} = 0.36 \times 10^{-3} \times (1\text{-}20\%) = 0.29 \times 10^{-3} \text{ mol·h}^{-1}$

$F_{BA} = 0.36 \times 10^{-3} \times 10\% = 0.036 \times 10^{-3} \text{ mol·h}^{-1}$

$F_{TOL} = 0.36 \times 10^{-3} \times 10\% = 0.036 \times 10^{-3} \text{ mol·h}^{-1}$

$F_{2\text{-propanol}} = 12.67 \times 1.2 \times 10^{-3} = 3.8 \times 10^{-3} \text{ mol·h}^{-1}$

$F_{H_2} = 160 \times 10^{-3} \text{ mol·h}^{-1}$

Molar fraction of each component,

$$x_{BN} = \frac{0.29}{0.29 + 0.036 + 0.036 + 3.8 + 160} = 1.75 \times 10^{-3}$$

$$x_{BA} = \frac{0.036}{0.29 + 0.036 + 0.036 + 3.8 + 160} = 0.22 \times 10^{-3}$$

$$x_{TOL} = \frac{0.036}{0.29 + 0.036 + 0.036 + 3.8 + 160} = 0.22 \times 10^{-3}$$

$$x_{2\text{-propanol}} = \frac{3.8}{0.29 + 0.036 + 0.036 + 3.8 + 160} = 0.023 \times 10^{-3}$$

$P_{BN} = P_{Total} \times x_{BN} = 101325 \times 1.75 \times 10^{-3} = 177 \text{ Pa}$

$P_{BA} = P_{Total} \times x_{BA} = 101325 \times 0.22 \times 10^{-4} = 22.3 \text{ Pa}$

$P_{TOL} = P_{Total} \times x_{TOL} = 101325 \times 0.22 \times 10^{-4} = 22.3 \text{ Pa}$

To calculate the saturated vapour pressure of toluene at (P_{TOL}^*) at T = 353 K, according to Antoine equation,

$$LogP_{TOL}^{*} = A - \frac{B}{T + C}$$

P_{TOL}^{*} = Saturated vapour pressure (bar)

T = Temperature (K)

The coefficient A, B and C for benzylamine are, A = 4.07827; B = 1343.943; C = -53.773

$$LogP_{TOL}^{*} = 4.07827 - \frac{1343.943}{353 - 53.773} = -0.413$$

P_{TOL}^{*} = 0.386 Bar = 0.386 × 101325 × 0.98692 = 38636 Pa

$$P_{BN} << P_{BN}^{*}$$

$$P_{BA} << P_{BA}^{*}$$

$$P_{TOL} << P_{TOL}^{*}$$

Benzonitrile, benzylamine and toluene were in the gas phase at this reaction conditions.

Appendix 3

Hydrogenation of *p*-chloronitrobenzene (*p*-CNB) at T = 453 K, P = 1 atm,

$$p\text{-CNB} + 3H_2 \rightarrow p\text{-CAN} + NB + AN$$

To calculate the saturated vapour pressure of each component at this reaction temperature,

For *p*-CNB,

$$T_B = 386.2 \text{ K}, P_B = 0.01 \text{ Bar}$$

T_B, temperature of boiling point;

P_B, vapour pressure at boiling point temperature

$$\frac{P_B}{T_B} = \frac{P_{CNB}^*}{453}$$

$$\frac{0.01}{386.2} = \frac{P_{CNB}^*}{453}$$

$$P_{CNB}^* = 0.0117 \text{ Bar} = 0.0117 \times 101325 \times 0.98692 = 1188 \text{ Pa}$$

For *p*-CAN, according to Antoine equation,

$$Log P_{p\text{-}CAN}^* = A - \frac{B}{T + C}$$

$P_{p\text{-}CAN}^*$ = Saturated vapour pressure (bar)

T = Temperature (K)

The coefficient A, B and C for *p*-CAN are, A = 4.87876; B = 2254.26; C = - 41.619

$$Log P_{p\text{-}CAN}^* = 4.87876 - \frac{2254.26}{453 - 41.619} = -0.1488$$

$$P_{p\text{-}CAN}^* = 0.7099 \text{ Bar} = 0.7099 \times 101325 \times 0.98692 = 70997.6 \text{ Pa}$$

For NB, according to Antoine equation,

$$Log P_{NB}^* = A - \frac{B}{T + C}$$

P_{NB}^* = Saturated vapour pressure (bar)

T = Temperature (K)

The coefficient A, B and C for NB are, A = 4.21553; B = 1727.592; C = - 73.438

$$LogP_{NB}^{*} = 4.21553 - \frac{1727.592}{453 - 73.438} = -0.336$$

$$P_{NB}^{*} = 0.4613 \text{ Bar} = 0.4613 \times 101325 \times 0.98692 = 46130.4 \text{ Pa}$$

For AN, according to Antoine equation,

$$LogP_{AN}^{*} = A - \frac{B}{T + C}$$

P_{AN}^{*} = Saturated vapour pressure (bar)

T = Temperature (K)

The coefficients A, B and C for AN are, A = 4.34541; B = 1661.858; C = - 74.048

$$LogP_{AN}^{*} = 4.34541 - \frac{1661.858}{453 - 74.048} = -0.03999$$

$$P_{AN}^{*} = 0.912 \text{ Bar} = 0.912 \times 101325 \times 0.98692 = 91200.3 \text{ Pa}$$

The highest partial pressure for each component at this reaction conditions,

$F_{p\text{-}CNB} = 0.24 \times 10^{-3}$ mol·h^{-1}

$$F_{Butanol} = 1.2 \times 10^{-3} \times \frac{\frac{810 \times 1000}{74.12}}{1000} = 13.11 \times 10^{-3} \text{ mol·h}^{-1}$$

$$F_{H_2} = \frac{\frac{60 \times 0.001}{22.4}}{\frac{1}{60}} = 160 \times 10^{-3} \text{ mol·h}^{-1}$$

To calculate the molar fraction of each component

$$x_{p\text{-}CNB} = \frac{0.24}{0.24 + 13.11 + 160} = 1.38 \times 10^{-3}$$

$P_{p\text{-}CNB} = P_{Total} \times x_{p\text{-}CNB} = 101325 \times 1.38 \times 10^{-3} = 140.2$ Pa

$$P_{p\text{-}CNB} << P_{p\text{-}CNB}^{*}$$

At the conversion of $X_{p\text{-}CNB}$ = 20%, to calculate the molar fraction of each component,

$$x_{p-CAN} = x_{p\text{-}CNB} \times 20\% = 1.38 \times 10^{-3} \times 20\% = 0.276 \times 10^{-3}$$

$$P_{p\text{-}CAN} = P_{Total} \times x_{p\text{-}CAN} = 101325 \times 0.276 \times 10^{-3} = 27.9 \text{ Pa}$$

$$P_{AN} = P_{Total} \times x_{AN} = 101325 \times 0.276 \times 10^{-3} = 27.9 \text{ Pa}$$

$$P_{NB} = P_{Total} \times x_{NB} = 101325 \times 0.276 \times 10^{-3} = 27.9 \text{ Pa}$$

$$P_{p\text{-}CAN} << P_{p\text{-}CAN}^*$$

$$P_{AN} << P_{CAN}^*$$

$$P_{NB} << P_{NB}^*$$

Ensuring all the components are in gas phase at this reaction conditions.

Appendix 4

Hydrogenation of benzaldehyde at T = 413 K, P = 1 atm,

To calculate the partial pressure of each component at this reaction condition,

$F_{Benzaldehyde} = 0.06 \times 10^{-3}$ mol·h^{-1}

$$F_{H_2O} = 1.2 \times 10^{-3} \times \frac{\frac{917 \times 10^3}{18}}{1 \times 10^3} = 61.1 \times 10^{-3} \text{ mol·h}^{-1}$$

$$F_{H_2} = \frac{\frac{60 \times 0.001}{22.4}}{\frac{1}{60}} = 160 \times 10^{-3} \text{ mol·h}^{-1}$$

$$x_{Benzaldehyde} = \frac{0.06}{0.06 + 61.1 + 160} = 0.27 \times 10^{-3}$$

$P_{Benzaldehyde} = P_{Total} \times x_{Benzaldehyde} = 101325 \times 0.27 \times 10^{-3} = 27.5$ Pa

At the conversion of $X_{Benzaldehyde}$ = 10%, to calculate the partial pressure of benzyl alcohol,

$x_{Benzyl\ alcohol} = 10\% \times 0.27 \times 10^{-3} = 0.027 \times 10^{-3}$

$P_{Benzyl\ alcohol} = P_{Total} \times x_{Benzyl\ alcohol} = 101325 \times 0.027 \times 10^{-3} = 2.75$ Pa

To compare with the saturated vapour pressure of each component at this reaction conditions,

For benzaldehyde, according to Antoine equation,

$$LogP_{Benzaldehyde}^{*} = A - \frac{B}{T + C}$$

$P_{Benzaldehyde}$* = Saturated vapour pressure (bar)

T = Temperature (K)

The coefficient A, B and C for benzaldehyde are, A = 3.87652; B = 1380.729; C = -94.98

$$LogP_{Benzaldehyde}^{*} = 3.87652 - \frac{1380.729}{413 - 94.98} = -0.465$$

$$P_{Benzaldehyde}^{*} = 0.3426 \text{ Bar} = 0.3426 \times 101325 \times 0.98692 = 34266.8 \text{ Pa}$$

For benzyl alcohol, according to Antoine equation,

$$LogP_{Benzyl\ alcohol}^{*} = A - \frac{B}{T + C}$$

$P_{Benzyl\ alcohol}^{*}$ = Saturated vapour pressure (bar)

T = Temperature (K)

The coefficient A, B and C for benzaldehyde are, A = 4.47713; B = 1738.9; C = - 89.559

$$LogP^{*} = 4.47713 - \frac{1738.9}{413 - 89.559} = -0.899$$

$$P_{Benzyl\ alcohol}^{*} = 0.126 \text{ Bar} = 0.126 \times 101325 \times 0.98692 = 12614.7 \text{ Pa}$$

$$P_{Benzaldehyde} << P_{Benzaldehyde}^{*}$$

$$P_{Benzyl\ alcohol} << P_{Benzyl\ alcohol}^{*}$$

Ensuring all the components were in gas phase at this reaction conditions.